64-9

LMSC-895304 • AUGUST 1963

MODEL ENGINE FLAME SPECTRAL STUDIES

(FOUR VOLUMES)

SPECTRAL RADIANCE OF ROCKET PLUMES

VOLUME I

LMSC-895304 • AUGUST 1963

LMSC-895304

MODEL ENGINE FLAME SPECTRAL STUDIES

(FOUR VOLUMES)

SPECTRAL RADIANCE OF ROCKET PLUMES

VOLUME I

by

T. J. KOWALL
R. C. TUTTLE

Prepared Under Air Force Contract AF 04(647)-767

R.C. REDDEN
Manager, Infrared and Optical Devices

H.W. BATTEN
Manager, Payload 461 Payload Development/ Data Processing

J.C. SOLVASON
Manager, Program 461

Lockheed

MISSILES & SPACE COMPANY

A GROUP DIVISION OF LOCKHEED AIRCRAFT CORPORATION

SUNNYVALE, CALIFORNIA

FOREWORD

This is Volume I of a four-volume report of Model Engine Flame Spectral Studies carried out under Air Force Contract AF 04(647)-787 during the period May, 1962 to October, 1963.

T. J. Kowall, who co-authored Volumes I and IV, was responsible for technically organizing and supervising the material for all volumes. Titles and authors are listed below.

Volume I: Spectral Radiance of Rocket Plumes
(T. J. Kowall, R. C. Tuttle)

Volume II: Model Engine Research Tests and Facilities
(H. J. Hemesath, B. L. Coffey, C. E. Tamagni)

Volume III: Engine Performance Computer Studies
(H. J. Hemesath)

Volume IV: Spectral Radiance Calibration Data (C)
(T. J. Kowall, R. C. Tuttle)

ABSTRACT

Infrared spectral measurements were made on three combinations of rocket engine fuels and oxidizers: UDMH/nitrogen tetroxide, hydrazine/nitrogen tetroxide, and RP-1/LOX. Each combination was used in a 1000-lb thrust model engine developed for the tests. Important parameters were varied over a wide range, primarily those of mixing ratios and different conditions of nitrogen purge. The objective was to produce high resolution spectra of small regions of the flame without the usual atmospheric absorption due to water vapor and carbon dioxide. A special test facility was established at the Lockheed Santa Cruz Test Base for spectral measurements, and a special model engine was developed to permit varying fuels and oxidizers. A nitrogen gas system was used to purge the spectrometer paths and to blanket the exhaust flame. The Perkin -Elmer 112 and other spectrometers, including the Block I-4 series were evaluated, but the P-E 112 was selected as the primary instrument. Ninety infrared emission spectra in the one-to-five-micron region were obtained and are published. Conversion of relative spectra to absolute radiance units is achieved by a novel technique using overlays, which are included in the report.

CONTENTS

Appendixes

ILLUSTRATIONS

Section 1
INTRODUCTION

1.1 OBJECTIVES

The primary objective of a Model Engine Flame Measurements Program (MIST) at the Lockheed Missiles & Space Company was to provide useful information on the spectra of new fuels and oxidizers, as and when these became important to satellite-borne surveillance systems. The utility of the data was considered to be meaningful if it permitted the weapons-system engineer to predict performance of a particular system. The need for such a program arose out of discussions with officials of the Department of Defense and the Air Force; concurrence was obtained for implementing and conducting the measurements program within the scope of the larger weapons-system program.

The general objective of MIST was initially considered in terms of comparisons between captive engine flame spectral radiance measurements and full-scale engine-spectral-intensity measurements made in flight from airborne platforms. The difficulty and cost of obtaining high-resolution spectra by airborne instrumentation as compared to static test site measurements, was offset by the obvious utility of the airborne data in predicting system response to such parameters as flame size, altitude, and thrust. However, the airborne measurements programs could not control the selection of fuels and oxidizers, nor could it produce large amounts of data at will. The captive engine measurements program could employ model engines and, with relatively simple modifications, different fuels and oxidizers could be used. Furthermore, these engines could be operated repeatedly. The major problem, however, was the "scaling" of near-sea-level spectral radiance data to the intensity spectra as seen at high altitude from a total exhaust.

To minimize the above problem, it was decided to operate both the spectral measuring apparatus and the model engine in an environment of dry nitrogen gas. It was believed

that this would at least eliminate absorbing constituents in the optical path and minimize the afterburning due to interaction with the low-altitude atmosphere. The problems of (1) scaling the model engine spectral data to higher altitudes and (2) integrating over the flame area were considered at the time to be progressing toward solution because of the known work being done at other companies. The effects of dry nitrogen gas on the flame spectra were considered to be secondary, although measurements of these effects were to be an important part of the MIST Program planning.

1.2 IMPLEMENTATION AND HISTORY

The MIST Program was initiated in May 1962. The planning was implemented by development of the following items at the Lockheed Santa Cruz Test Base:

- A model engine producing 1000-lb thrust
- A spectrometer and optical collector enclosure that was closely coupled to the model-engine firing stand
- A nitrogen injector and drum arrangement for blanketing the flame
- A nitrogen purge system for the spectrometer enclosure
- Transducers for monitoring many parameters for assessment of engine and spectrometer performance
- Methods for data recording and reduction

The model engine was segmented to permit use of different injectors, combustion chambers, and nozzles. The spectrometer installation was set up with two spectrometers, a Perkin-Elmer Model 112, and a Block Associates Model I-4. Other spectrometers were also tried but were not considered to be useful. The "front-optics" consisted primarily of an off-axis F:3.8 parabolic mirror and first-surface mirrors.

In November 1962 the first successful spectral data runs were achieved. These runs represented the combination of intensive activities of engine design and development and spectrometer installation and alignment. The measurements program thereafter emphasized the following activities.

- Three combinations of fuels and oxidizers were used as propellants for the model engine: UDMH/N_2O_4, Hydrazine/N_2O_4, and RP-1/LOX.
- Multiplicity of spectra were obtained to permit statistical averaging for obtaining a "model spectrum."
- The nitrogen blanket around the flame was optimized to obtain the minimum interaction as determined by the spectra.
- Continuous assessment of the data and improvements in the installations and equipments were conducted.
- Measurements were made on RP-1/LOX at the exit plane of the nozzle so as to permit correlation and comparison with previously published data.
- Multiple methods and devices were developed for calibration of the spectrometer output, both in wavelength and in absolute radiance units.

The model engine spectral runs were completed in mid-August 1963. The following three months were concerned with data reduction, calibration verifications, and writing a comprehensive report on activities and results to date.

1.3 RESULTS

The most significant results of the model engine flame spectral studies are the following:

(1) Successful measurements of flame emission in the spectral 1-5 micron band regions. The firings were made on a 1,000-lb-thrust model engine at the LMSC Santa Cruz Test Base, at an elevation of 2,000 feet, on three series of fuel and oxidizer combinations. A total of ninety spectra was obtained in the one-to-five-micron region: twenty-three spectra were of UDMH-N_2O_4, twenty-six were in the N_2H_4-N_2O_4 series, and forty-one were in the RP-1/LOX series. All three series of measurements were made viewing the first Mach disc at two nozzle diameters aft of the exit plane. The undisturbed cone of radiation was also observed during a portion of the RP-1/LOX series. In all spectra obtained, emission in the absorption band regions was well above the noise level of the measuring instrument, even in the case of extreme purge cooling of the flame.

The RP-1/LOX measurements were favorably compared with previous reported measurements made from small-scale model engines (100-lb thrust) in a vacuum chamber, and captive firings of full-scale engines (with associated long optical paths with atmospheric absorption).

The many spectra produced are displayed in several different manners in the report. It is believed that the data as presented can be directly utilized by the weapons-system engineer to optimize his systems response.

(2) Successful developments of a general purpose model engine of 1,000-lb thrust. All the performance characteristics of an operational engine are included in this segmented-type motor with the capability of operation on the following fuels and oxidizers:

Fuels	Oxidizers
Liquid Hydrogen	Liquid Fluorine
Ammonia	IRFNA
Acrozine	ClF_3
Hydyne	OF_2
Hydrazine	LOX
UDMH	N_2O_4
RP-1	

(3) Successful use of a nitrogen blanket around the flame, to suppress the afterburning due to atmospheric interaction with the exhaust. The nitrogen was introduced into a drum surrounding the flame. It was believed that this was important to permit extrapolation of spectral radiance to flames at higher altitudes. The opinions on the need for such suppression have not been fully evaluated; however, the nitrogen blanket has produced data that are useful for further studies on flame structures. Optimum nitrogen flow was

defined as that rate producing minimum absorption at selected bands. The effects of the nitrogen blanket and drum are summarized below:

- There was no apparent difference between optimum flow rates for UDMH/N_2O_4 and Hydrazine/N_2O_4.
- The use of the nitrogen blanket around the flame did show an effect on RP-1/LOX spectra, indicating cooling of the flame. For measurements at the first Mach disc, the magnitude of this effect was small, nominally around 10 percent for 100 psig and one configuration of nitrogen nozzle and drum as compared with no purge. The RP-1/LOX absorption spectra in the significant bands at this flame region were better with low nitrogen flows, or with none. The results showed no important statistical deviation with or without low nitrogen flow. At the exit plane of the engine nozzle, a slight improvement in the spectra was obtained with nitrogen at 100 psig.
- The use of a drum surrounding the flame was experimentally evaluated for RP-1/LOX, and no significant change in spectra was detectable between drum and no-drum firings. The drum did apparently provide a uniform background under wide variations in atmospheric conditions, as evidenced by uniformity of results over long periods of time.

(4) Studies of spectral-radiance variation with mixing ratio of oxidizer to fuel. In all three fuel-oxidizer combinations no significant changes in spectral distribution of radiance occurred in the significant IR emission bands of interest while viewing the flame at two nozzle diameters from the exit plane of the engine, except the slight change due to temperature variation with mixing ratio. There was, however, a noticeable difference in the radiance at the exit plane as a function of mixing ratio for RP-1/LOX in the short wavelength region.

The MIST Program was initiated in May 1962, and the final data runs were completed in August 1963. A preliminary report on the UDMH-N_2O_4 and the Hydrazine/N_2O_4 test data were published (Ref. 1) in May 1963. The following report covers this entire period of time.

Section 2
INSTRUMENTATION AND CALIBRATION

This section of the report is concerned mainly with spectroscopy, or radiation measurements, since the model engine and associated test facilities are described in detail in Volume II. The primary objective of the design and operation of the spectral recording system described below was to record flame emission spectra of the highest possible resolution with a minimum of atmospheric attenuation.

2.1 INSTRUMENTATION

The two major units of instrumentation used in this study consisted of an Astrosystems 1,000-lb (nominal) -thrust engine designed to burn a variety of fuel and oxidizer combinations, and a single beam, prism-type spectrometer for radiation measurements.

2.1.1 Model Engine and Accessory Equipment

The model engine and the accessory nitrogen-purge equipment are described in Volume II, but the operational details pertaining to radiation shall be discussed in this section. The purge-ring system and the drum configuration were used in attempts to eliminate all possible sources of atmospheric attenuation, and, also, to minimize afterburning. The purge efficiency of the spectrometer system was clearly demonstrated and is shown in Fig. 2-1. The experimentation with purge nozzles and rings took many forms; the two main configurations evolved from the many types evaluated. Purge ring A consisted of a 3/4-in. pipe rolled to a diameter of 5 in. and slit on one side to an opening 3/32-in. wide. The purge ring used in A is shown in Fig. 2-2. Table 2-1 contains the information on the various experimental configurations. Listed in the table are the purge-ring types, drum configurations, and the optical systems used in the various runs.

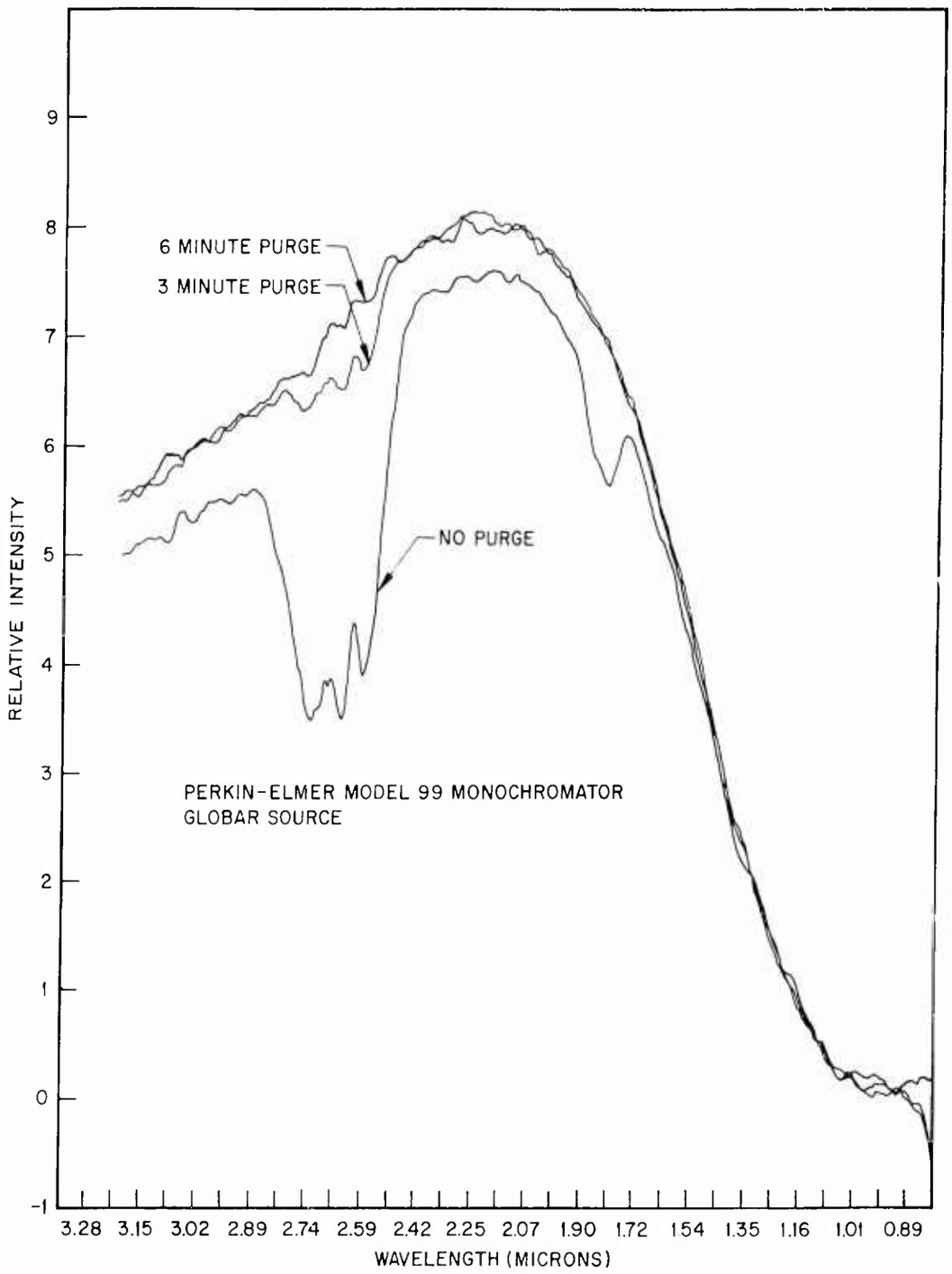

Fig. 2-1 Purge Efficiency of the Perkin-Elmer Spectrometer System

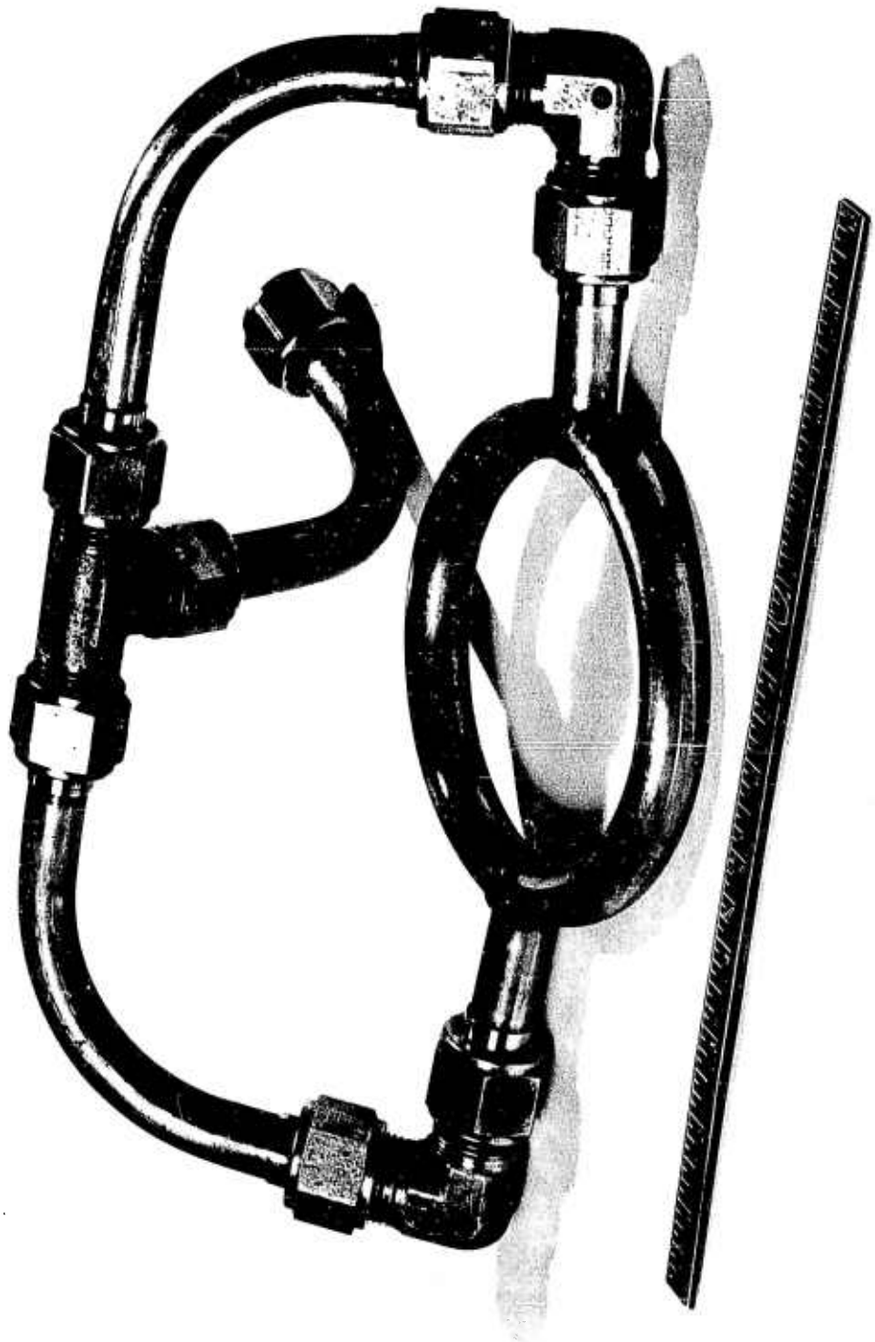

Fig. 2-2 Purge Ring A

Purge-ring B consisted of a metal ring surrounding the exit nozzle. The exit slit had a diameter of 5-3/8 in., and an 0.02-in. opening provided the exit for the purging gases. A photograph of the B system in shown (Fig. A-15) in Volume II.

The two main drum configurations are identified as Drum A and Drum B, and their dimensions are described in Fig. 2-3. The two configurations differ mainly in relative sizes of drums, view port, and most important, from the IR standpoint, the position of the flame viewed. Drum A views the flame at the first mach disc, and B views it immediately aft of the exit plane.

Table 2-1

EXPERIMENTAL CONFIGURATIONS
NITROGEN PURGE AND OPTICAL SYSTEMS

Run Number	Purge Drum	Purge Ring	Optical System
659 and 611	A	A	A
611 thru 681	A	A	B
698 thru 717	A	A	C
718 thru 728	A	B	C
729 thru 731	None	B	C
732 and 733	None	None	C
734	None	A	C
735 thru 745	B	B	D

2.1.2 Spectrometer Evaluation

Although other spectrometers were evaluated, the most efficient proved to be the Perkin-Elmer Model 112. Also evaluated were the Block I-4T and I-4E, and the Beckman IR-7. The Blocks were unsuccessful because of the microphonic problems and the complexities of data reduction of Fourier transforms. The Beckman

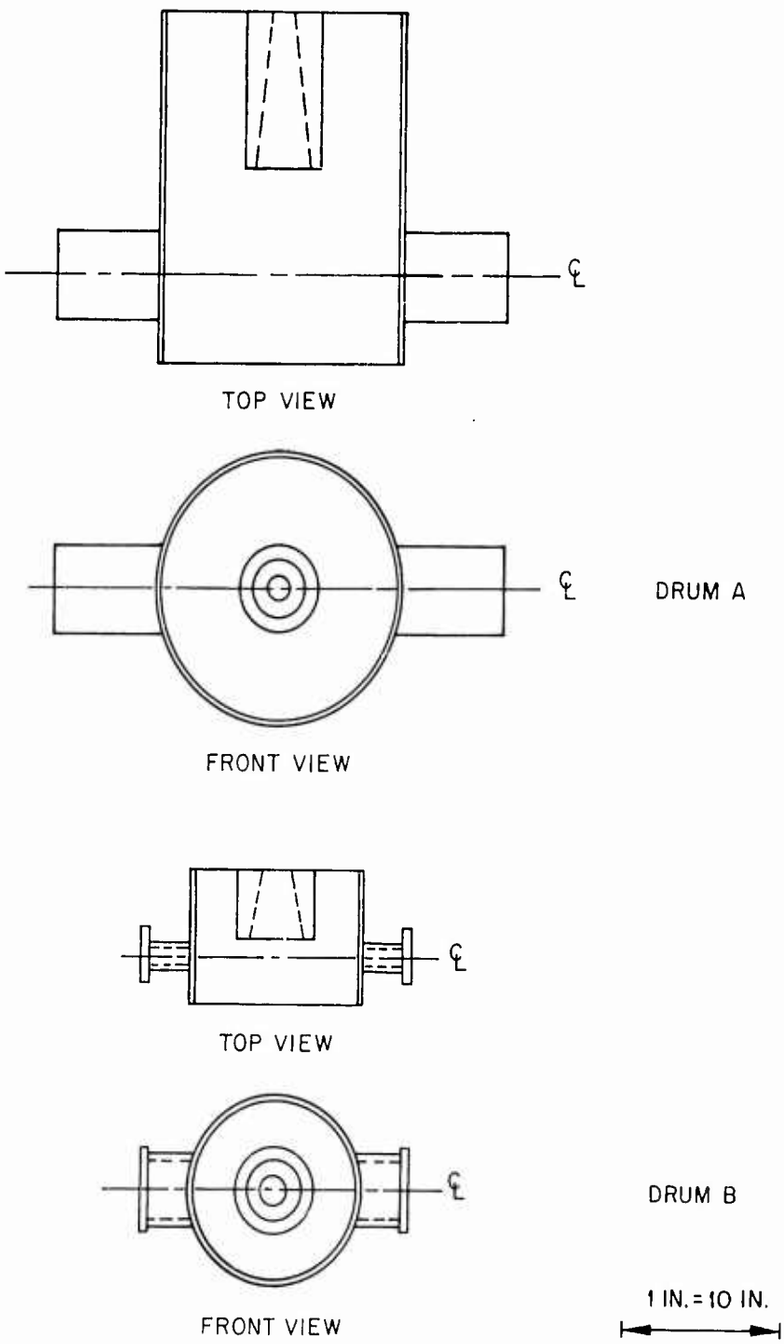

Fig. 2-3 Drum and Nozzle Geometry

nitrogen-purge system was inadequate in this instance. The purge system had so many small openings that when used under laboratory conditions the nitrogen pressure had to be excessively increased until a satisfactory purge was attained. When used under conditions of the model engine flame measurement the spectrometer was aspirated (Bernoulli effect). This caused an introduction of atmosphere into the optical path of the spectrometer. This so attentuated the signal in the emission region that the Beckman was not considered adequate without further modification.

Perkin-Elmer 112 Spectrometer. The Perkin-Elmer 112 Spectrometer is a single beam, double-pass instrument equipped with a thermocouple detector. The double-pass feature of the Model 99 monochromator reduces the scattered radiation to less than 0.1 percent and improves overall resolution. A calcium fluoride (CaF_2) prism was installed in order to obtain the highest possible resolution in the area of interest. The standard model 107 pre-amp and amplifier system was used and the scan speed was modified to scan one through five microns in 100 seconds at a recorder speed of 0.165 in. per sec. Engine flame spectra were recorded simultaneously on the Leeds-Northrup chart recorder located next to the monochromator, and on an oscillograph (Datarite) in the blockhouse. A second pen was installed on the L-N recorder to indicate drum numbers at the top of the chart, and the normal drum-number signal was applied to a Datarite channel in the blockhouse so that Datarite spectra contained an accurate wavelength scale. The monochromator and exterior optical system were purged with dry nitrogen. The operation of the spectral recording system was remotely controlled from the blockhouse. Four separate optical systems, shown in Fig. 2-4, A, B, C, and D, were used with the Perkin-Elmer 112 spectrometer. System A was used to demonstrate feasibility of the 112; System B was used on the UDMH and Hydrazine series; and Systems C and D were used in the RP-1/LOX series. Systems B, C, and D were designed to image the observed portion of the flame on the monochromator slit. The off-axis parabolloid collecting mirror used in systems B, C, and D has a diameter of 6.5 in. and a focal length of 25 in.

Michelson (Block) Interferometers I-4E and I-4T. The rapid-scan features of the Michelson (Block) Interferometer Spectrometer made it an attractive system to evaluate for use in the model engine flame studies. Preliminary spectra of the propane

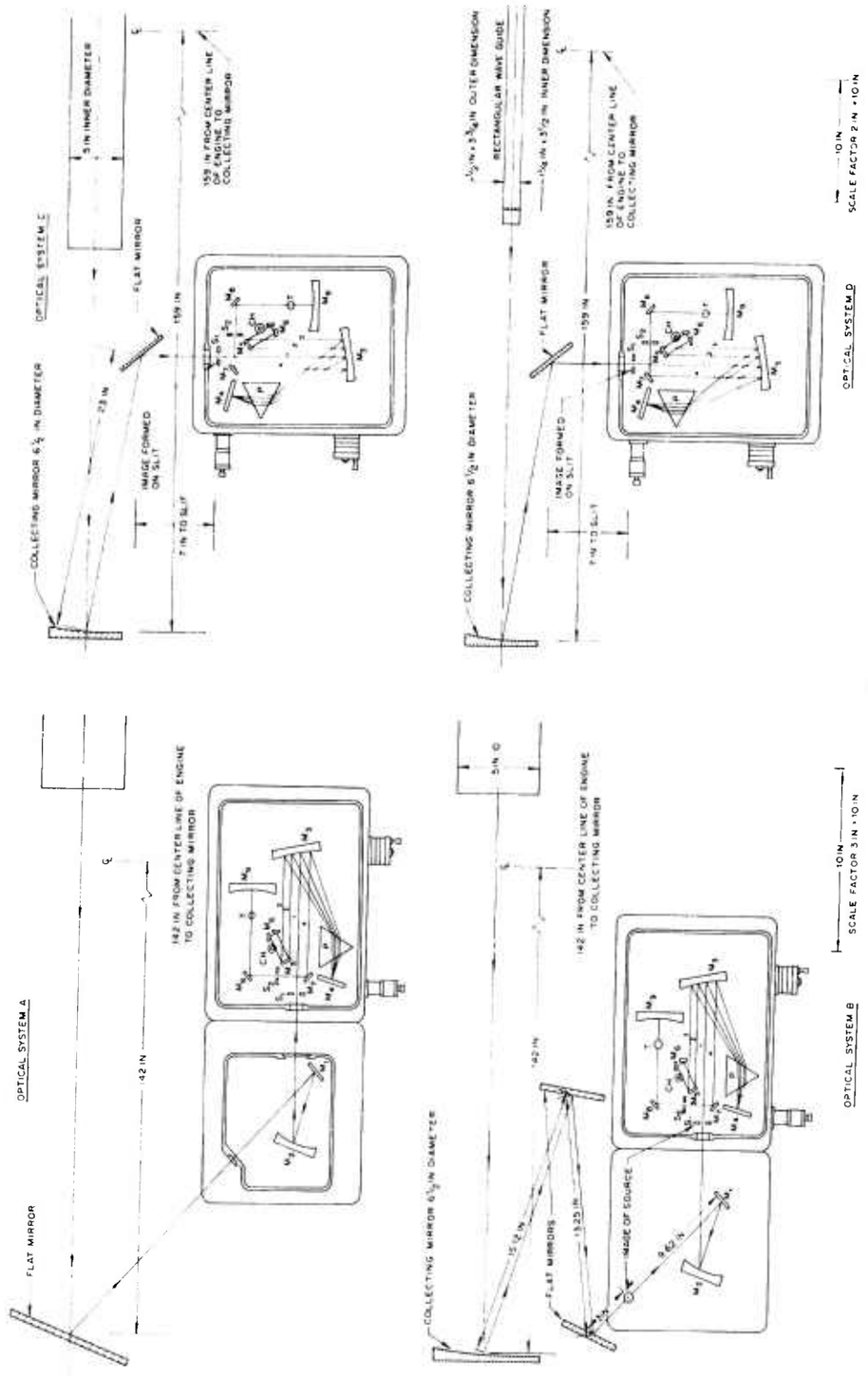

Fig. 2-4 Optical Configurations Used in Model Engine Flame Spectral Studies

torch, other small flames, and the usual greybody and blackbody sources recorded under laboratory conditions compared favorably with spectra obtained with a prism-type spectrometer. An absorption spectrum of polystyrene with a blackbody source, for example, was similar to the standard spectrum found in the NBS publication (Ref. 2). Subsequent spectral recording of the model engine flame was unsuccessful due to microphonics from the excessive engine vibration and the difficulties in reducing the complex data so obtained.

Appendix C of this volume is devoted to a theoretical discussion of calibration of the Michelson (Block) interferometer spectrometer.

2.2 CALIBRATION PROCEDURES

Calibration of the spectrometers is recognized to be the most important feature of a measurement program and consists of two calibration procedures, namely, wavelength and absolute radiance. The calibration procedures described in the Nicodemus-Zissis publication (Ref. 3) are followed whenever applicable. The two types of systems, radiometric and spectrometric have so many basic features in common that the same calibration techniques apply to either system.

Because the relationship between absolute radiance values and relative intensity values are classified, this information is presented in Volume IV, the only classified volume in this report. Consequently, Volume IV contains replotted spectra and absolute radiation calibration overlays.

2.2.1 Perkin-Elmer Spectrometer

The wavelength calibration is shown in Fig. 2-5, in which two separate curves appear. The second calibration was necessary because, after the UDMH and Hydrazine series, a second pen was installed on the recorder to record the drum number markings on the top of the chart during a spectral measurement. The new pen was displaced three drum numbers from the original pen marking. This displacement is illustrated by the dotted

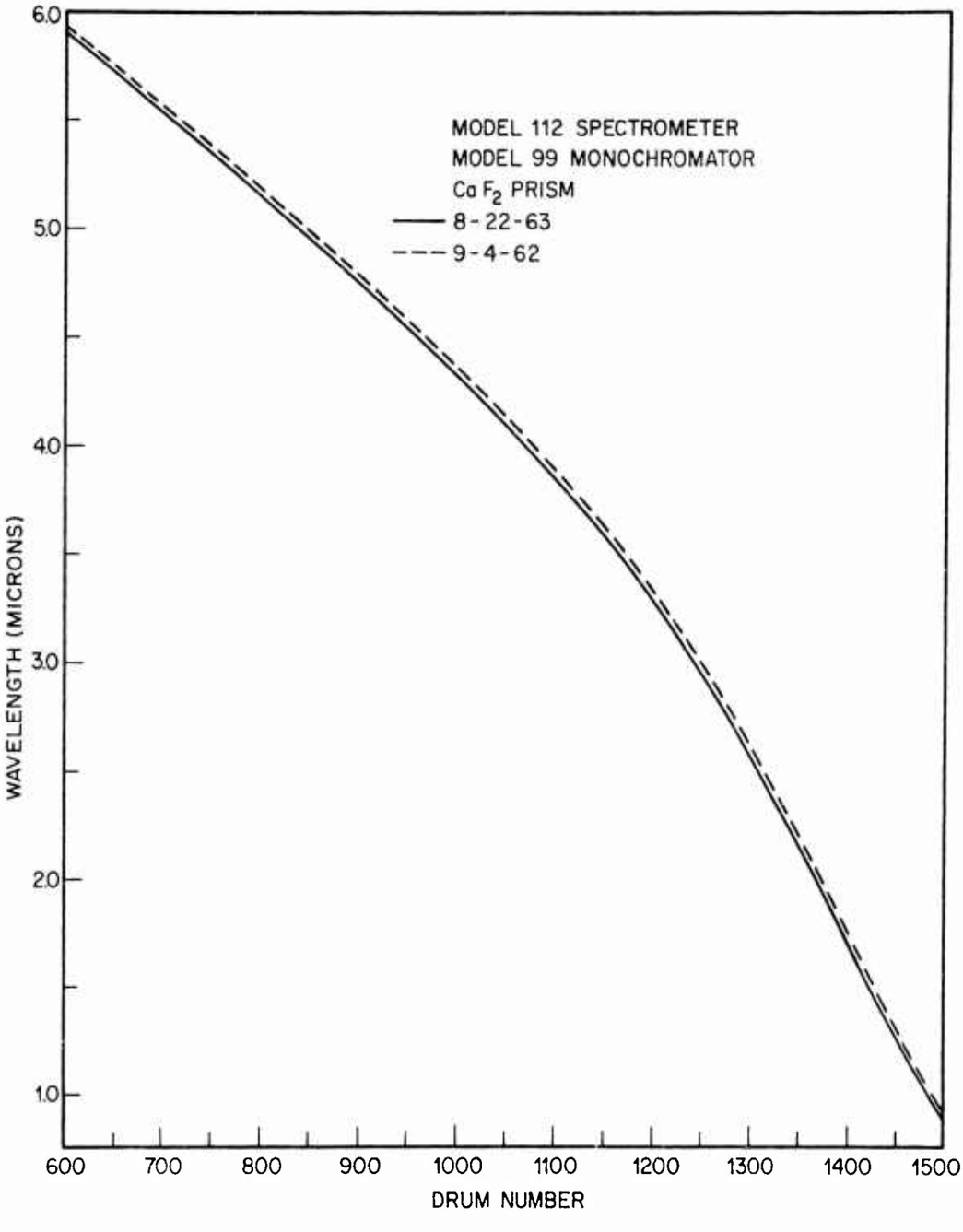

Fig. 2-5 Wavelength Calibration Curve

line in Fig. 2-5. The absorption bands used in the wavelength calibration were the atmospheric constituents, H_2O at 6.3, 2.62, 2.58 and 1.90 microns; CO_2 at 4.26, 2.76 and 2.68 microns; the C-H stretching bands of polysyrene at 3.30 and 3.51 microns; and the series of Mercury lines in the UV, visible, and the near IR. Figures 2-6 and 2-7 are charts showing the spectra of common absorbing constituents encountered in this study. The spectra are replotted from curves in E.K. Plyler's article (Ref. 2), the Ritland report (Ref. 4), and the work of Pierson, Fletcher, and Gantz (Ref. 5). Wavelength calibrations were performed in conjunctions with each set of measurements.

The absolute radiance measurements were made with the source placed at the center line of the engine and imaged on the spectrometer slit. The optical system was designed to reduce a 5-in. source to an image whose height and width more than covered the slit and made possible spectral measurements using low slit widths, thereby increasing spectral resolution. The data for the wavelength calibration curve were obtained with the optical path completely purged with dry nitrogen except in the case of spectra of atmospheric H_2O and CO_2. Inasmuch as the high-speed purge flowed through the monochromator and out of the environmental chamber to the source,the source was cooled slightly. Therefore, spectral calibration measurements were carried out after the calibration source had dropped to a constant temperature. The removal (purge) of atmospheric constituents between spectral measurements was monitored by setting the spectrometer on a known atmospheric absorption band and running the recorder until there was no further response from the pen. The speed of removal of atmospheric constituents is illustrated by the spectra in Fig. 2-1. The purge procedure was carried out between spectral measurements, and the spectrum that shows a negligible amount of atmospheric attenuation is representative of the optical path prior to a spectral measurement. Radiance data were obtained by recording a series of emission spectra of sources of known temperature and emissivity under purged conditions at the various settings of slit width used in the flame measurement. The recorder sensitivity was maintained at a standard setting for calibration, but some drift was noted during the firings. The effect of this drift is discussed in Volume IV. The L-N chart was cali brated in terms of radiance units within the range of slit widths used in the actual flame measurements. A series of curves was drawn relating spectral radiance, pen deflection, wavelength and slit width. Values of model engine flame radiance were calculated by comparing the flame spectrum to the corresponding calibration curve. Calculations and calibration curves appear in Volume IV.

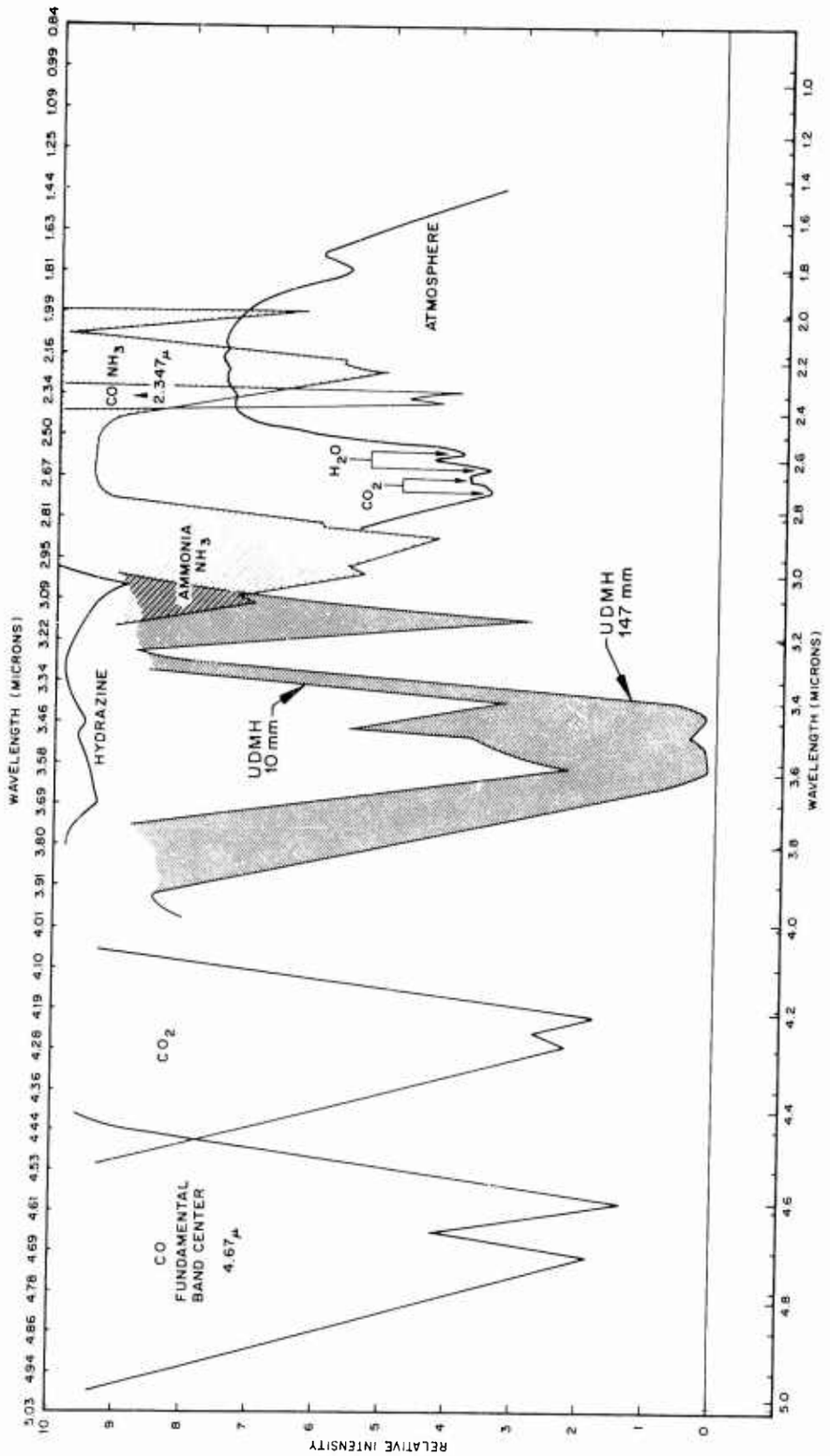

Fig. 2-6 Absorption Spectra for Common Exhaust Species at 300°K (for Wavelength Reference Only). Scale Value = 100% Transmission

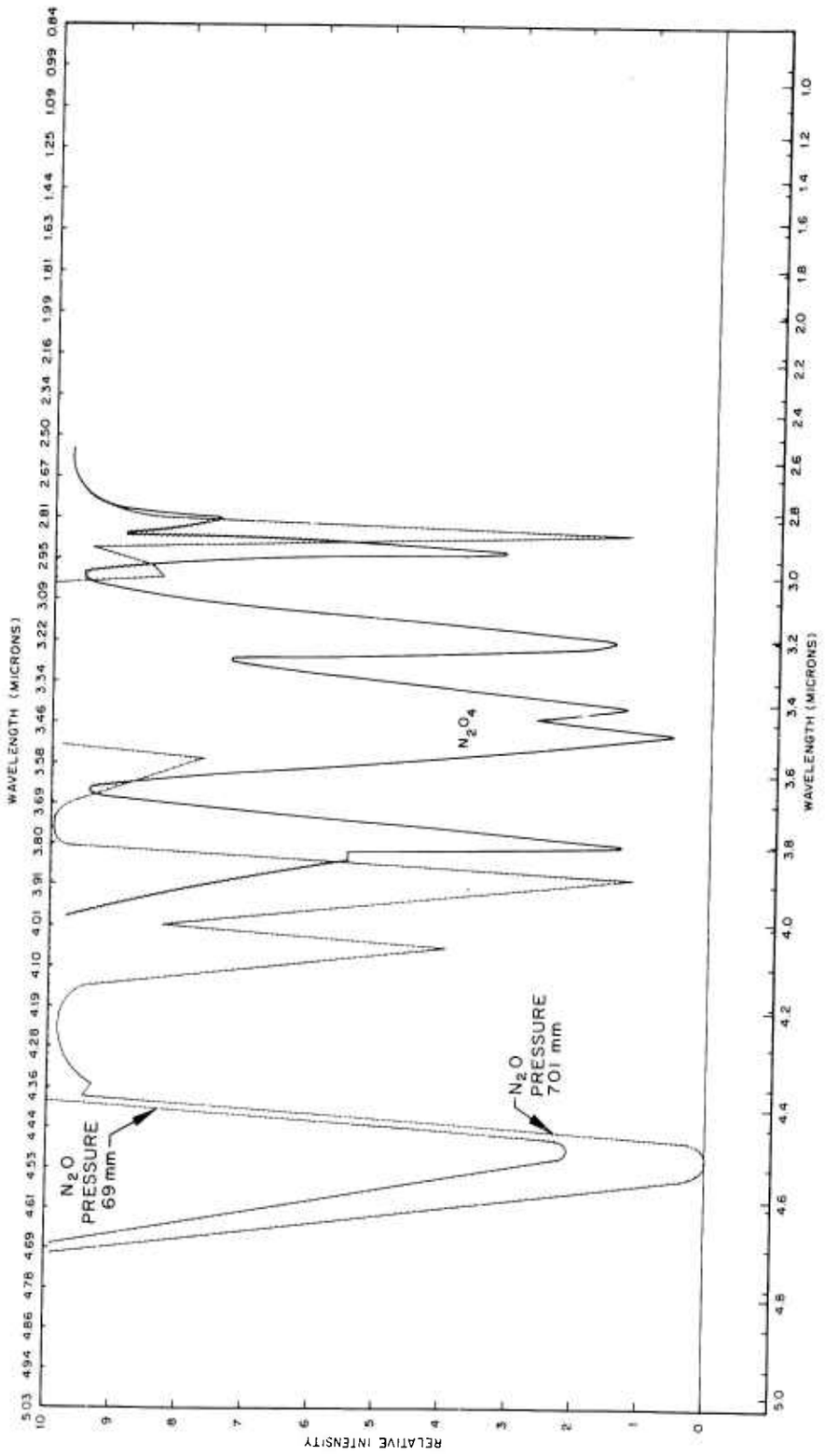

Fig. 2-7 Absorption Spectra for Nitrogen Oxides at 300°K (for Wavelength Reference Only)
Scale Valve 10 = 100 Percent Transmission

Four separate overlays for conversion of relative spectra into absolute values are included in Vol. IV. They are a plot of N_λ from 1 to 5 microns and they allow the direct conversion of any point on the curve to spectral radiance. The calibration source used in the RP-1/LOX portion of the study was a Globar rod of silicon carbide. The dimensions of the rod were 5/16 in. in diameter by 13 in. overall length with 6 in. of radiating surface in the center. A photograph of the drum B purge ring B configuration with the Globar rod calibration source in position for calibration is shown on Page A-17 of Vol. II.

The temperature of the Globar rod was determined with a Leeds-Northrup optical pyrometer that had been calibrated against a National Bureau of Standards tungsten lamp. The temperature read from the dial of the instrument is shown plotted against the current of the Globar in Fig. 2-8. The calibration of the pyrometer against the NBS tungsten lamp shows that the dial reading, or indicated temperature T_i is normally 25° C too high, so that, in converting to brightness temperature T_B and true temperature T_T the following relations hold.

$$T_B = T_i - 25^\circ C$$

$$T_T = \frac{1}{T_B} - \frac{\lambda}{C_2} \ell n \frac{1}{\epsilon(\lambda,T)}$$

where

$$\epsilon(\lambda,T) = 0.73$$

$$\lambda = 0.665\mu$$

$$T_T = 1248^\circ K$$

$$T_i = 1250^\circ K$$

The true temperature T_T is 1248°K as compared to a T_i of 1250° K. As this small difference is found to be within the experimental error, T_i is considered to be equal to T_T for this temperature range.

The emissivity of silicon carbide is found in Refs. 6, 7, and 8 to be quite uniform at 1250°K, and a mean curve was plotted in Fig. 2-8. The 2-5 micron region agreement was good between Silverman, Brugel, and the NBS data. In the 1-2 micron region the

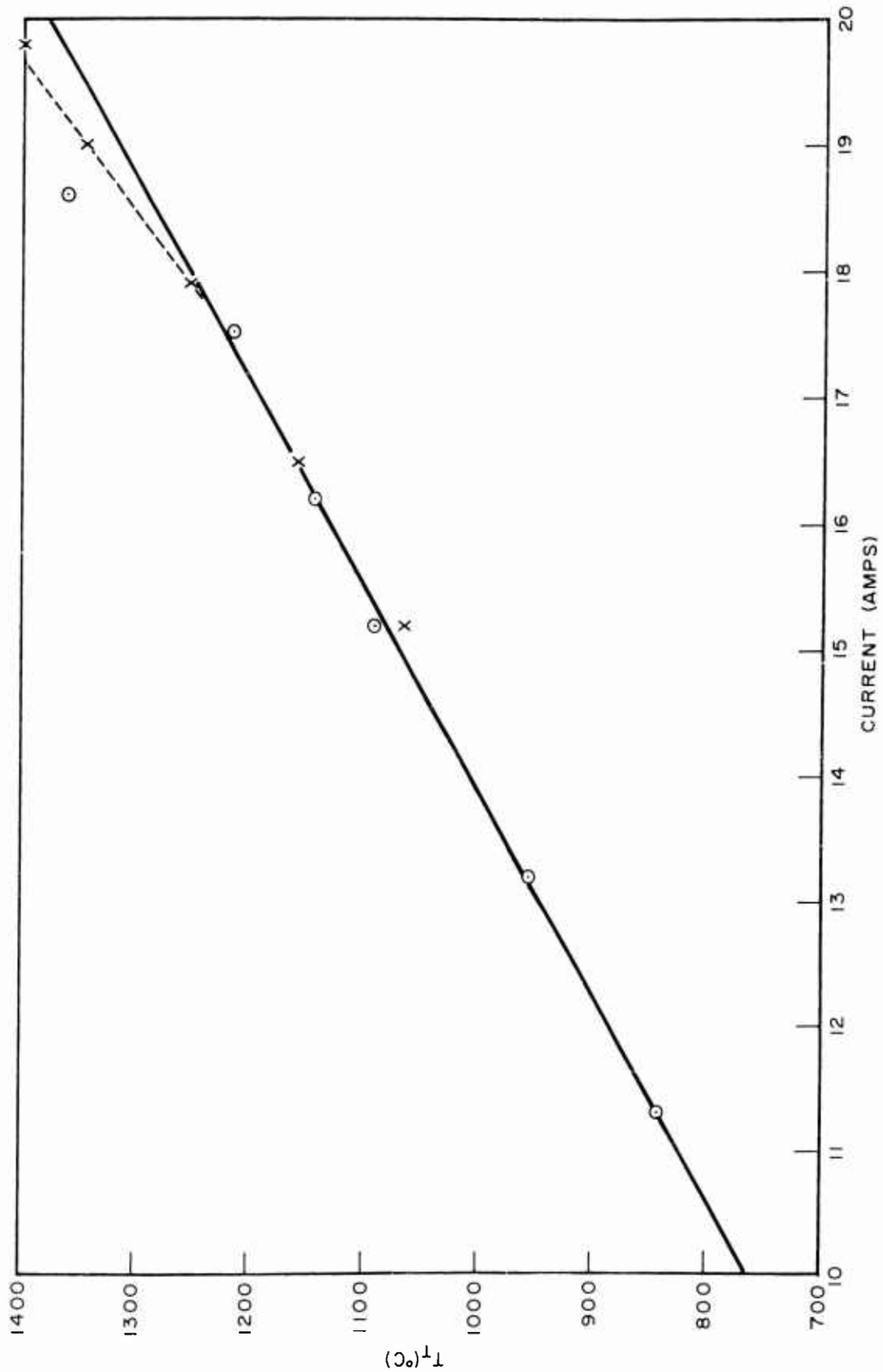

Fig. 2-8 Calibration of Globar Rod With Optical Pyrometer. Leeds-Northrup Optical Pyrometer Calibrated Against NBS Tungsten Lamp

NBS data were 10 percent lower than the other two. Therefore, emissivity curve, Fig. 2-9, reflects all results except the 1-2 micron NBS data.

In addition to the globar, a 1000°C blackbody with a 0.2564-in. aperture was used. The image of the source falling on the slit was too small, so it was decided to use the blackbody to obtain the shape factor of the calibration curve and the globar extended source for intensity. This procedure was necessary in order to eliminate a small error (10%) in the longer wavelength region when the two calibration curves are compared. The difference is possibly attributed to the use of literature values of emissivity as compared to an accurate measurement conducted on the actual globar source used.

Table 2-2 contains a schedule of spectral resolution for the present Perkin-Elmer system. For the range of slits used, the resolution was 0.003 to 0.015 microns.

Table 2-2

SPECTRAL RESOLUTION

Wavelength (μ)	Spectral Resolution ($\Delta\mu$)					
Slit Width (mm) →	0.05	0.1	0.2	0.3	0.4	0.5
1.0	0.0057	0.0107	0.0207	0.0307	0.0407	0.0507
1.5	0.0061	0.0111	0.0211	0.0311	0.0411	0.0511
2.0	0.0062	0.0109	0.0204	0.0299	0.0394	0.0489
2.5	0.0059	0.0102	0.0188	0.0274	0.0360	0.0446
3.0	0.0053	0.0090	0.0174	0.0230	0.0330	0.0403
3.5	0.0048	0.0080	0.0144	0.0280	0.0272	0.0336
4.0	0.0043	0.0071	0.0127	0.0183	0.0239	0.0295
4.5	0.0038	0.0062	0.0110	0.0158	0.0206	0.0254
5.0	0.0035	0.0057	0.0101	0.0145	0.0189	0.0233

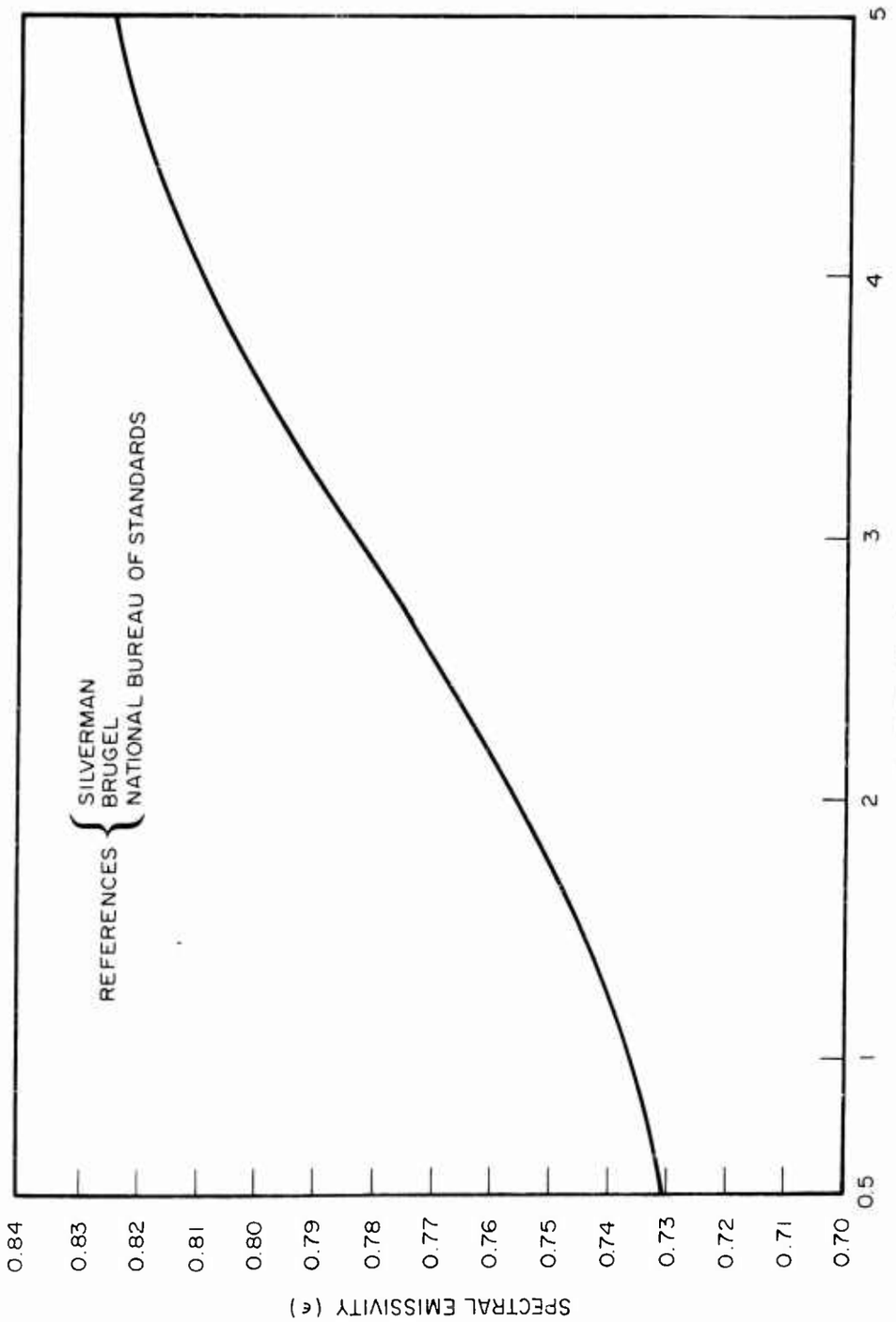

Fig. 2-9 Globar Emissivity

2.2.2 Michelson (Block) Interferometer Spectrometer

The Michelson (Block) Interferometer Spectrometer Models I-4T and I-4E were both found to have a nonlinear response when observing a blackbody source. The peaks were not in the proper location for the temperature of the source, and other nonlinearities were apparent. The response of the I-4E is shown in Fig. 2-10. In order to use the instrument with any degree of certainty that meaningful results would be obtained, a theoretical study of calibration procedures was initiated by R. G. Clow, and the results of that study are presented in Appendix C of this volume.

The practical calibration of the instrument is possible, despite nonlinearities, so long as the blackbody spectra of the nitrogen-purged systems are reproducible from day to day. The difficulties are mainly involved with the microphonics, or susceptibility of the optical system to vibrations. The usual method of processing the interferometer data is to employ a standard wave analyzer to extract the frequencies of interest from the raw data which are a series of interference fringes, or interferograms. Each interferogram can be reduced, theoretically, to a complete spectrum of the source. In practice, however, this is extremely difficult to do since an interferogram occurs every tenth of a second on the tape; therefore, one or more loops are made out of the taped data and are subjected to a wave analysis. This yields an average spectrum of a loop of data. Variations in flame intensity are reflected in the intensity of the individual interferograms, and the final spectrum may vary from analysis to analysis, depending upon where the analysis started on the loop. The quantitative reproducibility in this method of data reduction is open to question. An example of the data obtained under laboratory conditions is shown in Fig. 2-10. Some of the results are discussed in Section 3.5

2.2.3 Silicon Photovoltaic Light Sensor

The Silicon (diffused junction) photovoltaic light sensors (LS 222) are mounted on a terminal board with central portion cut out (so that the radiant energy coming from the flame can image on the slit of the spectrometer). A drawing of the actual position of

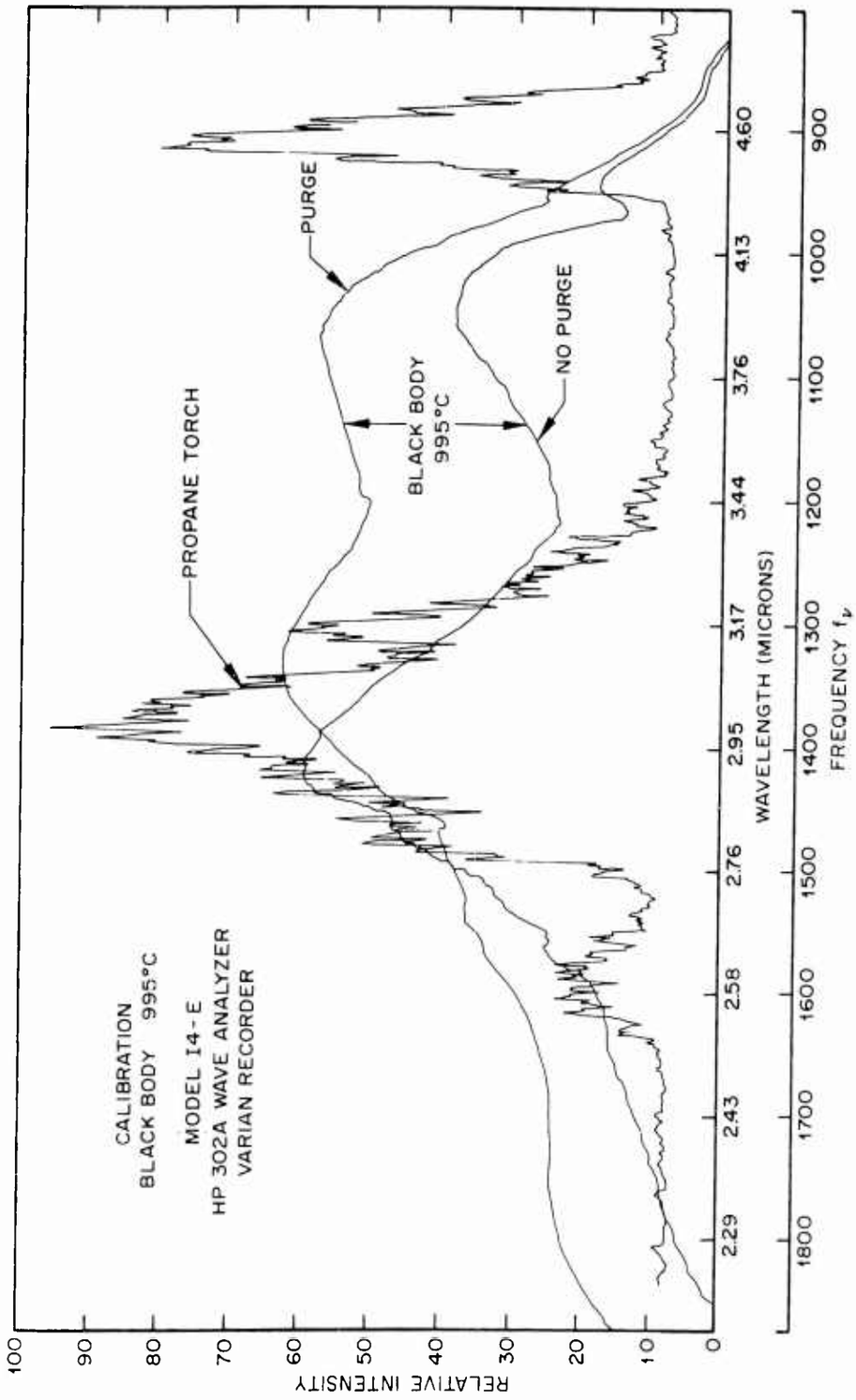

Fig. 2-10 Michelson (Block) Interferometer Spectrometer Calibration

each sensor, and the geometry of the slit are shown in Fig. 2-11. The board is then slipped into position in the slot for holding samples at the entrance slit. A photograph of optical system D shows the terminal board in place. (See Fig. A-21, Vol. II.)

A spectral measurement of a globar source with and without the sensors in place showed that the positioning of the sensors did not affect the validity of the P-E 112 plume spectral measurements.

The output of each sensor during a spectral measurement was recorded directly on the Datarite recorder. A typical trace of the sensors' response to a model engine flame is shown in Fig. 2-12, along with the Datarite representation of the flame spectrum and drum numbers. Each sensor was calibrated with the use of the globar as a temperature source. The procedure was to image the globar on each sensor in succession, and then to optimize and calibrate the Datarite in temperature units. This calibration procedure was performed at three or more globar temperatures which were determined by an optical pyrometer.

The amount of deflection for each temperature indicates an apparent temperature which is lower than true temperature because of the unknown gas and carbon particle emissivity at 0.8 microns, which is the spectral peak of the sensor. The data derived from the procedure described above was useful for monitoring radiation in addition to temperature analysis and is discussed in Section 3.5.

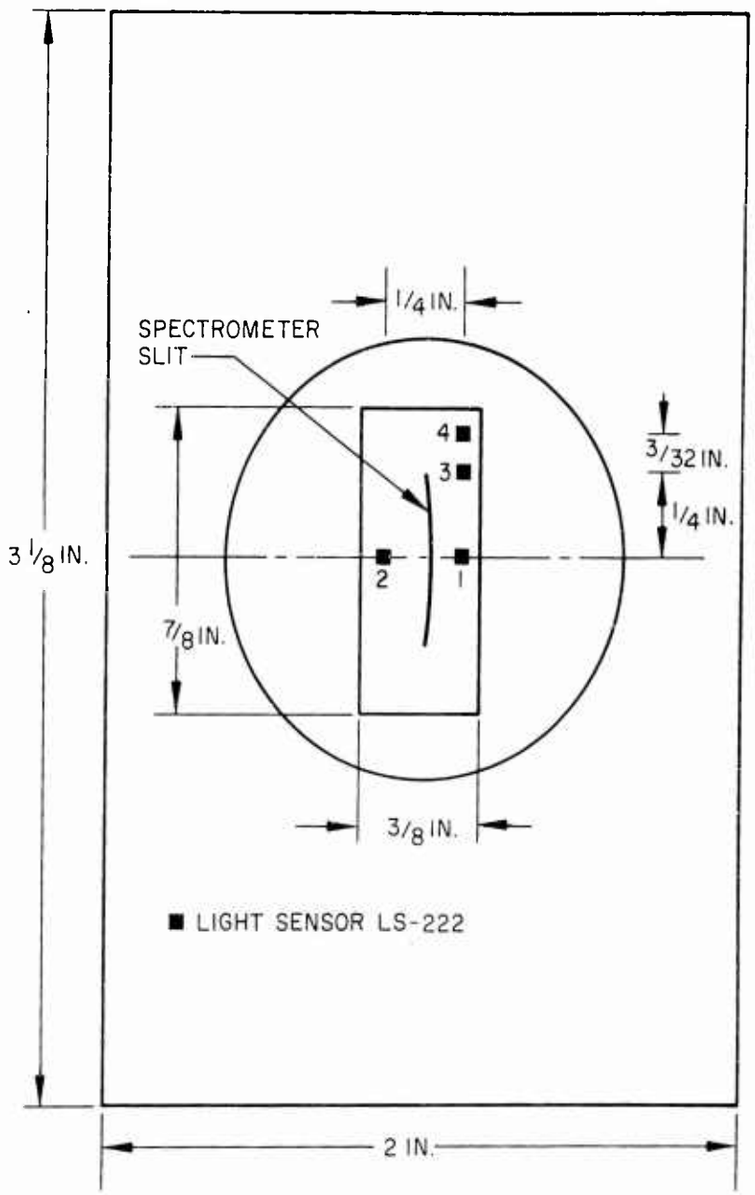

Fig. 2-11 Light Sensor Geometry With Reference to Spectrometer Slit and Flame Image

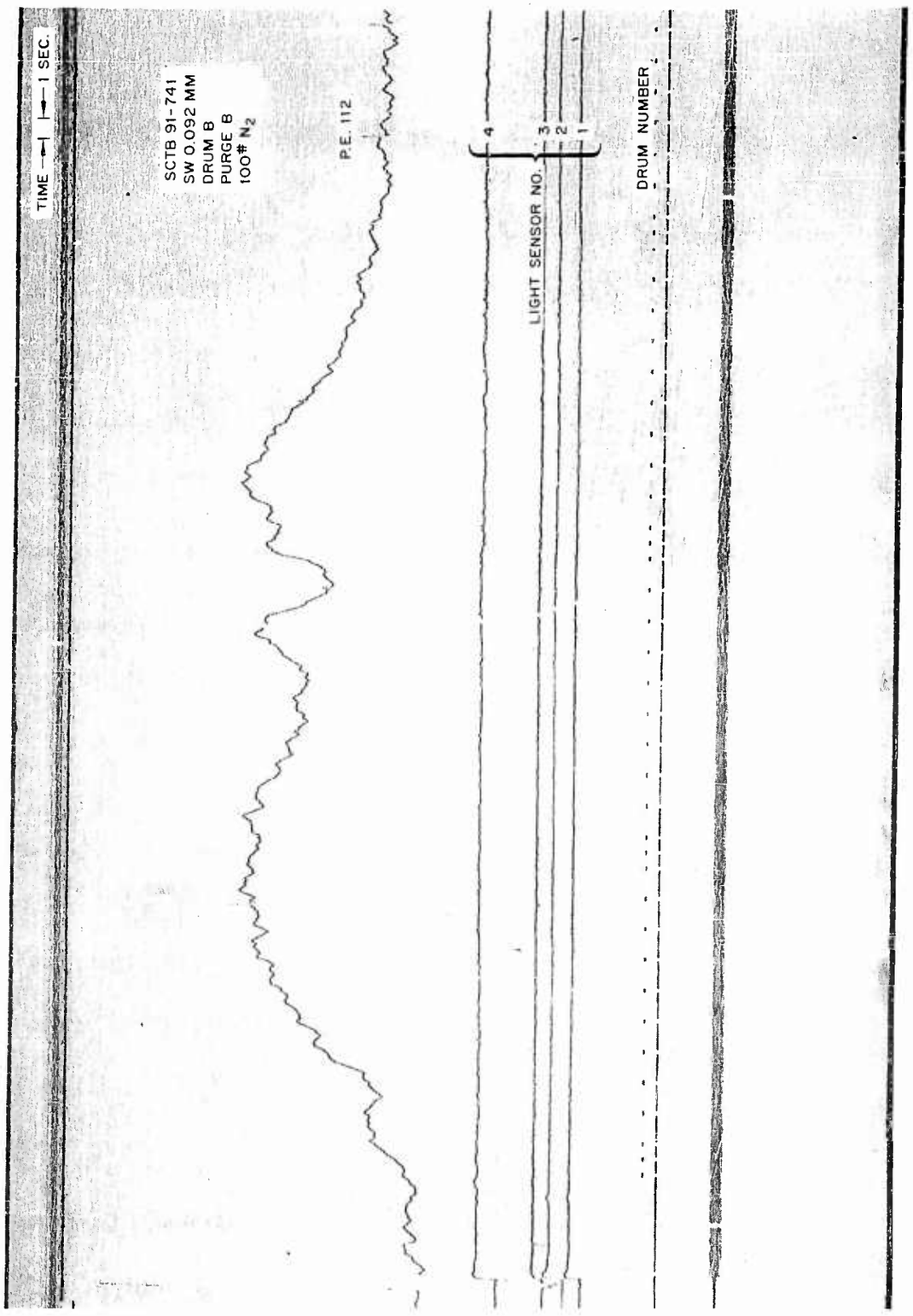

Fig. 2-12 Datarite Recorder Trace of Light Sensor and P. E.-112 Response

Section 3
INFRARED SPECTRAL DATA (ONE-TO-FIVE-MICRON REGION)

The total number of successful firings in which acceptable infrared spectral data were obtained is ninety. Twenty three for the UDMH-N_2O_4 series, twenty six for the N_2H_4 - N_2O_4 series, and forty-one for RP-1/LOX. All of the raw data spectra are included as Appendixes A and B.

In addition to having all of the relative spectra available, calibration overlays for conversion of relative to absolute values are presented in Volume IV.

The basic objective of the program was to obtain emission spectra with the least amount of absorption in the emission bands,and to eliminate afterburning with atmospheric oxygen which was suspected of changing the spectral distribution and temperature of the source. The study can be separated into four separate phases, namely, (1) composite spectra, or the best statistical averages possible, (2) nitrogen purge-rate studies in which the effects of flame cooling can be assessed, (3) mixing-ratio studies, and (4) slit-variation studies. The results of these study phases are shown in the following series of comparative spectra with each group compared at the same slit width. These comparative spectra have been traced from the original raw data curves.

3.1 COMPOSITE SPECTRA AND PURGE RATE STUDIES

The composite spectra and purge rate studies are not separable because they are truly composites in the nonabsorbing regions. However, in the absorption bands there is some deviation in relative intensity caused by purge cooling. This cooling results in self-absorption of the flame, a phenomenon discussed in Section 3.7.

3.1.1 RP-1/LOX

The RP-1/LOX series was the first selected for discussion because two positions in the flame were viewed. In one case the first Mach disc six inches from the exit plane and one inch aft of the exit plane were observed; in the other case, observation was made one inch aft of the exit plane only.

The exit plane spectra are presented in Fig. 3-1. This study shows the precision of the measurements as defined by Nicodemus and Zissis (Ref. 3). The features of the spectra that are immediately apparent are the continuum and the superimposed emission bands for H_2O, CO_2, and CO. The small quantity of absorption present is shown by the CO_2 bands at 4.23μ, 4.28μ, 2.76μ and 2.68μ. Water absorption is apparent at 2.58μ.

Purge rate studies carried out at the beginning of each series show the effect of flame cooling on radiance (Fig. 3-2). The effect is most pronounced in the absorption bands when viewing the first Mach disc. Little or no effect is shown for the nozzle exit spectra.

The spectra from the first Mach disc are shown in Figs. 3-3 through 3-6. All the runs are with the drum A configuration as described in Table 2-1. Figures 3-3 and 3-5 are for the purge ring A; 3-4 and 3-6 are for purge ring B. The major difference in the design of the purge rings is that nitrogen flow in B is directed toward the plume axis while in A the flow is parallel to the axis. This difference results in severe cooling as is shown by the comparison of Figs. 3-3 and 3-5 with 3-4 and 3-6. The cooling effect with increased purge is shown in all four illustrations with a critical purge rate indicated in the radiance values and corroborated by the enclosed shadowgraphs (Fig. 3-7) of the flow only from purge ring A. The top edge of each shadowgraph marks the centerline of the purge axis. The ordinate (left) marks the location of the nozzle exit plane. (See page 3-9.) Table 3-1 is a description of the pertinent features in Fig. 3-7 and is shown on page 3-10.

The shadowgraphs were obtained by use of an intense light source, the purge nozzle, a plate with a pin-hole and a photographic plate placed in that order.

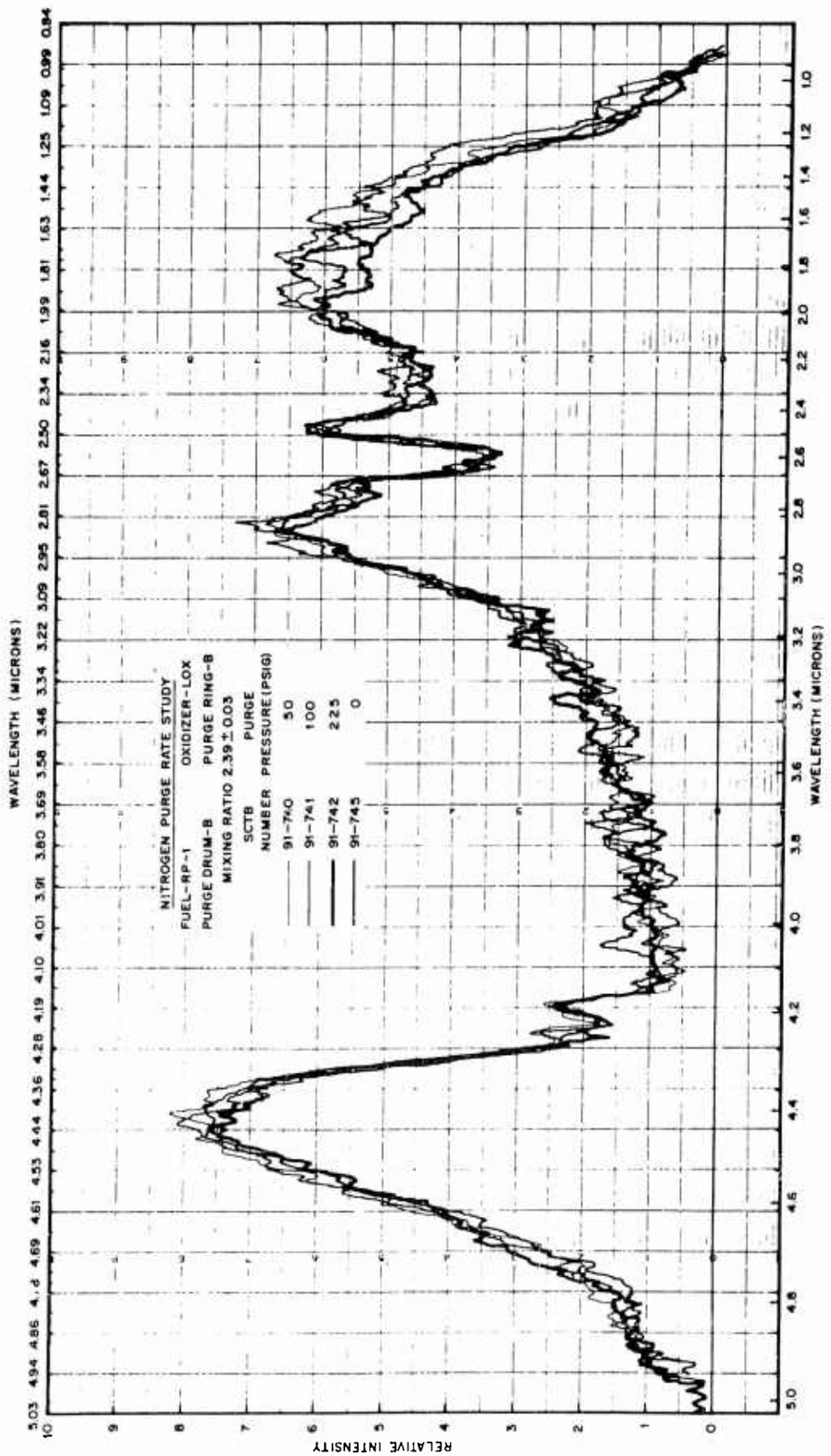

Fig. 3-1 Comparative Spectra: RP-1/LOX; No. 740, 741, 742, 745

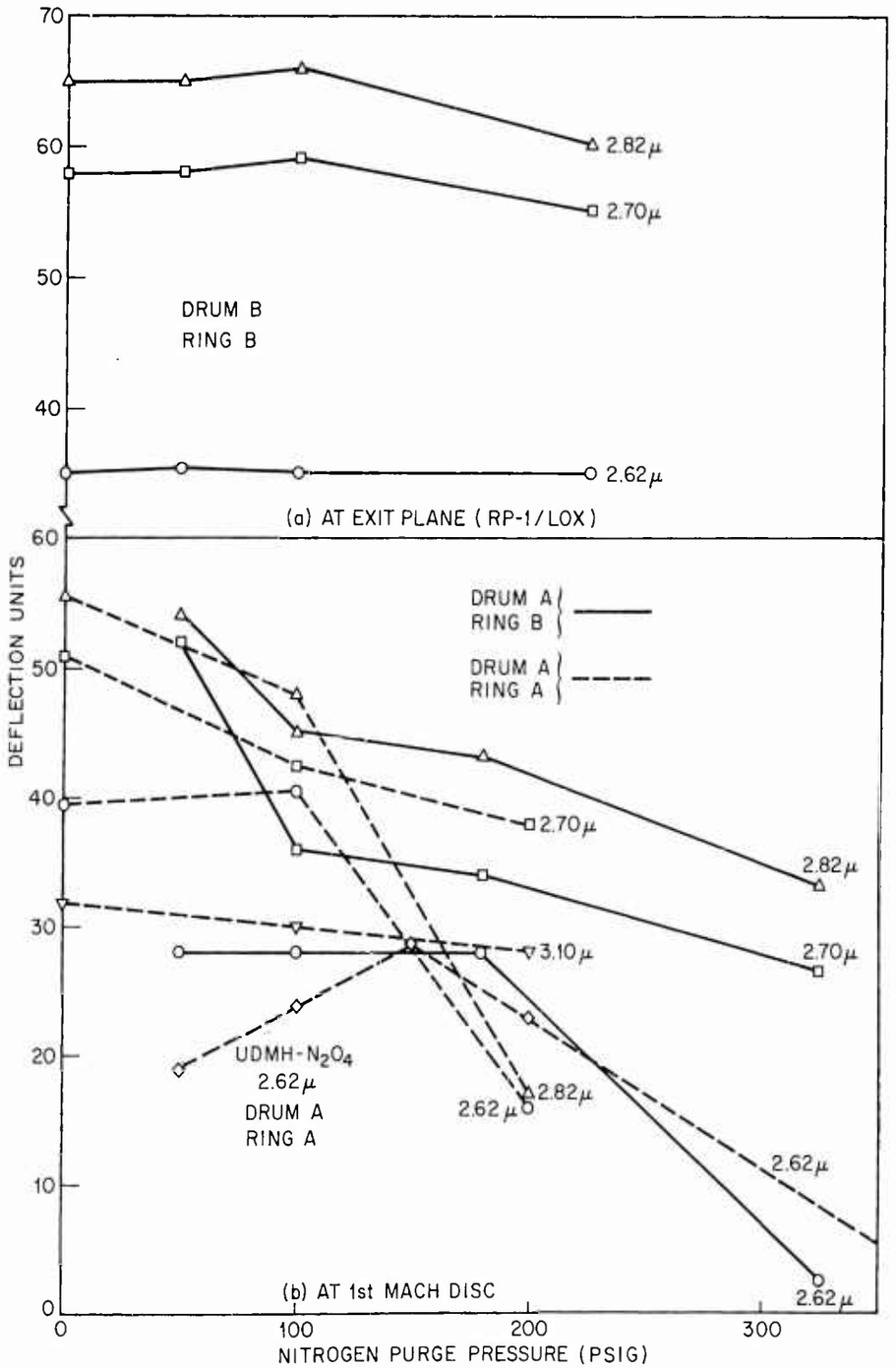

Fig. 3-2 Effect of Purge Rate on RP-1/LOX Flames

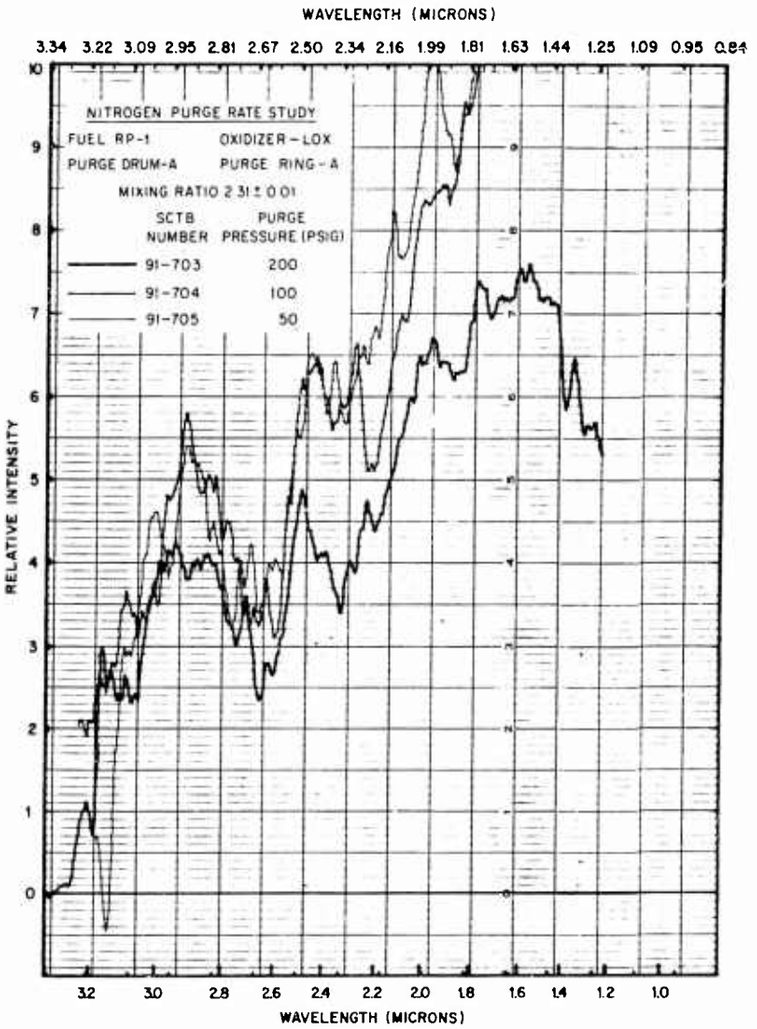

Fig. 3-3 Comparative Spectra: RP-1/LOX; No. 703, 704, 705

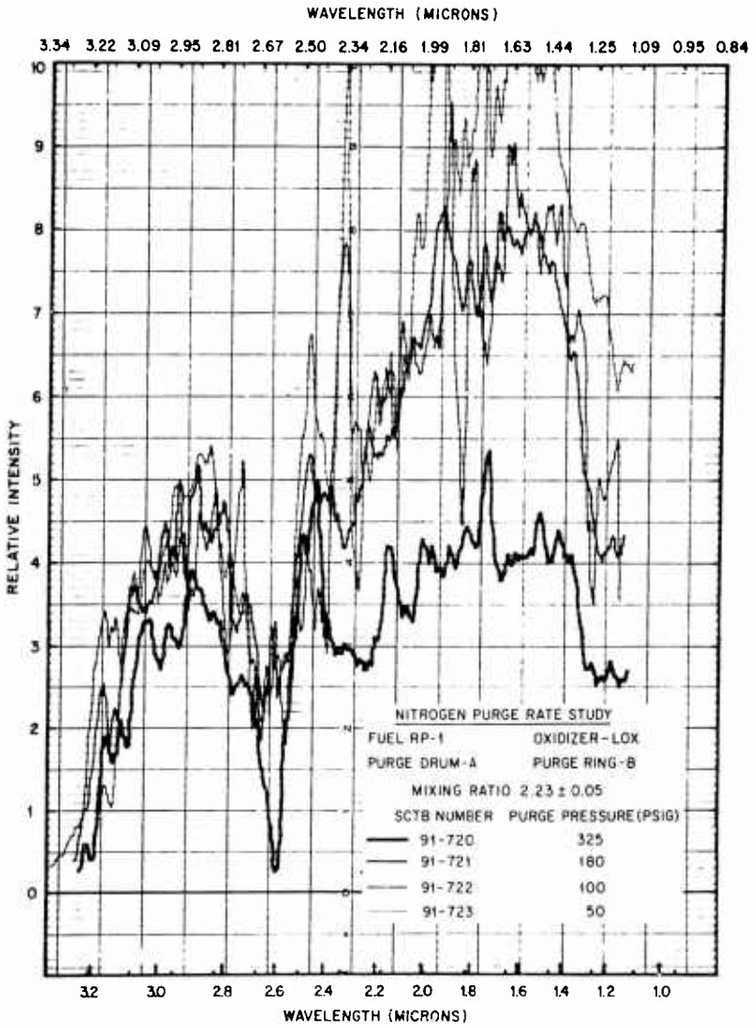

Fig. 3-4 Comparative Spectra: RP-1/LOX: No. 720, 721, 722, 723

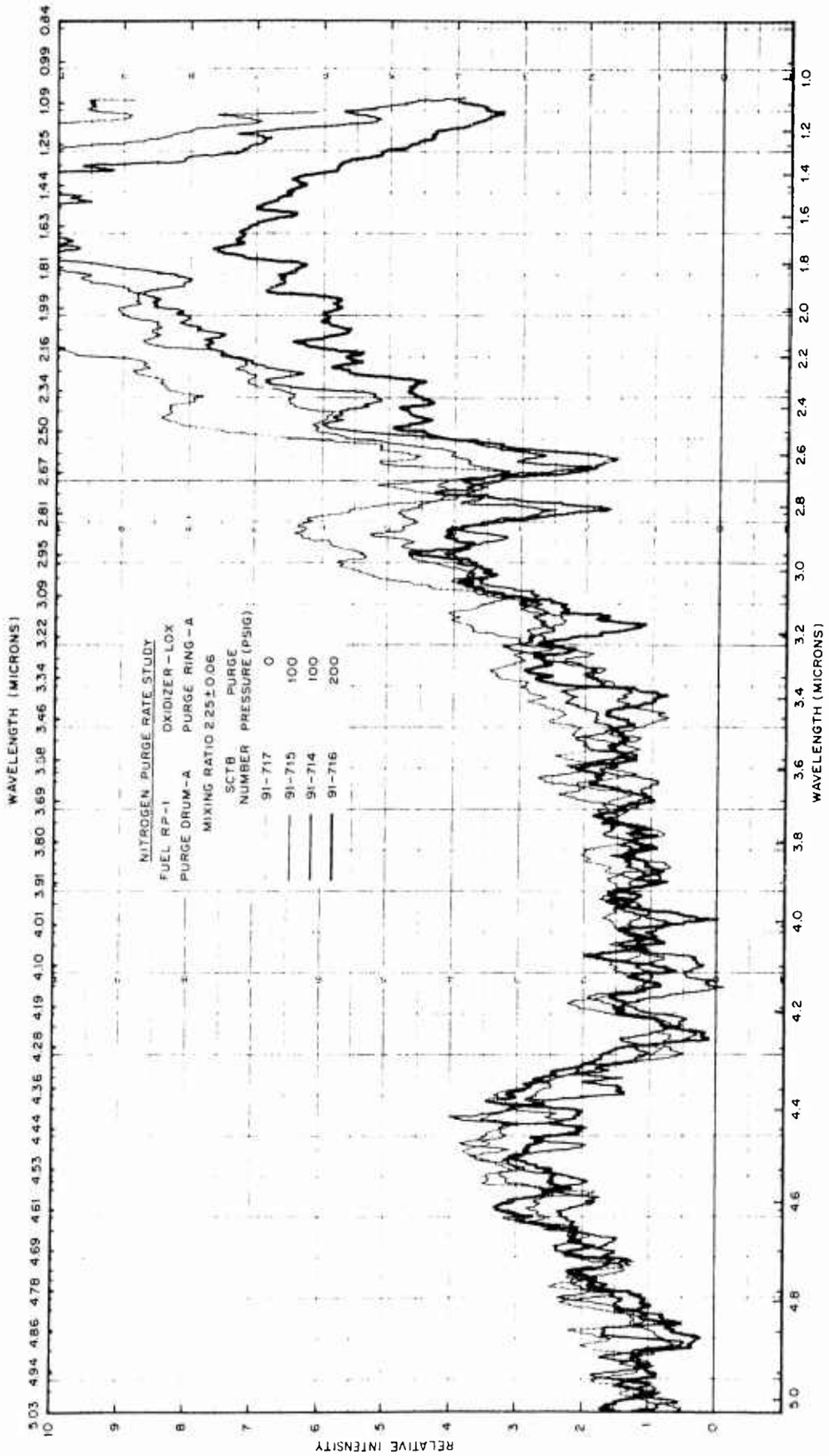

Fig. 3-5 Comparative Spectra: RP-1/LOX; No. 714, 715, 716, 717

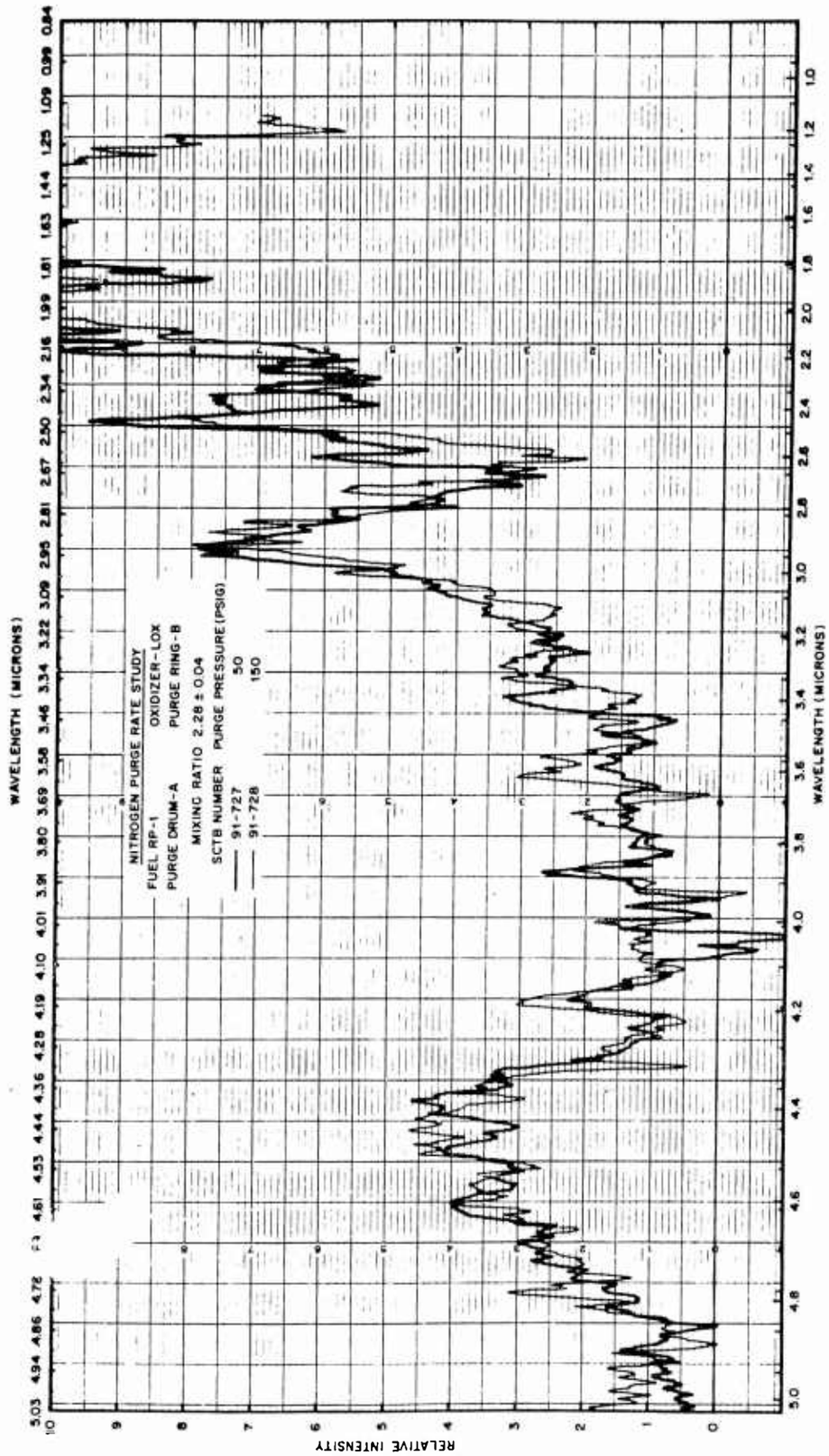

Fig. 3-6 Comparative Spectra: RP-1/LOX; No. 727, 728

(a) 100-lb N_2 Purge; 75° Angle of Flow

(b) 200-lb N_2 Purge; 80° Angle of Flow

(c) 225-lb N_2 Purge; 83° Angle of Flow

(d) 250-lb N_2 Purge; 70° Angle of Flow

Fig. 3-7 Shadographs of Purge Flow: Purge Drum B; Purge Ring B

Table 3-1

SHADOWGRAPH ANALYSIS OF FLOW FROM PURGE RING B
[(SHADOWGRAPH (FIG. 3-7), DATA (FIG. 3-4)]

Flow Rate (psig)	Angle of Direction* (deg)	Remarks
100	75	Thin stream
200	80	Turbulence indicated by increase in size of mach disc
225	83	More turbulence
250	70	Marked changes in shape
300	76	———

*90 deg. (parallel to plume axis)
0 deg. (normal to plume axis)

An additional piece of information that is indicated from the study of Figs. 3-4 and 3-6 are the sharp emission bands apparent at 2.34μ and 2.45μ. The 2.34μ band is attributed to CO emission while the 2.45μ band is not a real peak, but may be part of an attentuated H_2O band at 2.58μ.

A series of spectra viewing the first Mach disc were obtained with the purge drum A removed and a sintered-silica section of pipe placed on the end of the spectrometer viewing tube in order to bring the spectrometer purge gas into close proximity to the plume. Figure 3-8 is a picture of this set-up and flame. The data are shown in Fig. 3-9 and it indicates a minimum of absorption and the highest radiance of all of the spectra from the first Mach disc region of the plume. Figure 3-10 presents spectra for no drum but with purge ring B. A decrease in radiance is noted over the no purge situation indicating that cooling is observed without the drum.

(a) Perspective View

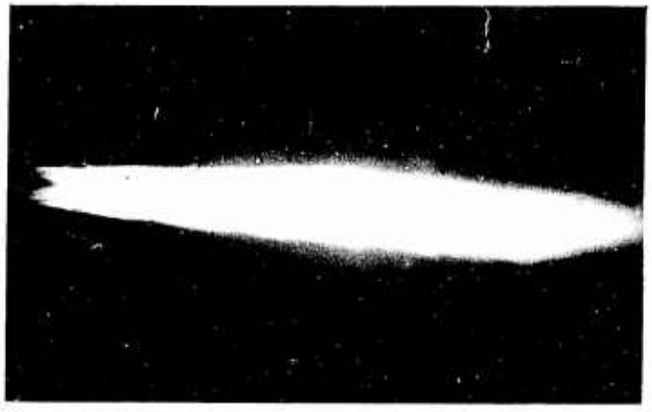

(b) Side View Ceramic Probe 5 in. Inside Dimension (normal exposure)

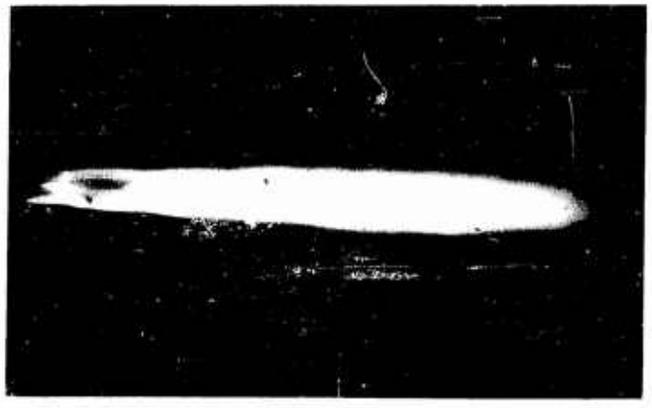

(c) Side View (under exposed)

Fig. 3-8 RP-1–LOX Plumes, Drum Removed

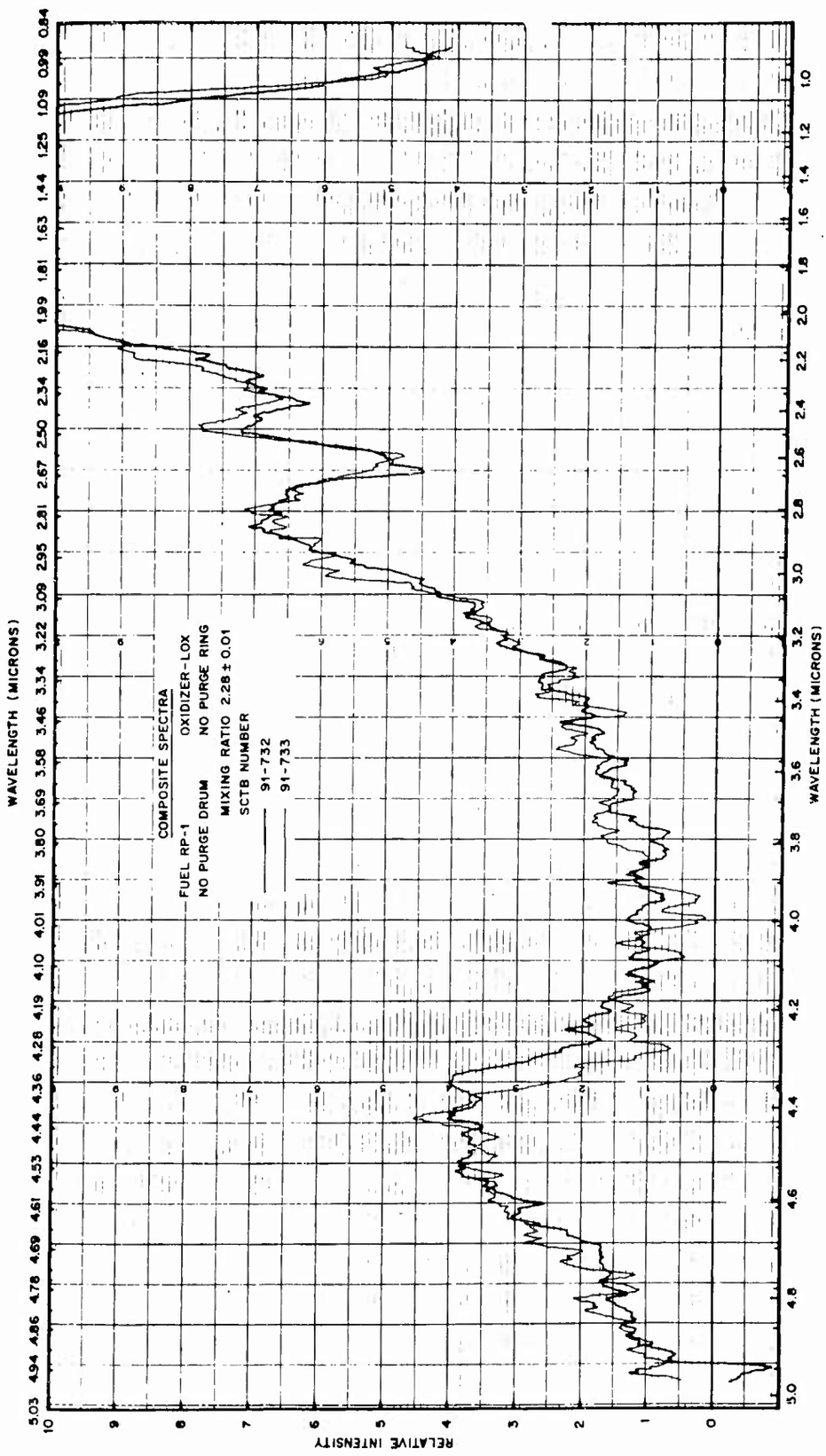

Fig. 3-9 Comparative Spectra: RP-1/LOX; No. 732, 733

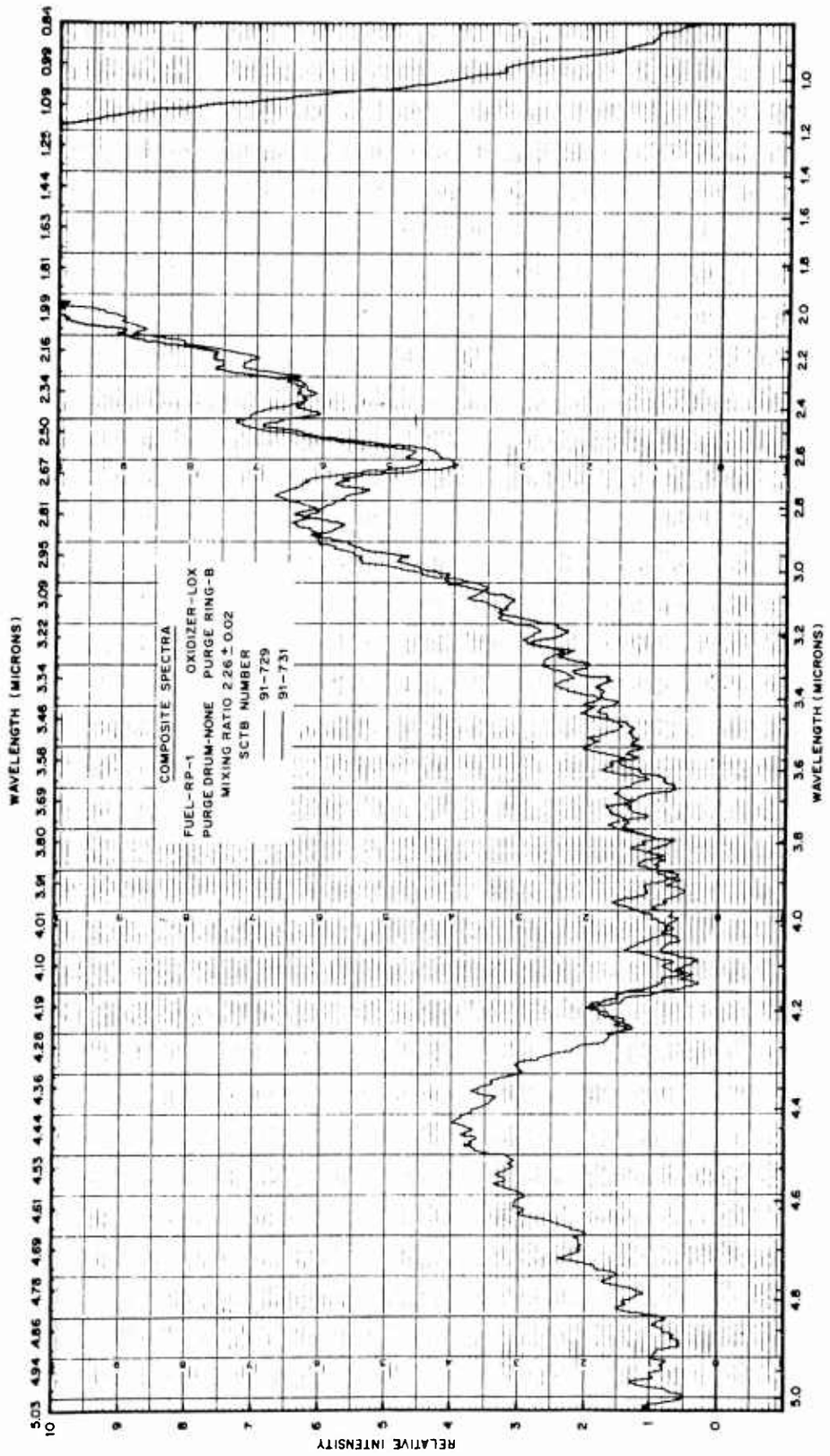

Fig. 3-10 Comparative Spectra: RP-1/LOX; No. 729, 731

3.1.2 Unsymetrical Dimethyl Hydrazine-Nitrogen Tetroxide (UDMH-N_2O_4)

The UDMH-N_2O_4 series was the first run, and drum A, with purge ring A was used. The spectrometer viewed the flame in the vicinity of the first Mach disc. Figure 3-11 indicates a series of composite spectra in which a purge-rate study was conducted. As in the case of the RP-1/LOX firings, consistency of the data is an indicator of the precision of the measurement. The only major deviation is the absorption bands at 2.58, 2.68, and 2.76 microns. A plot of the pen deflection against purge rate for the 2.58 micron region revealed that 150 psig nitrogen purge pressure was optimum (showed the least absorption) for the drum A, purge ring A experiments (Fig. 3-2).

Figure 3-12 is a similar composite study at 150 psig purge for the CO_2 region of the spectrum. The one major deviation from this composite occurred in run number 628, in which the chamber pressure was low. The elimination of this spectrum resulted in a set of curves with a small mean deviation. Some of the more important features of this spectral region are the increased resolution, the appearance of the CO emission at 4.67 microns, CO_2 at 4.8μ, and the absorption bands at 4.23 and 4.28 microns.

3.1.3 Hydrazine-Nitrogen Tetroxide (N_2H_4 - N_2O_4)

The N_2H_4 - N_2O_4 series of spectra are unique in that hydrazine is normally used as a 50-50 mixture with UDMH (Aerozine), and the spectra produced in our study are for pure N_2H_4. The composite spectra presented in Fig. 3-13, and the purge-rate study in Fig. 3-14 reveal a consistent set of data, but with strong fluctuations in the absorption bands.

A discussion of all of the intermediate species of oxidation or decomposition products for the N_2H_4 - N_2O_4 system are beyond the scope of this report. However, to identify

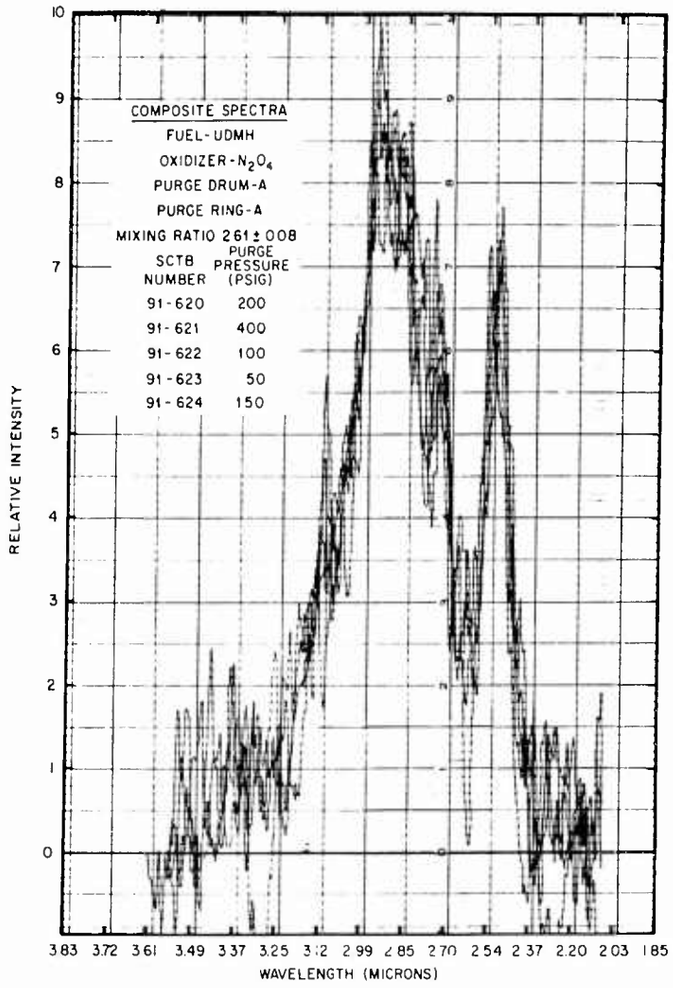

Fig. 3-11 Comparative Spectra: UDMH; No. 620, 631, 622, 623, 624

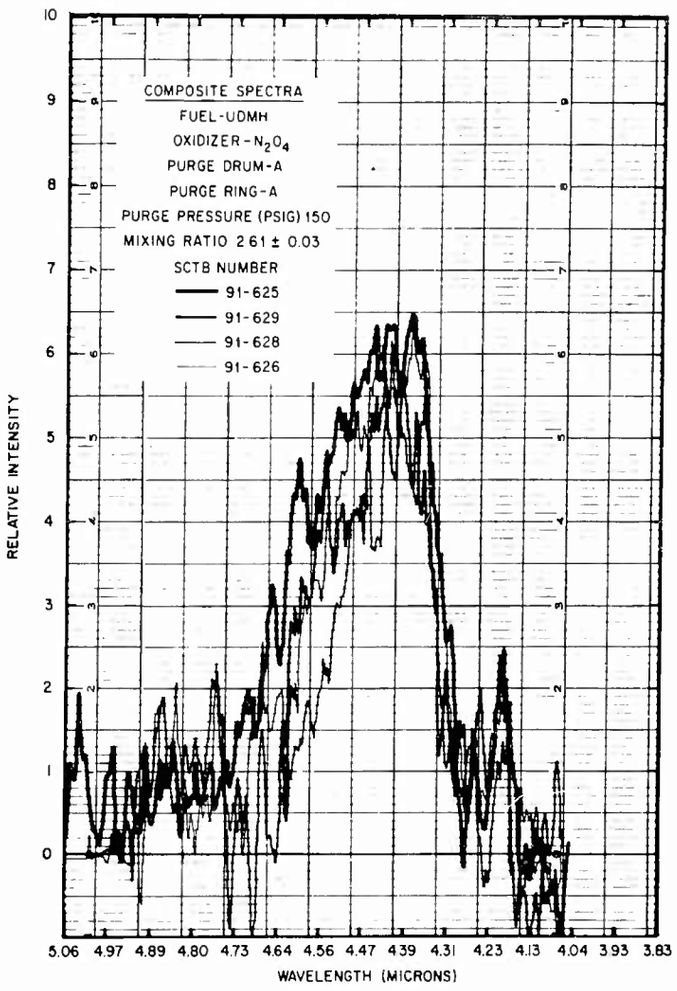

Fig. 3-12 Comparative Spectra: UDMH; No. 625, 626, 628, 629

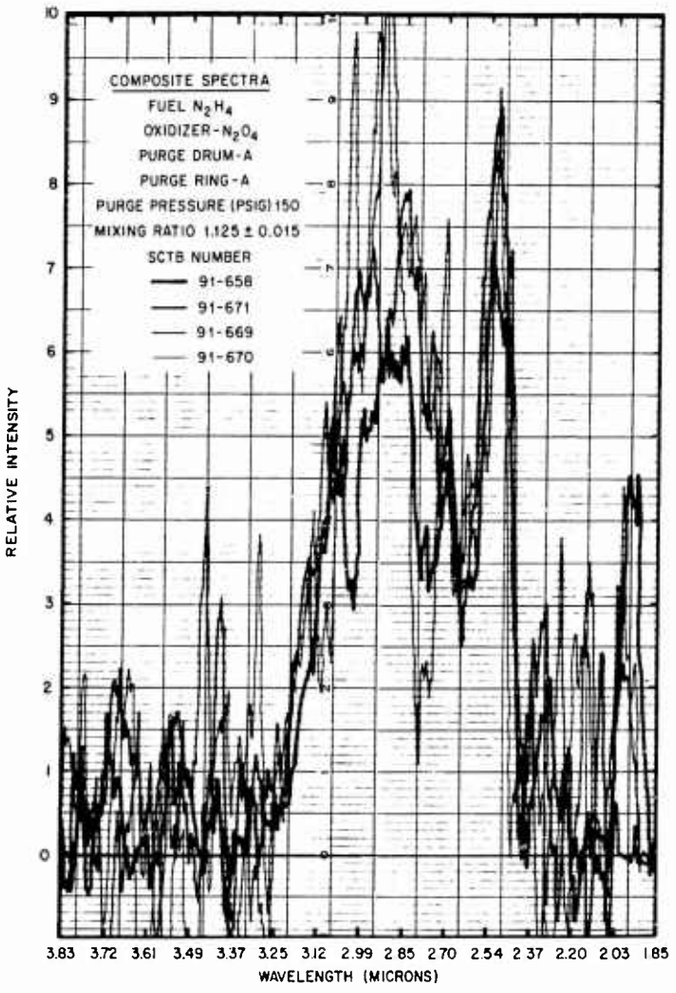

Fig. 3-13 Comparative Spectra: N_2H_4 / N_2O_4 : No. 658, 669, 670, 671

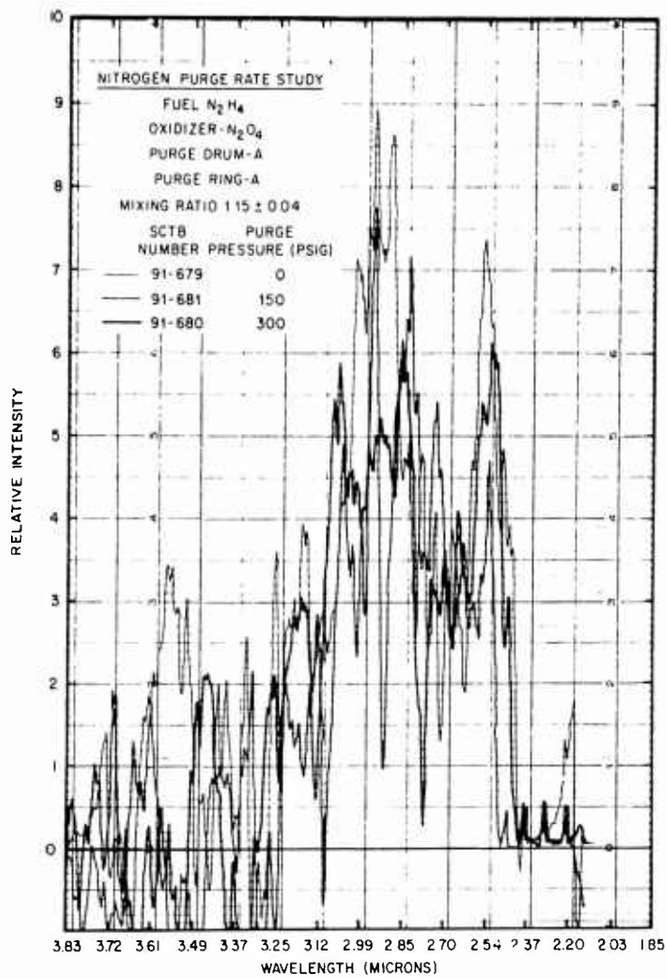

Fig. 3-14 Comparative Spectra: N_2H_4 / N_2O_4; No. 679, 680, 681

some of the species that influence the emission spectra and provide background to the N_2H_4 - N_2O_4 system, the following qualitative information is presented.

Oxidation→ ← Reduction

$$N_2H_4 \rightleftharpoons N_2 \rightleftharpoons N_2O \rightleftharpoons NO \rightleftharpoons N_2O_4$$

Decomposition ↓

$$N_2H_4 \rightarrow NH_3 \rightarrow N_2 + H_2$$

Both N_2O_4 and N_2O have absorption bands in the region of interest as shown in Figs. 2-6 and 2-7. Ammonia is a decomposition by-product and a spectral absorbing and emitting species. It is not likely that N_2O_4 is present in the exhaust, and NO does not have significant absorption bands in the one-to-five-micron region.

One of the difficulties encountered in this series was the unscheduled change in mixing ratio which occurred during each run. The spectra are included in Appendixes A and B but were not used in the comparative studies. There was no definite pattern to the occurrence, so further study would be required to explain this phenomenon. One known fact which may be related to this unusual occurrence is that hydrazine is a monopropellant (Ref. 9) of the class B type, which means that its decomposition energy is derived from a chemically unstable arrangement of atoms in the molecule. It is conceivable that decomposition is taking place prior to ignition at some time during the run when some portion of the system, such as the injector plate, heats up. A definite change in pitch of the sound of the rocket engine occurs. Propulsion engineers call this pitch change a "shift."

3.2 MIXING-RATIO STUDIES

This series of experiments was designed to vary the mixing ratio, within the limits of practicality for the model engine, in order to observe the spectral changes which occur in the relative proportions of CO, CO_2 and H_2O. In addition, the temperature increase with mixing ratio should be reflected in the amplitude of the peaks.

3.2.1 Rocket Propellant (Hydrocarbon) – Liquid Oxygen (RP-1/LOX)

The first illustration (Fig. 3-15) of this series shows the spectra for drum B and purge ring B. The flame is viewed just aft of the exit plane. The principal difference in the spectra appears in the shorter wavelength region. The variation appears to be related to change in temperature of the continuum or the change in amount of carbon particles present. The carbon content is inversely proportional to mixing ratio.

An interesting feature is apparent in 4.4μ region in that a difference in the shape of the spectral peak is noted. The curve for the 2.64 mixing ratio peaks at 4.4μ and has the appearance of the typical CO_2 curve. (Ref. 10)

The curve for the 2.40 mixing ratio reveals a shift in the peak to 4.44μ with a considerable change in the appearance. This change is attributed to the shift of CO to CO_2 ratio with more CO for the lower mixing ratio and an increase in the peak radiation of the 4.67μ CO band as compared to the 4.3μ peak for CO_2.

The only change in the H_2O emission region at 2.5μ, the 2.7μ radiation of H_2O-CO_2, and OH peak at 2.8μ appears to be related to the amount of continuum change rather than to a change in emitting gas species. Appearing in Volume III of this report are a group of curves that show how the amounts of the CO, CO_2 and H_2O in the exhaust product change with mixing ratio. The CO_2 and H_2O are comparatively insensitive to mixing ratio change from 2.3 to 2.6, while the CO decreases quite rapidly. This is borne out in the long wavelength region of our spectrum.

The comparative study for the drum A, purge ring A configuration in which the first Mach disc is viewed is shown in Fig. 3-16. The intensity variations are quite similar to those encountered previously for this fuel-oxidizer combination (Fig. 3-15). A significant magnitude change is noted in that the 2.5μ peak is greater at this point than the 2.85μ peak. This change in magnitude is accounted for by a comparison of the temperatures of the two positions of the flame wherein the carbon particles at the first

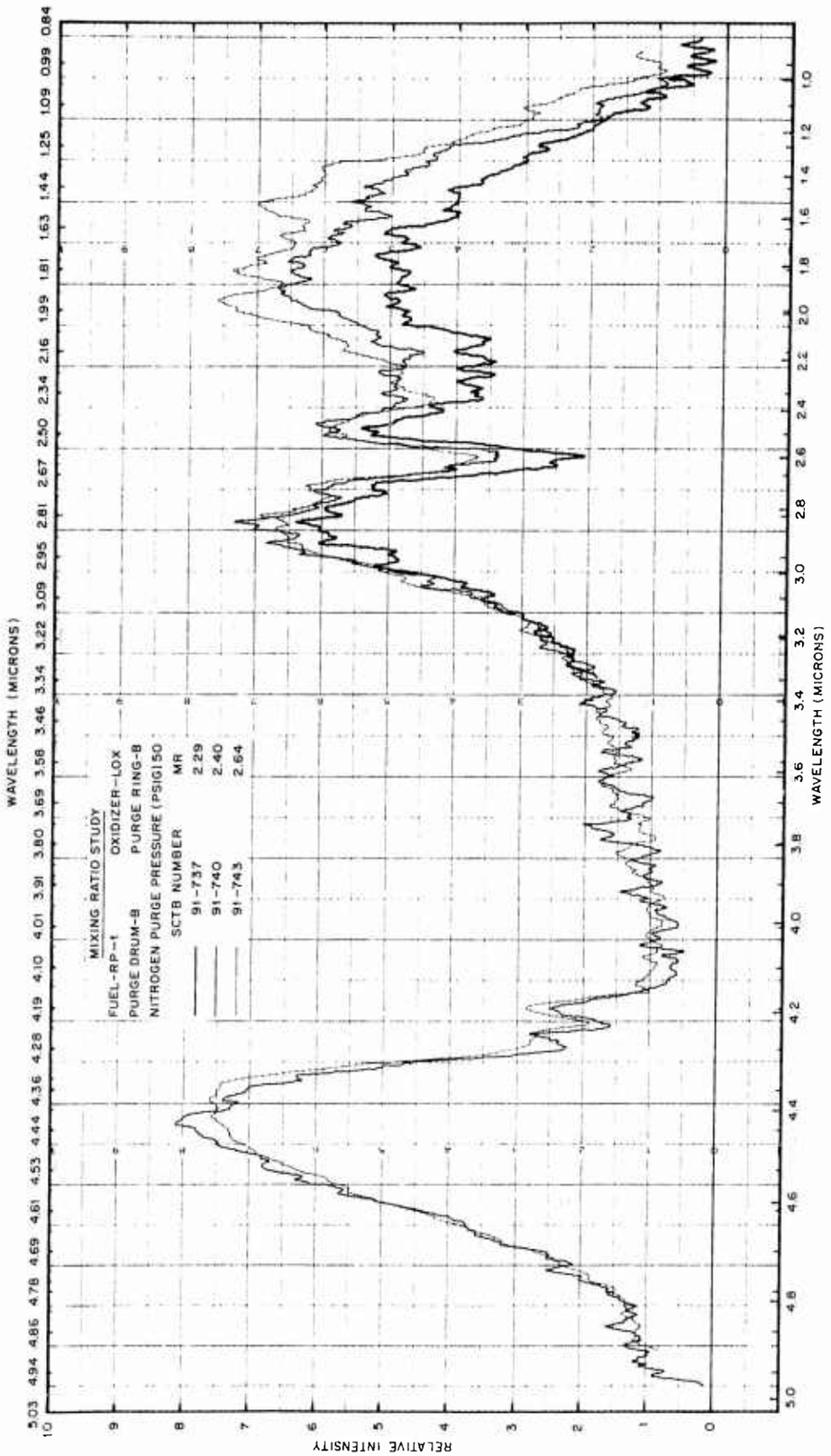

Fig. 3-15 Comparative Spectra: RP-1/LOX; No. 737, 740, 743

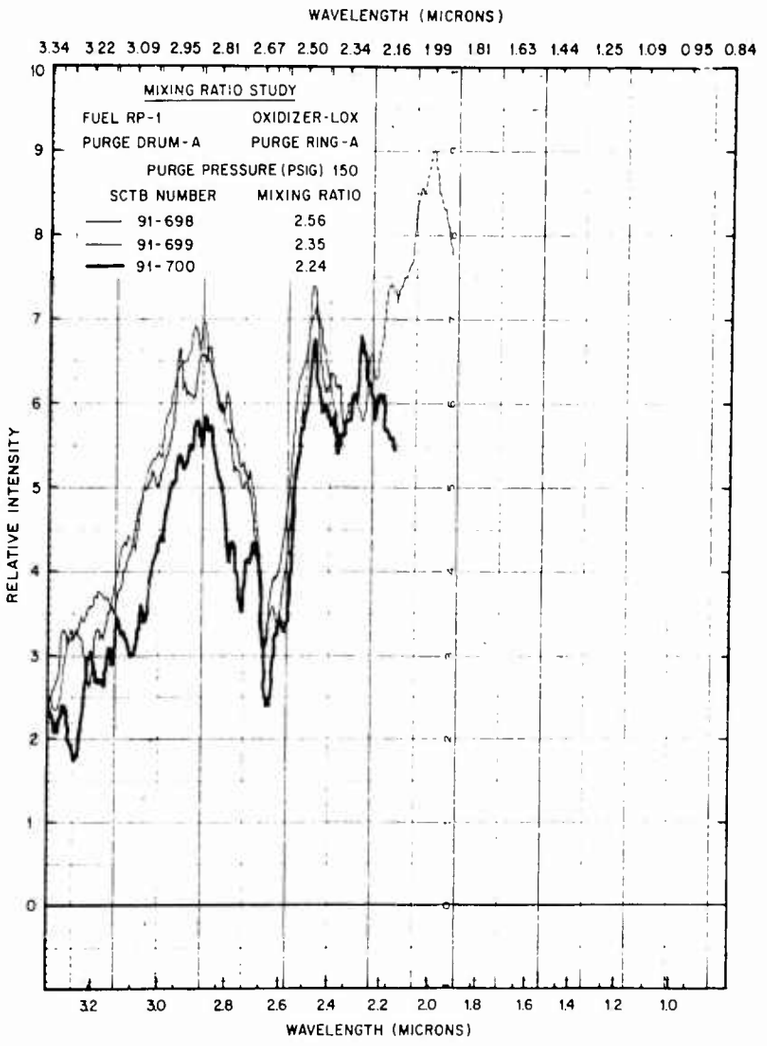

Fig. 3-16 Comparative Spectra: RP-1/LOX; No. 698, 699, 700

Mach disc are much hotter than they are aft of the exit plane. Although the slope of the continuum curve changes, the peak height above the continuum remains constant.

3.2.2 Unsymetrical Dimethyl Hydrazine – Nitrogen Tetroxide (UDMH-N_2O_4)

The UDMH-N_2O_4 mixing ratio study for drum A, purge ring A is presented in Fig. 3-17. These spectra are characterized by the lack of continuum, and the sharpness of the spectral peaks. An interesting feature is that the same type of CO, CO_2 shift occurs in the 4.4μ region as is noted in the RP-1/LOX mixing ratio studies. The CO band center, under higher resolution and higher temperature, 4.67μ, is now quite prominent, and some of the P branch lines are beginning to be resolved (Ref. 2).

3.2.3 Hydrazine-Nitrogen Tetroxide (N_2H_4-N_2O_4)

Two hydrazine mixing ratio series were run. They are illustrated in Figs. 3-18 and 3-19. The drum A, purge ring A configuration was used, and the first Mach disc region was viewed. In Fig. 3-18 the curves are fairly consistent, showing only minor variations in amplitude. Again, some of the absorption bands mentioned in the discussion of purge studies of N_2H_4-N_2O_4 are prominent. The most significant feature is that the amplitude of the 2.5μ peak is greater than that of the 2.85μ peak. This is to be expected, as there is no CO_2 in the exhaust of this fuel. The other fuel exhausts contain carbon dioxide.

Figure 3-19 illustrates the effect of a more fuel-rich series in which the longer wavelength peak is predominant. This predominance is due to the presence of more intermediate oxides of nitrogen, such as N_2O. In addition, as previously noted in regard to the hydrazine series, the fuel-rich mixture contains NH_3 as a decomposition product of N_2H_4 which is emitting in the 2.95μ and 3.05μ regions.

3.3 VARIABLE-SLIT STUDY

In the course of preliminary spectral measurements on a new fuel-oxidizer combination, or new experimental configuration, it was necessary to find the optimum slit

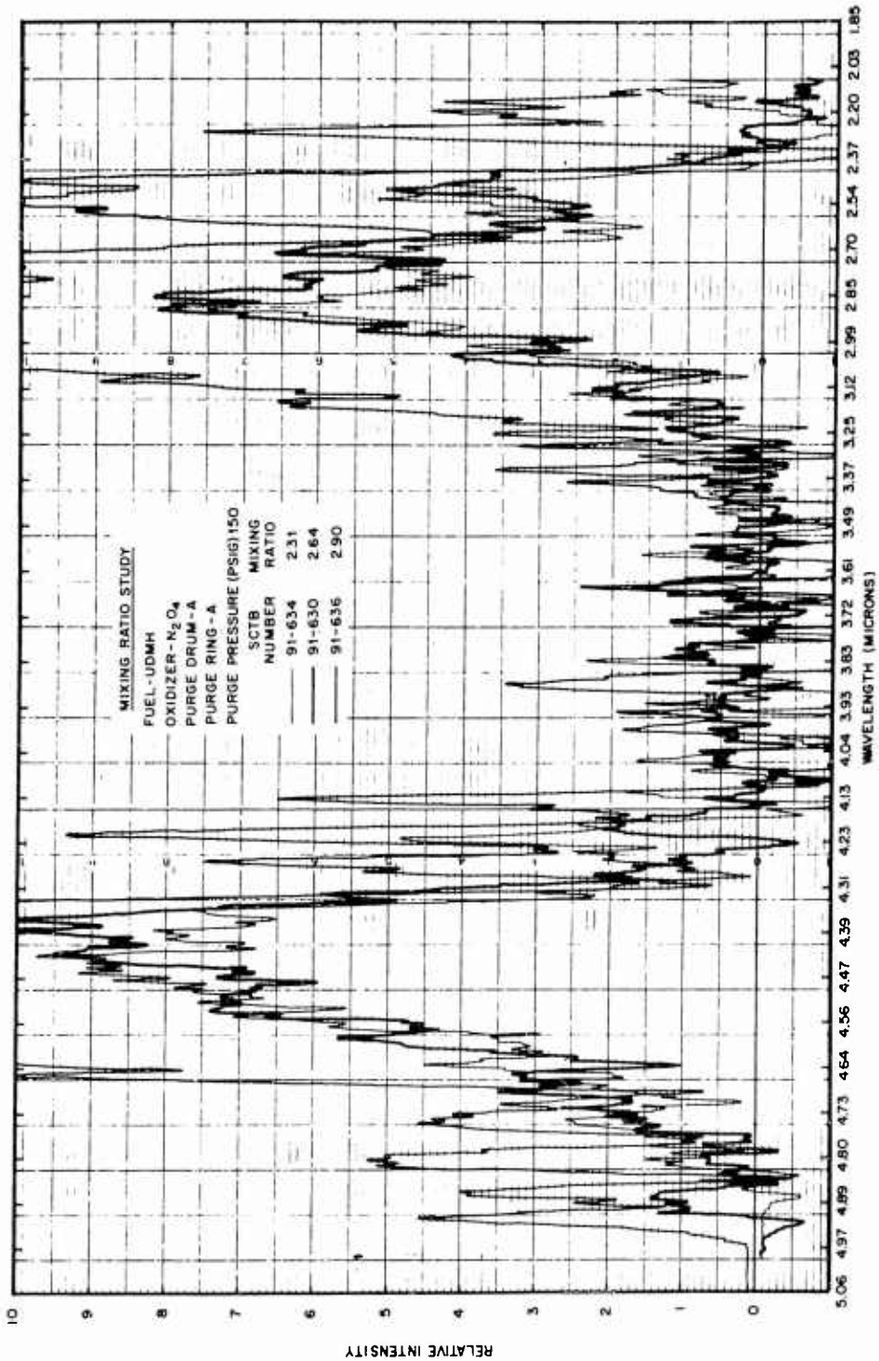

Fig. 3-17 Comparative Spectra: UDMH; No. 630, 634, 636

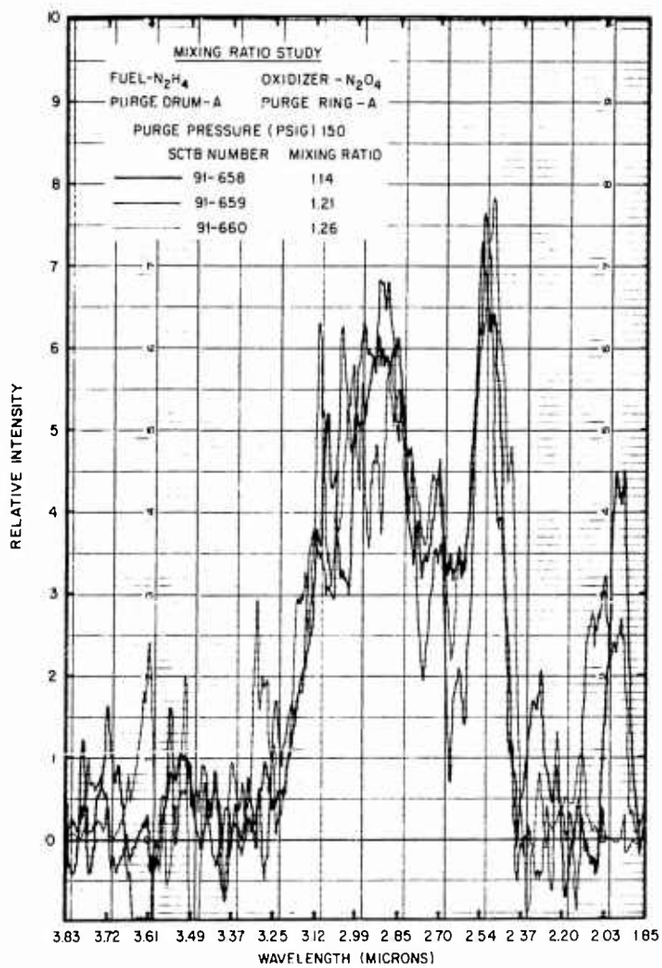

Fig. 3-18 Comparative Spectra: N_2H_4/N_2O_4; No. 658, 659, 660

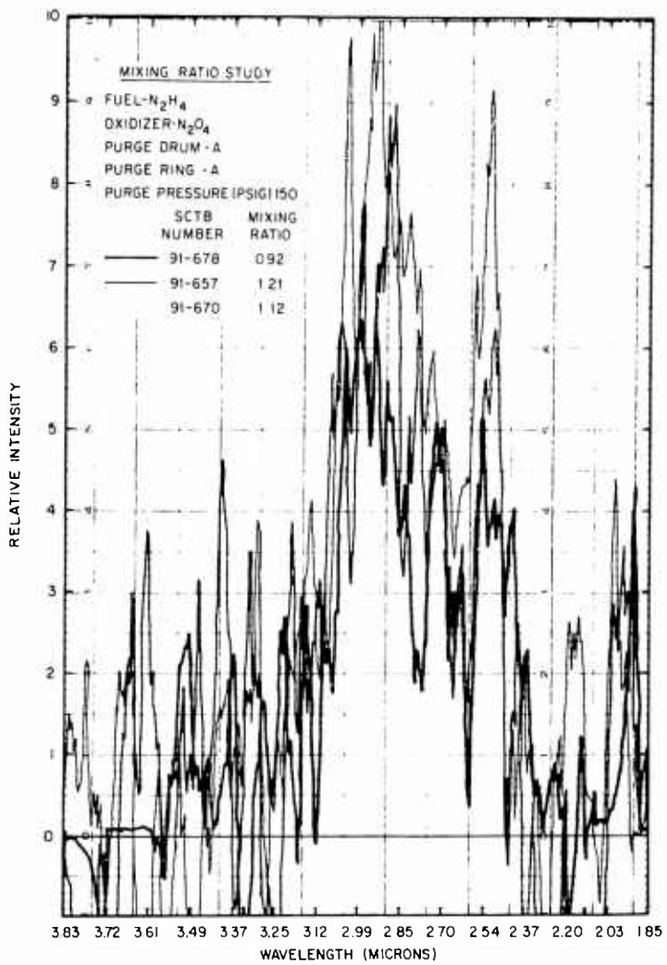

Fig. 3-19 Comparative Spectra: N_2H_4 / N_2O_4: No. 657, 670, 678 (Overlay No. 1)

conditions to make the comparative study. This effort resulted in a by-product which may not have great significance from the data standpoint, but which could point out some of the more salient features of the spectrometer itself. The resolution in the longer wavelength region is a case in point.

The study of drum B, purge ring B, for the RP-1/LOX system is shown in Fig. 3-20, and the drum A purge ring A is shown in Fig. 3-21. As anticipated, resolution of the spectral peaks improve when slit width is reduced.

The UDMH-N_2O_4 and N_2H_4-N_2O_4 on drum A, purge ring A show the typical spectra previously described in the other studies (Figs. 3-22 and 3-23). Advantage of these studies is to emphasize the importance of some of the sideband radiation.

3.4 RAW DATA LOG – PERKIN-ELMER SPECTROMETER

The chronological sequence of the raw data obtained with the Perkin-Elmer spectrometer is shown in Tables 3-2 and 3-3. In addition to the columnar data pertaining to the runs, these tables contain appendix-text-page information. The "Remarks" column presents information on optical, purge, and drum configuration used. See also Table 2-1.

3.5 RADIATION GEOMETRY

The experimental accessories required to perform the simple radiation geometry studies were described in Section 2.1.3. The calibration procedures were discussed in Section 2.2.3. Table 3-4 lists the runs made with the sensor system and identifies the experimental conditions. All temperatures in this study are termed "apparent" because the emissivity of the gas and carbon particle radiating source in the spectral region 0.5 to 1.0 microns, is unknown. It is recognized that the axial temperatures as observed by the sensors are considerably lower than the true core temperature because of flame self-absorption. The inherent temperature gradient of the flame produces some kind of average temperature which cannot be distinguished from the true

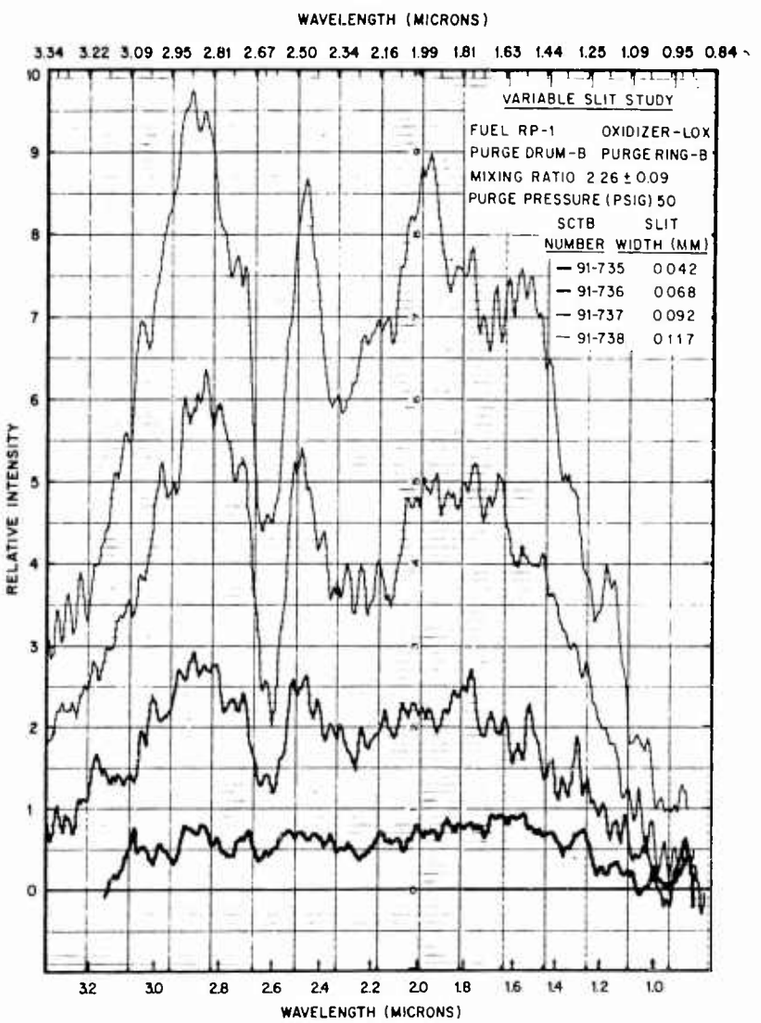

Fig. 3-20 Comparative Spectra: RP-1/LOX; No. 735, 736, 737, 738

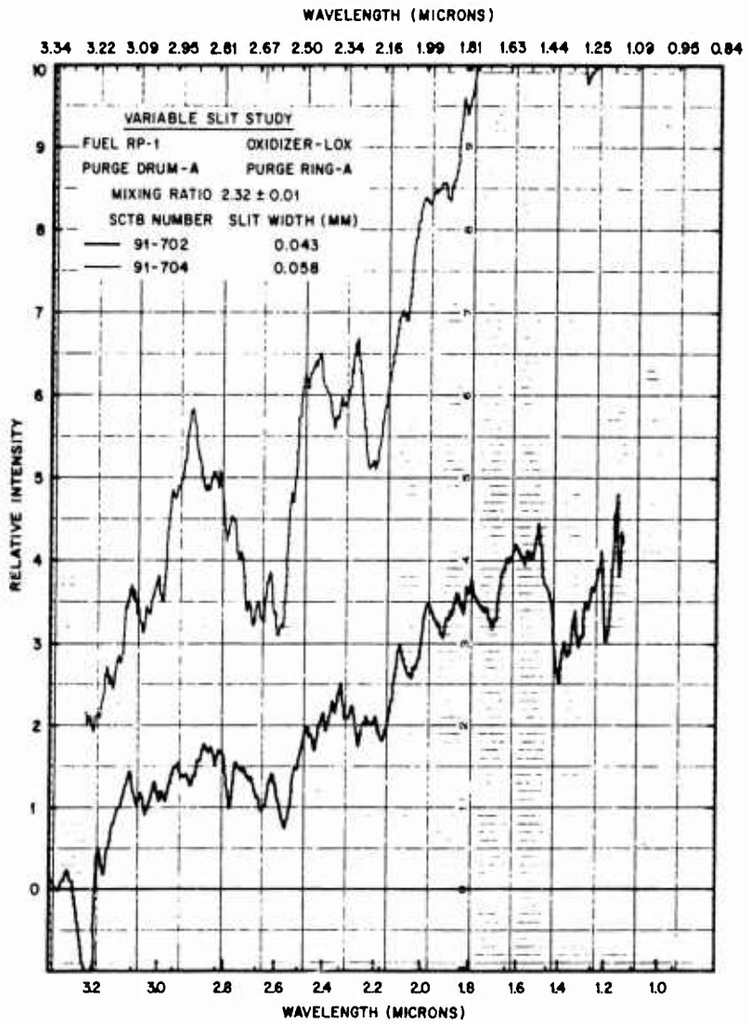

Fig. 3-21 Comparative Spectra: RP-1/LOX; No. 702, 704

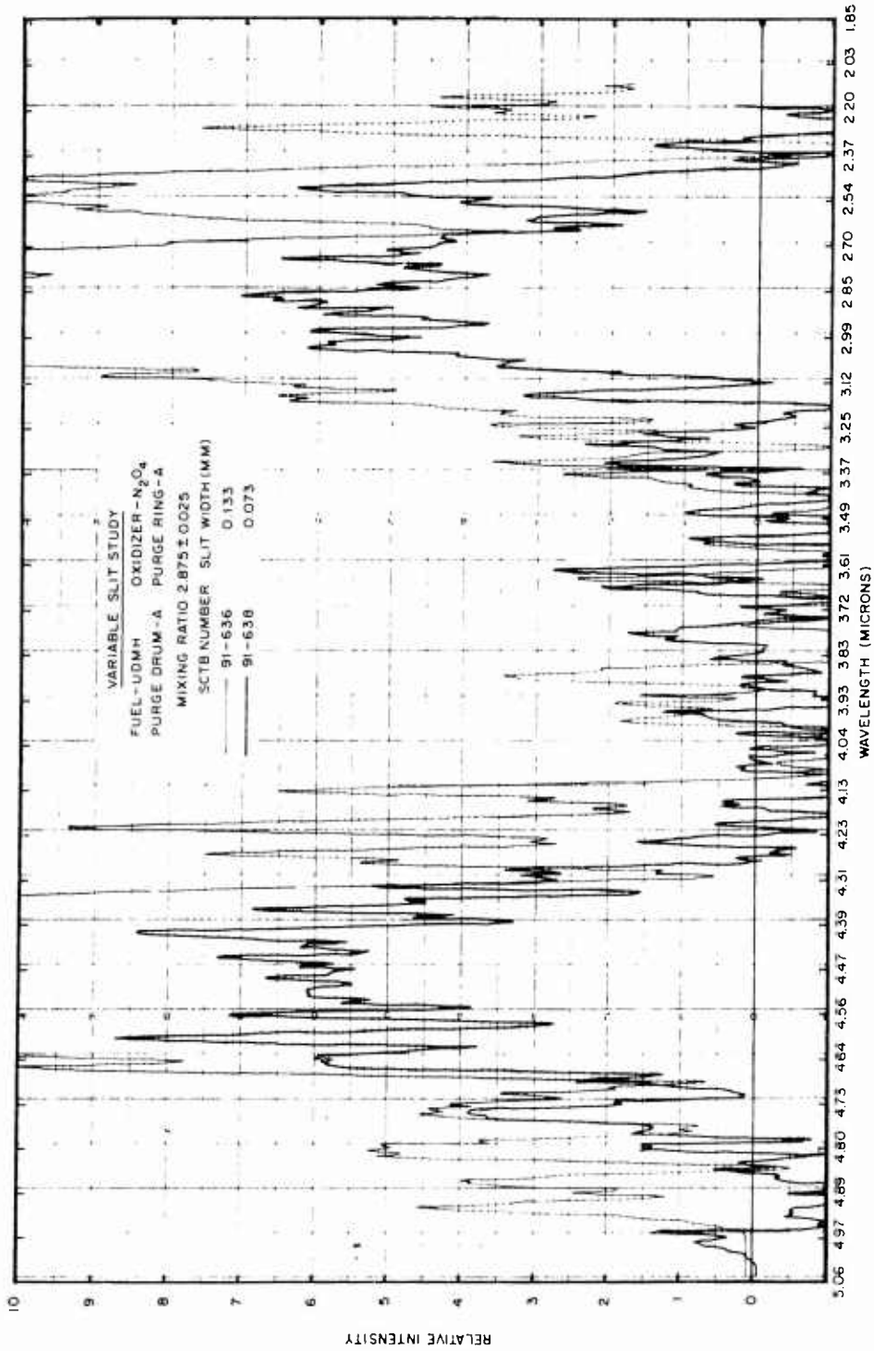

Fig. 3-22 Comparative Spectra: UDMH; No. 636, 638

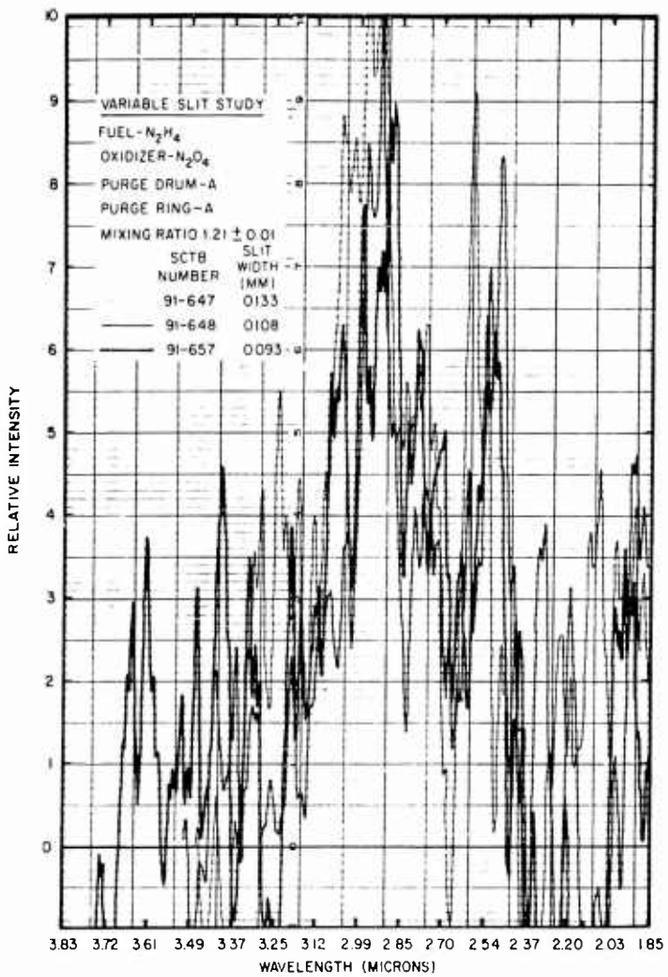

Fig. 3-23 Comparative Spectra: N_2H_4 / N_2O_4; No. 647, 648, 657

Table 3-2

ENGINE PERFORMANCE DATA (UDMH-N_2O_4 AND N_2H_4 - N_2O_4)

Appendix Page No	Run No +1-	Date	Duration (sec)	Chamber Pressure (psia)	Mixing Ratio (oxide/fuel)	Nitrogen Purge Pressure (psig)	Slit Width (mm)	Spectral Range (microns)	Remarks
A-2	609	10-4-62	20.04	497	2.62		0.358	2.2-3.6	Optical system A AA[1]
A-2	611	12-27-62	30.02	491	2.58	200	0.258	2.2-4.0	Optical system A
A-3	612	12-27-62	55.89	503	2.66	100	0.258	2.2-4.4	Optical system B
A-4	614	1-4-63	55.07	514	2.65	200	0.258	2.2-4.6	
A-5	615	1-4-63	60.02	515	2.66	200	0.158	2.2-4.6	
A-6	616	1-4-63	59.08	516	2.69	70	0.158	2.2-4.0	
A-6	618	1-10-63	30.02	505	2.63	200	0.158	2.2-3.6	New detector
A-7	620	1-10-63	30.02	506	2.64	200	0.133	2.2-3.6	
A-7	621	1-10-63	30.07	510	2.62	100	0.133	2.2-3.6	
A-8	622	1-10-63	23.11	509	2.63	100	0.133	2.2-3.7	
A-8	623	1-10-63	29.06	509	2.63	50	0.133	2.2-3.6	
A-9	624	1-10-63	20.05	504	2.53	150	0.133	2.2-3.3	
A-9	625	1-10-63	30.05	508	2.62	150	0.098	4.0-4.9	
A-10	626	1-11-63	20.04	512	2.58	150	0.108	4.0-4.9	
A-10	628	1-11-63	20.58	104	-	150	0.108	4.0-4.7	
A-11	629	1-11-63	20.04	508	2.62	150	0.108	4.0-4.9	
A-12	630	1-21-63	75.05	510	2.64	150	0.133	2.2-4.9	
A-13	631	1-11-63	75.01	405	2.31	150	0.133	2.2-4.9	
A-14	634	1-11-63	73.70	499	2.31	150	0.133	2.2-4.9	
A-15	636	1-18-63	75.09	494	2.40	150	0.133	2.2-4.9	
A-16	637	1-18-63	75.00	494	2.40	150	0.093	2.2-4.9	
A-17	638	1-18-63	71.06	493	2.85	150	0.073	2.2-4.9	
A-18	639	1-18-63	29.89	493	2.64	150	0.073	2.1-3.7	
A-18	643	2-12-63	20.09	508	1.36	150	0.133	2.0-3.5	Optical system B
A-19	647	2-14-63	32.83	173	1.22	150	0.133	1.8-3.5	
A-19	648	2-14-63	35.03	505	1.20	150	0.108	2.0-3.5	
A-20	650	2-14-63	40.06	505	1.18	150	0.108	1.8-3.6	
A-20	654	2-21-63	20.05	496	1.08	150	0.098	1.8-3.5	
A-21	655	2-21-63	40.04	505-522	1.08-1.11	150	0.088	1.8-3.8	17.8 sec[b]
A-21	656	2-21-63	40.08	500	1.17	150	0.093	1.8-3.8	
A-22	657	2-21-63	39.99	502	1.21	150	0.093	1.8-3.7	
A-22	658	2-22-63	40.06	502	1.14	150	0.093	1.8-3.8	
A-23	659	2-22-63	40.01	500	1.21	150	0.093	1.8-3.8	
A-23	660	2-22-63	17.41	504	1.21	150	0.093	2.3-3.7	
A-24	663	2-28-63	40.00	482-474	1.33-1.30	150	0.093	1.8-3.8	16.5 sec[b]
A-24	664	2-28-63	40.03	476-505	1.20-1.29	150	0.093	1.8-3.7	25.5 sec[b]
A-25	665	2-28-63	40.02	478-504	1.14-1.24	150	0.093	1.8-3.7	19.8 sec[b]
A-25	666	2-28-63	40.05	476	1.14-1.19	150	0.093	1.8-3.7	1.2 sec[b]
A-26	667	2-28-63	40.04	484-511	1.12-1.22	150	0.093	1.8-3.7	13.2 sec[b]
A-26	668	2-28-63	40.02	484	1.11-1.20	150	0.093	1.8-3.7	6.4 sec[b]
A-27	669	2-28-63	40.00	486	1.11	150	0.093	1.8-3.7	
A-27	670	2-28-63	40.09	489	1.12	150	0.093	1.8-3.7	
A-28	671	2-28-63	40.01	488	1.13	150	0.093	1.8-3.7	
A-28	672	3-4-63	40.00	502-509	1.12-1.27	150	0.093	1.9-3.8	27.0 sec[b]
A-29	674	3-4-63	40.00	519-501	1.38-1.23	150	0.093	1.8-3.8	18.0 sec[b]
A-29	675	3-4-63	40.06	482	0.92	150	0.093	2.0-3.5	
A-30	679	3-4-63	20.02	503	1.19	0	0.093	2.2-3.8	
A-30	680	3-4-63	40.01	506	1.13	300	0.093	2.2-3.8	
A-31	681	3-4-63	70.06	501	1.13	150	0.093	2.2-5.0	

(a) AA is Purge Drum A and Purge Ring A
(b) Unscheduled change in mixing ratio and chamber pressure at time indicated

Table 3-3

ENGINE PERFORMANCE DATA (RP-1/LOX)

Appendix Page No	Run No 91-	Date	Duration (sec)	Chamber Pressure (psia)	Mixing Ratio (oxide fuel)	Nitrogen Purge Pressure (psig)	Slit Width (mm)	Spectral Range (microns)	Remarks	
B-2	698	7-11-63	30 03	498	2 56	150	0 058	2 3-3 5	Optical System C	AA[a]
B-2	699	7-11-63	40 00	502	2 35	150	0 058	2 0-3 5		
B-3	700	7-11-63	40 05	501	2 24	150	0 058	2 2-3 8		
B-3	701	7-12-63	40 00	490	2 46	150	0.043	2.2-3 8		
B-4	702	7-12-63	40 86	487	2 33	100	0 043	2 2-3.8		
B-4	703	7-12-63	40 00	491	2 32	200	0 058	2.2-3.8		
B-5	704	7-12-63	40 00	494	2 31	100	0 058	2.2-3 8		
B-5	705	7-12-63	40 00	494	2 31	50	0 058	2.2-3.8		
B-6	713	7-25-63	90 03	503	2 38	100	0 058	1 1-4.7		
B-7	714	7-25-63	99 93	503	2 26	100	0 058	1 1-5 0		
B-8	715	7-25-63	100 00	505	2.31	100	0.058	1 1-5 0		
B-9	716	7-25-63	100 06	504	2.19	200	0 058	1 1-5 0		
B-10	717	7-25-63	100 00	508	2 23	0	0.058	1 1-5 0		
B-11	718	7-26-63	40 01	511	2 18	100	0 058	1.1-3 2		AB
B-11	719	7-26-63	39 98	510	2 23	200	0 058	1 1-3 2		
B-12	720	8-1-63	39 95	511	2 18	325	0 058	1.1-3 2		
B-12	721	8-1-63	40 02	515	2 24	150	0.058	1.1-3.2		
B-13	722	8-1-63	39.99	514	2.18	100	0 058	1.1-3.2		
B-13	723	8-1-63	39.98	517	2.26	50	0 058	1 1-3.1		
B-14	724	8-1-63	100 01	512	2.20	50	0 058	1 1-5 0		
B-15	725	8-1-63	94 05	508	2.14	50	0.058	1.1-4.9		
B-16	726	8-2-63	100 00	505	2 33	50	0 058	1.1-5.0		
B-17	727	8-2-63	100 03	504	2 31	50	0.058	1 1-5.0		
B-18	728	8-2-63	100.02	503	2 24	150	0.058	1 1-5.0		
B-19	729	8-2-63	100 02	503	2 28	50	0.058	1 1-5 0	No Drum, Purge Ring B	
B-20	730	8-2-63	100 06	502	2.24	150	0.058	1.1-5.0	No Drum, Purge Ring B	
B-21	731	8-2-63	100 03	504	2.24	50	0 058	0.5-4 3	No Drum, Purge Ring B	
B-22	732	8-2-63	100 03	504	2 27	0	0 058	0 9-4 9	No Drum, No Ring, Moly Extender	
B-23	733	8-2-63	100 04	504	2 28	0	0 058	0 9-4 9	No Drum, No Ring, No Moly Extender	
B-24	734	8-2-63	100 06	503	2 28	100	0 058	0 9-4 9	No Drum, Purge Ring A Smoked Optics, No Data	
B-25	735	8-7-63	42 62	513	2 17	50	0 042	0 9-3 1	Optical System D	BB
B-25	736	8-7-63	50 00	517	2 21	50	0 067	0 9-3.3		
B-26	737	8-7-63	50 00	513	2.29	50	0.092	0 9-3 3		
B-26	738	8-7-63	50 02	509	2 35	50	0 117	0 9-3 3		
B-27	739	8-7-63	100 03	502	2 32	50	0 117	0 9-4 9		
B-28	740	8-7-63	100 07	505	2 40	50	0 092	0 9-4 9		
B-29	741	8-7-63	100.01	506	2 41	100	0 092	0 9-4 9		
B-30	742	8-7-63	100 02	509	2 40	225	0 092	0 9-4.9		
B-31	743	8-7-63	100 05	486	2 64	50	0 092	0 9-4 9		
B-32	744	8-7-63	100 01	505	2 21	0	0.092	0 9-4 9		
B-33	745	8-7-63	100 01	511	2 36	0	0 092	0 9-4.9		

(a) AA is Purge Drum A and Purge Ring A. AB is Purge Drum A and Purge Ring B.
BB is Purge Drum B and Purge Ring B

Table 3-4

RADIATION GEOMETRY STUDY TO DETERMINE APPARENT TEMPERATURE WITH A SILICON PHOTOVOLTAIC LIGHT SENSOR (LS222)

Run No. 91-	Experimental Configuration	Mixing Ratio	Purge Pressure (Psig)	Temp °C(a) Sensor 1	ΔT(b)	Temp °C Sensor 2	ΔT	Temp °C Sensor 3	ΔT	Temp °C Sensor 4	ΔT
720	A-B	2.18	325	217	10	302	18	214	2	214	44
722	A-B	2.18	100	268	28	348	25	229	18	211	10
723	A-B	2.26	50	278	23	360	--	224	8	214	8
724	A-B	2.20	50	290	5	361	2	225	7	218	4
725	A-B	2.14	50	290	17	361	--	225	9	217	6
726	A-B	2.33	50	286	38	352	16	236	3	219	2
727	A-B	2.31	50	300	15	356	10	235	--	220	4
728	A-B	2.24	150	293	37	340	40	225	7	215	7
729	No Drum-B	2.28	50	283	15	352	16	221	--	218	4
731	No Drum-B	2.24	50	284	5	348	25	224	9	217	4
732	No Drum No Ring	2.27	0	290	--	360	--	228	--	219	--
733	No Drum No Ring	2.28	0	294	8	360	--	228	--	219	2
739	B-B	2.32	50	112	17	158	15	91	11	71	13
740	B-B	2.40	50	109	17	58	1	89	22	75	27
741	B-B	2.41	100	92	5	57	11	90	14	72	21
742	B-B	2.40	225	87	4	52	12	76	8	47	7
743	B-B	2.64	50	103	4	67	21	87	3	65	--
744	B-B	2.21	0	125	29	55	11	106	6	86	33
745	B-B	2.36	0	125	40	65	29	96	15	96	14

(a) $(T - T_o)$ where T_o is a constant temperature value specified in Vol. IV.

(b) Peak-to-peak temperature variation during the run.

core temperature: however, the average temperatures of outer portions of the flame are quite useful for flame analysis to assess self-absorption.

Figure 3-24 shows the apparent temperature profile of the axial region from the exit plane to slightly beyond the first Mach disc. The small deviation of the measured points indicates the reliability, or precision of the measurement. The effect of flame cooling due to the purge with dry nitrogen is demonstrated. The magnitude of cooling increases with distance downstream ranging from 10°C near the exit plane to 68°C at two nozzle diameters.

The off-axis apparent temperature profiles at 1/2 nozzle diameter and 2 nozzle diameters down-stream are shown in Fig. 3-25. The indicated off-axis gradient in apparent temperature is 36°C at 1/2 nozzle diameter and 67°C at 2 nozzle diameter for unpurged conditions. The slightly larger deviations for the sensor No. 4 measurements are possibly attributed to the proximity of the boundary layer as the sensor is outside the nozzle diameter. The expansion of the plume places the sensor in the boundary layer whereas for the 2D position, the plume has expanded so that the sensor view is well within the flame and not subjected to large fluctuations.

Using this data, one can observe the radiation entering the spectrometer slit for the drum A configuration has an apparent (or minimum) gradient of 57°C while the drum B gradient shows it to be 22°C. The comparison of Figs. 3-1 and 3-4 reflects this as a difference in "optical noise" which appears to be approximately 3 units in "A" and less than 1 unit in "B".

Although caution must be used in the acceptance of the radiation distribution data, the value of the sensor arrangement as an experimental aid for radiation fluctuation monitoring and for data analysis of flame structures is evident.

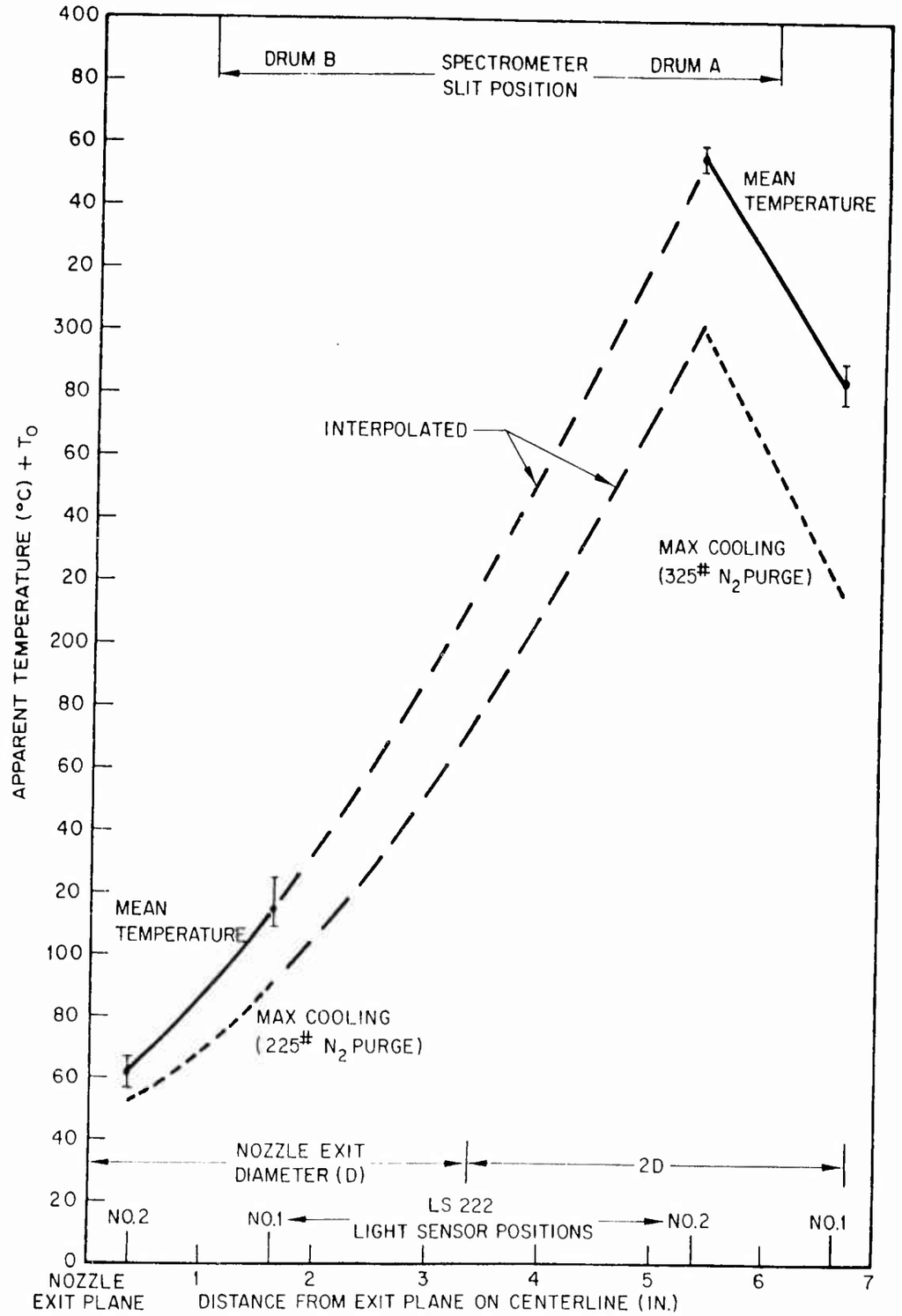

Fig. 3-24 Axial Apparent Temperature Profile; RP-1/LOX; Spectral Bandwidth (0.5 - 1.0μ)

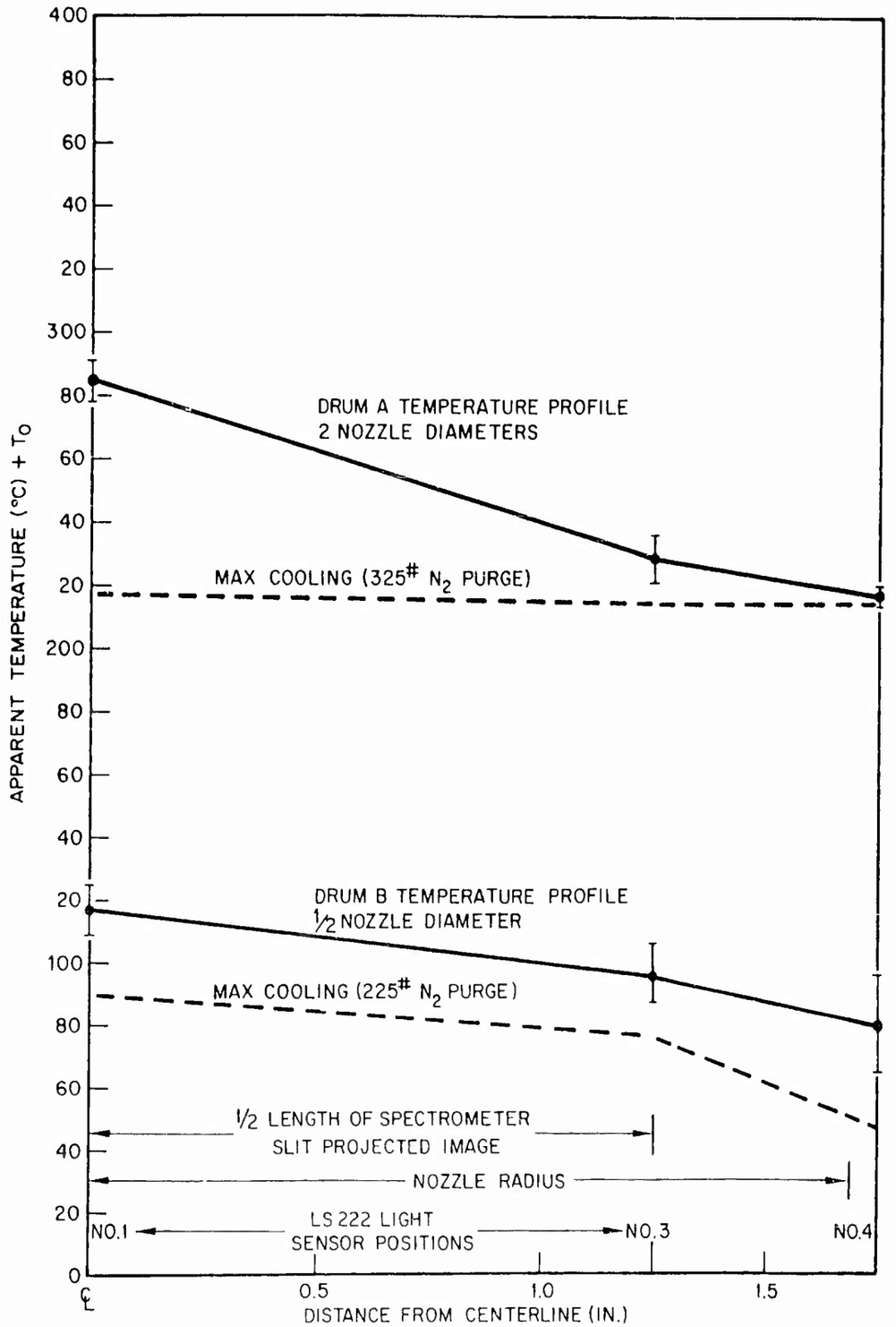

Fig. 3-25 Off-Axis Apparent Temperature; RP-1/LOX; Spectral Bandwidth (0.5 - 1.0μ)

3.6 MICHELSON (BLOCK) INTERFEROMETER SPECTROMETER DATA

The engine flame spectral data obtained with the Michelson (Block)Interferometer spectrometer was not considered satisfactory for presentation in this report for the reasons discussed in Section 2. Figure 2-10 shows examples of spectra of a blackbody source recorded with the optical path purged and unpurged, and an emission spectrum of a propane flame. This interferometer (I-4E) employs an uncooled lead-selenide (PbSe) detector.

The blackbody spectra clearly show the inability of this particular instrument to record the true spectral response of the source. This is attributed in part to the spectral response of the PbSe detector which begins to cut off at 4 microns. The effect of the detector response is also indicated in the propane torch spectra where the CO_2 emission intensity at 4.4 microns is apparently less than the CO_2-H_2O emission band at 2.95 microns. The propane torch flame had considerably more CO_2 than this spectrum indicates, and, using a prism, or grating spectrometer, the spectrum would record the 4.4-micron emission band five to ten times the amplitude of the 2.95-micron emission band. In order to obtain valid quantitative interferometer spectra, the application of a system response correction factor to the raw data would be necessary.

In a vibration-free laboratory setup where a good measure of control can be exercised over the source, useful qualitative emission and absorption spectra can be obtained. In order to withstand the effects of the "13-G" environment of the test site, some redesign of the instrument would be necessary to permit proper operation. In addition to these problems, the raw data requires complex data reduction procedures in order to obtain the detailed quantitative analysis of both the setup and the flame source necessary to any spectral measurement.

3.7 DISCUSSION OF FLAME COOLING BY NITROGEN SHROUD

The discussion of specific studies, such as composite spectra, purge rate, mixing ratio, and variation of slit have been carried out during the analysis of the comparative spectra for each fuel-oxidizer combination. The following is a general discussion emphasizing the important spectral parameter of flame cooling.

The two important objectives of this discussion are: (1) to assess the extent to which absorption bands were eliminated from the spectra obtained, and (2) to evaluate the effects of flame cooling.

A study of the various spectra reveal that Fig. 3-9 which contains both of the runs without a purge ring and with the purge drum removed exhibits the highest value of radiation in the absorption bands. In this series the first Mach disc is viewed, and a ceramic extension to the viewing port prevents entrainment of atmosphere (Fig. 3-8). The next important series of spectra in which the absorption bands are minimized is shown in Fig. 3-1. This is for the RP-1/LOX fuel-oxidizer combination with the B drum and ring viewing the flame one inch aft of the exit plane. The radiance values are lower because of the portion of the flame being viewed, but the absorption bands are present although minimized. The best spectral region to observe absorption is in the 4.23 and 4.26 micron CO_2 bands. Both of the spectral cases cited do show less absorption in this region without nitrogen blanketing. Preliminary torch studies were carried out in which the nitrogen shroud was preheated by the hot metal torch tip. This reduced cooling in the outer layer of the flame, and self-absorption was indicated by the spectrum to be negligible.

The effects of flame cooling are best demonstrated (Fig. 3-2) in the study of the purge-rate spectra and the radiation-geometry data. Figure 3-1 shows the minimum effect of purge rate because the least variant portion of the flame is viewed, although some change is apparent. Comparison of Fig. 3-1 with Fig. 3-6 reveals that much greater radiation occurs when viewing two exit diameters downstream, but the effects of flame cooling are magnified. The greatest effect of flame cooling is probably to be found where the radiation maximum appears downstream.

A most significant feature of the results on flame cooling is shown in the radiation-geometry data. The temperature profile of the axial radiation in Fig. 3-24 shows a typical result in which the temperature increases to the first Mach disc and then begins to decrease; but the maximum cooling curve increases with distance from the nozzle. The upper curve in Fig. 3-25 shows that little or no cooling results at the outer envelope, but rather that the greatest cooling occurs at the view of the axis.

Self-absorption of the flame caused by the temperature gradient of the radiating species is indicated in the curves in Fig. 3-26. The theoretical emission curve of a carbon dioxide source (2400°K) with a uniform temperature is compared with one of our experimental curves for the 4.3-micron band of CO_2. Shown also is a short-path absorption curve of carbon dioxide at 300°K. The theoretical emission and absorption curves are based on data from G. N. Plass in his "Emissivity of the 4.3 Micron Band of CO_2" (AFCRC No. TN-58-604, 7-31-51).

The experimental curve reveals the type of spectrum one would expect to observe from a hot spectral source emitting through a cold absorbing gas. This phenomenon is called self-absorption.

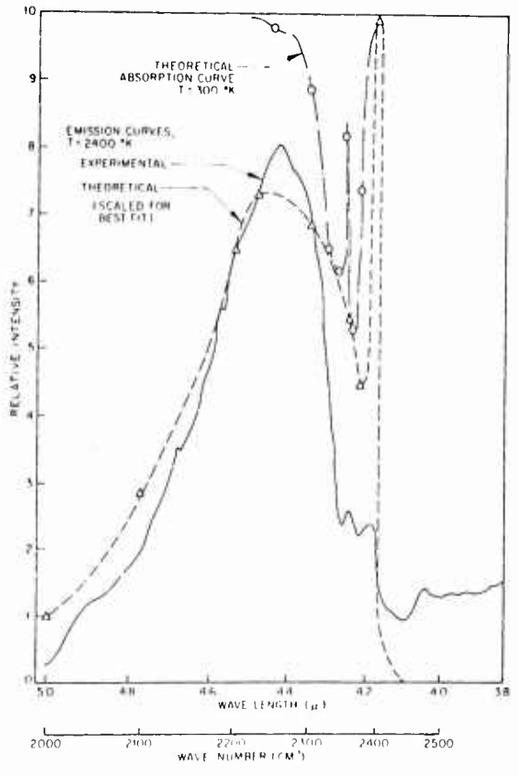

Fig. 3-26 The Effect of Self-Absorption on the Emissivity of the 4.3 Micron Band of CO_2

Section 4

REFERENCES

1. Lockheed Missiles & Space Company, Quick Look Report of Model Engine Flame Spectral Studies, UDMH-N_2O_4 and N_2H_4-N_2O_4 (U), by T. J. Kowall, R. C. Tuttle, and W. N. Tuttle, LMSC-8-19-63-10, May 1963

2. E. K. Plyler, et al, "Vibration-rotation Structure in Absorption Bands for Calibration of Spectrometers from 2 to 16 Microns," J. Res. NBS, Vol. 64, No. 1, Jan–Feb 1960

3. University of Michigan, Method of Radiometric Calibration, by F. E. Nicodemus and G. J. Zissis, Report of BAMIRAC, Report No. 4613-20-R, Oct 1962

4. Lockheed Missiles & Space Company, The Infrared Absorption Spectrum of Water Vapor and Carbon Dioxide (U), by H. N. Ritland, LMSC-5-77-62-2, Feb 1962

5. R. H. Pierson, A. N. Fletcher, and E. A. Gantz, "Catalog of Infrared Spectra for Qualitative Analysis of Gases," NOTS, China Lake, Anal. Chem. Vol. 28, No. 8, Aug 1956

6. S. Silverman, "Emissivity of Globar," J. Opt. Soc. Am., Vol. 38, No. 11, Nov 1948, p. 989

7. W. Brügel, "Radiation Measurements of Electrically Heated SiC Rods," Z. Physic, Vol. 127, 1950, p. 400

8. J. E. Stewart and J. C. Richmond, "IR Emission Spectrum of SiC Heating Elements," J. Res. NBS, Vol. 59, No. 6, Dec 1957, p. 405

9. D. Altman, J. M. Carter, S. S. Penner, and M. Summerfield, Liquid Propellant Rockets, Princeton U. Press, 1960, p. 85

10. Aeronutronics, IR Radiation Emitted by Hot Gases and Its Transmission Through Synthetic Atmospheres, by D. E. Burch and D. A. Gryvnak, Report No. U-1929, 31 Oct 1962

Appendix A

SPECTRAL RADIANCE CHARTS – RAW DATA ($UDMH-N_2O_4$ AND $N_2H_4-N_2O_4$)

A.1 SPECTRAL RANGE AND INSTRUMENTATION

The charts in this appendix encompass a spectral radiance of 1-5 microns. The LMSC-modified Astrosystems 1,000-lb thrust hypergolic engine and the Perkin-Elmer 112 spectrometer were used to botain these data.

A.2 SCALE-CONVERSION OVERLAY

Overlays for conversion of the ordinate scale from relative intensity to apparent spectral radiance are "Confidential" and therefore are included in Volume IV.

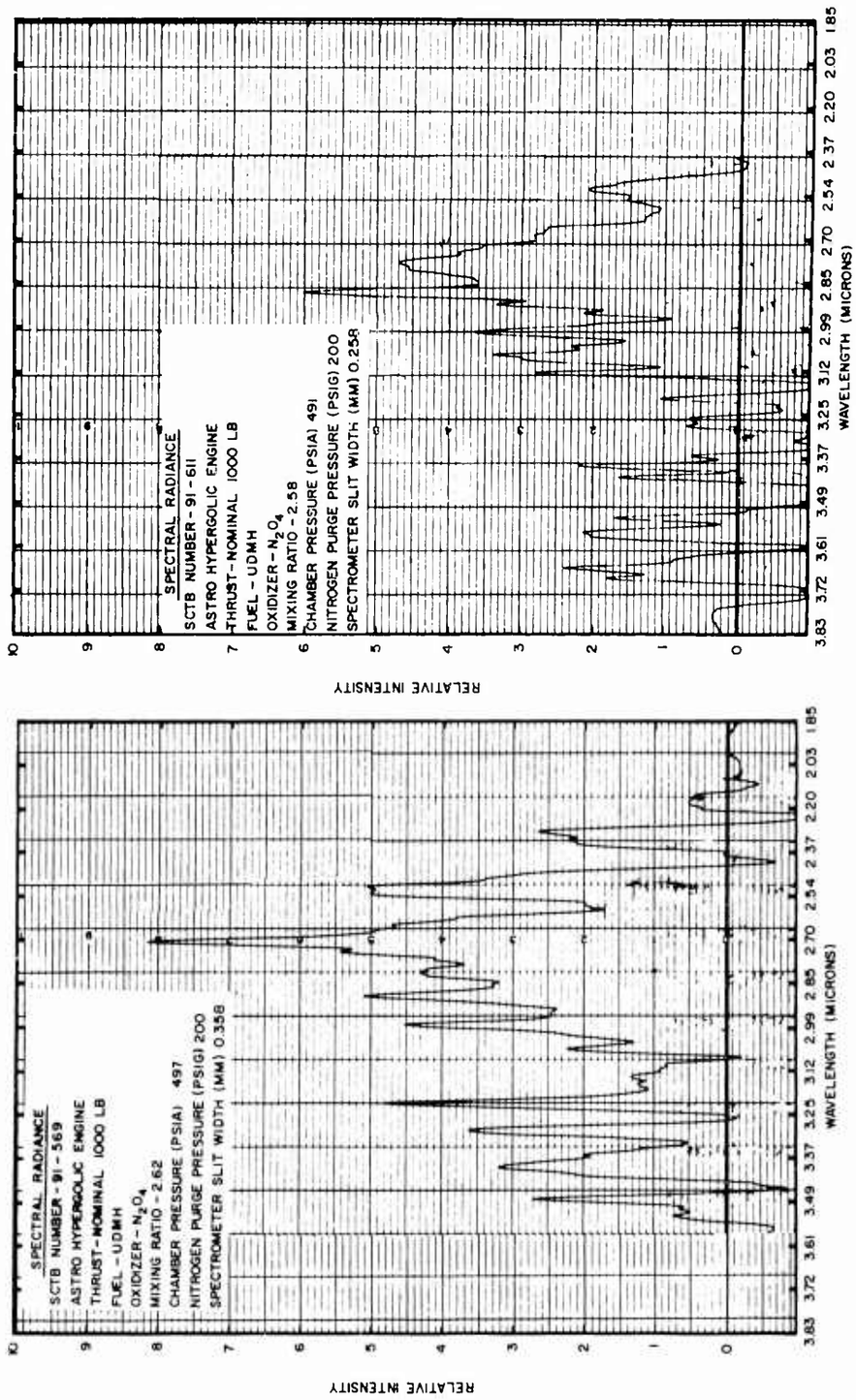
SPECTRAL RADIANCE
SCTB NUMBER - 91 - 569
ASTRO HYPERGOLIC ENGINE
THRUST - NOMINAL 1000 LB
FUEL - UDMH
OXIDIZER - N_2O_4
MIXING RATIO - 2.62
CHAMBER PRESSURE (PSIA) 497
NITROGEN PURGE PRESSURE (PSIG) 200
SPECTROMETER SLIT WIDTH (MM) 0.358
RELATIVE INTENSITY
WAVELENGTH (MICRONS)
3.83 3.72 3.61 3.49 3.37 3.25 3.12 2.99 2.85 2.70 2.54 2.37 2.20 2.03 1.85
SPECTRAL RADIANCE
SCTB NUMBER - 91 - 611
ASTRO HYPERGOLIC ENGINE
THRUST - NOMINAL 1000 LB
FUEL - UDMH
OXIDIZER - N_2O_4
MIXING RATIO - 2.58
CHAMBER PRESSURE (PSIA) 491
NITROGEN PURGE PRESSURE (PSIG) 200
SPECTROMETER SLIT WIDTH (MM) 0.258
RELATIVE INTENSITY
WAVELENGTH (MICRONS)
3.83 3.72 3.61 3.49 3.37 3.25 3.12 2.99 2.85 2.70 2.54 2.37 2.20 2.03 1.85

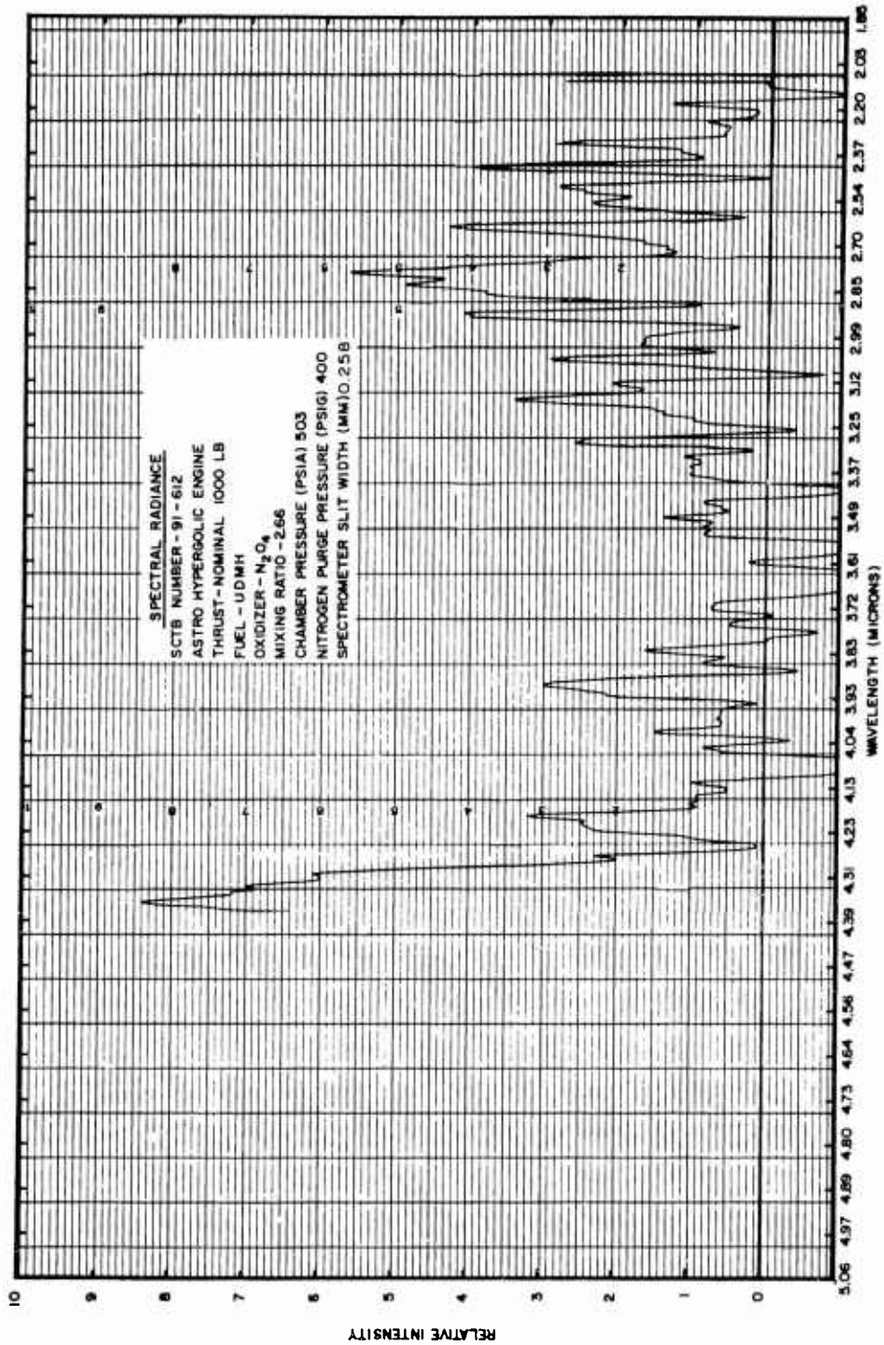
SPECTRAL RADIANCE
SCTB NUMBER - 91 - 612
ASTRO HYPERGOLIC ENGINE
THRUST - NOMINAL 1000 LB
FUEL - UDMH
OXIDIZER - N_2O_4
MIXING RATIO - 2.66
CHAMBER PRESSURE (PSIA) 503
NITROGEN PURGE PRESSURE (PSIG) 400
SPECTROMETER SLIT WIDTH (MM) 0.258
RELATIVE INTENSITY
WAVELENGTH (MICRONS)
5.06 4.97 4.89 4.80 4.73 4.64 4.56 4.47 4.39 4.31 4.23 4.13 4.04 3.93 3.83 3.72 3.61 3.49 3.37 3.25 3.12 2.99 2.85 2.70 2.54 2.37 2.20 2.03 1.85

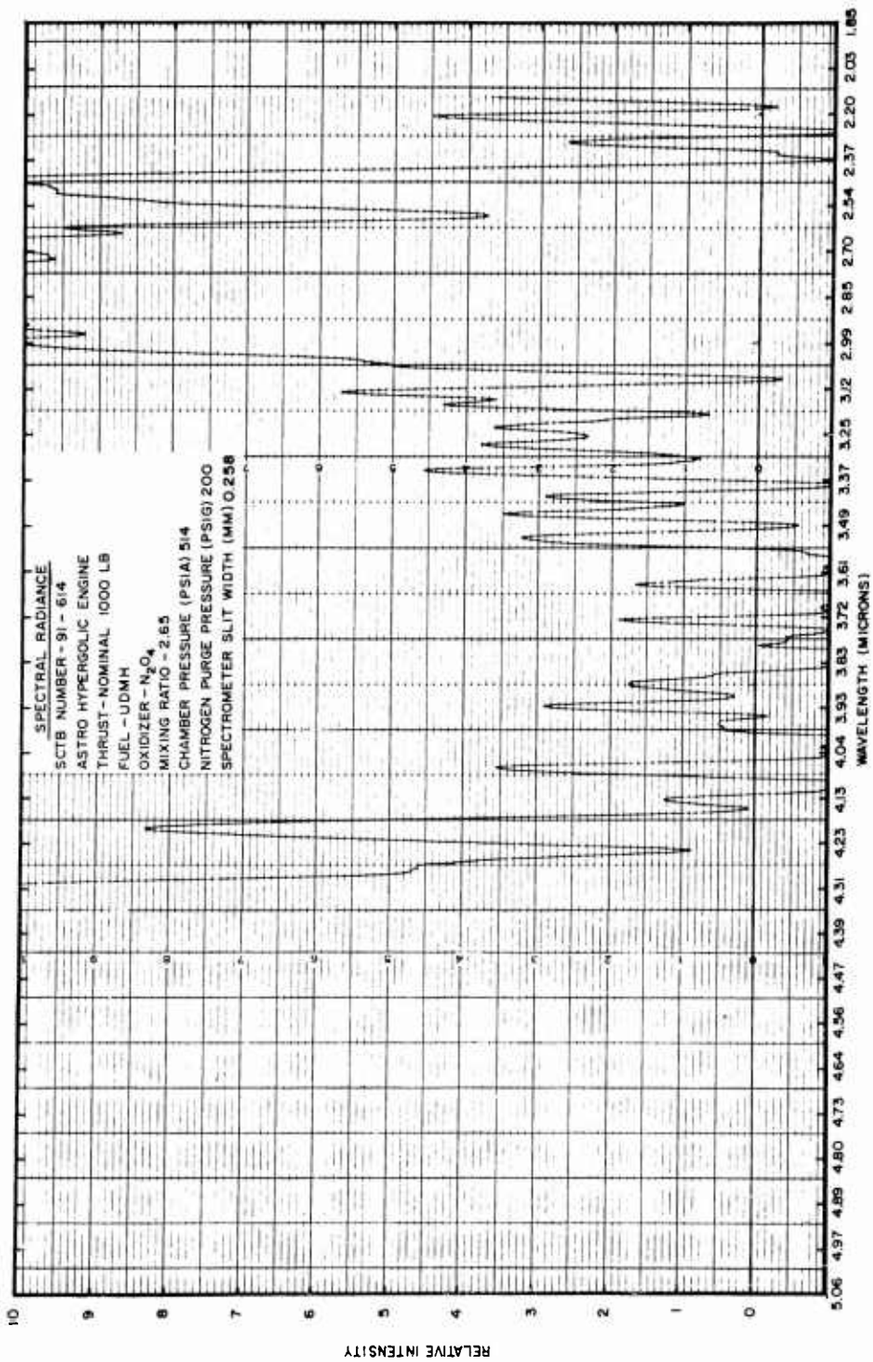
SPECTRAL RADIANCE
SCTB NUMBER - 91 - 614
ASTRO HYPERGOLIC ENGINE
THRUST - NOMINAL 1000 LB
FUEL - UDMH
OXIDIZER - N_2O_4
MIXING RATIO - 2.65
CHAMBER PRESSURE (PSIA) 514
NITROGEN PURGE PRESSURE (PSIG) 200
SPECTROMETER SLIT WIDTH (MM) 0.258
RELATIVE INTENSITY
WAVELENGTH (MICRONS)
10
9
8
7
6
5
4
3
2
1
0
5.06 4.97 4.89 4.80 4.73 4.64 4.56 4.47 4.39 4.31 4.23 4.13 4.04 3.93 3.83 3.72 3.61 3.49 3.37 3.25 3.12 2.99 2.85 2.70 2.54 2.37 2.20 2.03 1.85

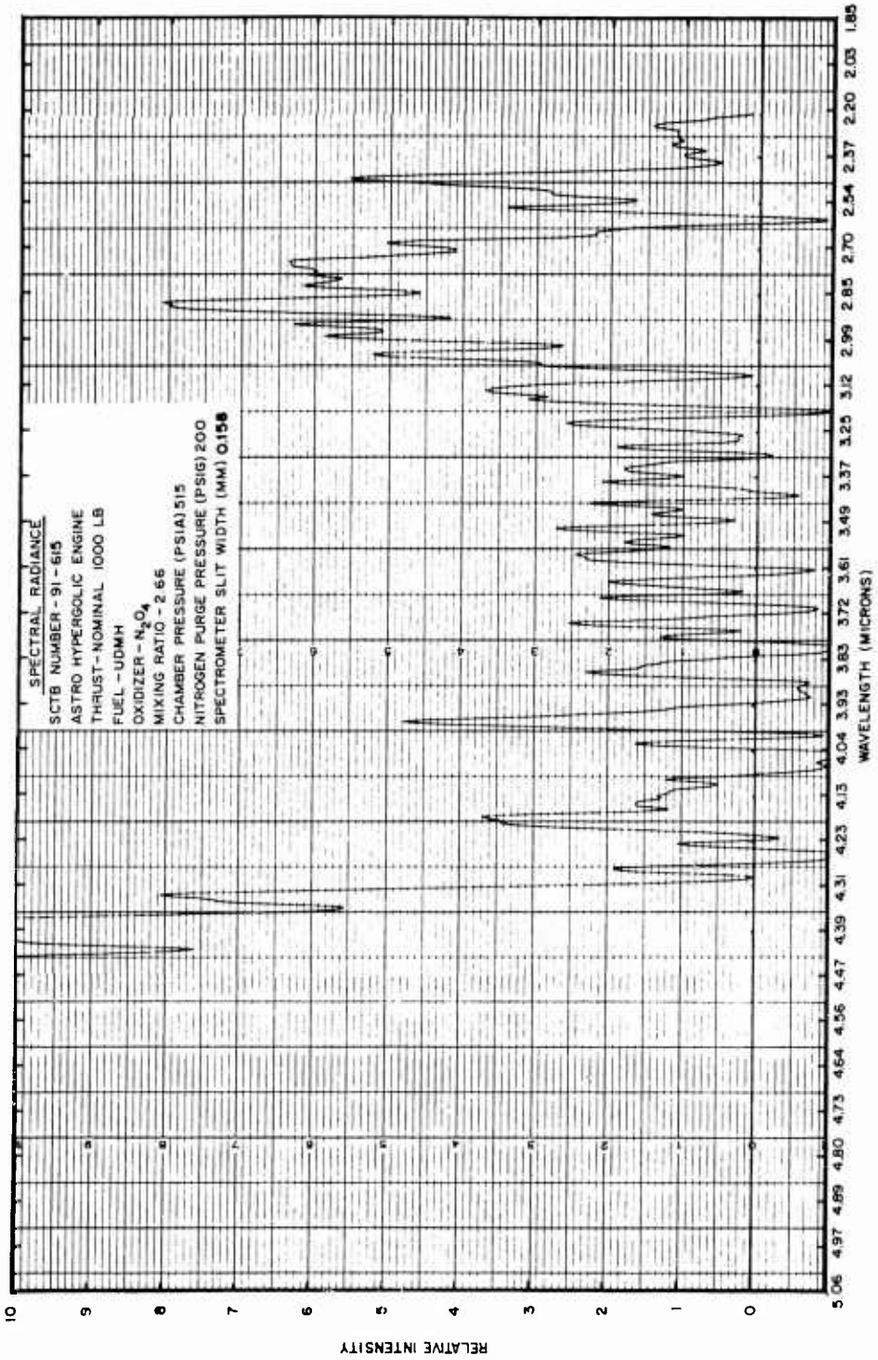
SPECTRAL RADIANCE
SCTB NUMBER - 91 - 615
ASTRO HYPERGOLIC ENGINE
THRUST - NOMINAL 1000 LB
FUEL - UDMH
OXIDIZER - N_2O_4
MIXING RATIO - 2.66
CHAMBER PRESSURE (PSIA) 515
NITROGEN PURGE PRESSURE (PSIG) 200
SPECTROMETER SLIT WIDTH (MM) 0.158
RELATIVE INTENSITY
WAVELENGTH (MICRONS)
5.06 4.97 4.89 4.80 4.73 4.64 4.56 4.47 4.39 4.31 4.23 4.13 4.04 3.93 3.83 3.72 3.61 3.49 3.37 3.25 3.12 2.99 2.85 2.70 2.54 2.37 2.20 2.03 1.85

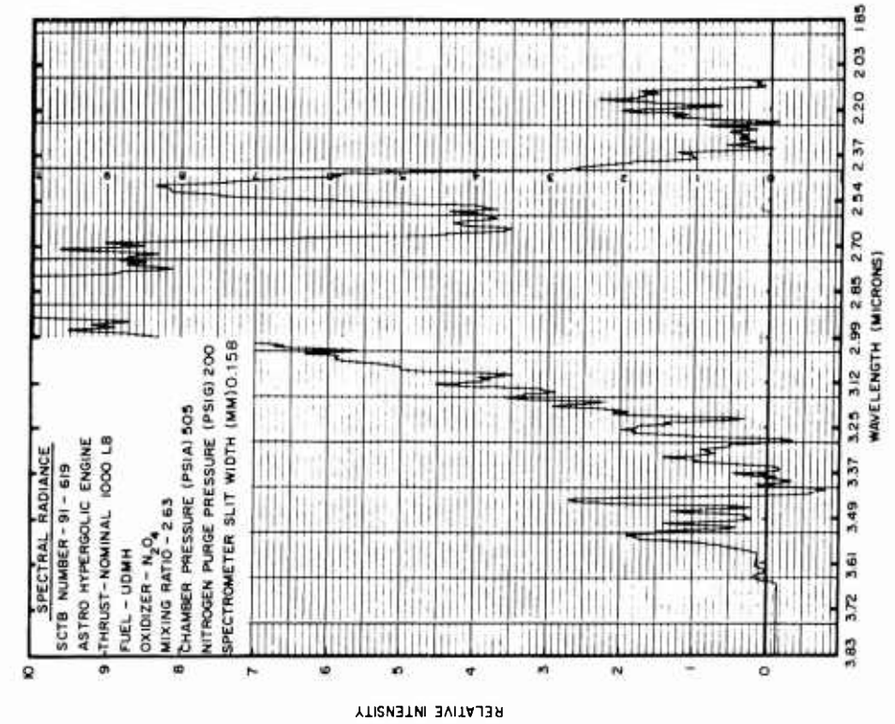
SPECTRAL RADIANCE
SCTB NUMBER - 91 - 619
ASTRO HYPERGOLIC ENGINE
THRUST - NOMINAL 1000 LB
FUEL - UDMH
OXIDIZER - N_2O_4
MIXING RATIO - 2.63
CHAMBER PRESSURE (PSIA) 505
NITROGEN PURGE PRESSURE (PSIG) 200
SPECTROMETER SLIT WIDTH (MM) 0.158
RELATIVE INTENSITY
WAVELENGTH (MICRONS)
3.83 3.72 3.61 3.49 3.37 3.25 3.12 2.99 2.85 2.70 2.54 2.37 2.20 2.03 1.85

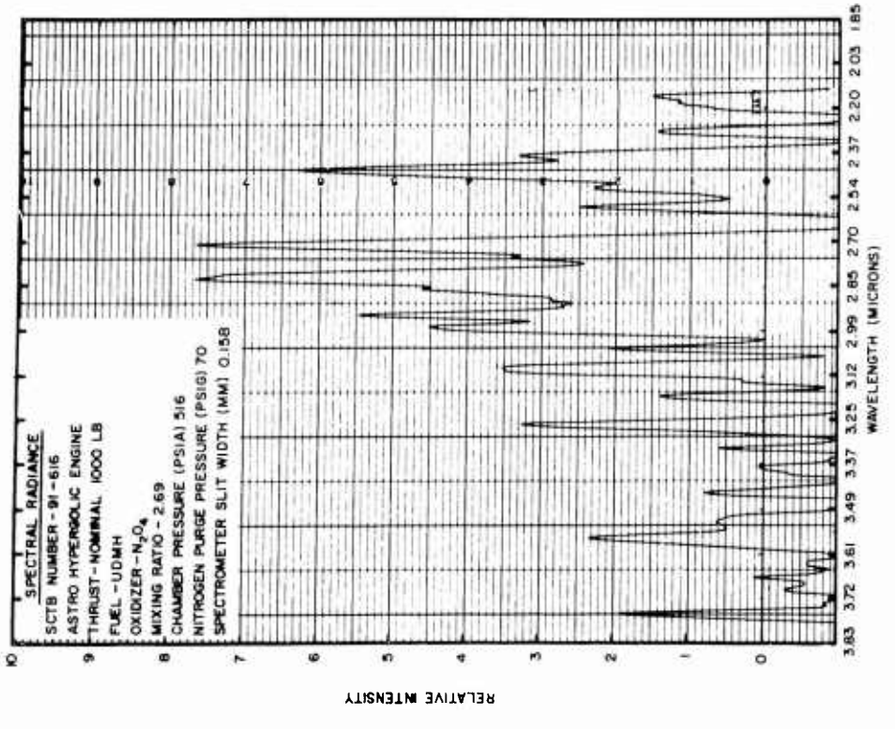
SPECTRAL RADIANCE
SCTB NUMBER - 91 - 616
ASTRO HYPERGOLIC ENGINE
THRUST - NOMINAL 1000 LB
FUEL - UDMH
OXIDIZER - N_2O_4
MIXING RATIO - 2.69
CHAMBER PRESSURE (PSIA) 516
NITROGEN PURGE PRESSURE (PSIG) 70
SPECTROMETER SLIT WIDTH (MM) 0.158
RELATIVE INTENSITY
WAVELENGTH (MICRONS)
3.83 3.72 3.61 3.49 3.37 3.25 3.12 2.99 2.85 2.70 2.54 2.37 2.20 2.03 1.85

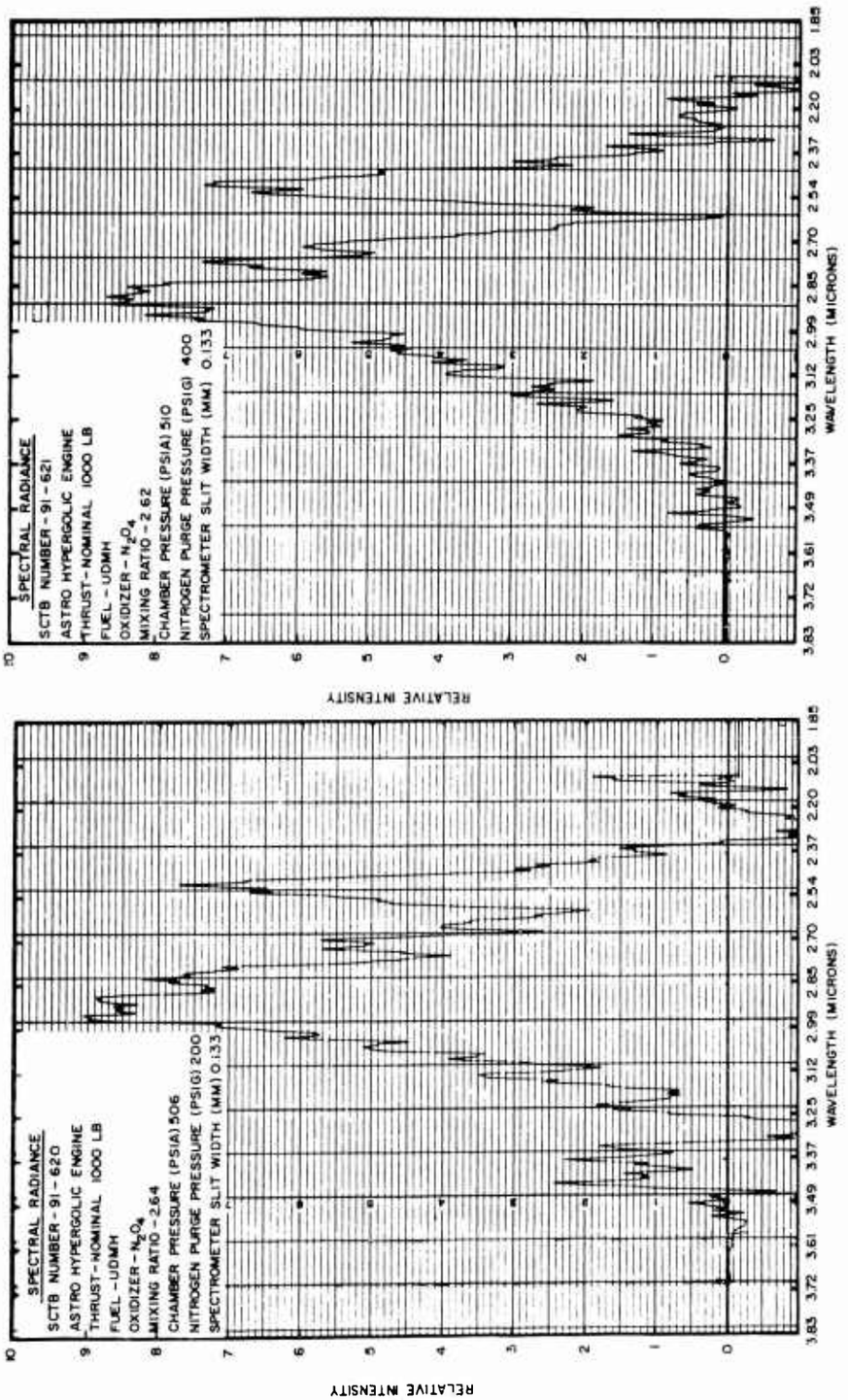
SPECTRAL RADIANCE
SCTB NUMBER - 91 - 621
ASTRO HYPERGOLIC ENGINE
THRUST - NOMINAL 1000 LB
FUEL - UDMH
OXIDIZER - N_2O_4
MIXING RATIO - 2.62
CHAMBER PRESSURE (PSIA) 510
NITROGEN PURGE PRESSURE (PSIG) 400
SPECTROMETER SLIT WIDTH (MM) 0.133
RELATIVE INTENSITY
WAVELENGTH (MICRONS)
SPECTRAL RADIANCE
SCTB NUMBER - 91 - 620
ASTRO HYPERGOLIC ENGINE
THRUST - NOMINAL 1000 LB
FUEL - UDMH
OXIDIZER - N_2O_4
MIXING RATIO - 2.64
CHAMBER PRESSURE (PSIA) 506
NITROGEN PURGE PRESSURE (PSIG) 200
SPECTROMETER SLIT WIDTH (MM) 0.133
RELATIVE INTENSITY
WAVELENGTH (MICRONS)

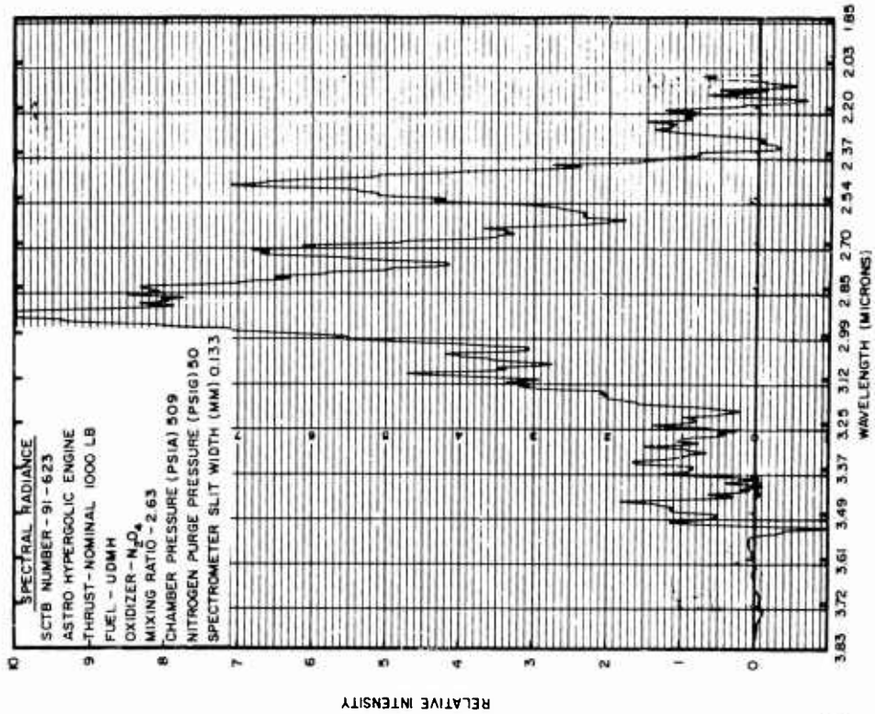
SPECTRAL RADIANCE
SCTB NUMBER - 91-623
ASTRO HYPERGOLIC ENGINE
THRUST - NOMINAL 1000 LB
FUEL - UDMH
OXIDIZER - N_2O_4
MIXING RATIO - 2.63
CHAMBER PRESSURE (PSIA) 509
NITROGEN PURGE PRESSURE (PSIG) 50
SPECTROMETER SLIT WIDTH (MM) 0.133
RELATIVE INTENSITY
WAVELENGTH (MICRONS)
3.83 3.72 3.61 3.49 3.37 3.25 3.12 2.99 2.85 2.70 2.54 2.37 2.20 2.03 1.85

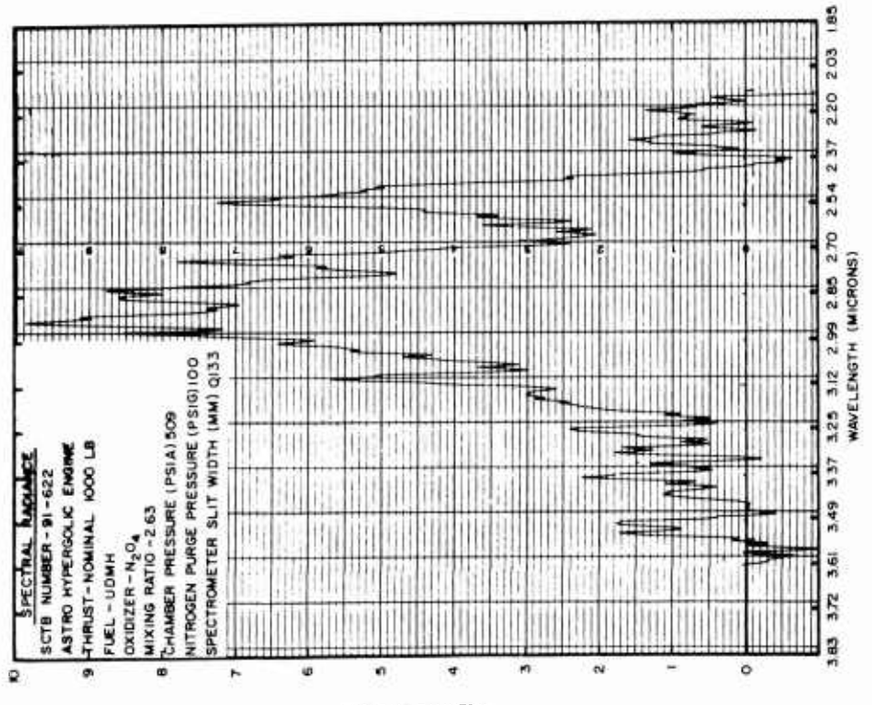
SPECTRAL RADIANCE
SCTB NUMBER - 91-622
ASTRO HYPERGOLIC ENGINE
THRUST - NOMINAL 1000 LB
FUEL - UDMH
OXIDIZER - N_2O_4
MIXING RATIO - 2.63
CHAMBER PRESSURE (PSIA) 509
NITROGEN PURGE PRESSURE (PSIG) 100
SPECTROMETER SLIT WIDTH (MM) 0.133
RELATIVE INTENSITY
WAVELENGTH (MICRONS)
3.83 3.72 3.61 3.49 3.37 3.25 3.12 2.99 2.85 2.70 2.54 2.37 2.20 2.03 1.85

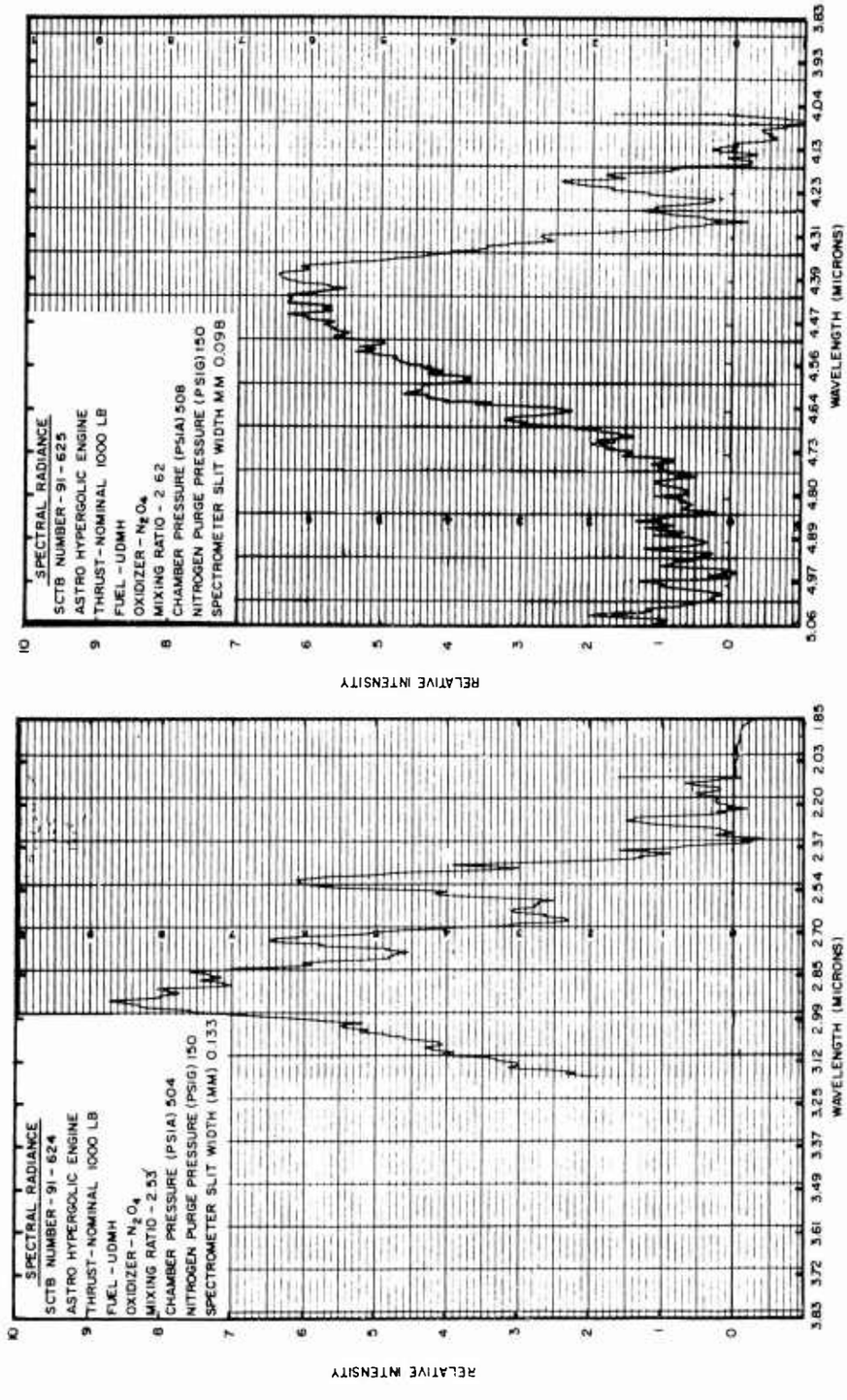
SPECTRAL RADIANCE
SCTB NUMBER - 91 - 624
ASTRO HYPERGOLIC ENGINE
THRUST - NOMINAL 1000 LB
FUEL - UDMH
OXIDIZER - N_2O_4
MIXING RATIO - 2.53
CHAMBER PRESSURE (PSIA) 504
NITROGEN PURGE PRESSURE (PSIG) 150
SPECTROMETER SLIT WIDTH (MM) 0.133
RELATIVE INTENSITY
WAVELENGTH (MICRONS)
3.83 3.72 3.61 3.49 3.37 3.25 3.12 2.99 2.85 2.70 2.54 2.37 2.20 2.03 1.85
SPECTRAL RADIANCE
SCTB NUMBER - 91 - 625
ASTRO HYPERGOLIC ENGINE
THRUST - NOMINAL 1000 LB
FUEL - UDMH
OXIDIZER - N_2O_4
MIXING RATIO - 2.62
CHAMBER PRESSURE (PSIA) 508
NITROGEN PURGE PRESSURE (PSIG) 150
SPECTROMETER SLIT WIDTH MM 0.098
RELATIVE INTENSITY
WAVELENGTH (MICRONS)
5.06 4.97 4.89 4.80 4.73 4.64 4.56 4.47 4.39 4.31 4.23 4.13 4.04 3.93 3.83

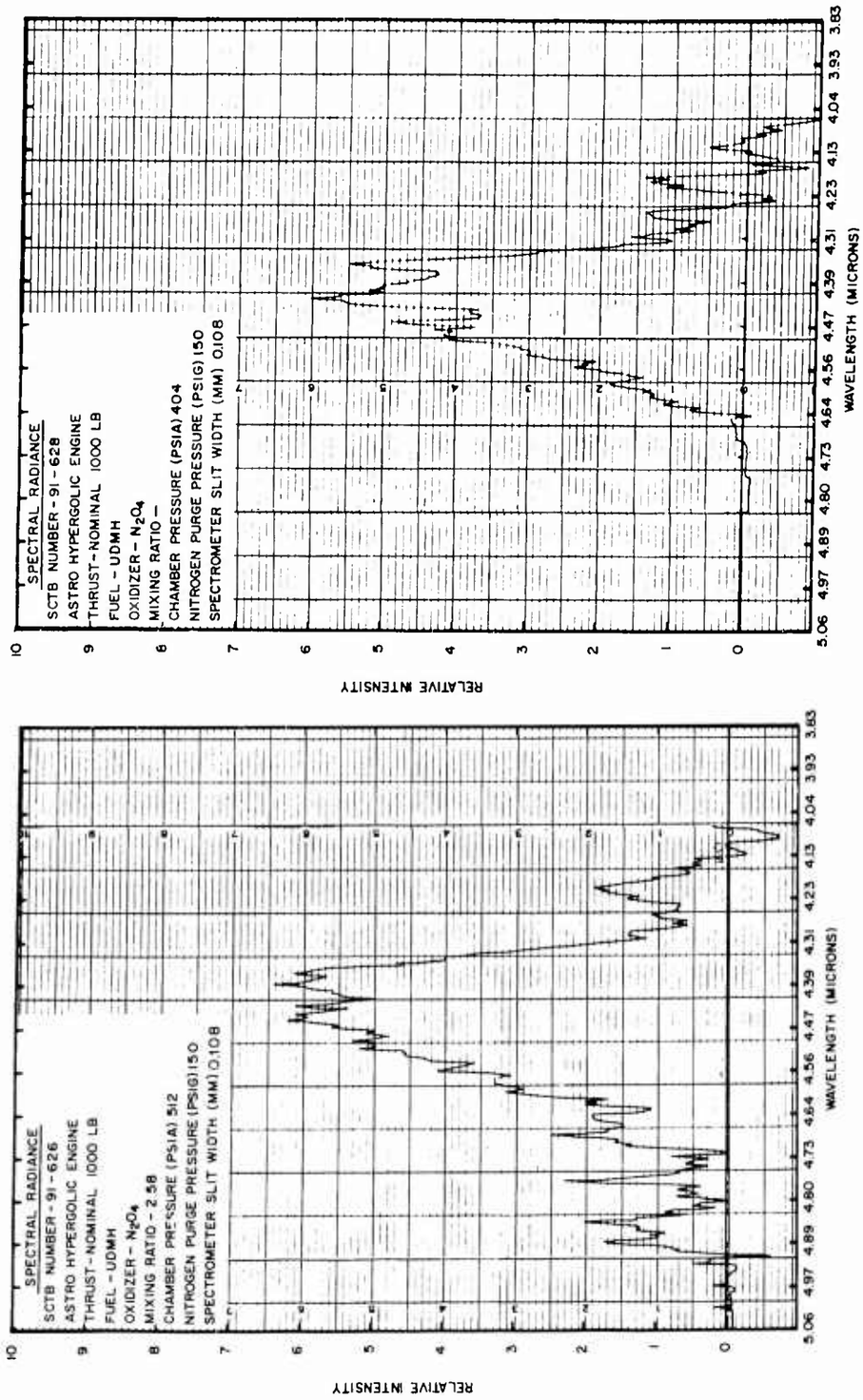
SPECTRAL RADIANCE
SCTB NUMBER - 91 - 626
ASTRO HYPERGOLIC ENGINE
THRUST - NOMINAL 1000 LB
FUEL - UDMH
OXIDIZER - N_2O_4
MIXING RATIO - 2.58
CHAMBER PRESSURE (PSIA) 512
NITROGEN PURGE PRESSURE (PSIG) 150
SPECTROMETER SLIT WIDTH (MM) 0.108
SPECTRAL RADIANCE
SCTB NUMBER - 91 - 628
ASTRO HYPERGOLIC ENGINE
THRUST - NOMINAL 1000 LB
FUEL - UDMH
OXIDIZER - N_2O_4
MIXING RATIO -
CHAMBER PRESSURE (PSIA) 404
NITROGEN PURGE PRESSURE (PSIG) 150
SPECTROMETER SLIT WIDTH (MM) 0.108
RELATIVE INTENSITY
WAVELENGTH (MICRONS)
5.06 4.97 4.89 4.80 4.73 4.64 4.56 4.47 4.39 4.31 4.23 4.13 4.04 3.93 3.83

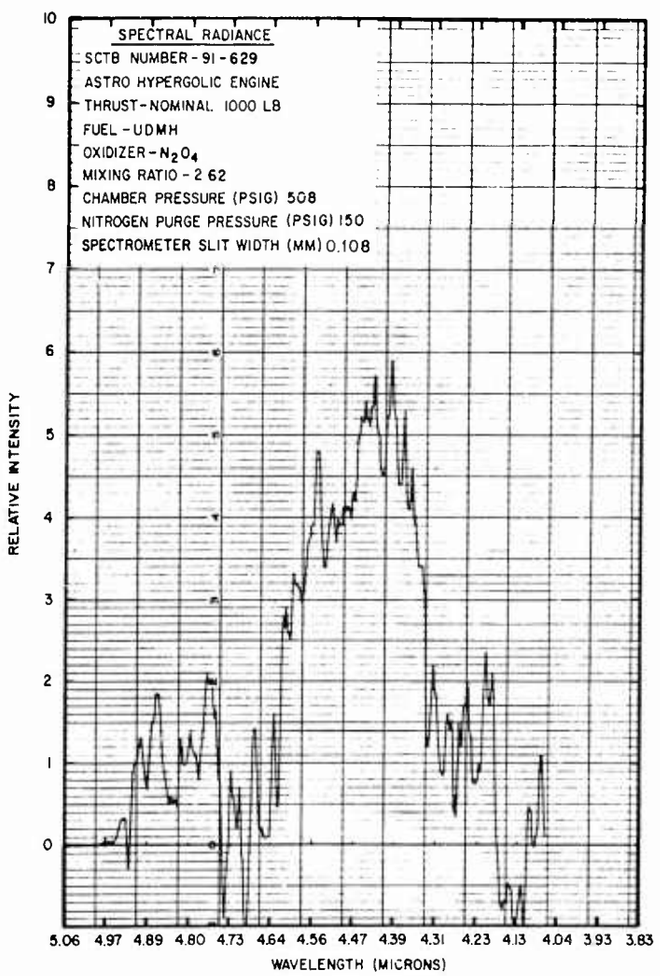
SPECTRAL RADIANCE
SCTB NUMBER - 91 - 629
ASTRO HYPERGOLIC ENGINE
THRUST - NOMINAL 1000 LB
FUEL - UDMH
OXIDIZER - N_2O_4
MIXING RATIO - 2 62
CHAMBER PRESSURE (PSIG) 508
NITROGEN PURGE PRESSURE (PSIG) 150
SPECTROMETER SLIT WIDTH (MM) 0.108
RELATIVE INTENSITY
10
9
8
7
6
5
4
3
2
1
0
5.06 4.97 4.89 4.80 4.73 4.64 4.56 4.47 4.39 4.31 4.23 4.13 4.04 3.93 3.83
WAVELENGTH (MICRONS)

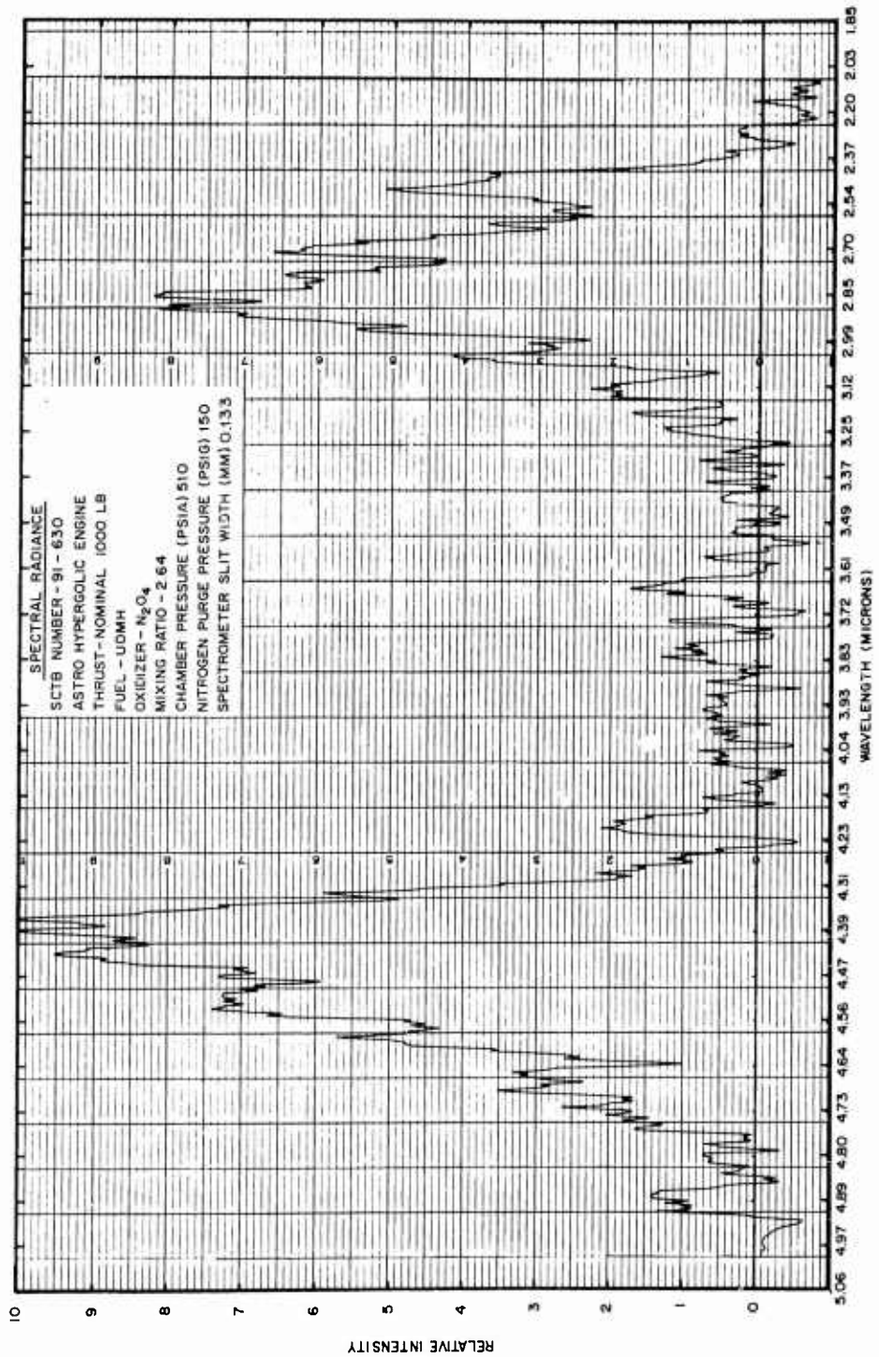
SPECTRAL RADIANCE
SCTB NUMBER - 91 - 630
ASTRO HYPERGOLIC ENGINE
THRUST - NOMINAL 1000 LB
FUEL - UDMH
OXIDIZER - N_2O_4
MIXING RATIO - 2.64
CHAMBER PRESSURE (PSIA) 510
NITROGEN PURGE PRESSURE (PSIG) 150
SPECTROMETER SLIT WIDTH (MM) 0.133
RELATIVE INTENSITY
10
9
8
7
6
5
4
3
2
1
0
5.06 4.97 4.89 4.80 4.73 4.64 4.56 4.47 4.39 4.31 4.23 4.13 4.04 3.93 3.83 3.72 3.61 3.49 3.37 3.25 3.12 2.99 2.85 2.70 2.54 2.37 2.20 2.03 1.85
WAVELENGTH (MICRONS)

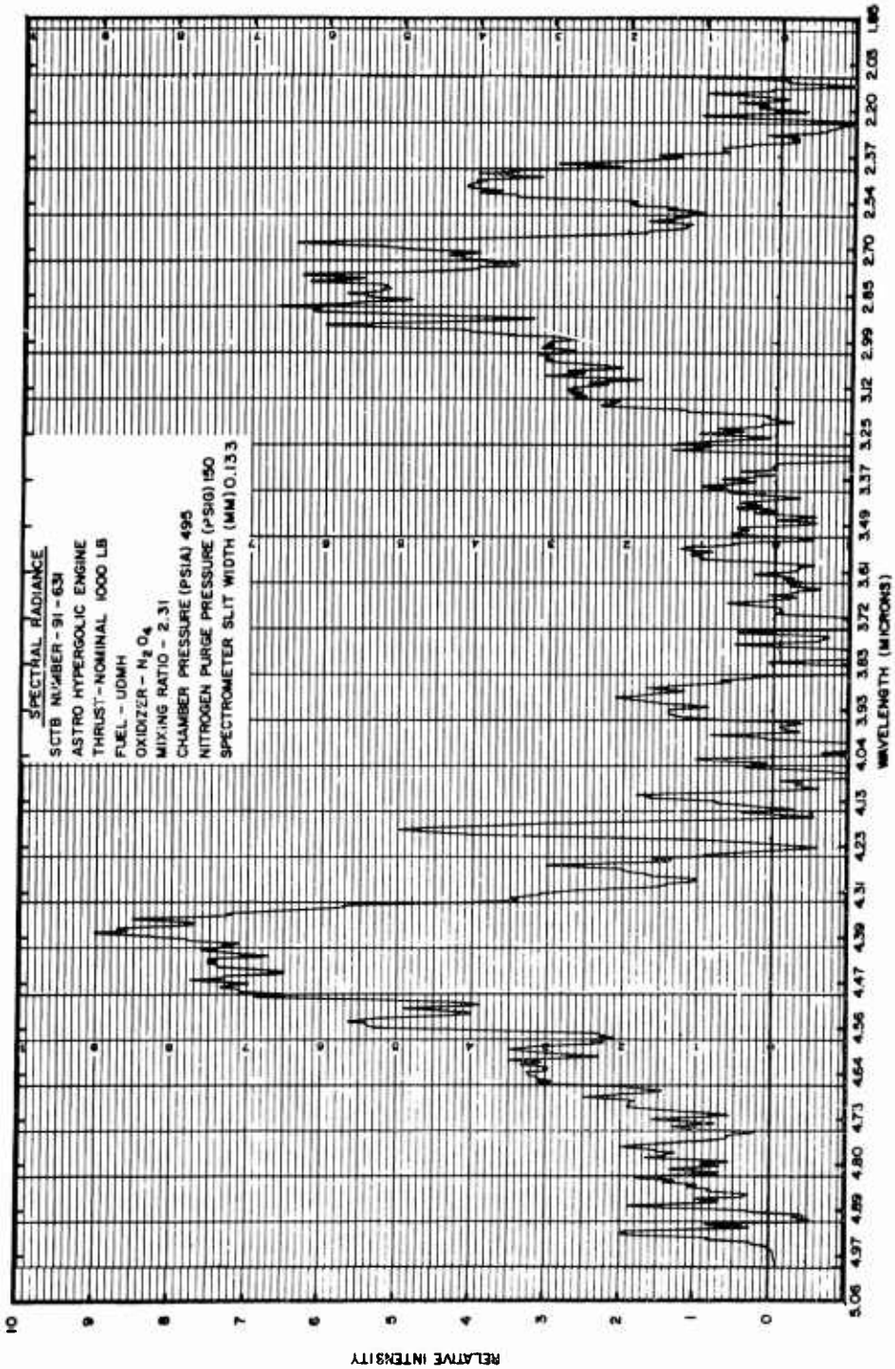
SPECTRAL RADIANCE
SCTB NUMBER - 91 - 631
ASTRO HYPERGOLIC ENGINE
THRUST - NOMINAL 1000 LB
FUEL - UDMH
OXIDIZER - N_2O_4
MIXING RATIO - 2.31
CHAMBER PRESSURE (PSIA) 495
NITROGEN PURGE PRESSURE (PSIG) 150
SPECTROMETER SLIT WIDTH (MM) 0.133
RELATIVE INTENSITY
WAVELENGTH (MICRONS)
10
9
8
7
6
5
4
3
2
1
0
4.97 4.89 4.80 4.73 4.64 4.56 4.47 4.39 4.31 4.23 4.15 4.04 3.93 3.83 3.72 3.61 3.49 3.37 3.25 3.12 2.99 2.85 2.70 2.54 2.37 2.20 2.05 1.86

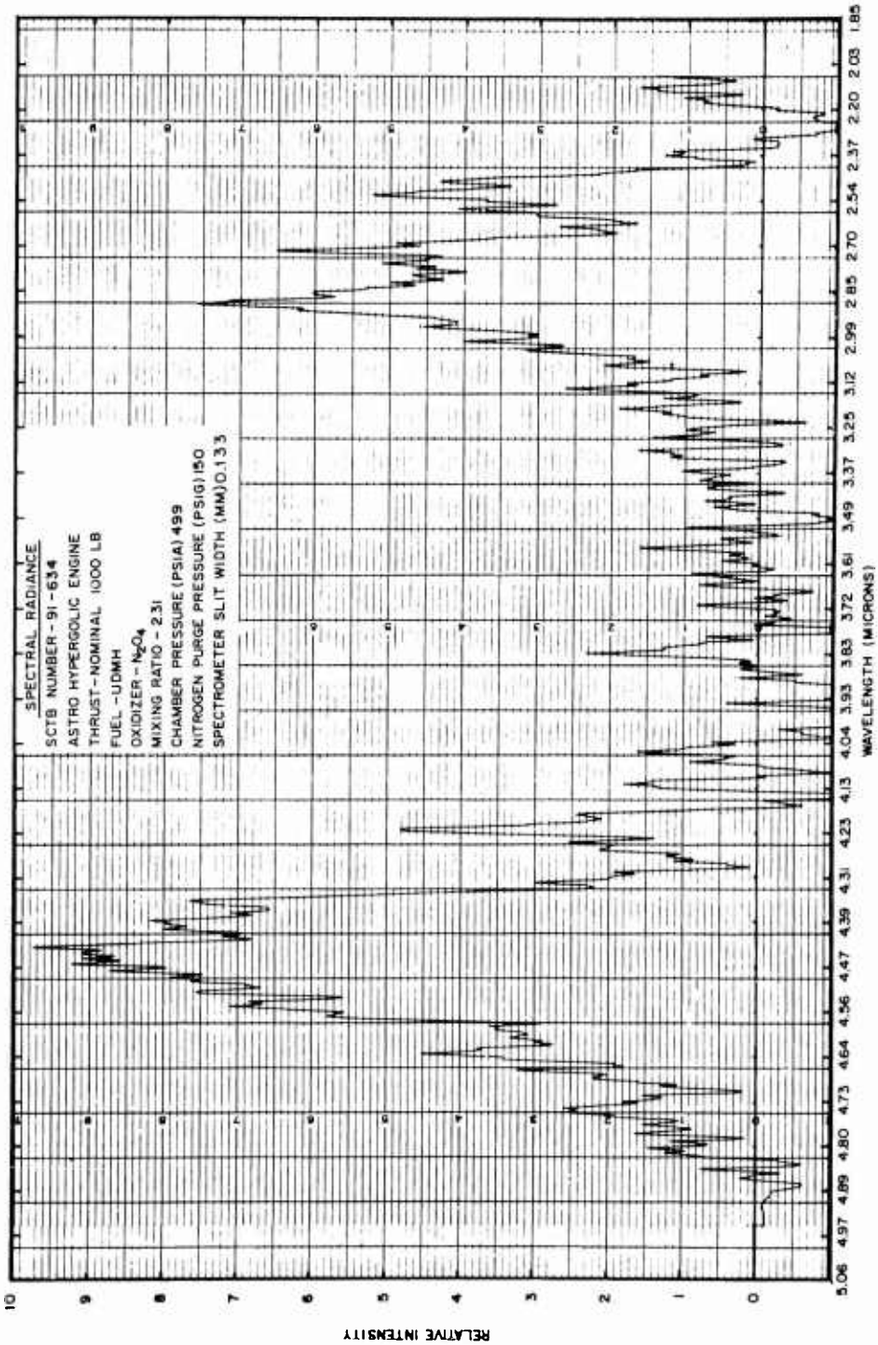
SPECTRAL RADIANCE
SCTB NUMBER - 91-634
ASTRO HYPERGOLIC ENGINE
THRUST - NOMINAL 1000 LB
FUEL - UDMH
OXIDIZER - N_2O_4
MIXING RATIO - 2.31
CHAMBER PRESSURE (PSIA) 499
NITROGEN PURGE PRESSURE (PSIG) 150
SPECTROMETER SLIT WIDTH (MM) 0.133
RELATIVE INTENSITY
WAVELENGTH (MICRONS)
10
9
8
7
6
5
4
3
2
1
0
5.06 4.97 4.89 4.80 4.73 4.64 4.56 4.47 4.39 4.31 4.23 4.13 4.04 3.93 3.83 3.72 3.61 3.49 3.37 3.25 3.12 2.99 2.85 2.70 2.54 2.37 2.20 2.03 1.85

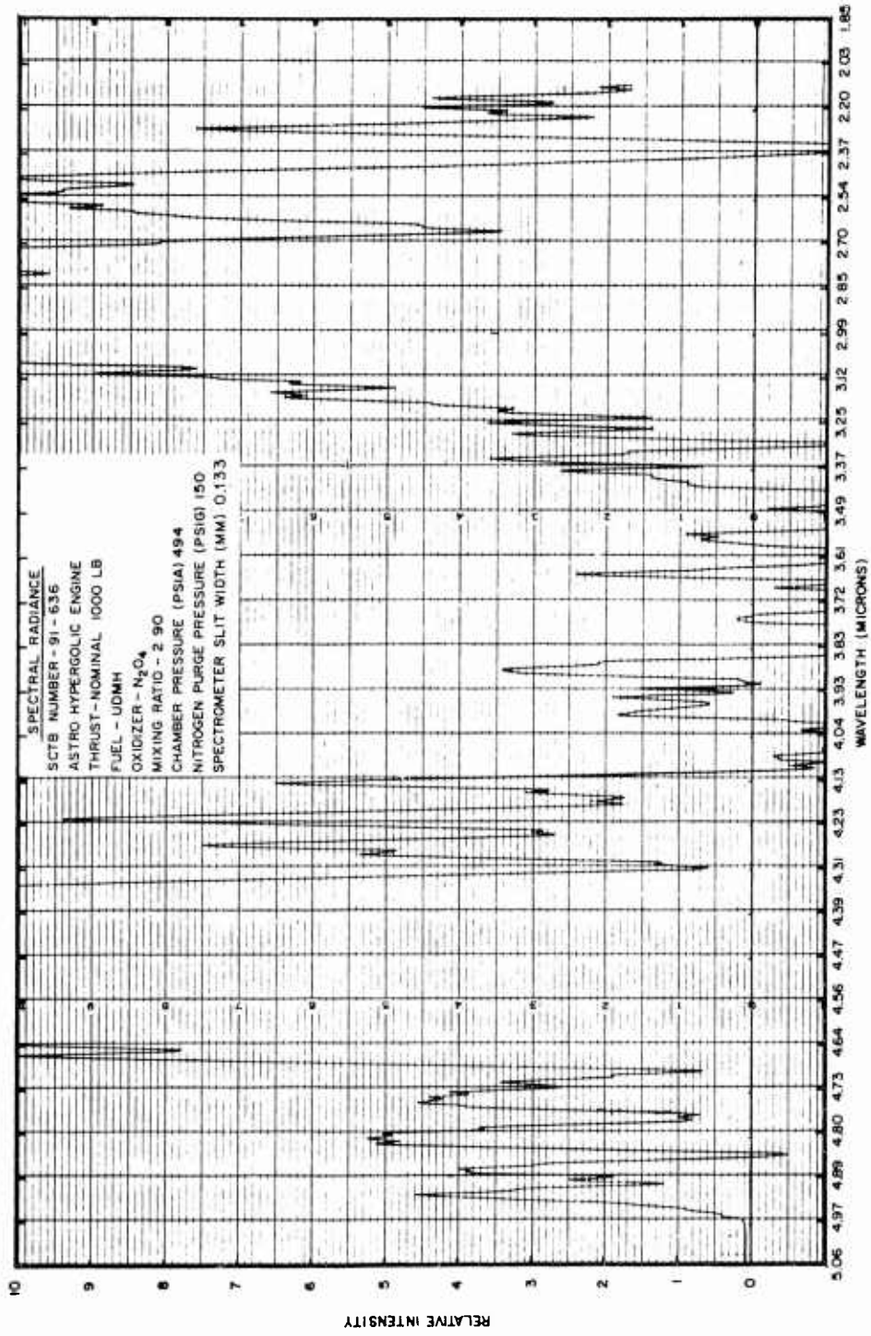
SPECTRAL RADIANCE
SCTB NUMBER - 91-636
ASTRO HYPERGOLIC ENGINE
THRUST - NOMINAL 1000 LB
FUEL - UDMH
OXIDIZER - N_2O_4
MIXING RATIO - 2.90
CHAMBER PRESSURE (PSIA) 494
NITROGEN PURGE PRESSURE (PSIG) 150
SPECTROMETER SLIT WIDTH (MM) 0.133
RELATIVE INTENSITY
10
9
8
7
6
5
4
3
2
1
0
5.06 4.97 4.89 4.80 4.73 4.64 4.56 4.47 4.39 4.31 4.23 4.13 4.04 3.93 3.83 3.72 3.61 3.49 3.37 3.25 3.12 2.99 2.85 2.70 2.54 2.37 2.20 2.03 1.85
WAVELENGTH (MICRONS)

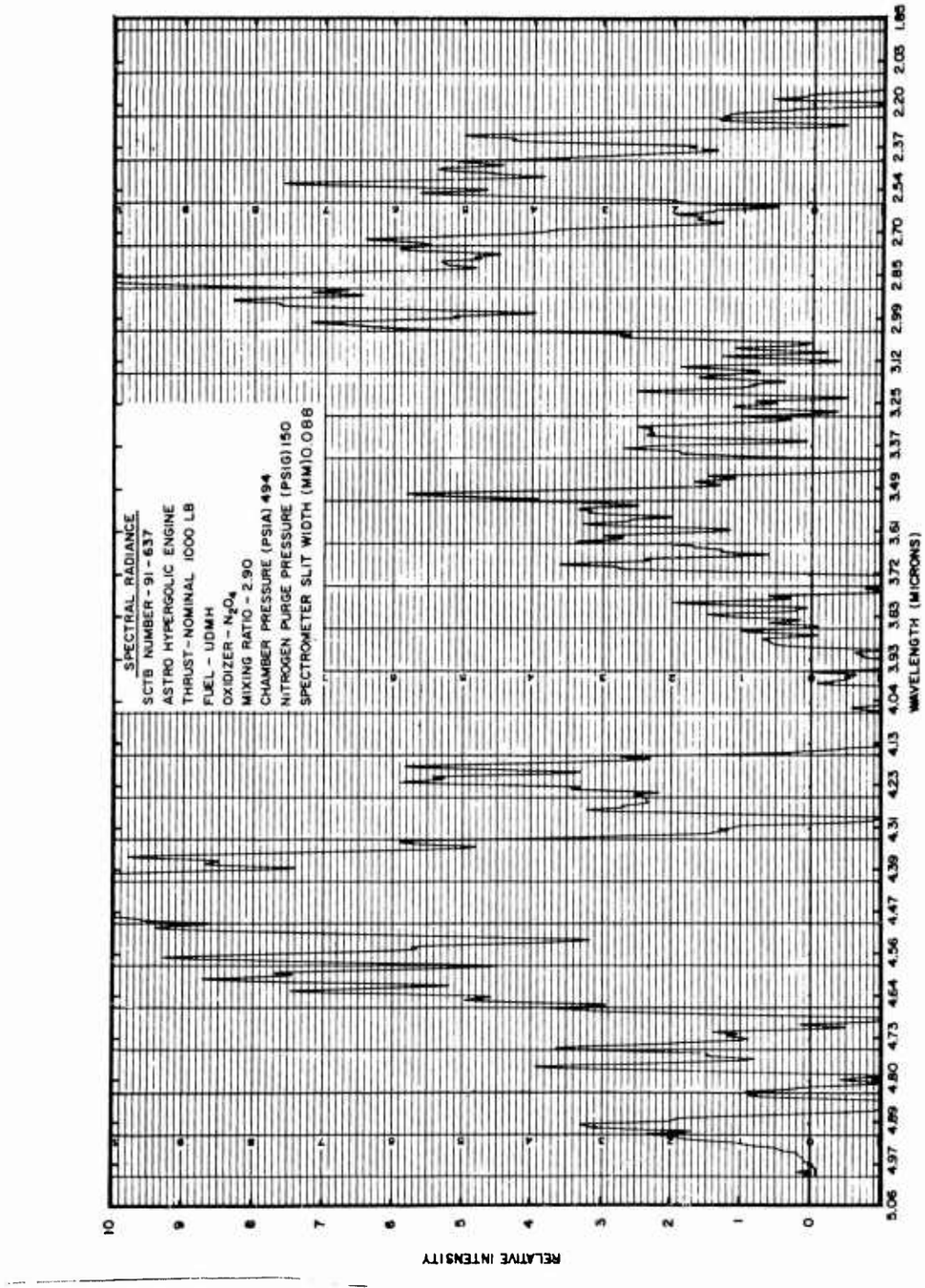
SPECTRAL RADIANCE
SCTB NUMBER - 91 - 637
ASTRO HYPERGOLIC ENGINE
THRUST - NOMINAL 1000 LB
FUEL - UDMH
OXIDIZER - N_2O_4
MIXING RATIO - 2.90
CHAMBER PRESSURE (PSIA) 494
NITROGEN PURGE PRESSURE (PSIG) 150
SPECTROMETER SLIT WIDTH (MM) 0.088
RELATIVE INTENSITY
WAVELENGTH (MICRONS)

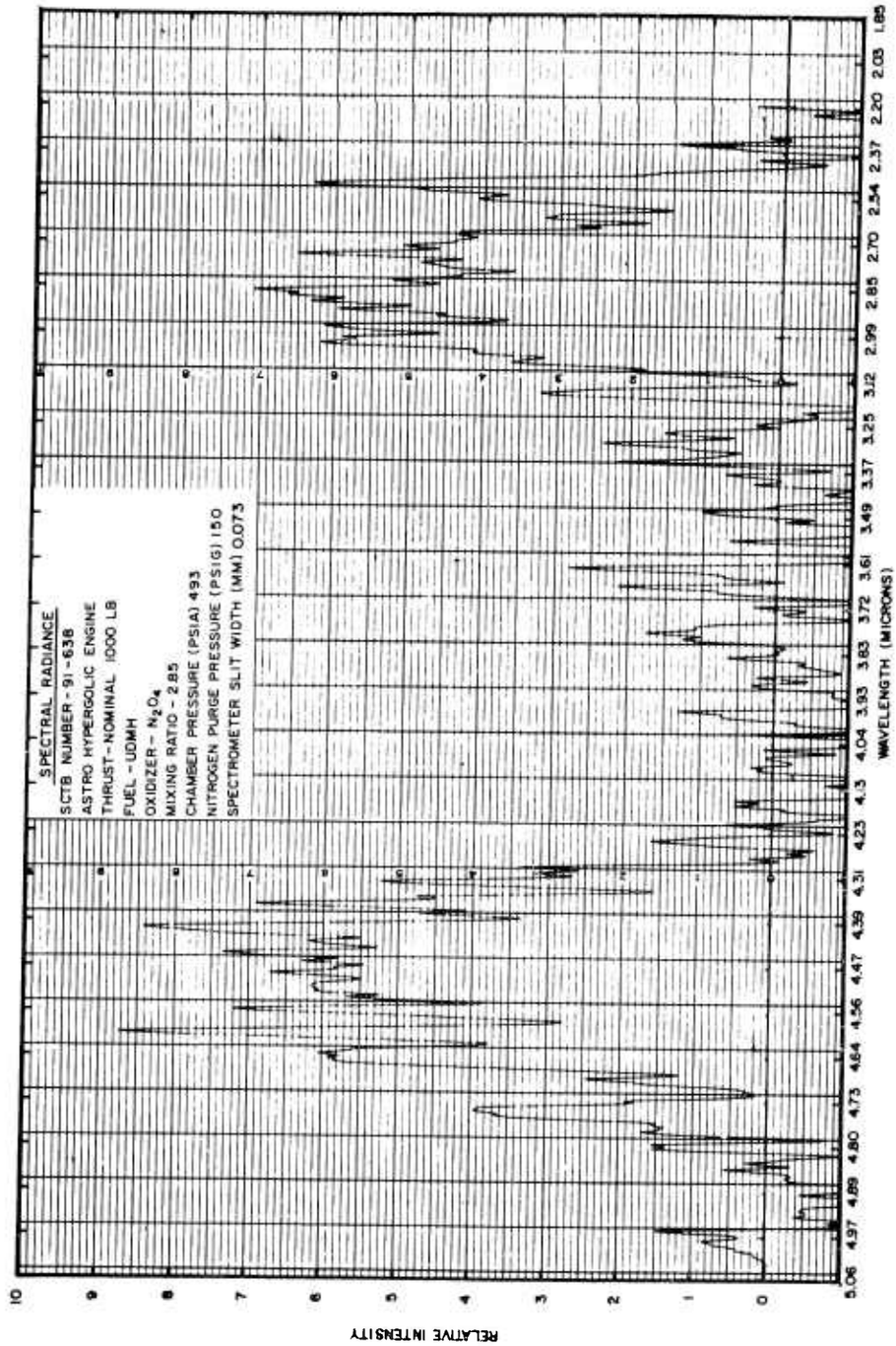
SPECTRAL RADIANCE
SCTB NUMBER - 91-638
ASTRO HYPERGOLIC ENGINE
THRUST-NOMINAL 1000 LB
FUEL - UDMH
OXIDIZER - N_2O_4
MIXING RATIO - 2.85
CHAMBER PRESSURE (PSIA) 493
NITROGEN PURGE PRESSURE (PSIG) 150
SPECTROMETER SLIT WIDTH (MM) 0.073
RELATIVE INTENSITY
WAVELENGTH (MICRONS)
10
9
8
7
6
5
4
3
2
1
0
5.06 4.97 4.89 4.80 4.73 4.64 4.56 4.47 4.39 4.31 4.23 4.3 4.04 3.93 3.83 3.72 3.61 3.49 3.37 3.25 3.12 2.99 2.85 2.70 2.54 2.37 2.20 2.03 1.85

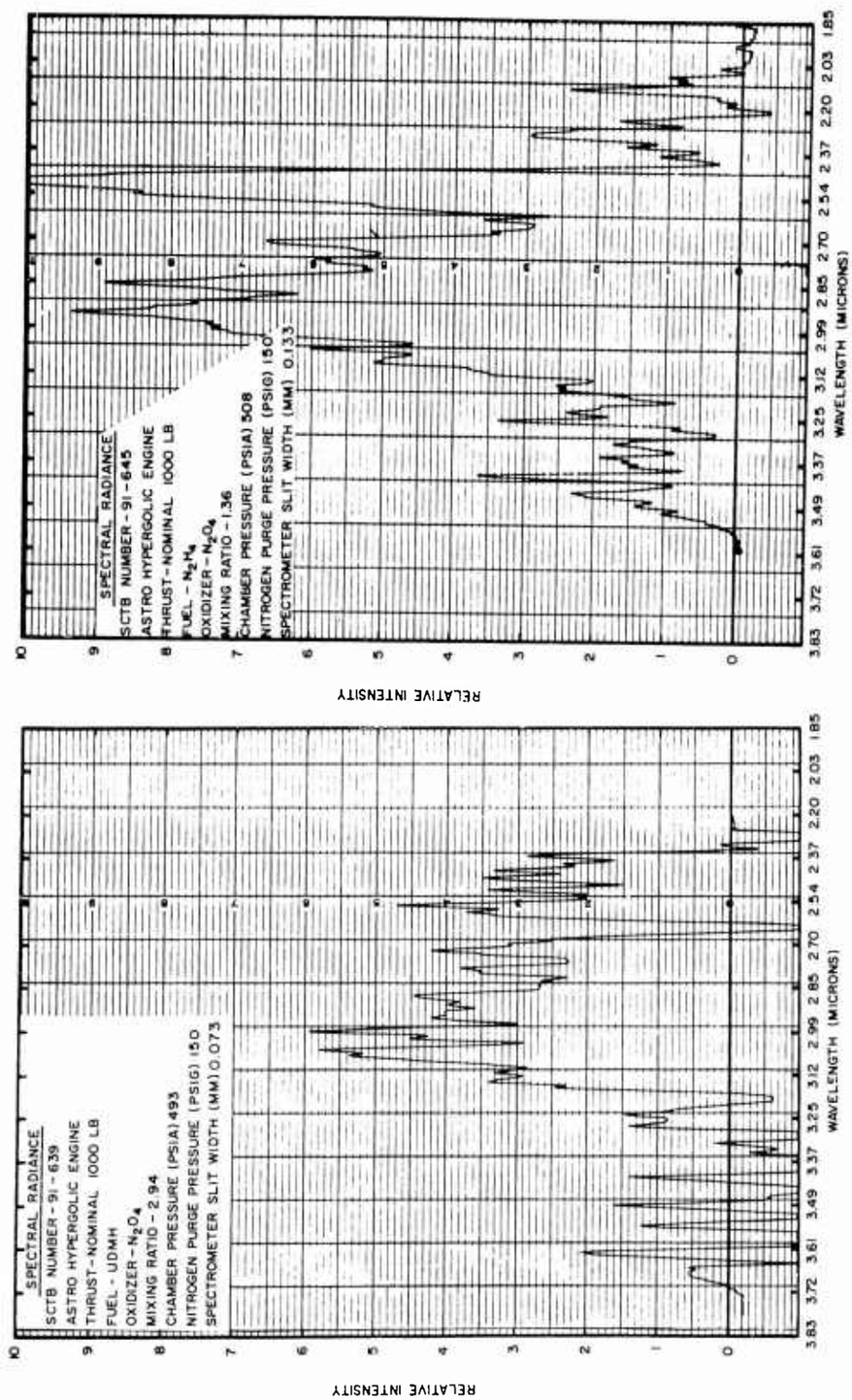
SPECTRAL RADIANCE
SCTB NUMBER - 91 - 645
ASTRO HYPERGOLIC ENGINE
THRUST - NOMINAL 1000 LB
FUEL - N_2H_4
OXIDIZER - N_2O_4
MIXING RATIO - 1.36
CHAMBER PRESSURE (PSIA) 508
NITROGEN PURGE PRESSURE (PSIG) 150
SPECTROMETER SLIT WIDTH (MM) 0.133
RELATIVE INTENSITY
WAVELENGTH (MICRONS)
SPECTRAL RADIANCE
SCTB NUMBER - 91 - 639
ASTRO HYPERGOLIC ENGINE
THRUST - NOMINAL 1000 LB
FUEL - UDMH
OXIDIZER - N_2O_4
MIXING RATIO - 2.94
CHAMBER PRESSURE (PSIA) 493
NITROGEN PURGE PRESSURE (PSIG) 150
SPECTROMETER SLIT WIDTH (MM) 0.073
RELATIVE INTENSITY
WAVELENGTH (MICRONS)

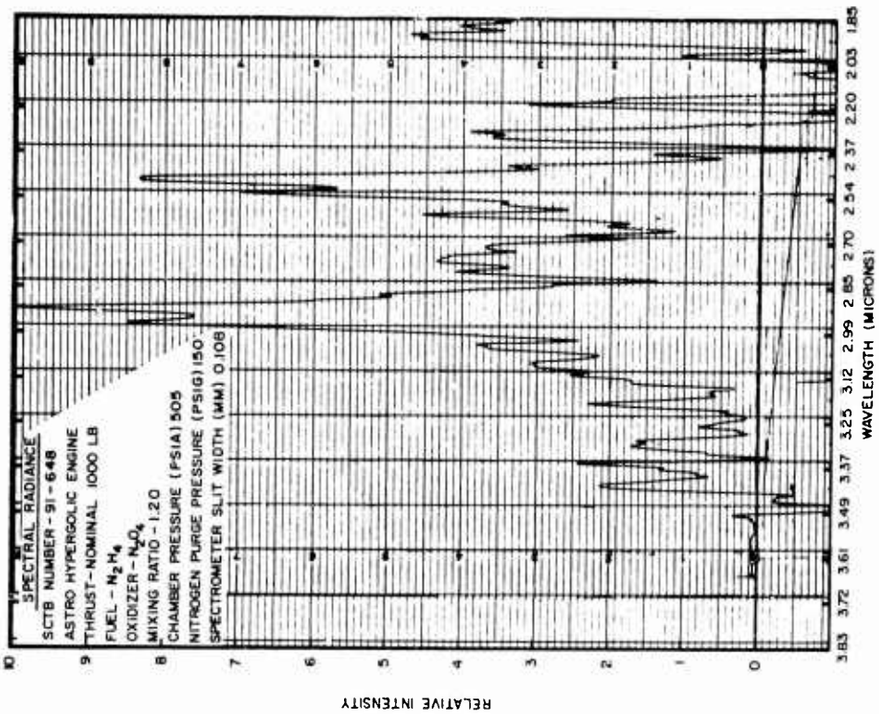
SPECTRAL RADIANCE
SCTB NUMBER - 91 - 648
ASTRO HYPERGOLIC ENGINE
THRUST - NOMINAL 1000 LB
FUEL - N_2H_4
OXIDIZER - N_2O_4
MIXING RATIO - 1.20
CHAMBER PRESSURE (PSIA) 505
NITROGEN PURGE PRESSURE (PSIG) 150
SPECTROMETER SLIT WIDTH (MM) 0.108
RELATIVE INTENSITY
WAVELENGTH (MICRONS)
3.83 3.72 3.61 3.49 3.37 3.25 3.12 2.99 2.85 2.70 2.54 2.37 2.20 2.03 1.85

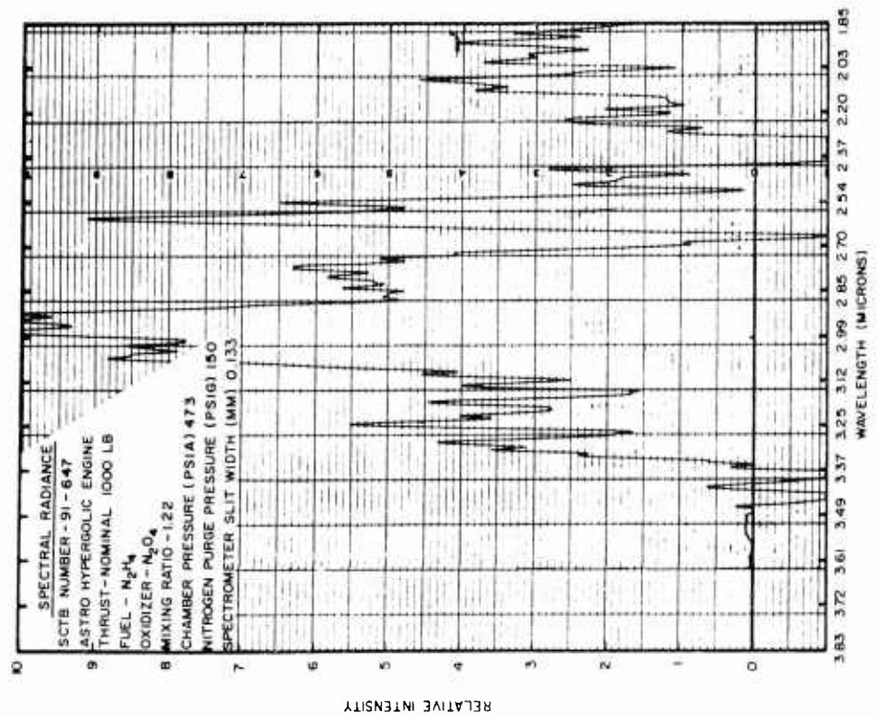
SPECTRAL RADIANCE
SCTB NUMBER - 91 - 647
ASTRO HYPERGOLIC ENGINE
THRUST - NOMINAL 1000 LB
FUEL - N_2H_4
OXIDIZER - N_2O_4
MIXING RATIO - 1.22
CHAMBER PRESSURE (PSIA) 473
NITROGEN PURGE PRESSURE (PSIG) 150
SPECTROMETER SLIT WIDTH (MM) 0.133
RELATIVE INTENSITY
WAVELENGTH (MICRONS)
3.83 3.72 3.61 3.49 3.37 3.25 3.12 2.99 2.85 2.70 2.54 2.37 2.20 2.03 1.85

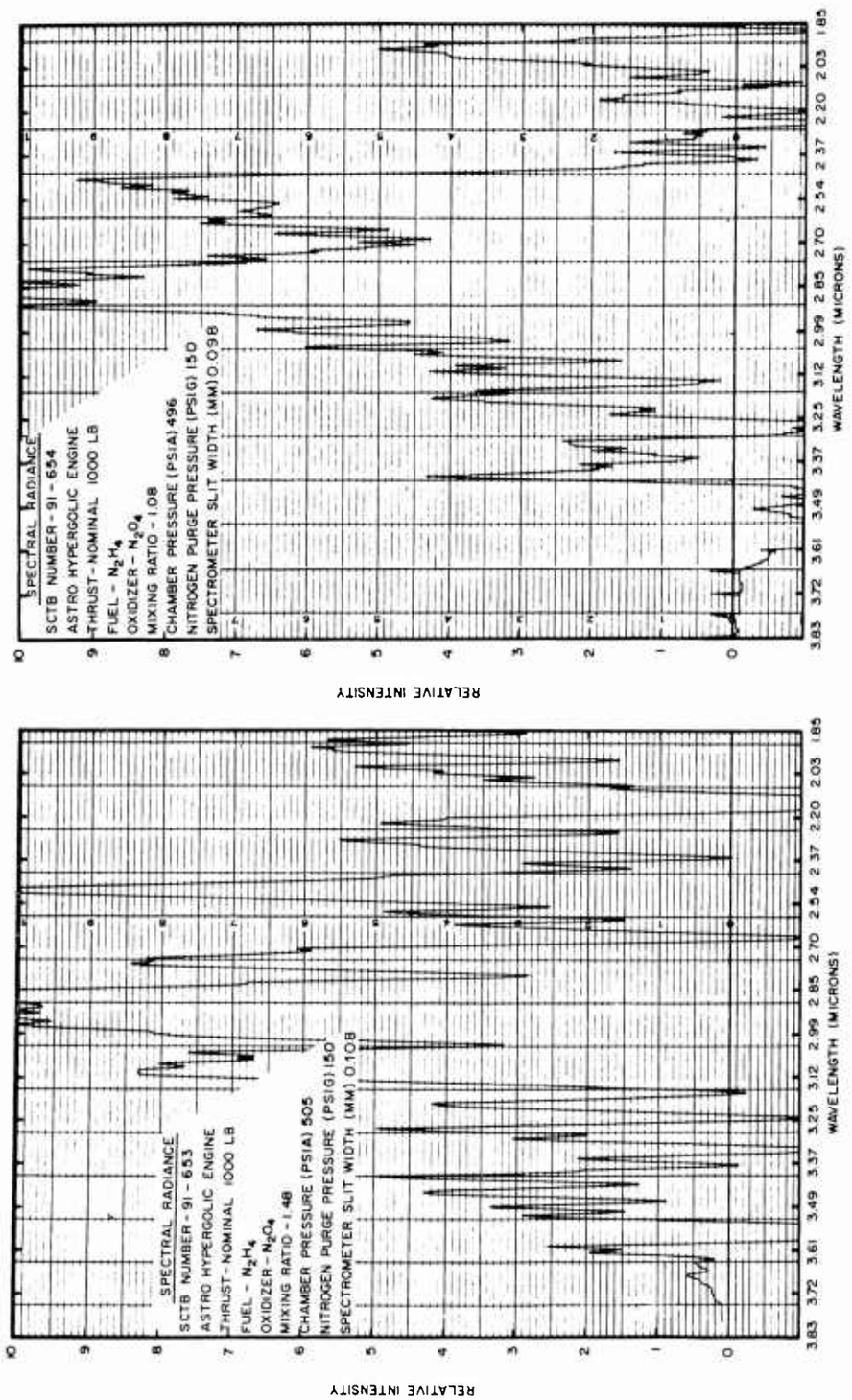
SPECTRAL RADIANCE
SCTB NUMBER - 91 - 654
ASTRO HYPERGOLIC ENGINE
THRUST - NOMINAL 1000 LB
FUEL - N_2H_4
OXIDIZER - N_2O_4
MIXING RATIO - 1.08
CHAMBER PRESSURE (PSIA) 496
NITROGEN PURGE PRESSURE (PSIG) 150
SPECTROMETER SLIT WIDTH (MM) 0.098
RELATIVE INTENSITY
WAVELENGTH (MICRONS)
3.83 3.72 3.61 3.49 3.37 3.25 3.12 2.99 2.85 2.70 2.54 2.37 2.20 2.03 1.85
SPECTRAL RADIANCE
SCTB NUMBER - 91 - 653
ASTRO HYPERGOLIC ENGINE
THRUST - NOMINAL 1000 LB
FUEL - N_2H_4
OXIDIZER - N_2O_4
MIXING RATIO - 1.48
CHAMBER PRESSURE (PSIA) 505
NITROGEN PURGE PRESSURE (PSIG) 150
SPECTROMETER SLIT WIDTH (MM) 0.108
RELATIVE INTENSITY
WAVELENGTH (MICRONS)
3.83 3.72 3.61 3.49 3.37 3.25 3.12 2.99 2.85 2.70 2.54 2.37 2.20 2.03 1.85

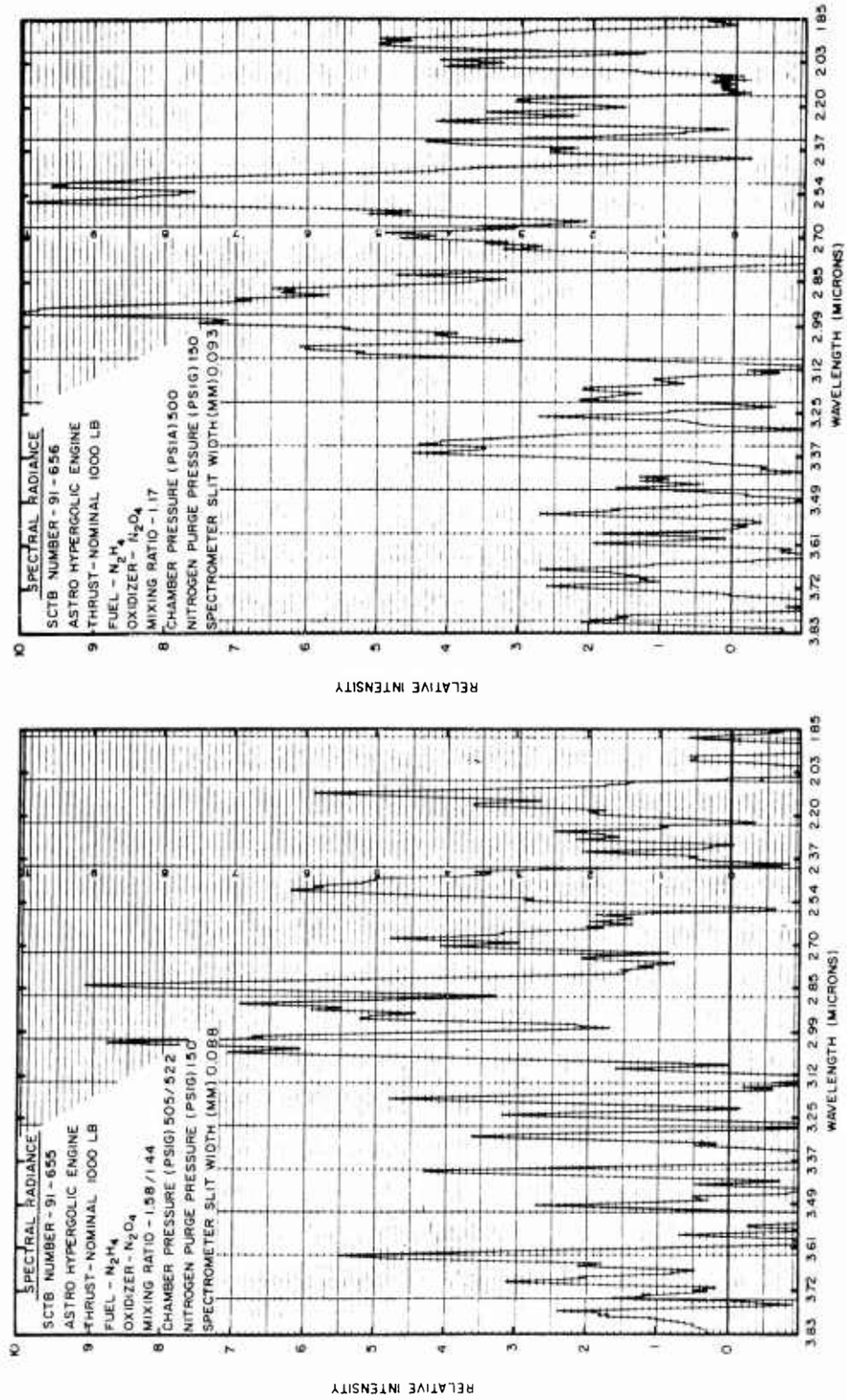
SPECTRAL RADIANCE
SCTB NUMBER - 91 - 655
ASTRO HYPERGOLIC ENGINE
THRUST - NOMINAL 1000 LB
FUEL - N_2H_4
OXIDIZER - N_2O_4
MIXING RATIO - 1.58 / 1.44
CHAMBER PRESSURE (PSIG) 505/522
NITROGEN PURGE PRESSURE (PSIG) 150
SPECTROMETER SLIT WIDTH (MM) 0.088
SPECTRAL RADIANCE
SCTB NUMBER - 91 - 656
ASTRO HYPERGOLIC ENGINE
THRUST - NOMINAL 1000 LB
FUEL - N_2H_4
OXIDIZER - N_2O_4
MIXING RATIO - 1.17
CHAMBER PRESSURE (PSIA) 500
NITROGEN PURGE PRESSURE (PSIG) 150
SPECTROMETER SLIT WIDTH (MM) 0.093
RELATIVE INTENSITY
WAVELENGTH (MICRONS)
3.83 3.72 3.61 3.49 3.37 3.25 3.12 2.99 2.85 2.70 2.54 2.37 2.20 2.03 1.85

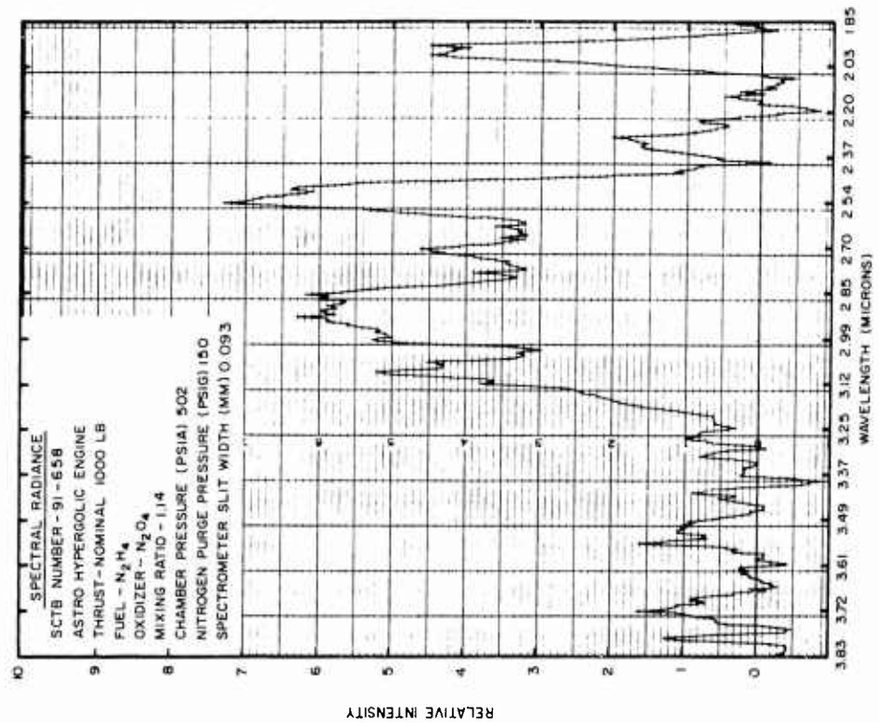
SPECTRAL RADIANCE
SCTB NUMBER - 91-658
ASTRO HYPERGOLIC ENGINE
THRUST - NOMINAL 1000 LB
FUEL - N_2H_4
OXIDIZER - N_2O_4
MIXING RATIO - 1.14
CHAMBER PRESSURE (PSIA) 502
NITROGEN PURGE PRESSURE (PSIG) 150
SPECTROMETER SLIT WIDTH (MM) 0.093
RELATIVE INTENSITY
WAVELENGTH (MICRONS)
3.83 3.72 3.61 3.49 3.37 3.25 3.12 2.99 2.85 2.70 2.54 2.37 2.20 2.03 1.85

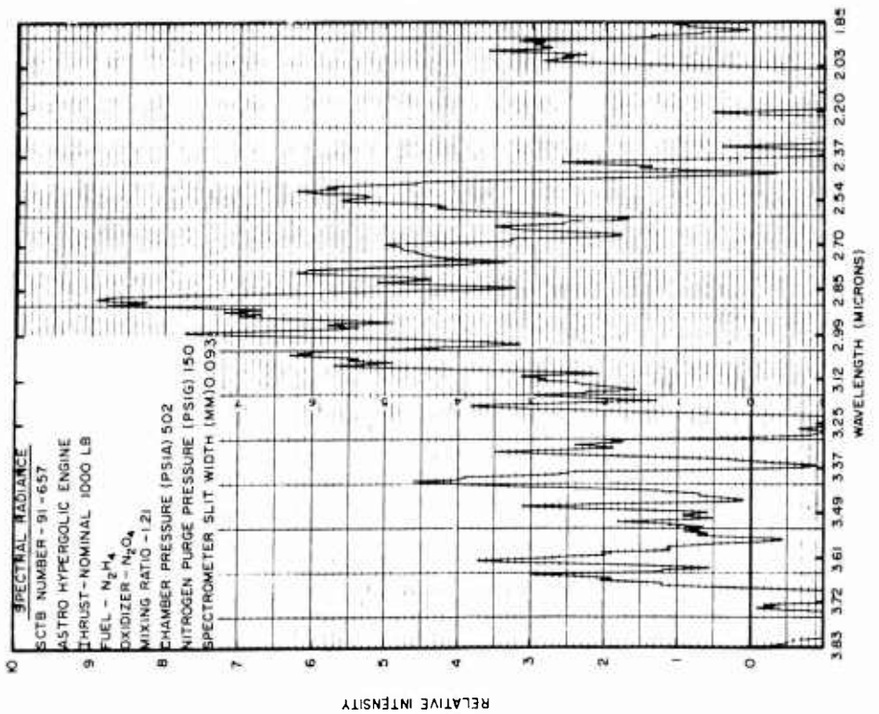
SPECTRAL RADIANCE
SCTB NUMBER - 91-657
ASTRO HYPERGOLIC ENGINE
THRUST - NOMINAL 1000 LB
FUEL - N_2H_4
OXIDIZER - N_2O_4
MIXING RATIO - 1.21
CHAMBER PRESSURE (PSIA) 502
NITROGEN PURGE PRESSURE (PSIG) 150
SPECTROMETER SLIT WIDTH (MM) 0.093
RELATIVE INTENSITY
WAVELENGTH (MICRONS)
3.83 3.72 3.61 3.49 3.37 3.25 3.12 2.99 2.85 2.70 2.54 2.37 2.20 2.03 1.85

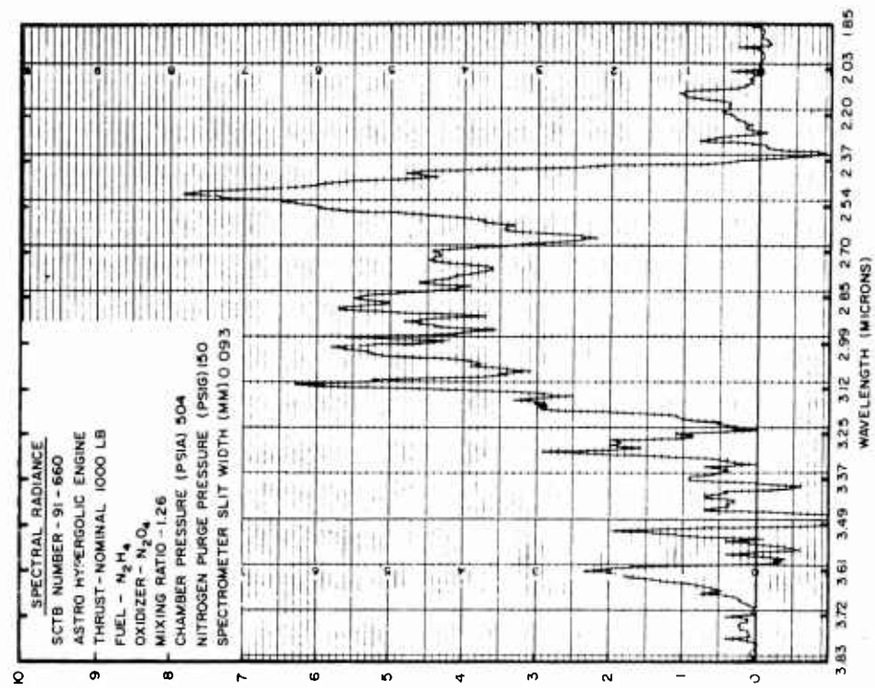
SPECTRAL RADIANCE
SCTB NUMBER - 91 - 660
ASTRO HYPERGOLIC ENGINE
THRUST - NOMINAL 1000 LB
FUEL - N_2H_4
OXIDIZER - N_2O_4
MIXING RATIO - 1.26
CHAMBER PRESSURE (PSIA) 504
NITROGEN PURGE PRESSURE (PSIG) 150
SPECTROMETER SLIT WIDTH (MM) 0.093
RELATIVE INTENSITY
WAVELENGTH (MICRONS)
3.83 3.72 3.61 3.49 3.37 3.25 3.12 2.99 2.85 2.70 2.54 2.37 2.20 2.03 1.85

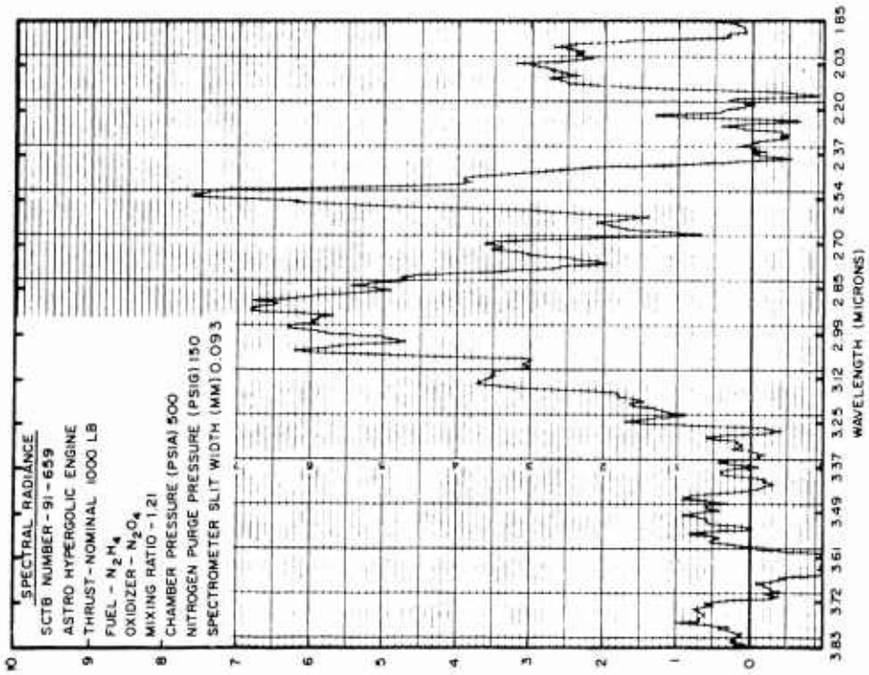
SPECTRAL RADIANCE
SCTB NUMBER - 91 - 659
ASTRO HYPERGOLIC ENGINE
THRUST - NOMINAL 1000 LB
FUEL - N_2H_4
OXIDIZER - N_2O_4
MIXING RATIO - 1.21
CHAMBER PRESSURE (PSIA) 500
NITROGEN PURGE PRESSURE (PSIG) 150
SPECTROMETER SLIT WIDTH (MM) 0.093
RELATIVE INTENSITY
WAVELENGTH (MICRONS)
3.83 3.72 3.61 3.49 3.37 3.25 3.12 2.99 2.85 2.70 2.54 2.37 2.20 2.03 1.85

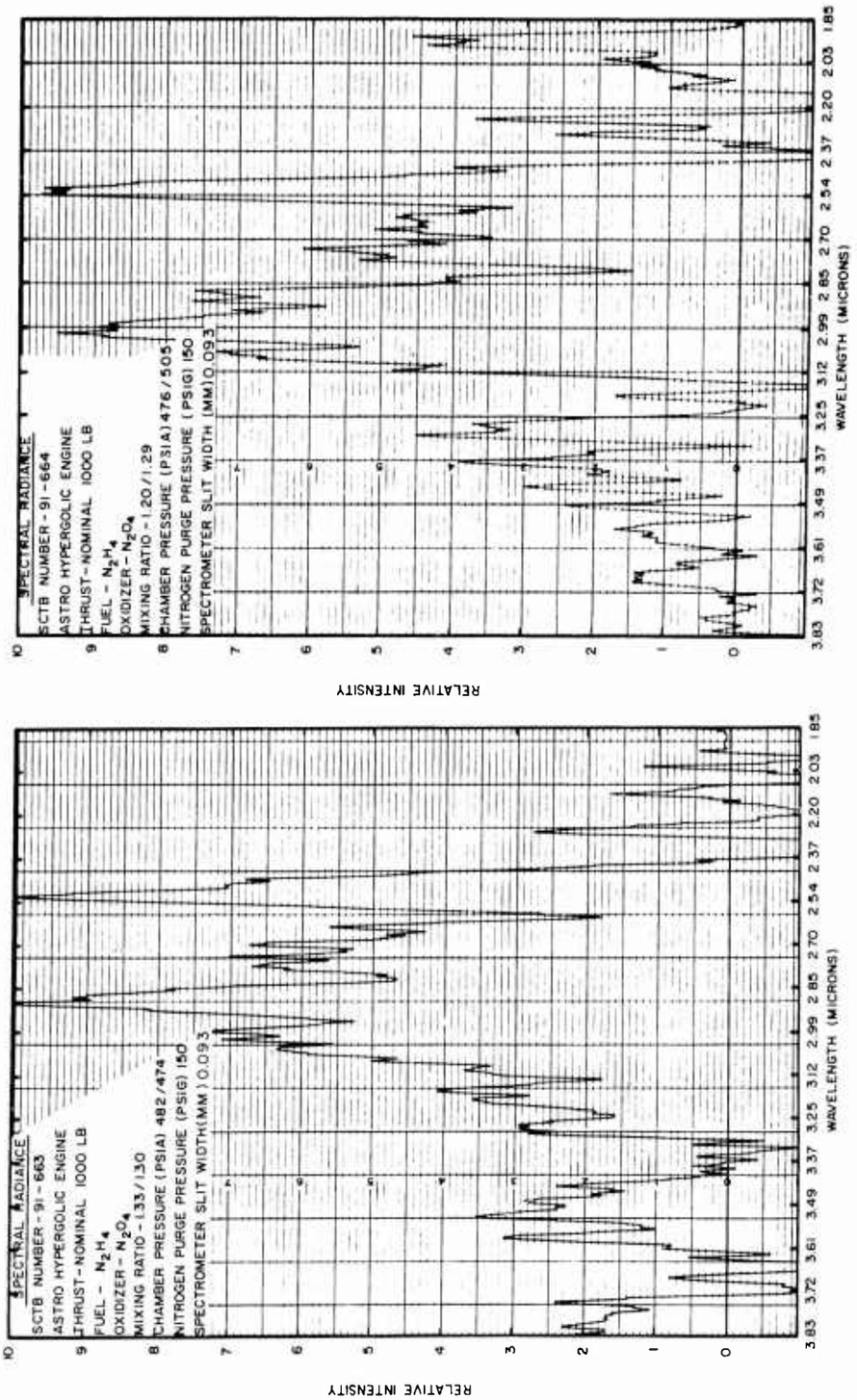
SPECTRAL RADIANCE
SCTB NUMBER - 91 - 664
ASTRO HYPERGOLIC ENGINE
THRUST - NOMINAL 1000 LB
FUEL - N_2H_4
OXIDIZER - N_2O_4
MIXING RATIO - 1.20 / 1.29
CHAMBER PRESSURE (PSIA) 476 / 505
NITROGEN PURGE PRESSURE (PSIG) 150
SPECTROMETER SLIT WIDTH (MM) 0.093
RELATIVE INTENSITY
WAVELENGTH (MICRONS)
3.83 3.72 3.61 3.49 3.37 3.25 3.12 2.99 2.85 2.70 2.54 2.37 2.20 2.03 1.85
SPECTRAL RADIANCE
SCTB NUMBER - 91 - 663
ASTRO HYPERGOLIC ENGINE
THRUST - NOMINAL 1000 LB
FUEL - N_2H_4
OXIDIZER - N_2O_4
MIXING RATIO - 1.33 / 1.30
CHAMBER PRESSURE (PSIA) 482 / 474
NITROGEN PURGE PRESSURE (PSIG) 150
SPECTROMETER SLIT WIDTH (MM) 0.093
RELATIVE INTENSITY
WAVELENGTH (MICRONS)
3.83 3.72 3.61 3.49 3.37 3.25 3.12 2.99 2.85 2.70 2.54 2.37 2.20 2.03 1.85

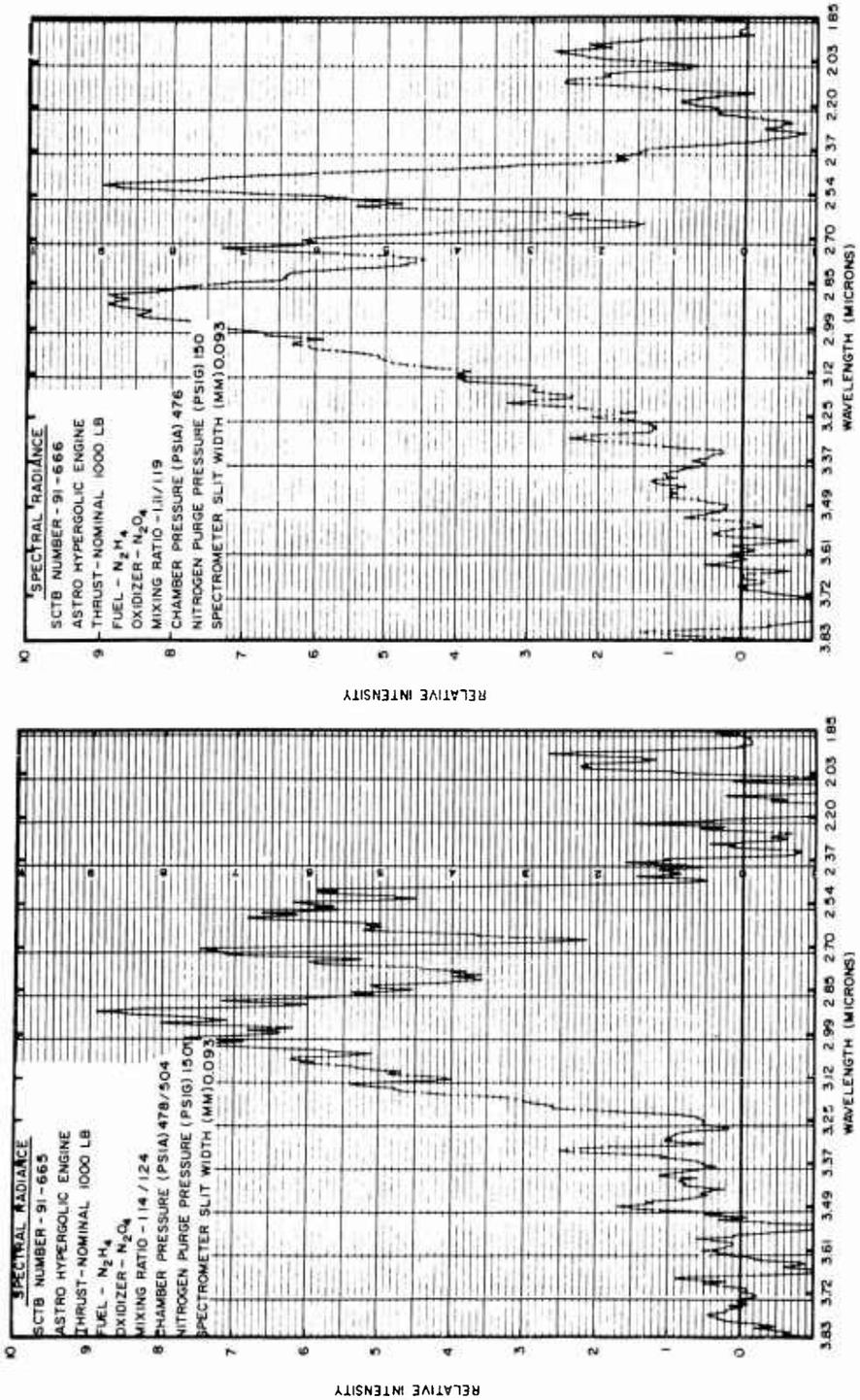
SPECTRAL RADIANCE
SCTB NUMBER - 91-665
ASTRO HYPERGOLIC ENGINE
THRUST - NOMINAL 1000 LB
FUEL - N_2H_4
OXIDIZER - N_2O_4
MIXING RATIO - 1.14 / 1.24
CHAMBER PRESSURE (PSIA) 478/504
NITROGEN PURGE PRESSURE (PSIG) 150
SPECTROMETER SLIT WIDTH (MM) 0.093
RELATIVE INTENSITY
WAVELENGTH (MICRONS)
3.83 3.72 3.61 3.49 3.37 3.25 3.12 2.99 2.85 2.70 2.54 2.37 2.20 2.03 1.85
SPECTRAL RADIANCE
SCTB NUMBER - 91-666
ASTRO HYPERGOLIC ENGINE
THRUST - NOMINAL 1000 LB
FUEL - N_2H_4
OXIDIZER - N_2O_4
MIXING RATIO - 1.11 / 1.19
CHAMBER PRESSURE (PSIA) 476
NITROGEN PURGE PRESSURE (PSIG) 150
SPECTROMETER SLIT WIDTH (MM) 0.093
RELATIVE INTENSITY
WAVELENGTH (MICRONS)
3.83 3.72 3.61 3.49 3.37 3.25 3.12 2.99 2.85 2.70 2.54 2.37 2.20 2.03 1.85

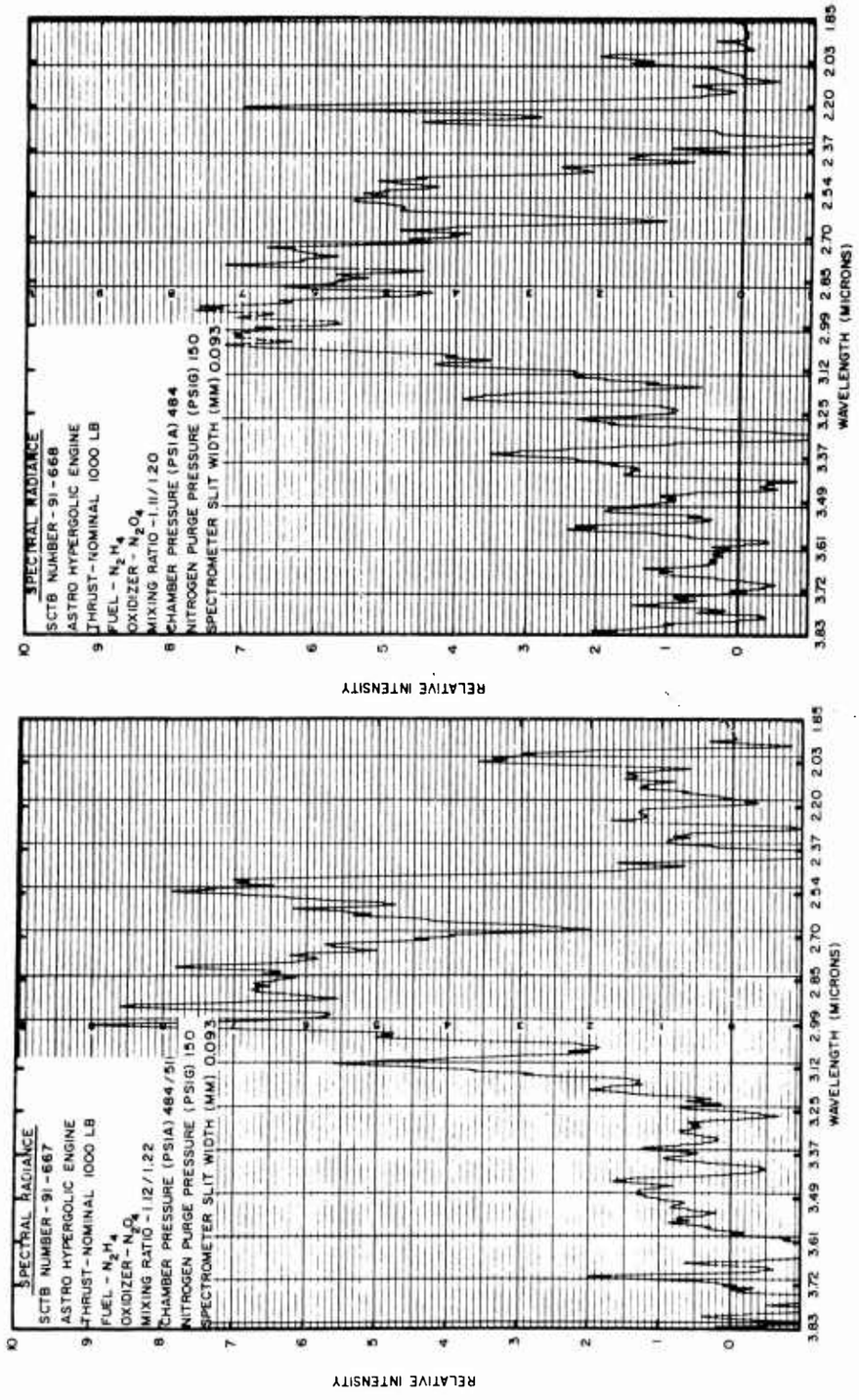
SPECTRAL RADIANCE
SCTB NUMBER - 91 - 668
ASTRO HYPERGOLIC ENGINE
THRUST - NOMINAL 1000 LB
FUEL - N_2H_4
OXIDIZER - N_2O_4
MIXING RATIO - 1.11/1.20
CHAMBER PRESSURE (PSIA) 484
NITROGEN PURGE PRESSURE (PSIG) 150
SPECTROMETER SLIT WIDTH (MM) 0.093
RELATIVE INTENSITY
WAVELENGTH (MICRONS)
3.83 3.72 3.61 3.49 3.37 3.25 3.12 2.99 2.85 2.70 2.54 2.37 2.20 2.03 1.85
SPECTRAL RADIANCE
SCTB NUMBER - 91 - 667
ASTRO HYPERGOLIC ENGINE
THRUST - NOMINAL 1000 LB
FUEL - N_2H_4
OXIDIZER - N_2O_4
MIXING RATIO - 1.12/1.22
CHAMBER PRESSURE (PSIA) 484/511
NITROGEN PURGE PRESSURE (PSIG) 150
SPECTROMETER SLIT WIDTH (MM) 0.093
RELATIVE INTENSITY
WAVELENGTH (MICRONS)
3.83 3.72 3.61 3.49 3.37 3.25 3.12 2.99 2.85 2.70 2.54 2.37 2.20 2.03 1.85

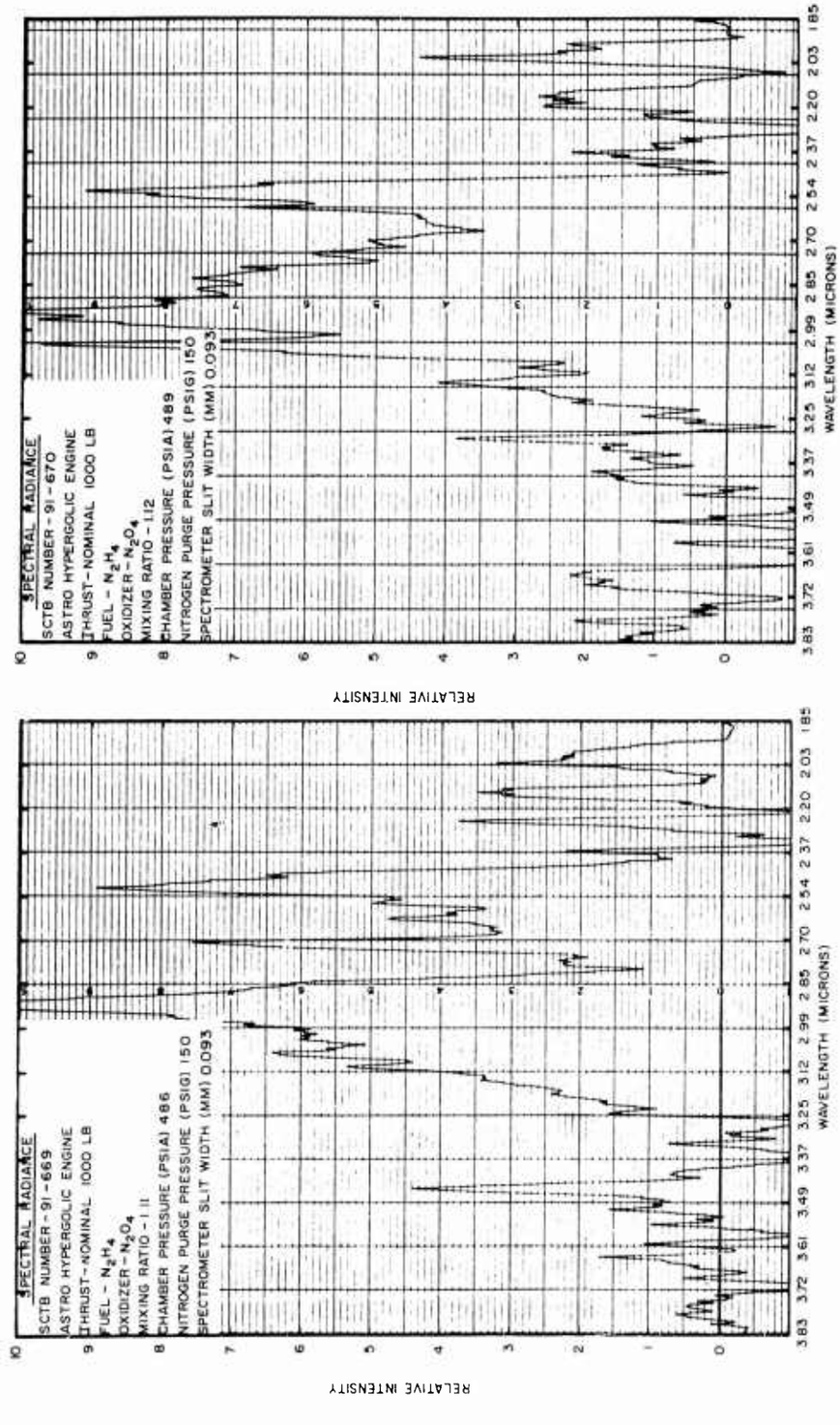
SPECTRAL RADIANCE
SCTB NUMBER - 91-669
ASTRO HYPERGOLIC ENGINE
THRUST - NOMINAL 1000 LB
FUEL - N_2H_4
OXIDIZER - N_2O_4
MIXING RATIO - 1.11
CHAMBER PRESSURE (PSIA) 486
NITROGEN PURGE PRESSURE (PSIG) 150
SPECTROMETER SLIT WIDTH (MM) 0.093
SPECTRAL RADIANCE
SCTB NUMBER - 91-670
ASTRO HYPERGOLIC ENGINE
THRUST - NOMINAL 1000 LB
FUEL - N_2H_4
OXIDIZER - N_2O_4
MIXING RATIO - 1.12
CHAMBER PRESSURE (PSIA) 489
NITROGEN PURGE PRESSURE (PSIG) 150
SPECTROMETER SLIT WIDTH (MM) 0.093
RELATIVE INTENSITY
WAVELENGTH (MICRONS)
383 372 361 349 337 325 312 299 285 270 254 237 220 203 185

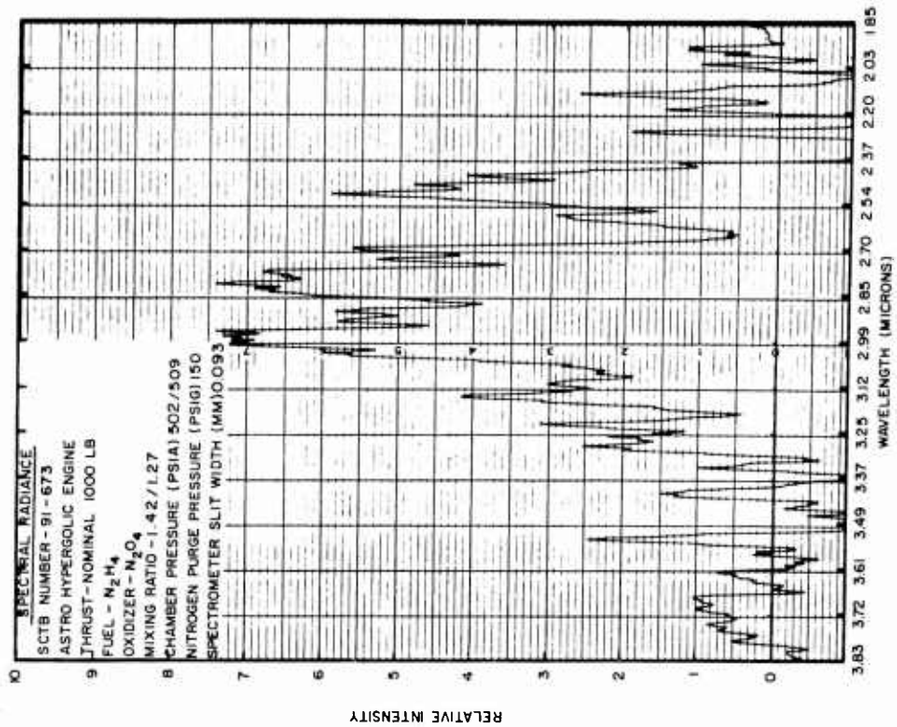
SPECTRAL RADIANCE
SCTB NUMBER - 91 - 673
ASTRO HYPERGOLIC ENGINE
THRUST - NOMINAL 1000 LB
FUEL - N_2H_4
OXIDIZER - N_2O_4
MIXING RATIO - 1.42 / 1.27
CHAMBER PRESSURE (PSIA) 502/509
NITROGEN PURGE PRESSURE (PSIG) 150
SPECTROMETER SLIT WIDTH (MM) 0.093
RELATIVE INTENSITY
WAVELENGTH (MICRONS)
3.83 3.72 3.61 3.49 3.37 3.25 3.12 2.99 2.85 2.70 2.54 2.37 2.20 2.03 1.85

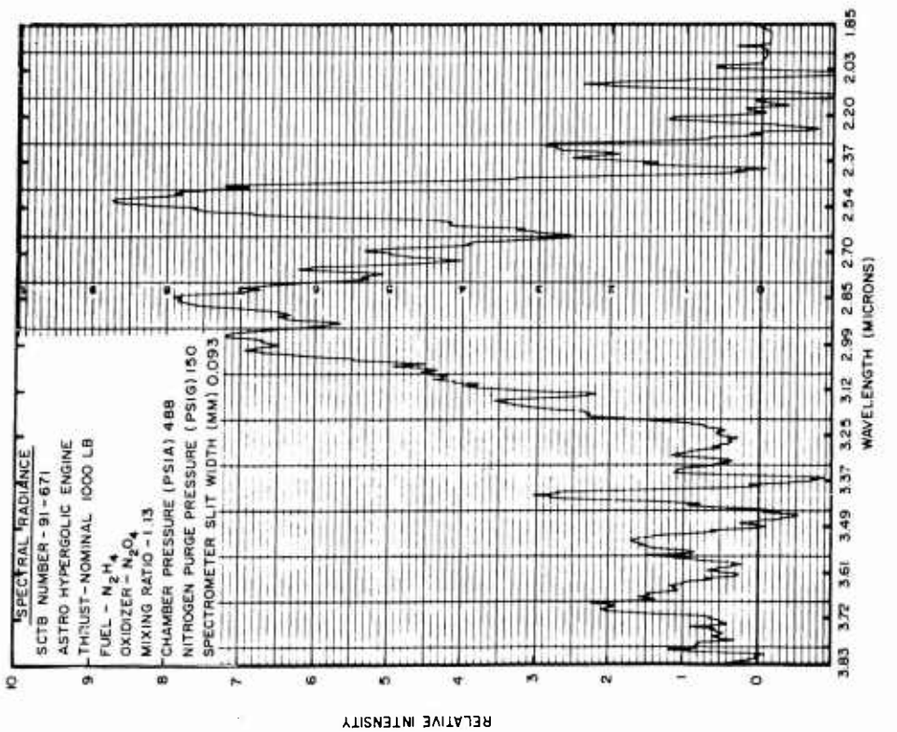
SPECTRAL RADIANCE
SCTB NUMBER - 91 - 671
ASTRO HYPERGOLIC ENGINE
THRUST - NOMINAL 1000 LB
FUEL - N_2H_4
OXIDIZER - N_2O_4
MIXING RATIO - 1.13
CHAMBER PRESSURE (PSIA) 488
NITROGEN PURGE PRESSURE (PSIG) 150
SPECTROMETER SLIT WIDTH (MM) 0.093
RELATIVE INTENSITY
WAVELENGTH (MICRONS)
3.83 3.72 3.61 3.49 3.37 3.25 3.12 2.99 2.85 2.70 2.54 2.37 2.20 2.03 1.85

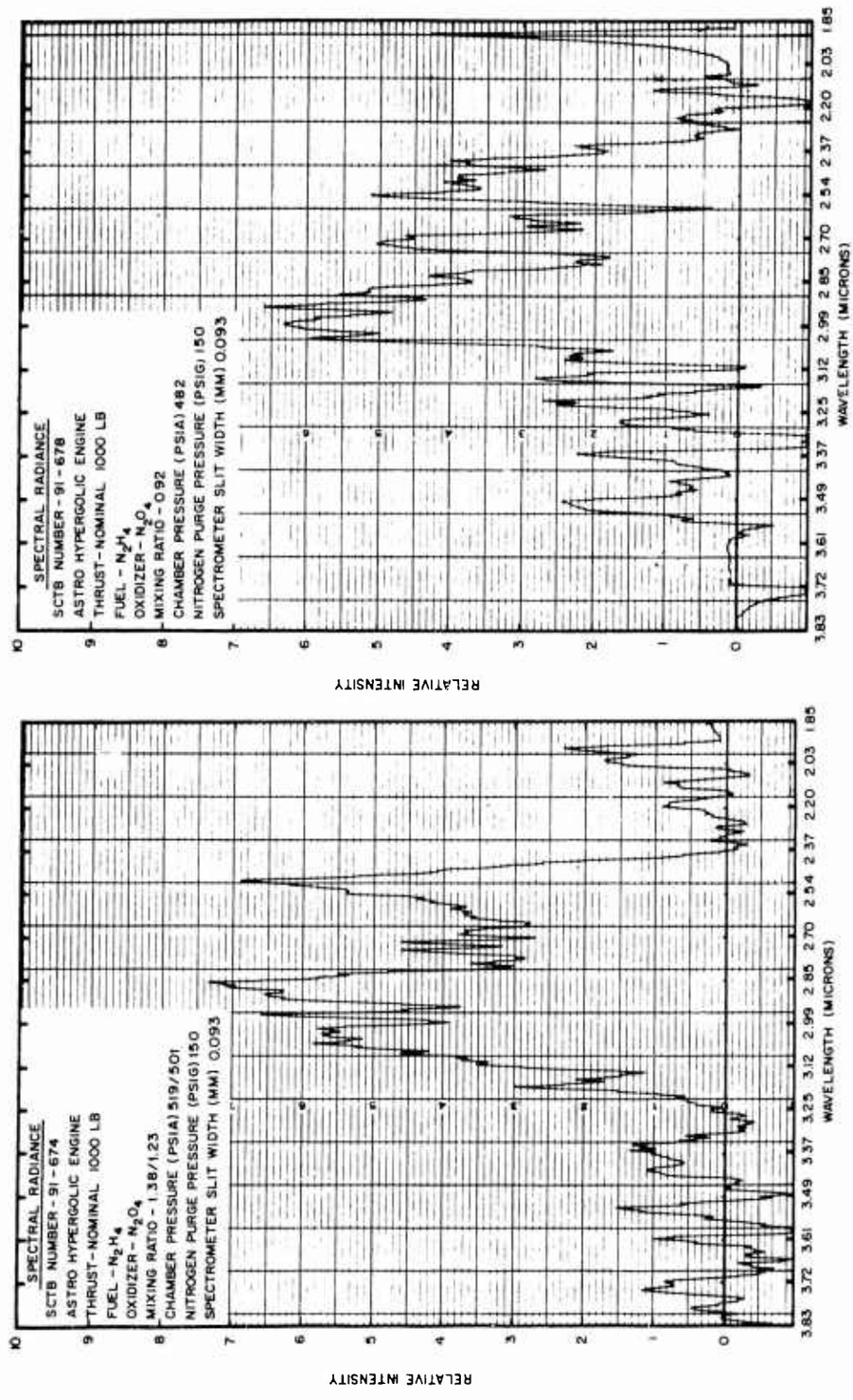
SPECTRAL RADIANCE
SCTB NUMBER - 91 - 678
ASTRO HYPERGOLIC ENGINE
THRUST - NOMINAL 1000 LB
FUEL - N_2H_4
OXIDIZER - N_2O_4
MIXING RATIO - 0.92
CHAMBER PRESSURE (PSIA) 482
NITROGEN PURGE PRESSURE (PSIG) 150
SPECTROMETER SLIT WIDTH (MM) 0.093
SPECTRAL RADIANCE
SCTB NUMBER - 91 - 674
ASTRO HYPERGOLIC ENGINE
THRUST - NOMINAL 1000 LB
FUEL - N_2H_4
OXIDIZER - N_2O_4
MIXING RATIO - 1.38/1.23
CHAMBER PRESSURE (PSIA) 519/501
NITROGEN PURGE PRESSURE (PSIG) 150
SPECTROMETER SLIT WIDTH (MM) 0.093
RELATIVE INTENSITY
WAVELENGTH (MICRONS)
3.83 3.72 3.61 3.49 3.37 3.25 3.12 2.99 2.85 2.70 2.54 2.37 2.20 2.03 1.85
0 1 2 3 4 5 6 7 8 9 10

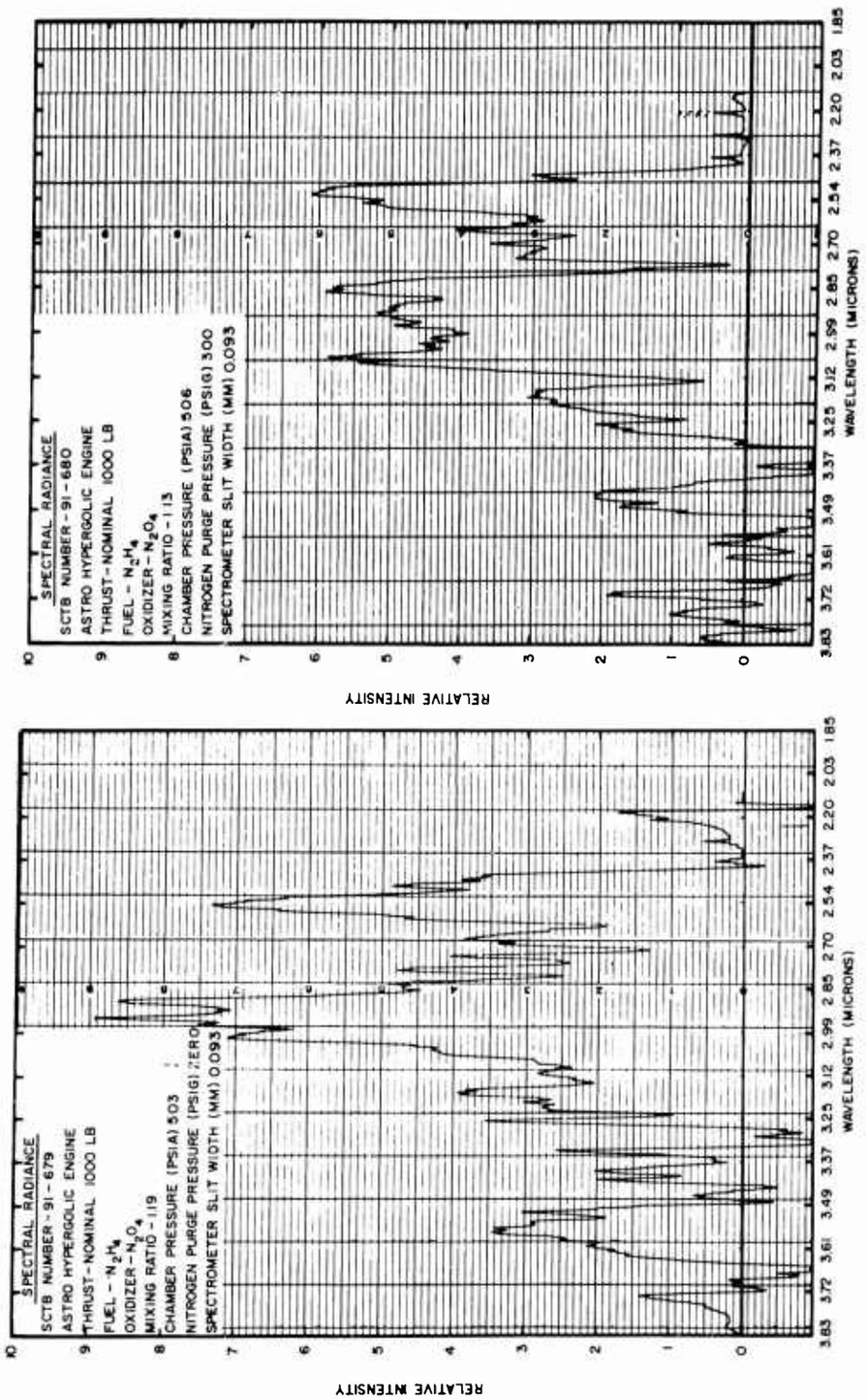
SPECTRAL RADIANCE
SCTB NUMBER - 91 - 679
ASTRO HYPERGOLIC ENGINE
THRUST - NOMINAL 1000 LB
FUEL - N_2H_4
OXIDIZER - N_2O_4
MIXING RATIO - 1.19
CHAMBER PRESSURE (PSIA) 503
NITROGEN PURGE PRESSURE (PSIG) ZERO
SPECTROMETER SLIT WIDTH (MM) 0.093
RELATIVE INTENSITY
WAVELENGTH (MICRONS)
3.83 3.72 3.61 3.49 3.37 3.25 3.12 2.99 2.85 2.70 2.54 2.37 2.20 2.03 1.85
SPECTRAL RADIANCE
SCTB NUMBER - 91 - 680
ASTRO HYPERGOLIC ENGINE
THRUST - NOMINAL 1000 LB
FUEL - N_2H_4
OXIDIZER - N_2O_4
MIXING RATIO - 1.13
CHAMBER PRESSURE (PSIA) 506
NITROGEN PURGE PRESSURE (PSIG) 300
SPECTROMETER SLIT WIDTH (MM) 0.093
RELATIVE INTENSITY
WAVELENGTH (MICRONS)
3.83 3.72 3.61 3.49 3.37 3.25 3.12 2.99 2.85 2.70 2.54 2.37 2.20 2.03 1.85

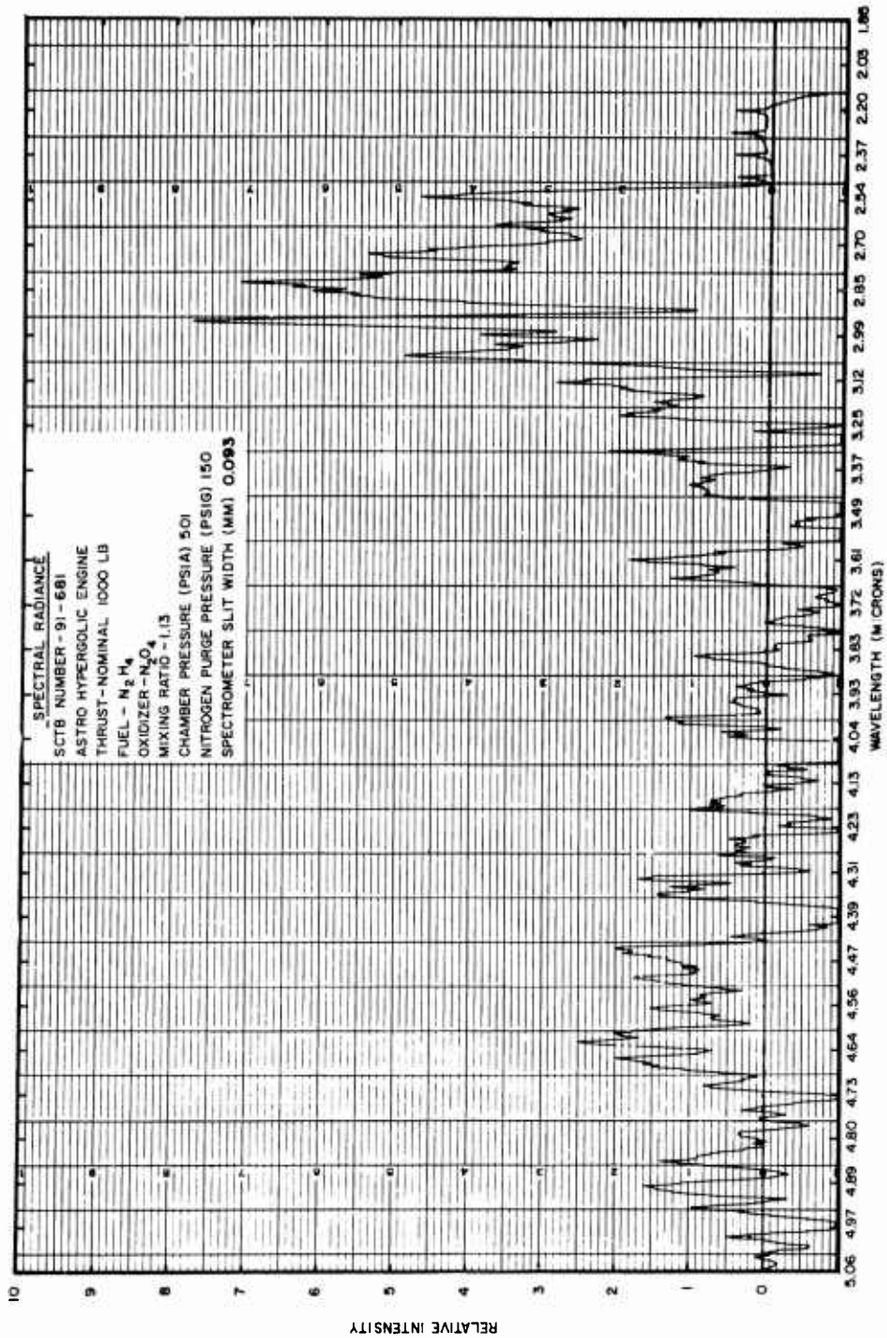
SPECTRAL RADIANCE
SCTB NUMBER - 91 - 681
ASTRO HYPERGOLIC ENGINE
THRUST - NOMINAL 1000 LB
FUEL - N_2H_4
OXIDIZER - N_2O_4
MIXING RATIO - 1.13
CHAMBER PRESSURE (PSIA) 501
NITROGEN PURGE PRESSURE (PSIG) 150
SPECTROMETER SLIT WIDTH (MM) 0.093
RELATIVE INTENSITY
WAVELENGTH (MICRONS)
5.06 4.97 4.89 4.80 4.73 4.64 4.56 4.47 4.39 4.31 4.23 4.13 4.04 3.93 3.83 3.72 3.61 3.49 3.37 3.25 3.12 2.99 2.85 2.70 2.54 2.37 2.20 2.08 1.86

Appendix B

SPECTRAL RADIANCE CHARTS – RAW DATA (RP-1/LOX)

B.1 SPECTRAL RANGE AND INSTRUMENTATION

The charts in this appendix encompass a spectral radiance of 1-5 microns. The LMSC-modified Astrosystems 1,000-lb thrust hypergolic engine and the Perkin-Elmer 112 spectrometer were used to obtain these data.

B.2 SCALE-CONVERSION OVERLAY

Overlays for conversion of the ordinate scale from relative intensity to apparent spectral radiance are "Confidential" and therefore are included in Volume IV.

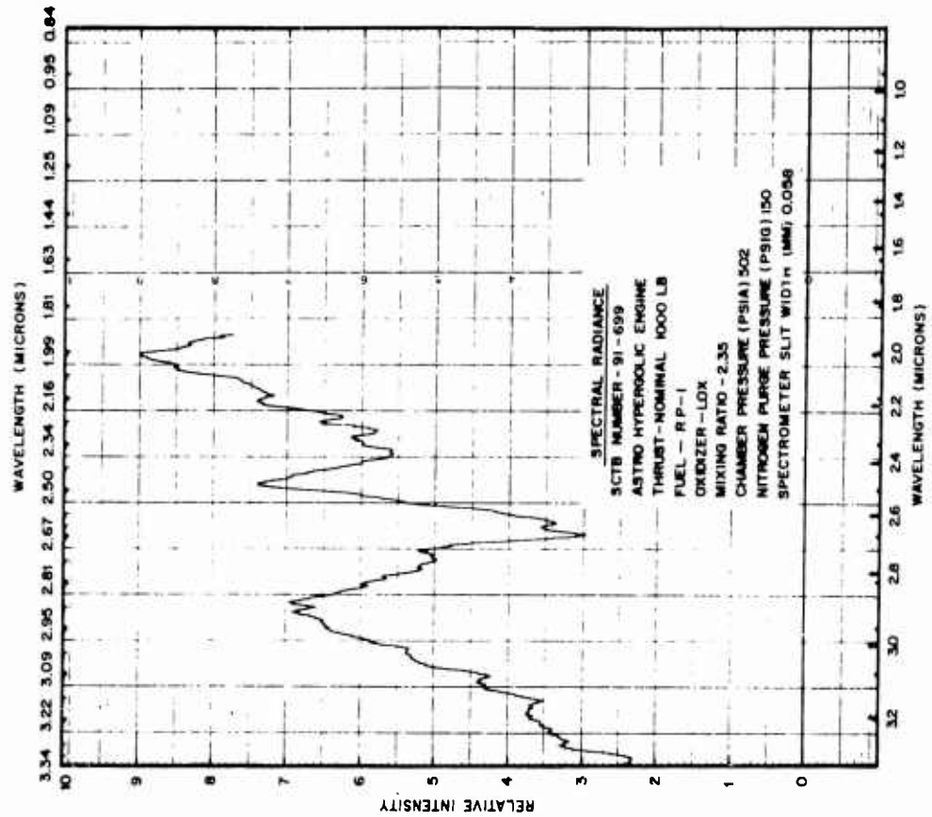
WAVELENGTH (MICRONS)
3.34 3.22 3.09 2.95 2.81 2.67 2.50 2.34 2.16 1.99 1.81 1.63 1.44 1.25 1.09 0.95 0.84
WAVELENGTH (MICRONS)
RELATIVE INTENSITY
SPECTRAL RADIANCE
SCTB NUMBER - 91-699
ASTRO HYPEROLIC ENGINE
THRUST - NOMINAL 1000 LB
FUEL — RP-1
OXIDIZER — LOX
MIXING RATIO - 2.35
CHAMBER PRESSURE (PSIA) 502
NITROGEN PURGE PRESSURE (PSIG) 150
SPECTROMETER SLIT WIDTH (MM) 0.058

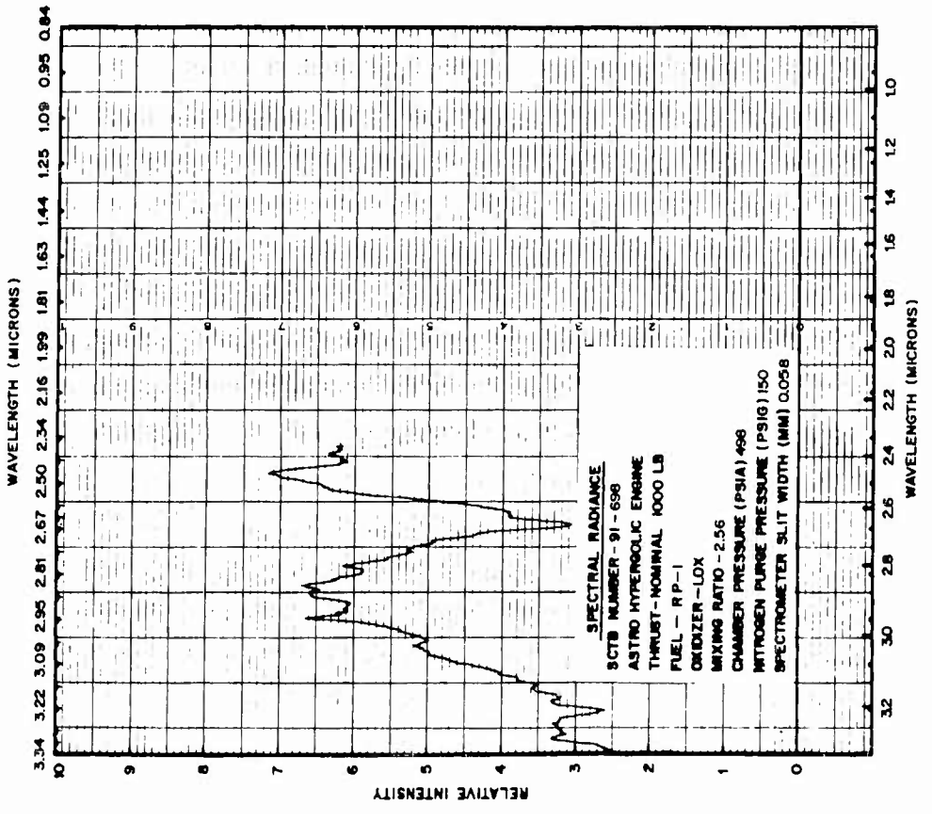
WAVELENGTH (MICRONS)
3.34 3.22 3.09 2.95 2.81 2.67 2.50 2.34 2.16 1.99 1.81 1.63 1.44 1.25 1.09 0.95 0.84
WAVELENGTH (MICRONS)
RELATIVE INTENSITY
SPECTRAL RADIANCE
SCTB NUMBER - 91-698
ASTRO HYPEROLIC ENGINE
THRUST - NOMINAL 1000 LB
FUEL — RP-1
OXIDIZER — LOX
MIXING RATIO - 2.56
CHAMBER PRESSURE (PSIA) 498
NITROGEN PURGE PRESSURE (PSIG) 150
SPECTROMETER SLIT WIDTH (MM) 0.058

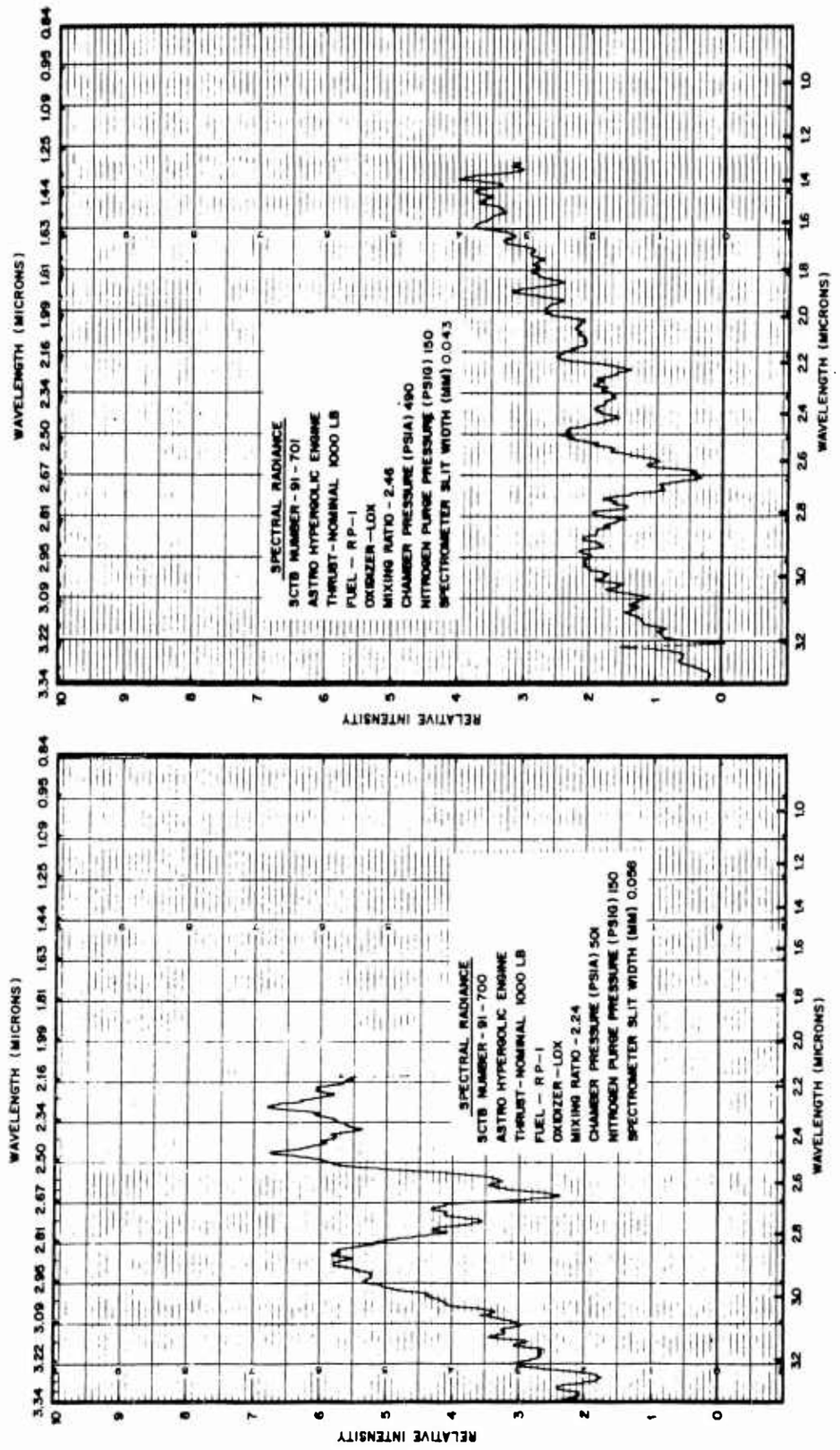
SPECTRAL RADIANCE
SCTB NUMBER - 91 - 701
ASTRO HYPERBOLIC ENGINE
THRUST - NOMINAL 1000 LB
FUEL - RP-1
OXIDIZER - LOX
MIXING RATIO - 2.46
CHAMBER PRESSURE (PSIA) 490
NITROGEN PURGE PRESSURE (PSIG) 150
SPECTROMETER SLIT WIDTH (MM) 0.043
SPECTRAL RADIANCE
SCTB NUMBER - 91 - 700
ASTRO HYPERBOLIC ENGINE
THRUST - NOMINAL 1000 LB
FUEL - RP-1
OXIDIZER - LOX
MIXING RATIO - 2.24
CHAMBER PRESSURE (PSIA) 501
NITROGEN PURGE PRESSURE (PSIG) 150
SPECTROMETER SLIT WIDTH (MM) 0.056
WAVELENGTH (MICRONS)
RELATIVE INTENSITY

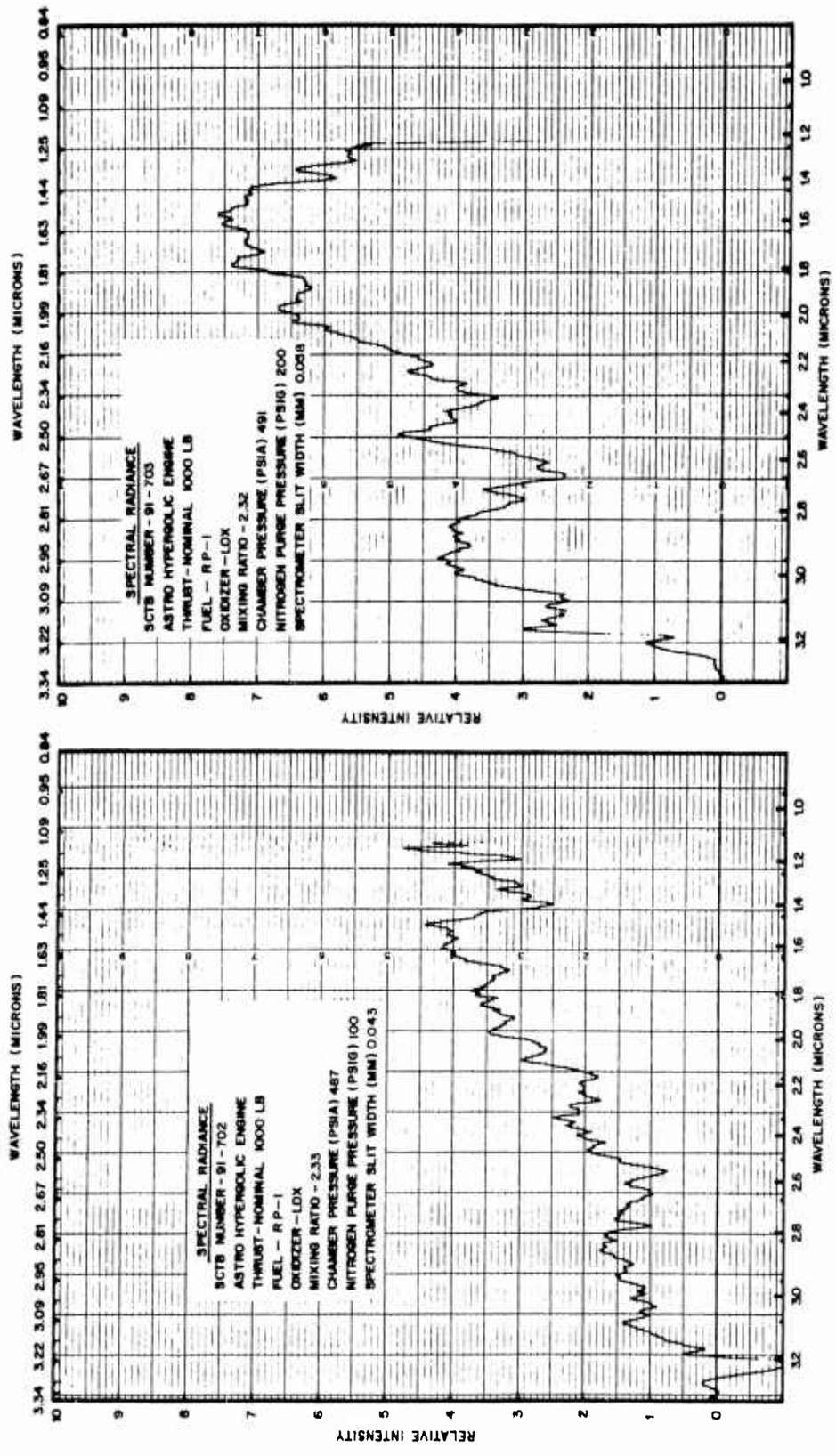
SPECTRAL RADIANCE
SCTB NUMBER - 91 - 702
ASTRO HYPERGOLIC ENGINE
THRUST - NOMINAL 1000 LB
FUEL — R P - 1
OXIDIZER - LOX
MIXING RATIO - 2.33
CHAMBER PRESSURE (PSIA) 487
NITROGEN PURGE PRESSURE (PSIG) 100
SPECTROMETER SLIT WIDTH (MM) 0.043
WAVELENGTH (MICRONS)
RELATIVE INTENSITY
SPECTRAL RADIANCE
SCTB NUMBER - 91 - 703
ASTRO HYPERGOLIC ENGINE
THRUST - NOMINAL 1000 LB
FUEL — R P - 1
OXIDIZER - LOX
MIXING RATIO - 2.32
CHAMBER PRESSURE (PSIA) 491
NITROGEN PURGE PRESSURE (PSIG) 200
SPECTROMETER SLIT WIDTH (MM) 0.058
WAVELENGTH (MICRONS)
RELATIVE INTENSITY

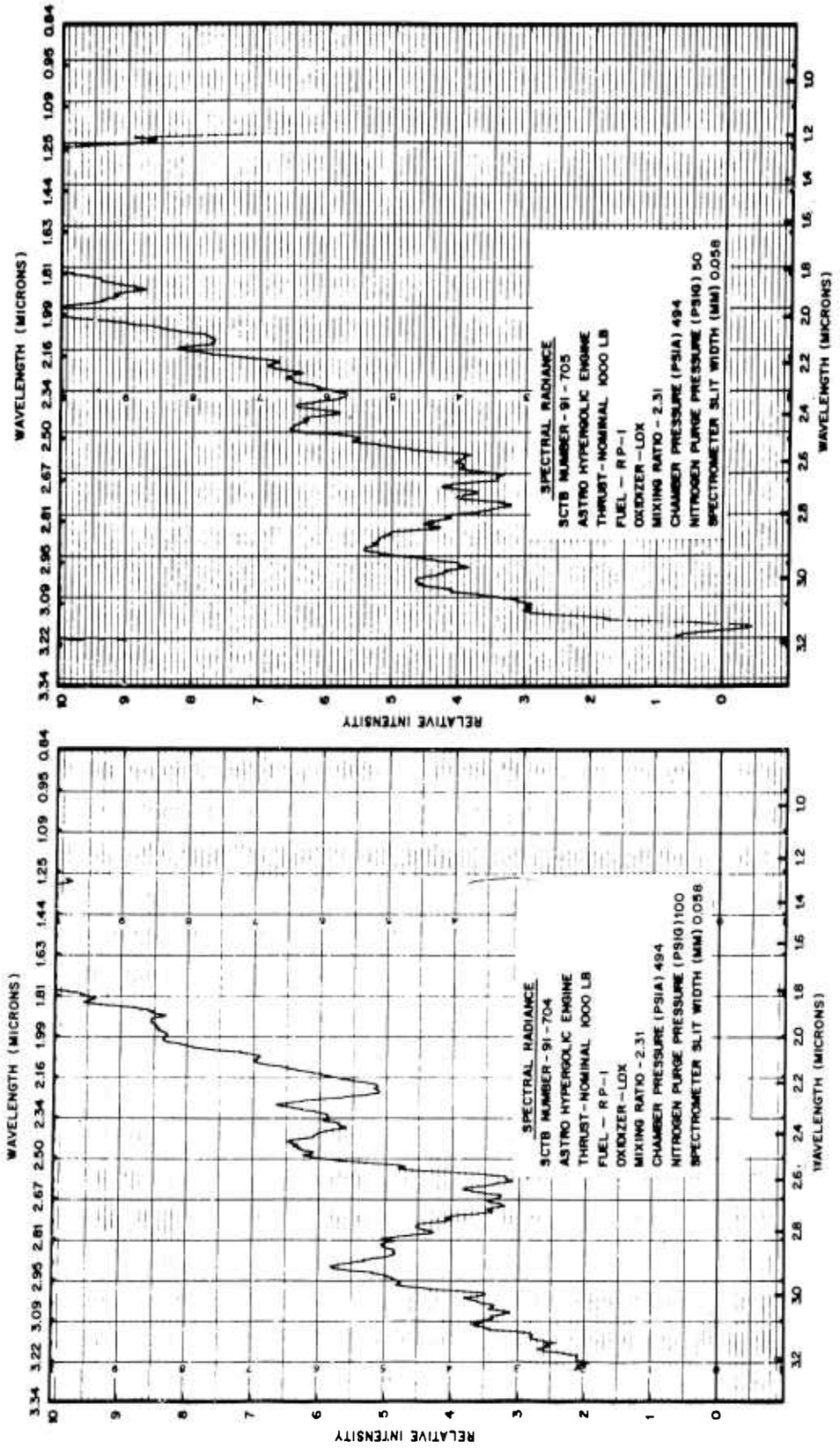
SPECTRAL RADIANCE
SCTB NUMBER - 91 - 705
ASTRO HYPERGOLIC ENGINE
THRUST - NOMINAL 1000 LB
FUEL - RP-1
OXIDIZER - LOX
MIXING RATIO - 2.31
CHAMBER PRESSURE (PSIA) 494
NITROGEN PURGE PRESSURE (PSIG) 50
SPECTROMETER SLIT WIDTH (MM) 0.058
WAVELENGTH (MICRONS)
RELATIVE INTENSITY
SPECTRAL RADIANCE
SCTB NUMBER - 91 - 704
ASTRO HYPERGOLIC ENGINE
THRUST - NOMINAL 1000 LB
FUEL - RP-1
OXIDIZER - LOX
MIXING RATIO - 2.31
CHAMBER PRESSURE (PSIA) 494
NITROGEN PURGE PRESSURE (PSIG) 100
SPECTROMETER SLIT WIDTH (MM) 0.058
WAVELENGTH (MICRONS)
RELATIVE INTENSITY

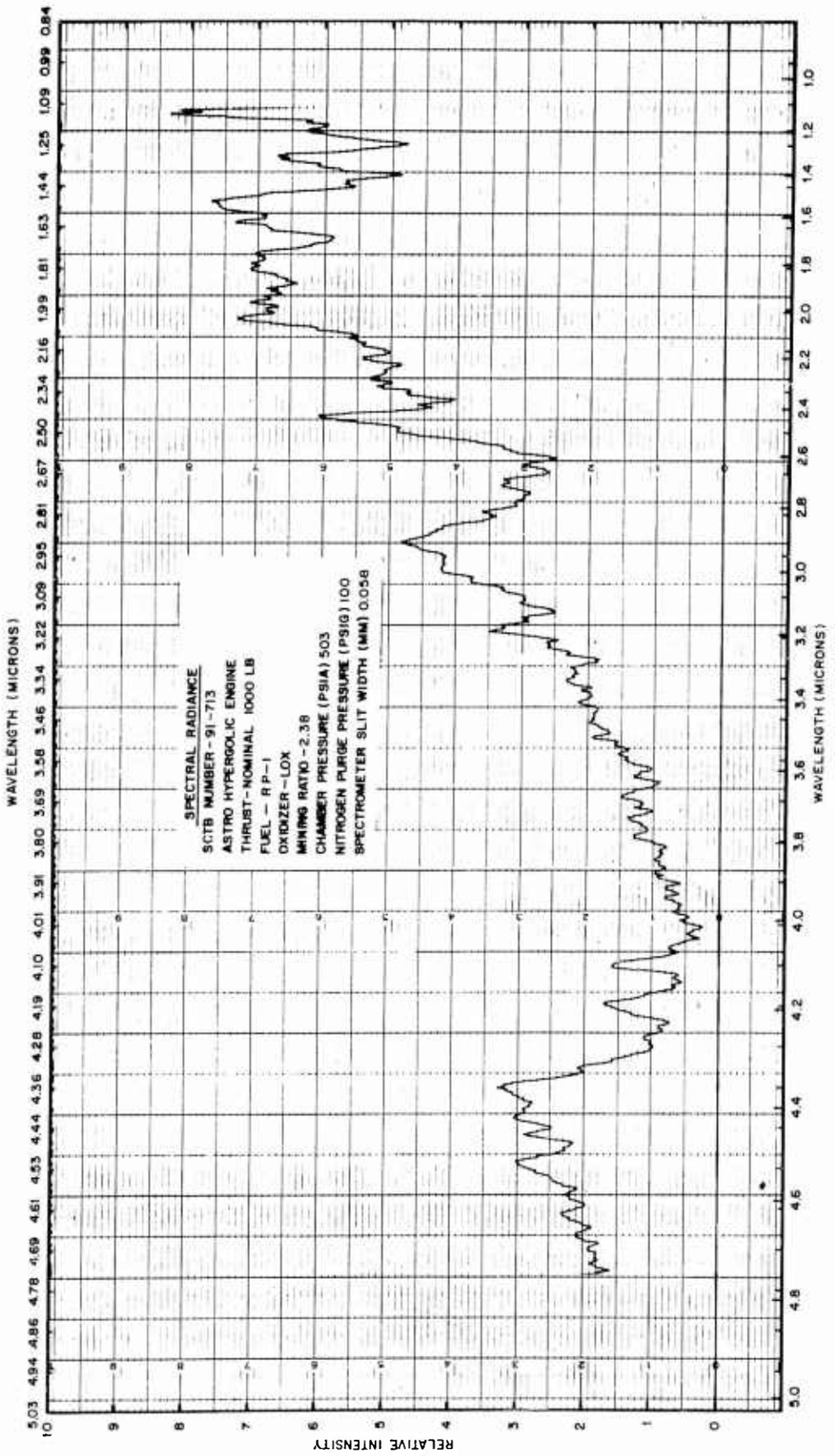
SPECTRAL RADIANCE
SCTB NUMBER - 91-713
ASTRO HYPERGOLIC ENGINE
THRUST - NOMINAL 1000 LB
FUEL — RP-1
OXIDIZER — LOX
MIXING RATIO - 2.38
CHAMBER PRESSURE (PSIA) 503
NITROGEN PURGE PRESSURE (PSIG) 100
SPECTROMETER SLIT WIDTH (MM) 0.058
WAVELENGTH (MICRONS)
RELATIVE INTENSITY

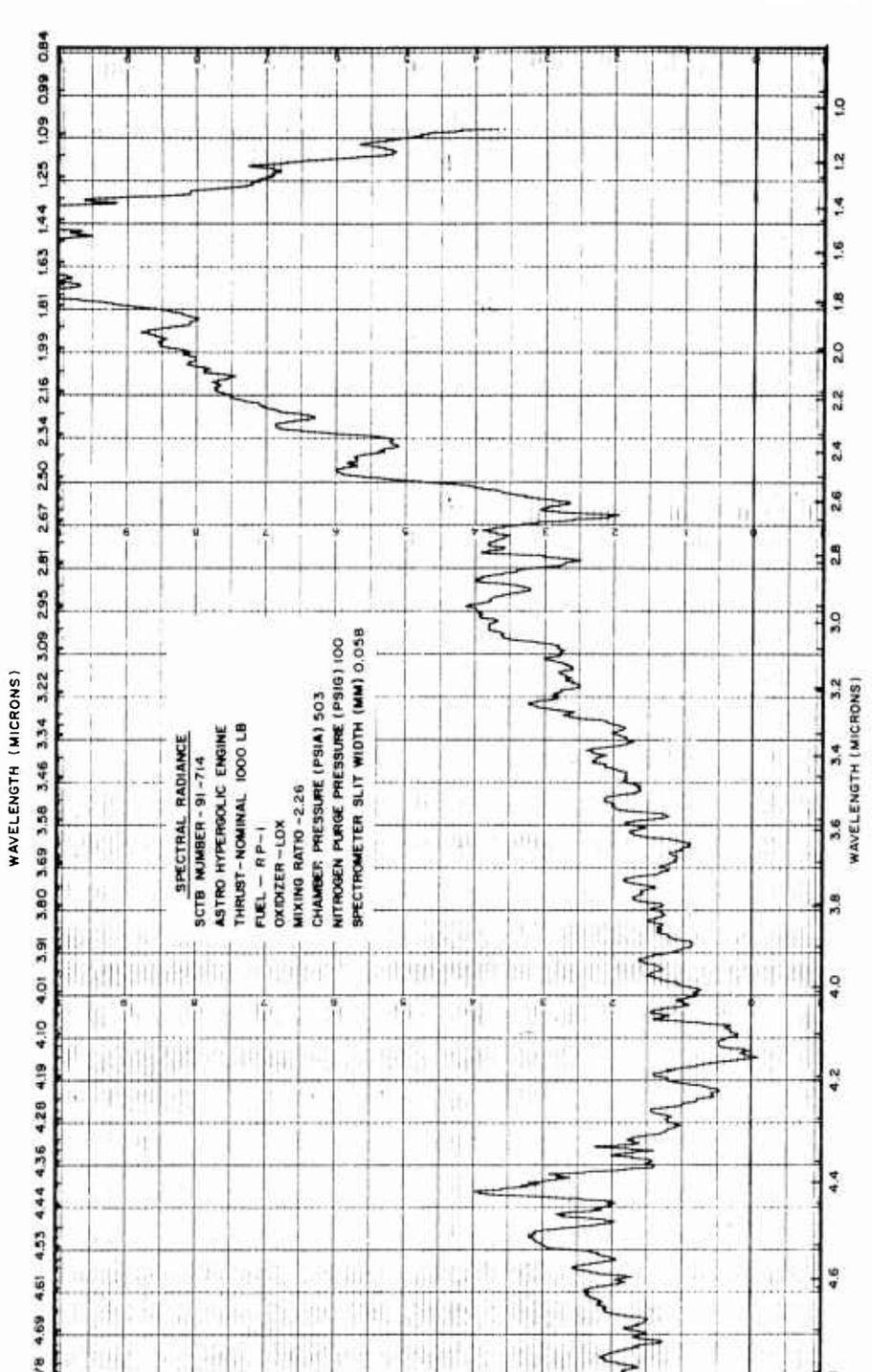
SPECTRAL RADIANCE
SCTB NUMBER - 91-7.4
ASTRO HYPERGOLIC ENGINE
THRUST - NOMINAL 1000 LB
FUEL — RP-1
OXIDIZER — LOX
MIXING RATIO - 2.26
CHAMBER PRESSURE (PSIA) 503
NITROGEN PURGE PRESSURE (PSIG) 100
SPECTROMETER SLIT WIDTH (MM) 0.058
WAVELENGTH (MICRONS)
RELATIVE INTENSITY
WAVELENGTH (MICRONS)

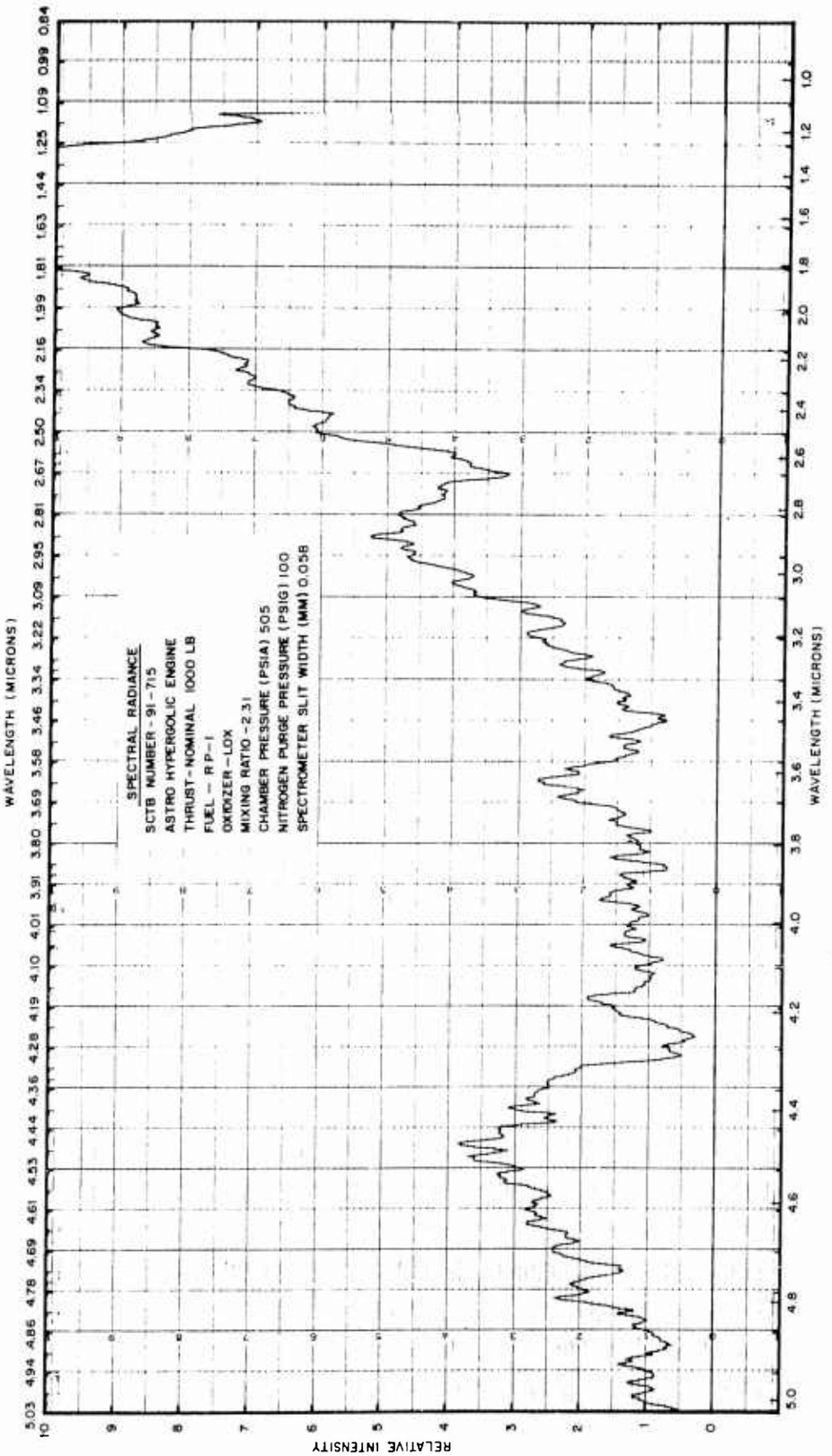
SPECTRAL RADIANCE
SCTB NUMBER - 91-715
ASTRO HYPERGOLIC ENGINE
THRUST - NOMINAL 1000 LB
FUEL — R P-1
OXIDIZER — LOX
MIXING RATIO - 2.31
CHAMBER PRESSURE (PSIA) 505
NITROGEN PURGE PRESSURE (PSIG) 100
SPECTROMETER SLIT WIDTH (MM) 0.058
WAVELENGTH (MICRONS)
RELATIVE INTENSITY

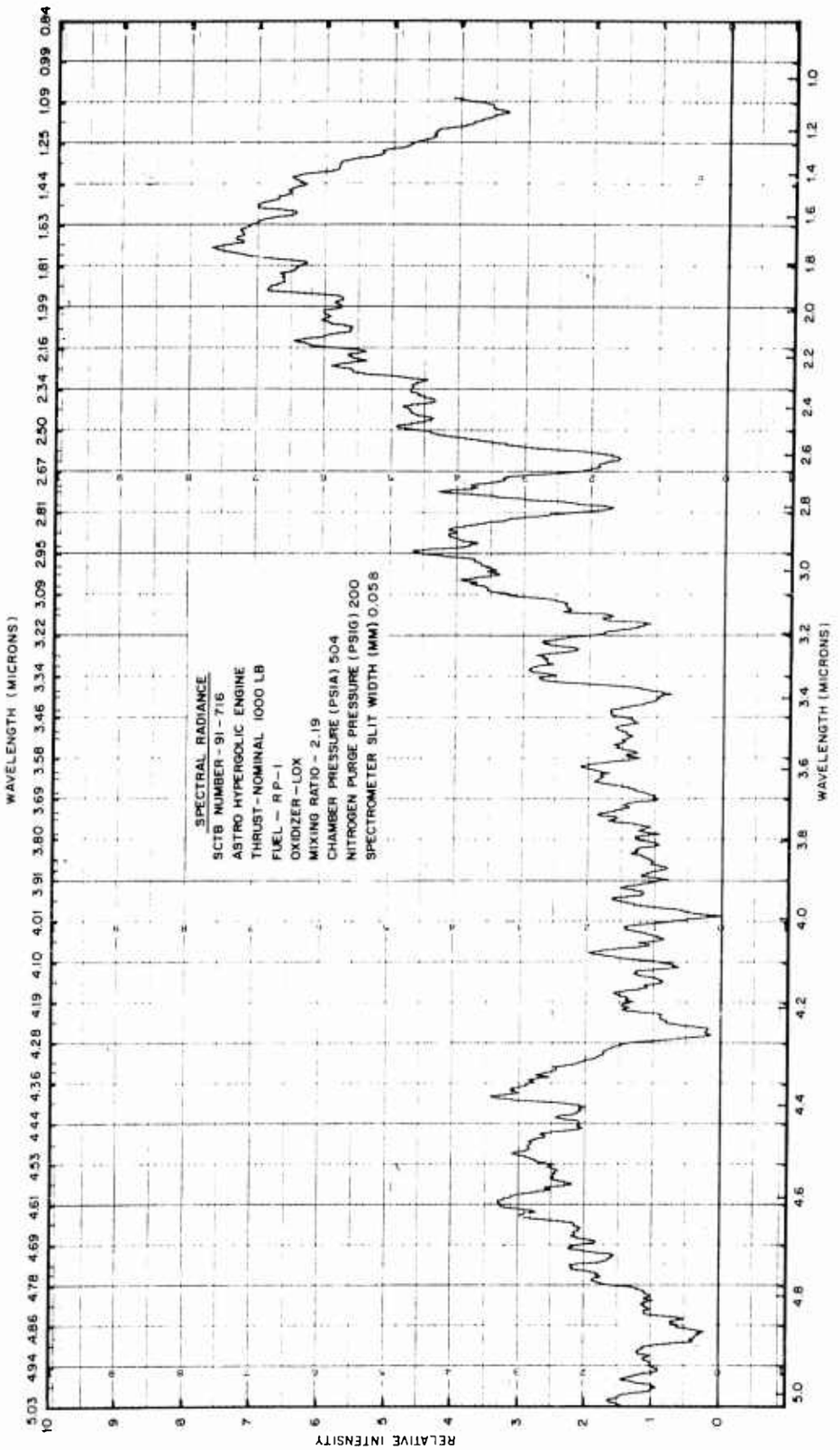
SPECTRAL RADIANCE
SCTB NUMBER - 91 - 716
ASTRO HYPERGOLIC ENGINE
THRUST - NOMINAL 1000 LB
FUEL - RP-1
OXIDIZER - LOX
MIXING RATIO - 2.19
CHAMBER PRESSURE (PSIA) 504
NITROGEN PURGE PRESSURE (PSIG) 200
SPECTROMETER SLIT WIDTH (MM) 0.058
WAVELENGTH (MICRONS)
RELATIVE INTENSITY

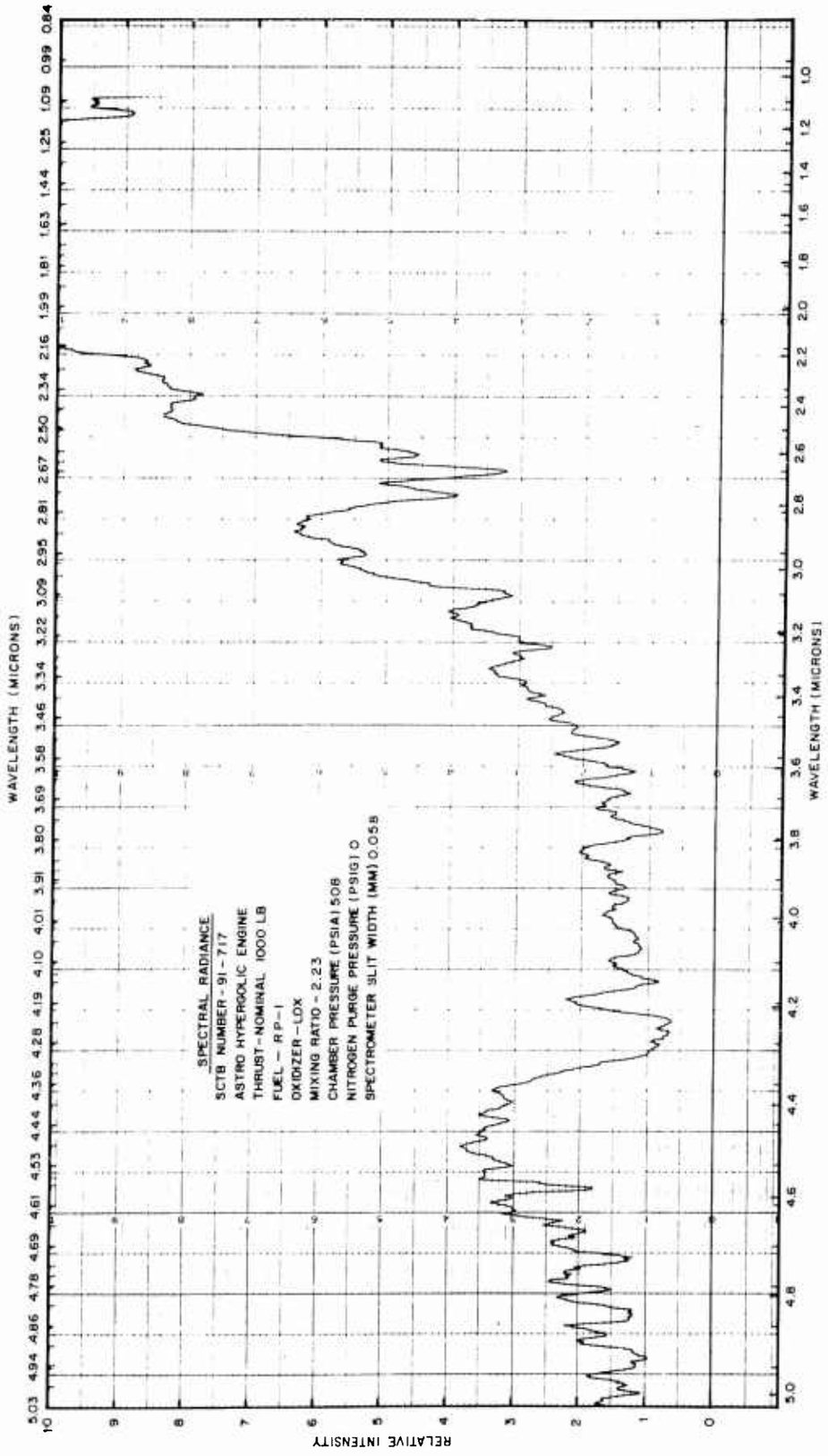
SPECTRAL RADIANCE
SCTB NUMBER - 91 - 717
ASTRO HYPERGOLIC ENGINE
THRUST - NOMINAL 1000 LB
FUEL - RP-1
OXIDIZER - LOX
MIXING RATIO - 2.23
CHAMBER PRESSURE (PSIA) 508
NITROGEN PURGE PRESSURE (PSIG) 0
SPECTROMETER SLIT WIDTH (MM) 0.058
WAVELENGTH (MICRONS)
WAVELENGTH (MICRONS)
RELATIVE INTENSITY

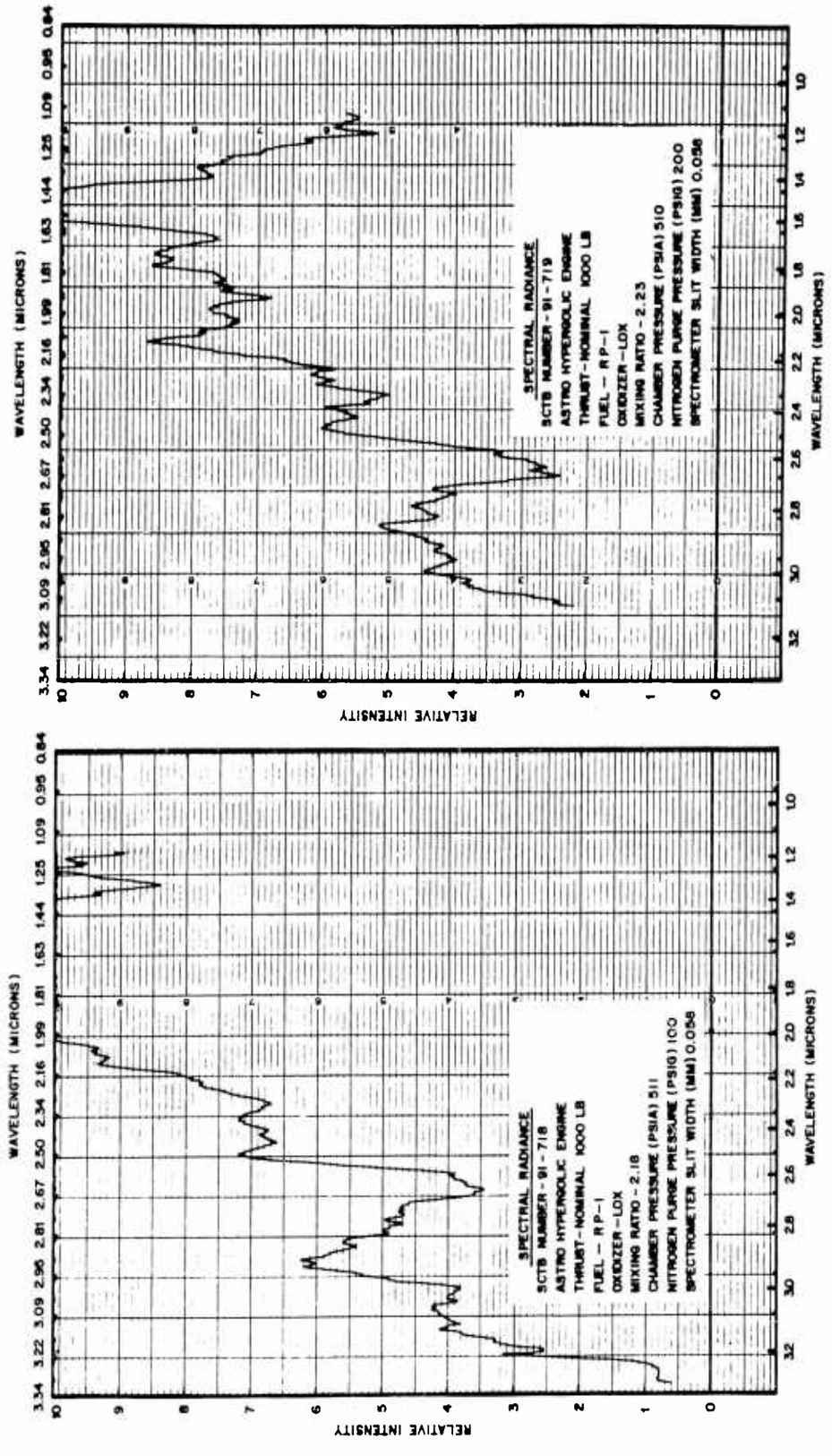
SPECTRAL RADIANCE
SCTB NUMBER - 91 - 719
ASTRO HYPERBOLIC ENGINE
THRUST - NOMINAL 1000 LB
FUEL -- RP-1
OXIDIZER -- LOX
MIXING RATIO - 2.23
CHAMBER PRESSURE (PSIA) 510
NITROGEN PURGE PRESSURE (PSIG) 200
SPECTROMETER SLIT WIDTH (MM) 0.056
WAVELENGTH (MICRONS)
RELATIVE INTENSITY
SPECTRAL RADIANCE
SCTB NUMBER - 91 - 718
ASTRO HYPERBOLIC ENGINE
THRUST - NOMINAL 1000 LB
FUEL -- RP-1
OXIDIZER -- LOX
MIXING RATIO - 2.18
CHAMBER PRESSURE (PSIA) 511
NITROGEN PURGE PRESSURE (PSIG) 100
SPECTROMETER SLIT WIDTH (MM) 0.058
WAVELENGTH (MICRONS)
RELATIVE INTENSITY

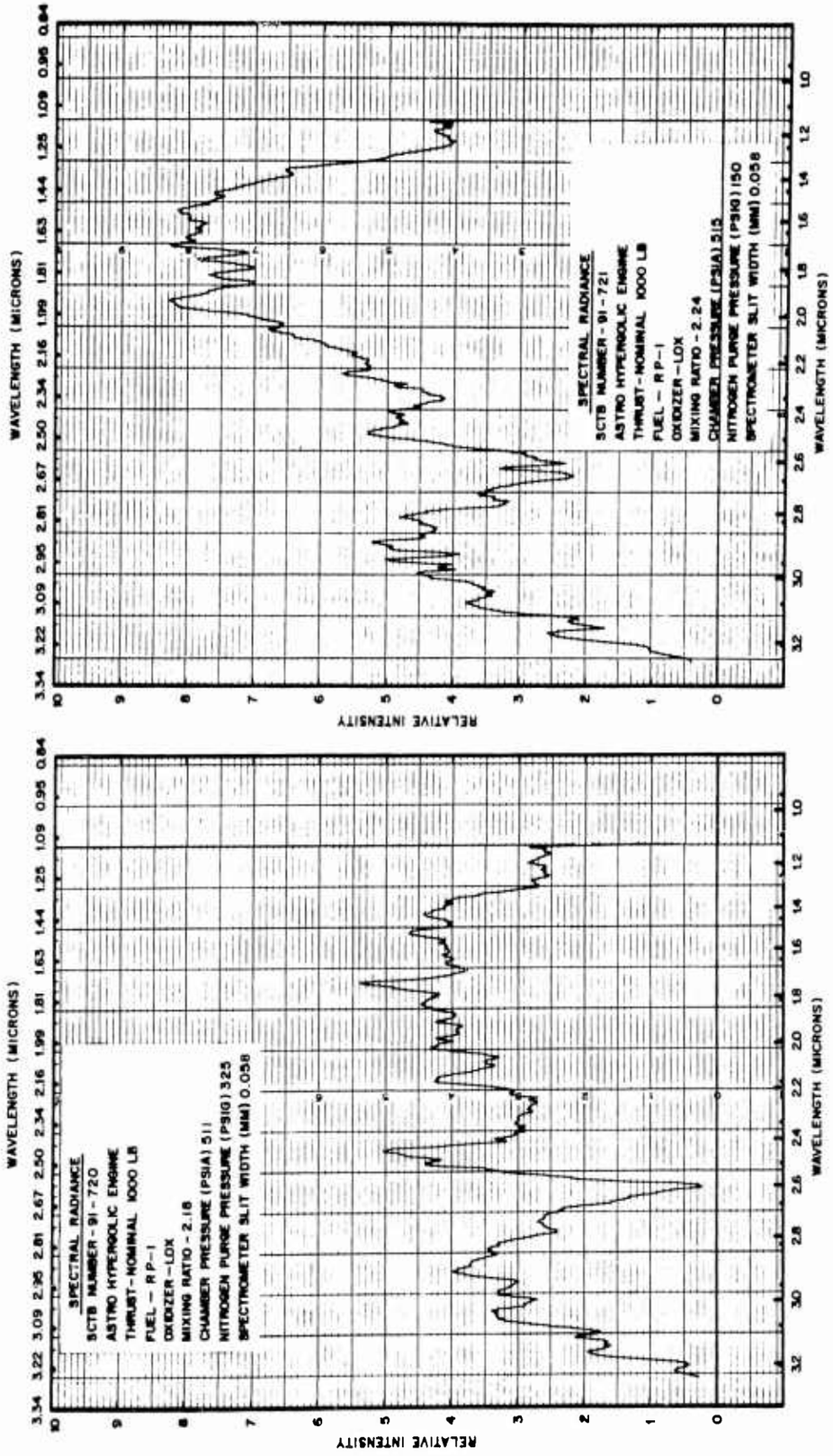
WAVELENGTH (MICRONS)
3.34 3.22 3.09 2.95 2.81 2.67 2.50 2.34 2.16 1.99 1.81 1.63 1.44 1.25 1.09 0.95 0.84
RELATIVE INTENSITY
WAVELENGTH (MICRONS)
SPECTRAL RADIANCE
SCTB NUMBER - 91-720
ASTRO HYPERGOLIC ENGINE
THRUST - NOMINAL 1000 LB
FUEL - RP-1
OXIDIZER - LOX
MIXING RATIO - 2.18
CHAMBER PRESSURE (PSIA) 511
NITROGEN PURGE PRESSURE (PSIG) 325
SPECTROMETER SLIT WIDTH (MM) 0.058
SPECTRAL RADIANCE
SCTB NUMBER - 91-721
ASTRO HYPERGOLIC ENGINE
THRUST - NOMINAL 1000 LB
FUEL - RP-1
OXIDIZER - LOX
MIXING RATIO - 2.24
CHAMBER PRESSURE (PSIA) 515
NITROGEN PURGE PRESSURE (PSIG) 150
SPECTROMETER SLIT WIDTH (MM) 0.058

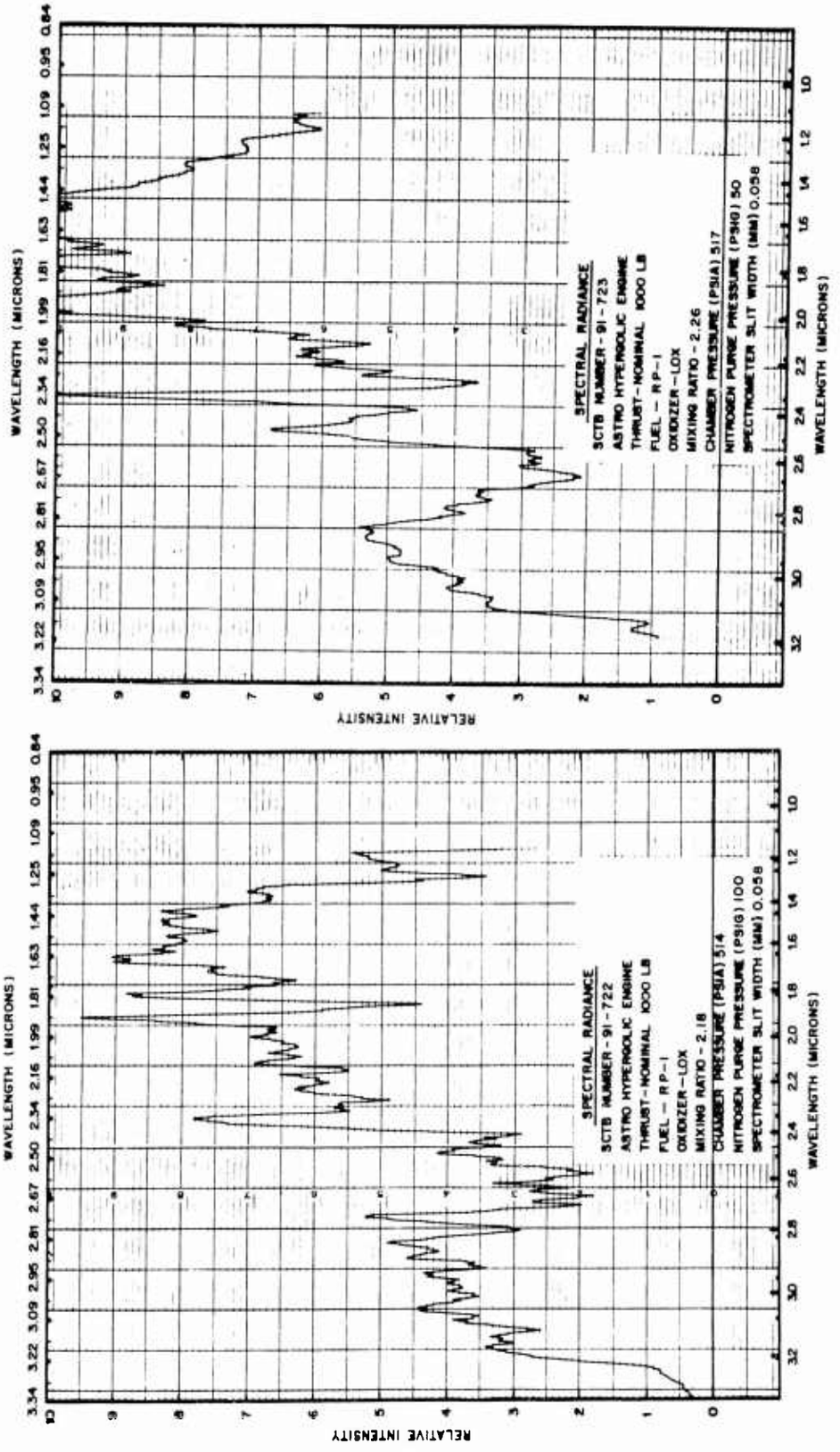
SPECTRAL RADIANCE
SCTB NUMBER - 91 - 723
ASTRO HYPERGOLIC ENGINE
THRUST - NOMINAL 1000 LB
FUEL - RP-1
OXIDIZER - LOX
MIXING RATIO - 2.26
CHAMBER PRESSURE (PSIA) 517
NITROGEN PURGE PRESSURE (PSIG) 50
SPECTROMETER SLIT WIDTH (MM) 0.058
SPECTRAL RADIANCE
SCTB NUMBER - 91 - 722
ASTRO HYPERGOLIC ENGINE
THRUST - NOMINAL 1000 LB
FUEL - RP-1
OXIDIZER - LOX
MIXING RATIO - 2.18
CHAMBER PRESSURE (PSIA) 514
NITROGEN PURGE PRESSURE (PSIG) 100
SPECTROMETER SLIT WIDTH (MM) 0.058
WAVELENGTH (MICRONS)
RELATIVE INTENSITY

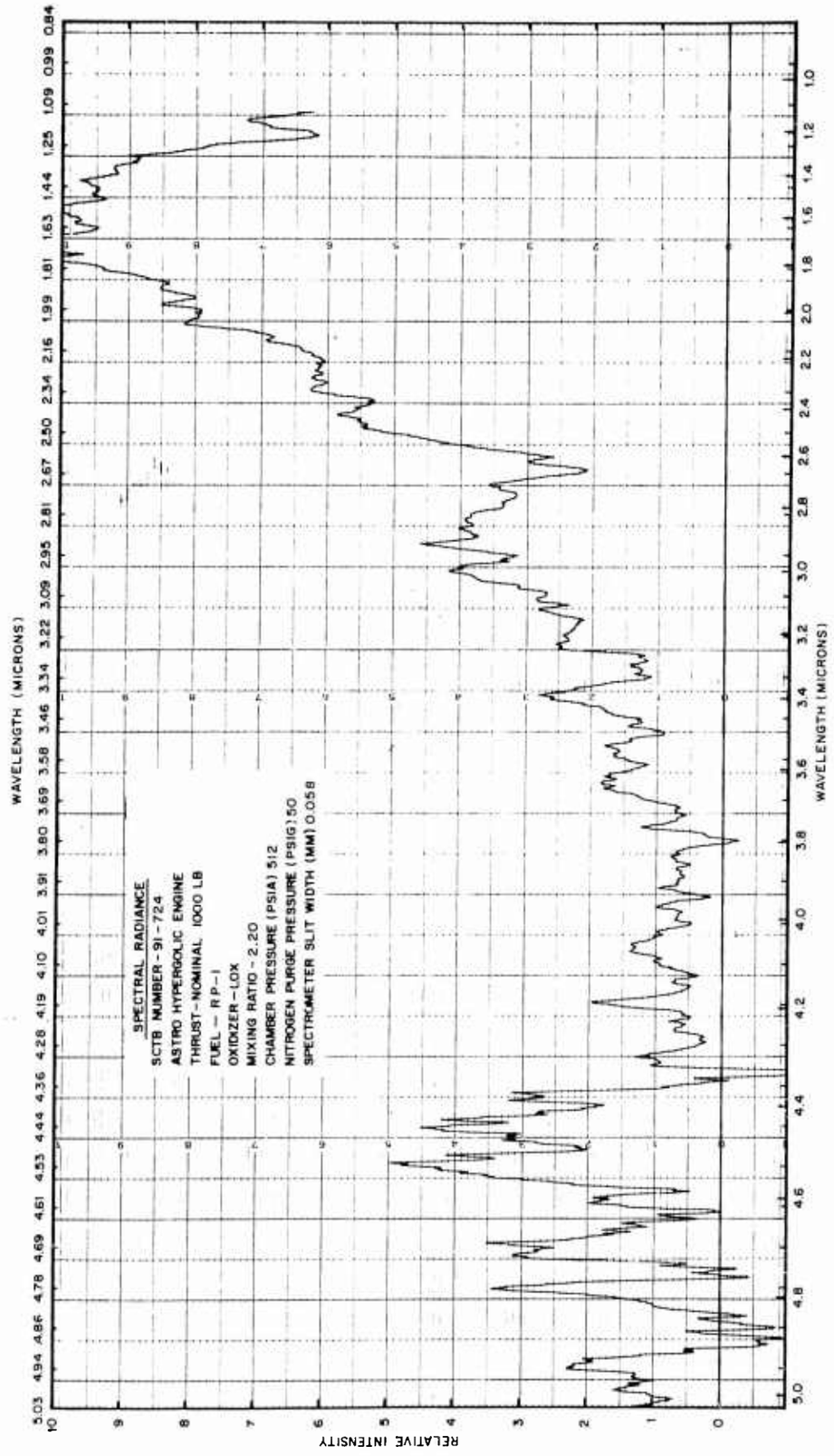
SPECTRAL RADIANCE
SCTB NUMBER - 91 - 724
ASTRO HYPERGOLIC ENGINE
THRUST - NOMINAL 1000 LB
FUEL — R P - 1
OXIDIZER — LOX
MIXING RATIO - 2.20
CHAMBER PRESSURE (PSIA) 512
NITROGEN PURGE PRESSURE (PSIG) 150
SPECTROMETER SLIT WIDTH (MM) 0.058
WAVELENGTH (MICRONS)
WAVELENGTH (MICRONS)
RELATIVE INTENSITY

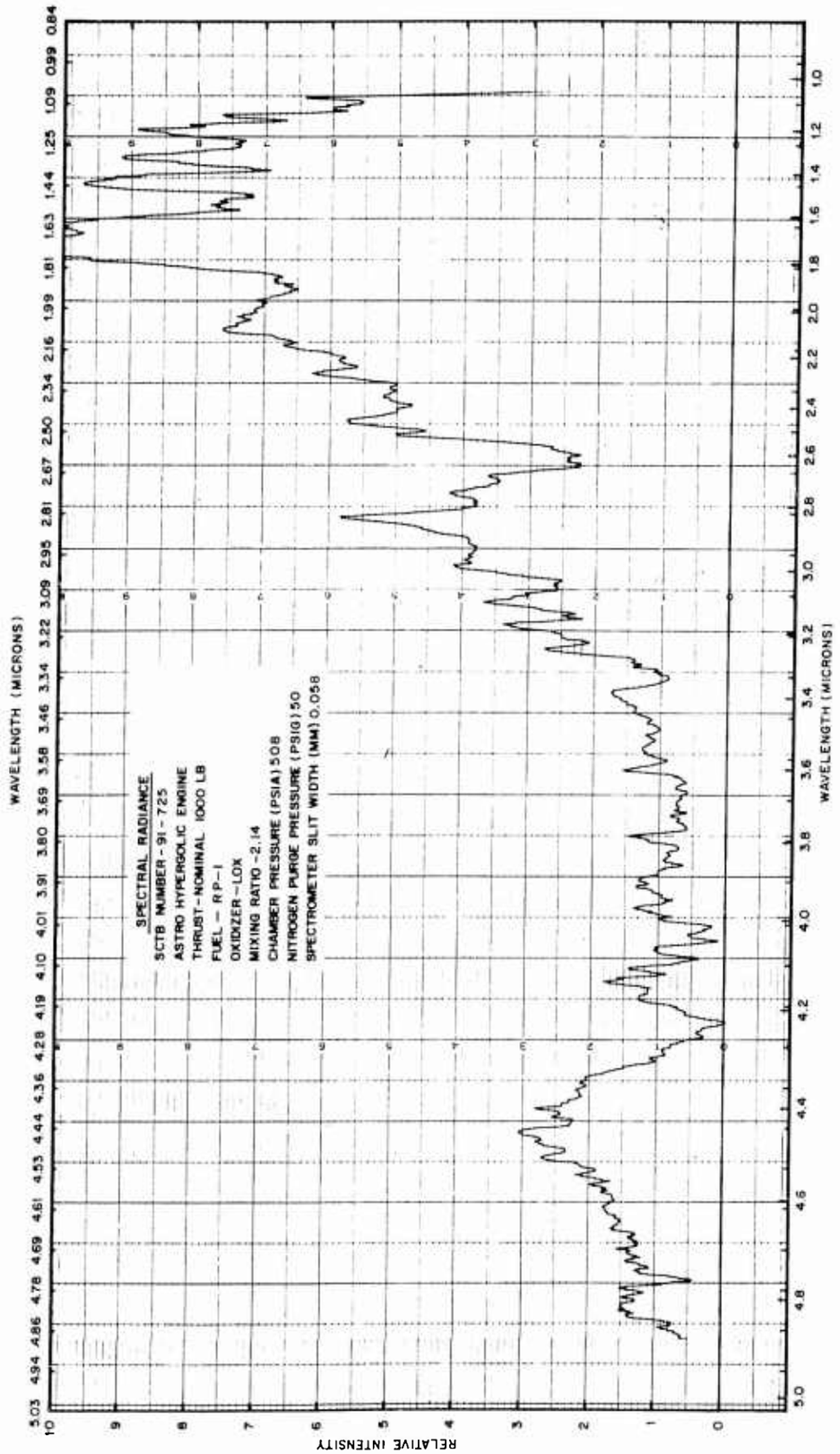
SPECTRAL RADIANCE
SCTB NUMBER - 91 - 725
ASTRO HYPERGOLIC ENGINE
THRUST - NOMINAL 1000 LB
FUEL — RP-1
OXIDIZER — LOX
MIXING RATIO - 2.14
CHAMBER PRESSURE (PSIA) 508
NITROGEN PURGE PRESSURE (PSIG) 50
SPECTROMETER SLIT WIDTH (MM) 0.058
WAVELENGTH (MICRONS)
RELATIVE INTENSITY

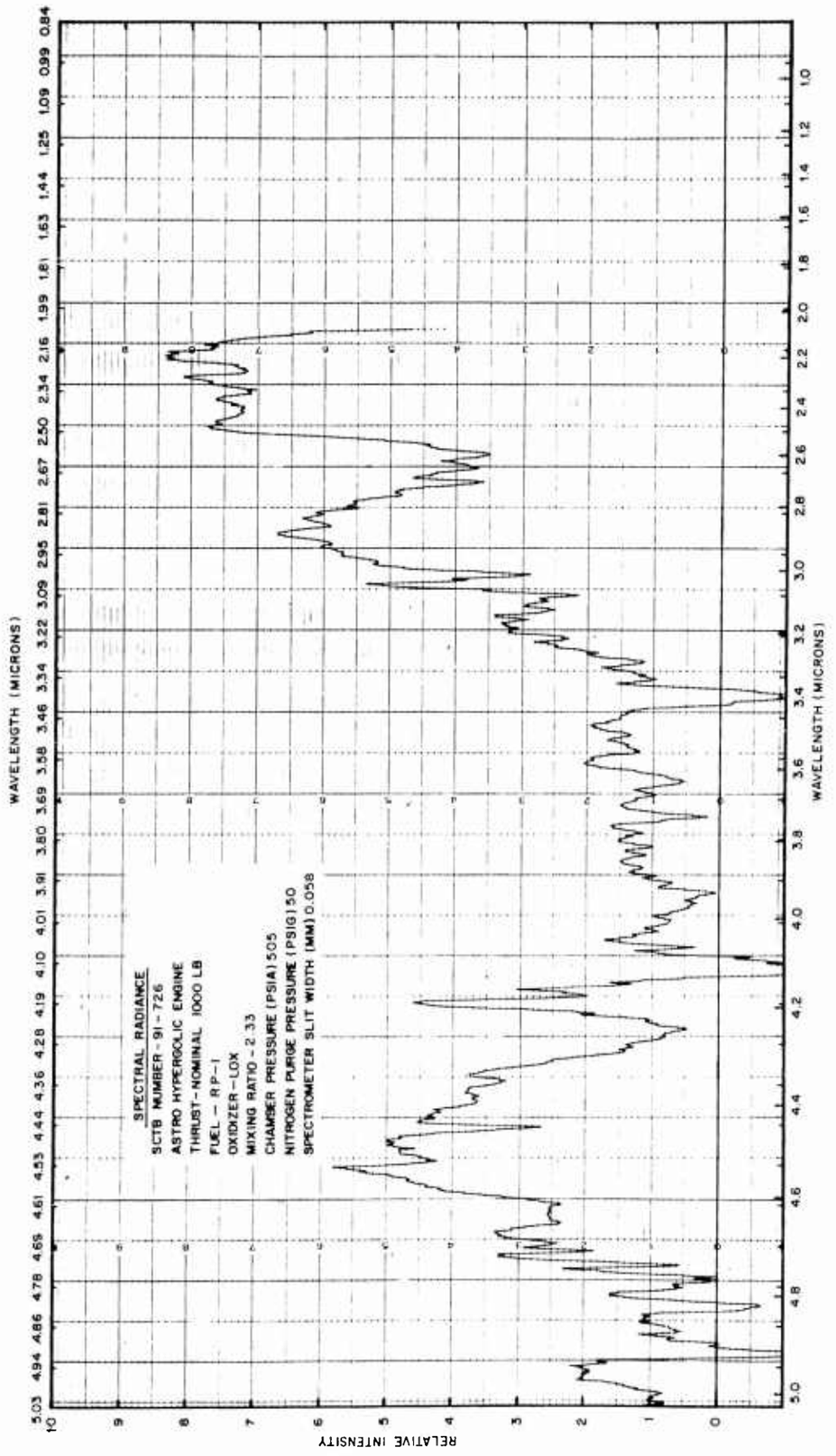
SPECTRAL RADIANCE
SCTB NUMBER - 91-726
ASTRO HYPERGOLIC ENGINE
THRUST-NOMINAL 1000 LB
FUEL - RP-1
OXIDIZER - LOX
MIXING RATIO - 2.33
CHAMBER PRESSURE (PSIA) 505
NITROGEN PURGE PRESSURE (PSIG) 50
SPECTROMETER SLIT WIDTH (MM) 0.058
WAVELENGTH (MICRONS)
WAVELENGTH (MICRONS)
RELATIVE INTENSITY

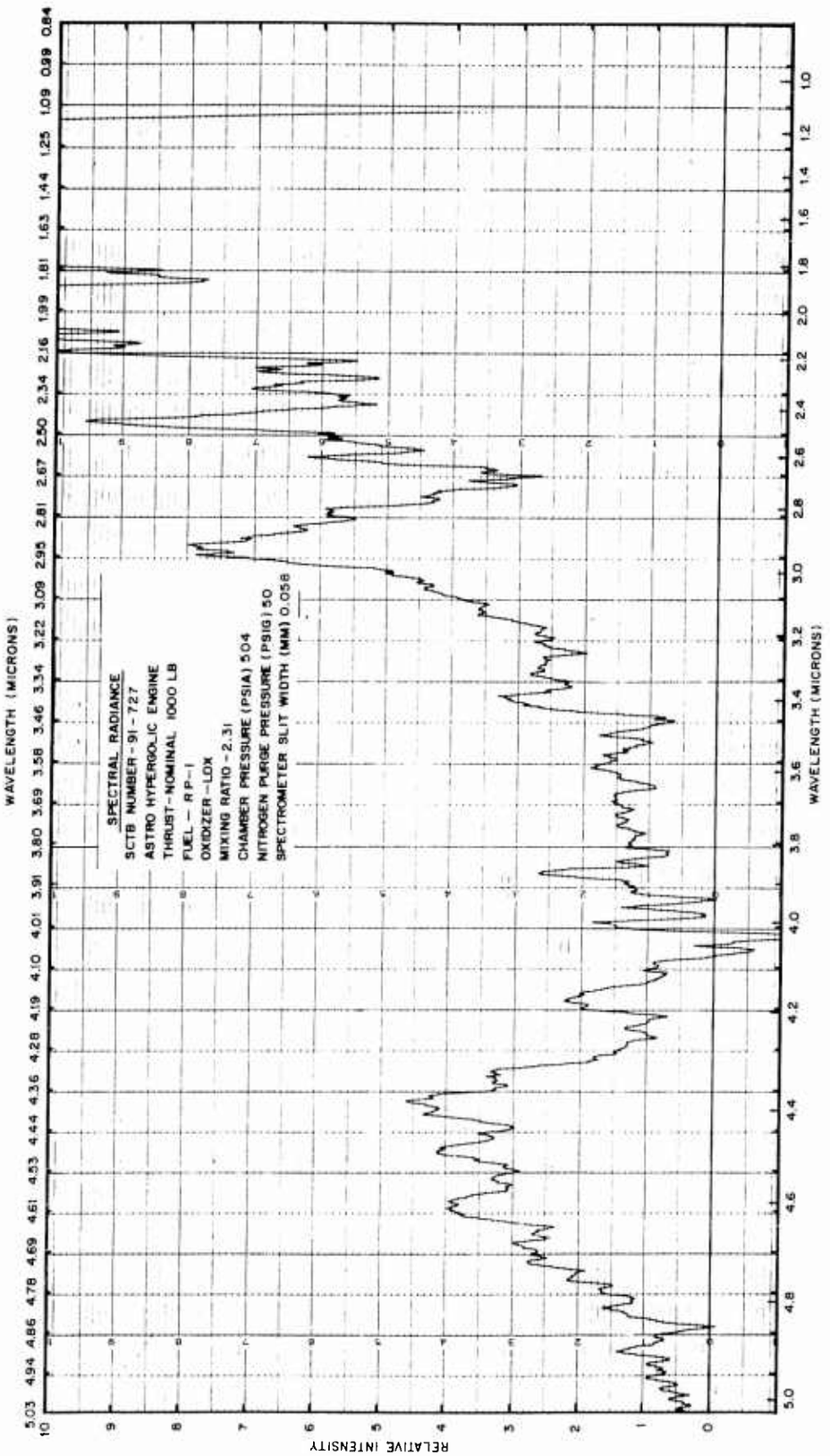
SPECTRAL RADIANCE
SCTB NUMBER - 91 - 727
ASTRO HYPERGOLIC ENGINE
THRUST - NOMINAL 1000 LB
FUEL - RP-1
OXIDIZER - LOX
MIXING RATIO - 2.31
CHAMBER PRESSURE (PSIA) 504
NITROGEN PURGE PRESSURE (PSIG) 50
SPECTROMETER SLIT WIDTH (MM) 0.058
WAVELENGTH (MICRONS)
RELATIVE INTENSITY

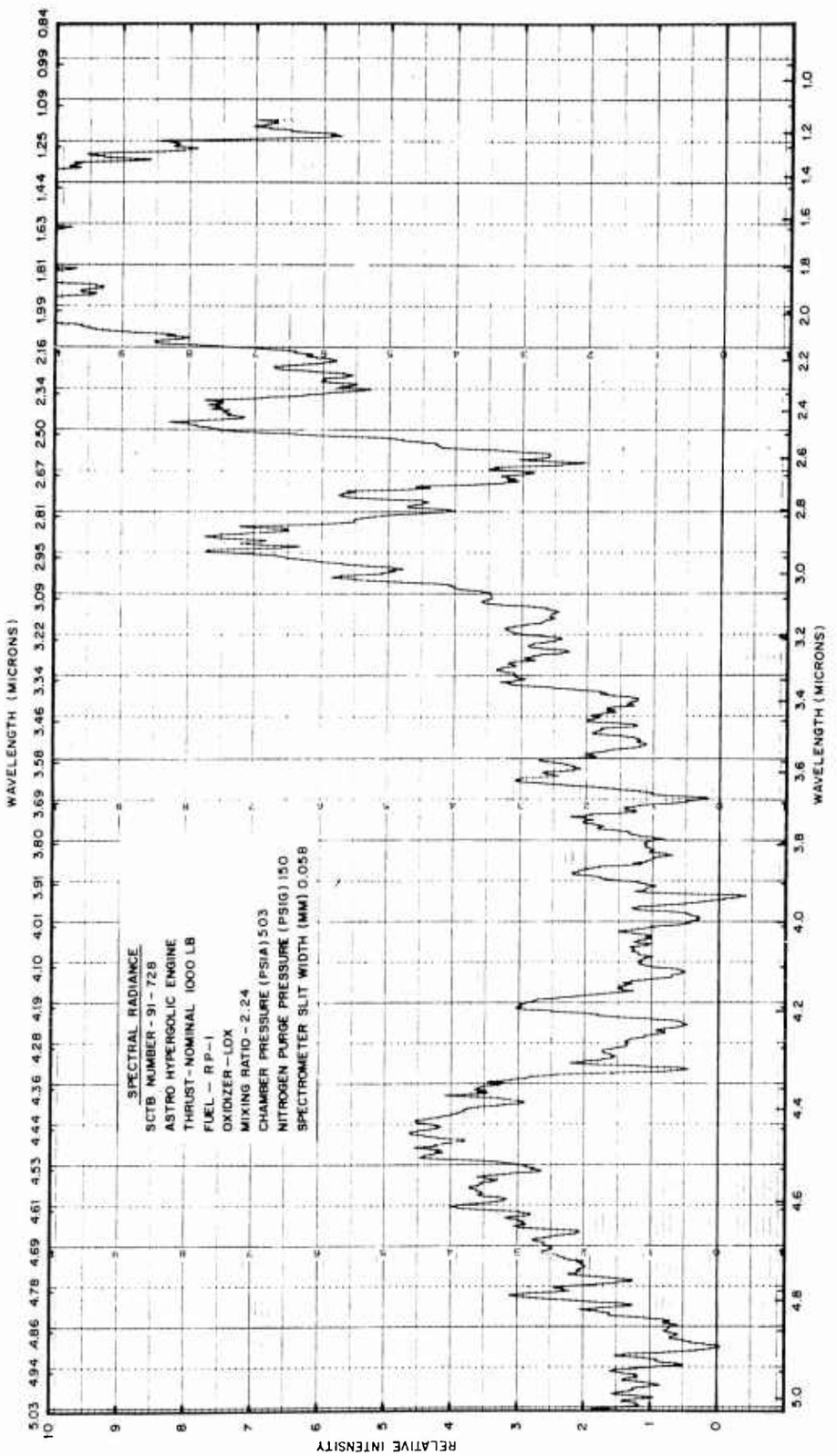
SPECTRAL RADIANCE
SCTB NUMBER - 91 - 728
ASTRO HYPERGOLIC ENGINE
THRUST - NOMINAL 1000 LB
FUEL — RP-1
OXIDIZER — LOX
MIXING RATIO - 2.24
CHAMBER PRESSURE (PSIA) 503
NITROGEN PURGE PRESSURE (PSIG) 150
SPECTROMETER SLIT WIDTH (MM) 0.058
WAVELENGTH (MICRONS)
WAVELENGTH (MICRONS)
RELATIVE INTENSITY

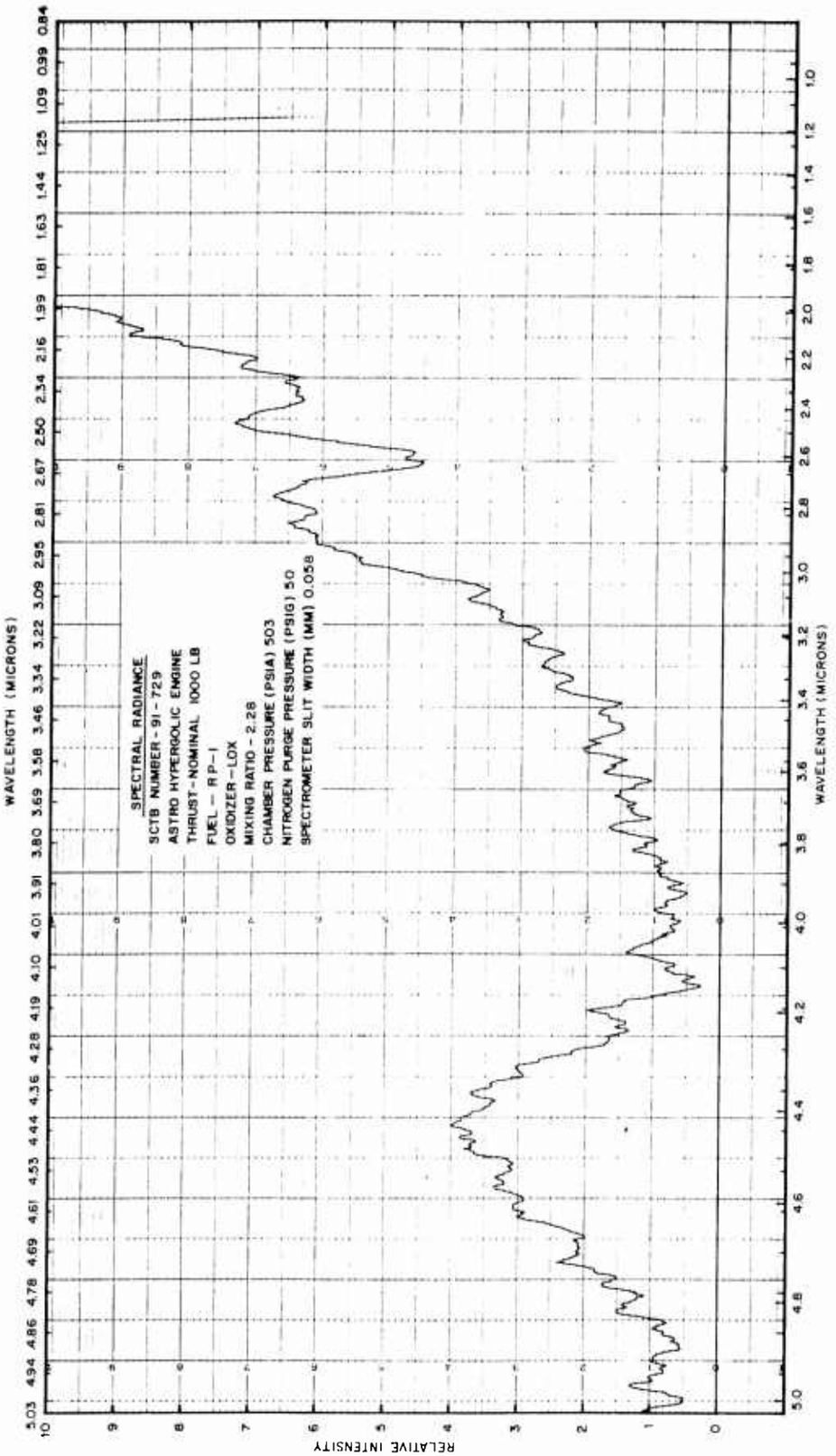
SPECTRAL RADIANCE
SCTB NUMBER - 91 - 729
ASTRO HYPERGOLIC ENGINE
THRUST - NOMINAL 1000 LB
FUEL — RP-1
OXIDIZER — LOX
MIXING RATIO - 2.28
CHAMBER PRESSURE (PSIA) 503
NITROGEN PURGE PRESSURE (PSIG) 50
SPECTROMETER SLIT WIDTH (MM) 0.058
WAVELENGTH (MICRONS)
RELATIVE INTENSITY

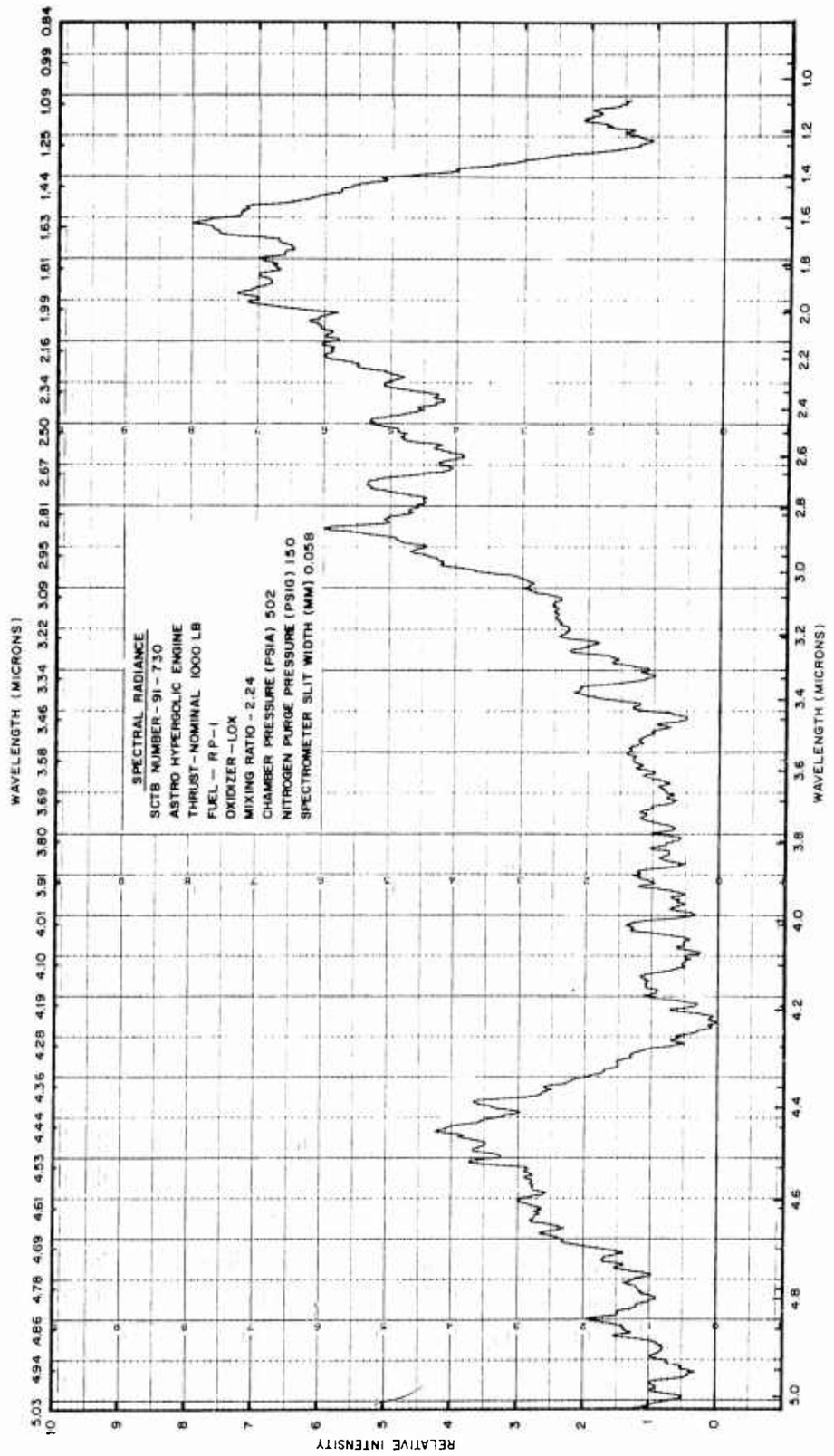
SPECTRAL RADIANCE
SCTB NUMBER - 91-730
ASTRO HYPERGOLIC ENGINE
THRUST - NOMINAL 1000 LB
FUEL — RP-1
OXIDIZER — LOX
MIXING RATIO - 2.24
CHAMBER PRESSURE (PSIA) 502
NITROGEN PURGE PRESSURE (PSIG) 150
SPECTROMETER SLIT WIDTH (MM) 0.058
WAVELENGTH (MICRONS)
RELATIVE INTENSITY

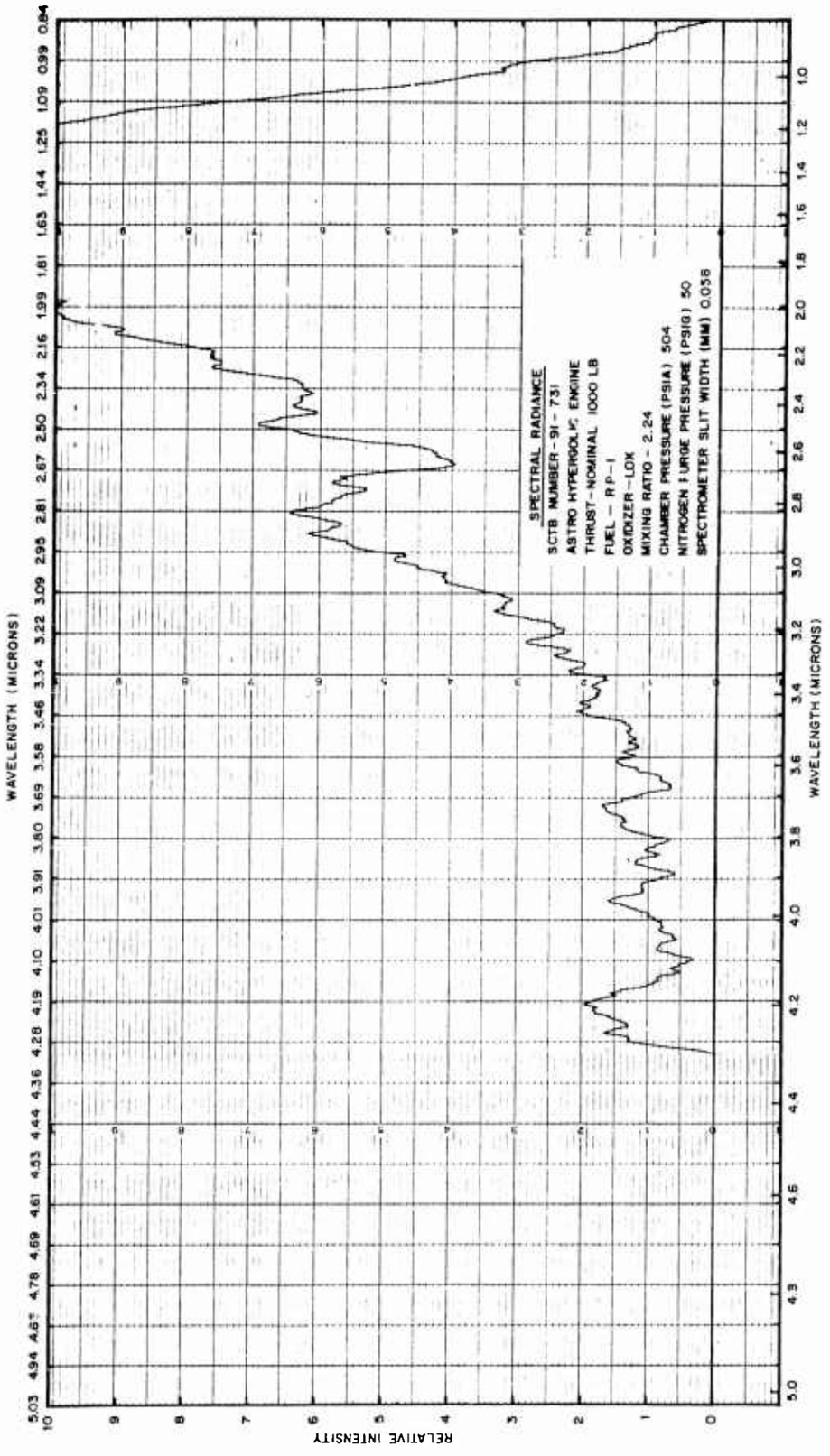
SPECTRAL RADIANCE
SCTB NUMBER - 91 - 731
ASTRO HYPERGOLIC ENGINE
THRUST - NOMINAL 1000 LB
FUEL — RP-1
OXIDIZER — LOX
MIXING RATIO - 2.24
CHAMBER PRESSURE (PSIA) 504
NITROGEN PURGE PRESSURE (PSIG) 50
SPECTROMETER SLIT WIDTH (MM) 0.058
WAVELENGTH (MICRONS)
RELATIVE INTENSITY

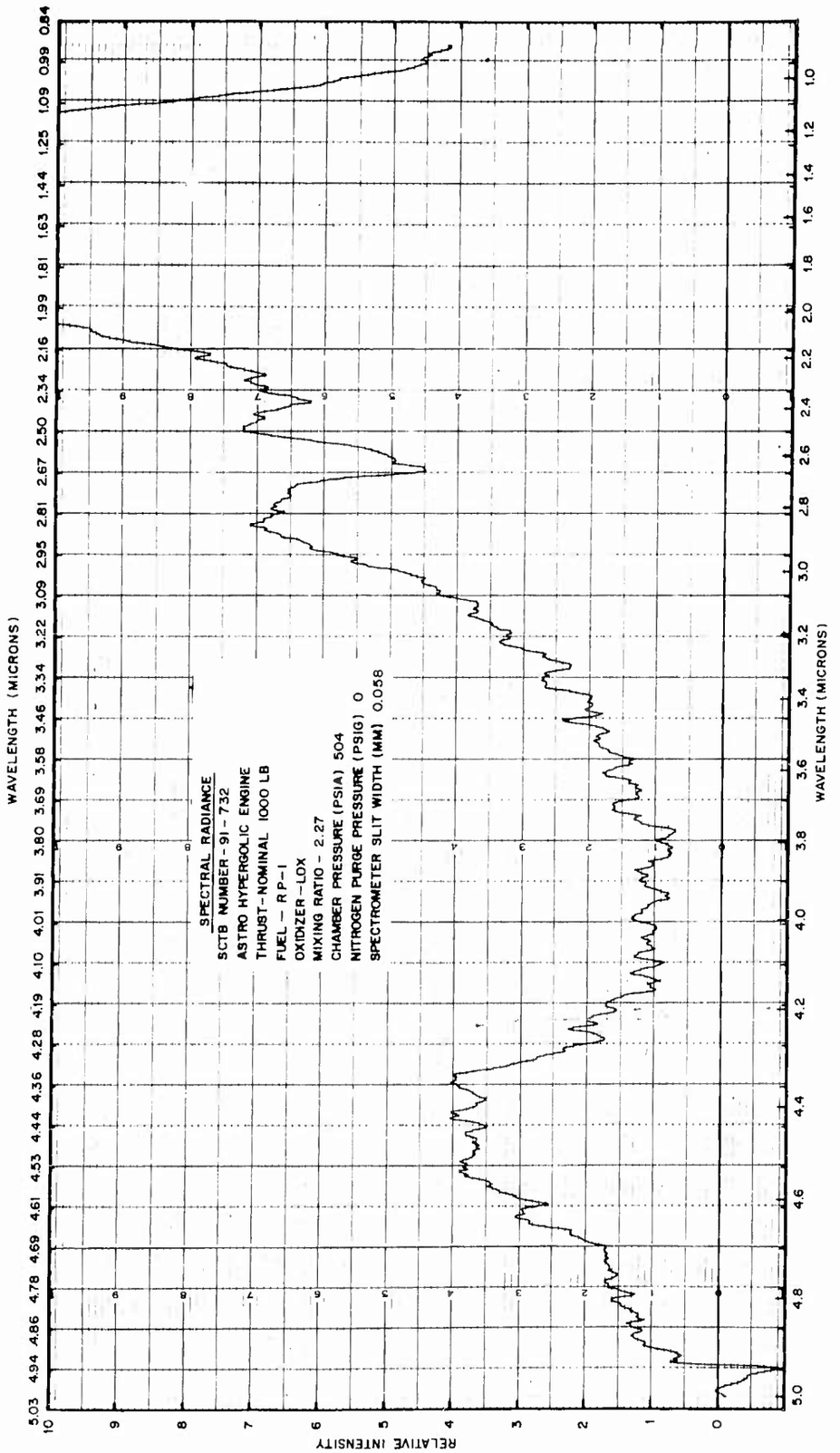
SPECTRAL RADIANCE
SCTB NUMBER - 91 - 732
ASTRO HYPERGOLIC ENGINE
THRUST - NOMINAL 1000 LB
FUEL - RP-1
OXIDIZER - LOX
MIXING RATIO - 2.27
CHAMBER PRESSURE (PSIA) 504
NITROGEN PURGE PRESSURE (PSIG) 0
SPECTROMETER SLIT WIDTH (MM) 0.058
WAVELENGTH (MICRONS)
WAVELENGTH (MICRONS)
RELATIVE INTENSITY

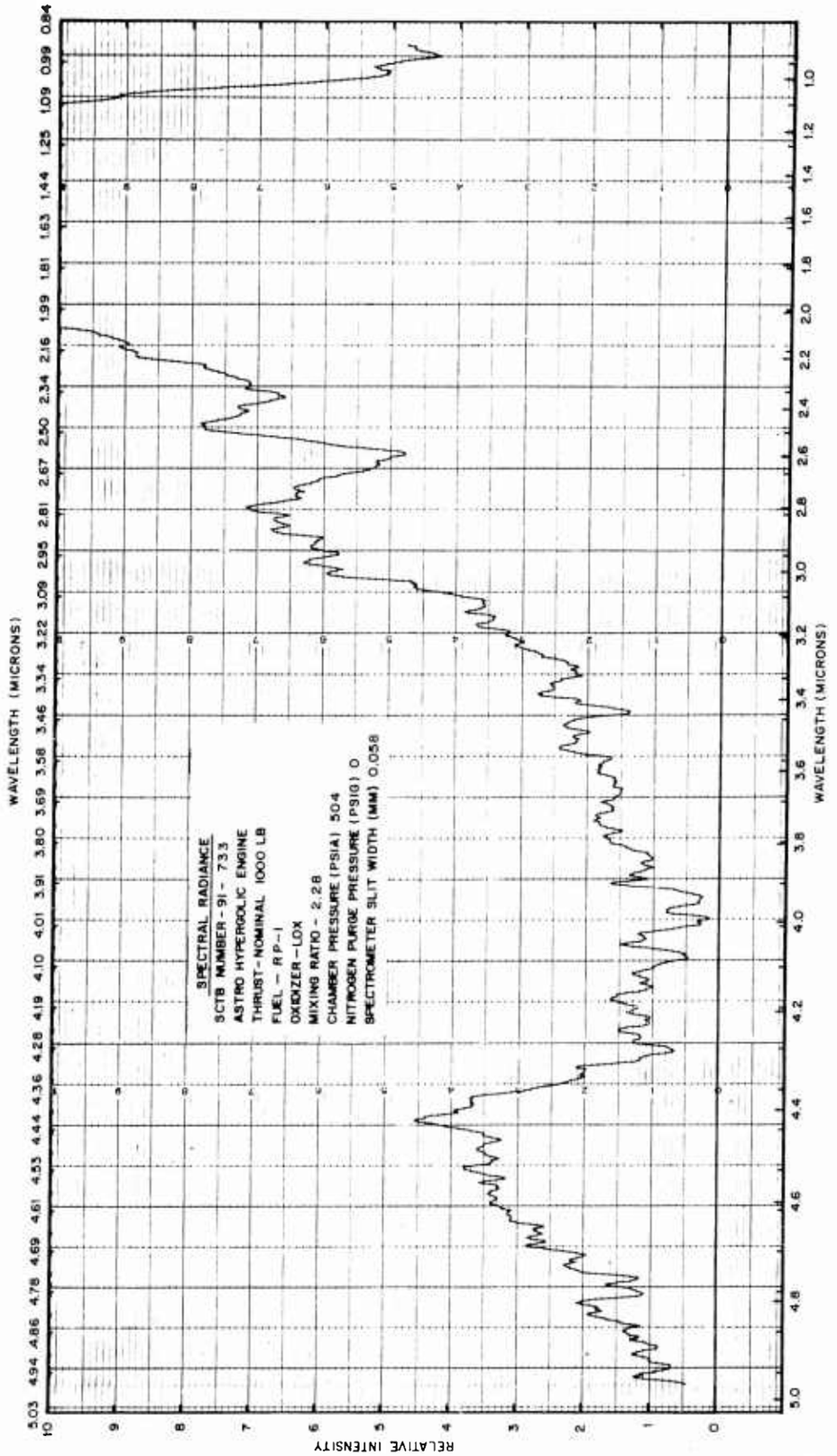
SPECTRAL RADIANCE
SCTB NUMBER - 91 - 733
ASTRO HYPERGOLIC ENGINE
THRUST - NOMINAL 1000 LB
FUEL - RP-1
OXIDIZER - LOX
MIXING RATIO - 2.28
CHAMBER PRESSURE (PSIA) 504
NITROGEN PURGE PRESSURE (PSIG) 0
SPECTROMETER SLIT WIDTH (MM) 0.058
WAVELENGTH (MICRONS)
RELATIVE INTENSITY

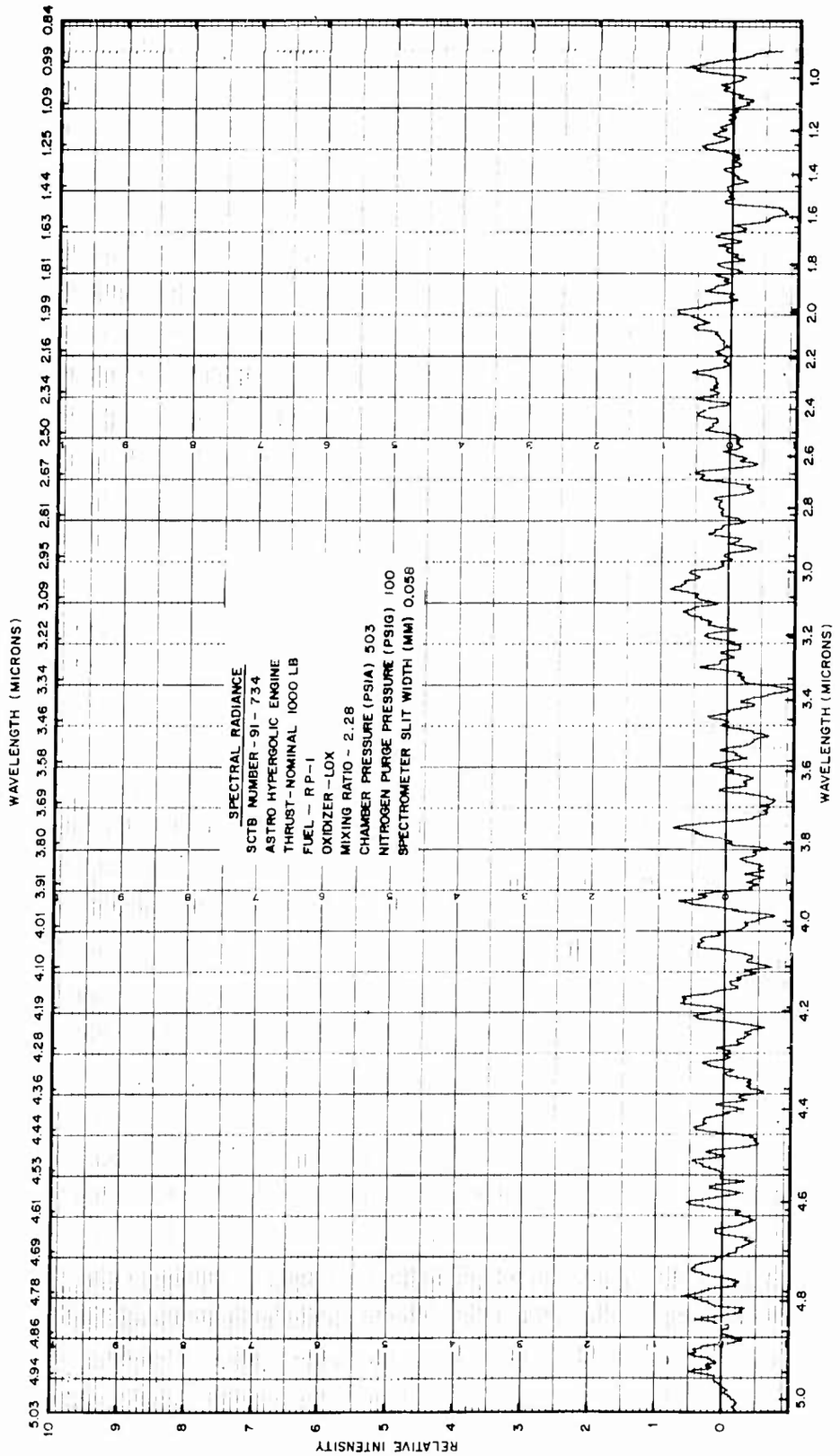
SPECTRAL RADIANCE
SCTB NUMBER - 91 - 734
ASTRO HYPERGOLIC ENGINE
THRUST - NOMINAL 1000 LB
FUEL - RP-1
OXIDIZER - LOX
MIXING RATIO - 2.28
CHAMBER PRESSURE (PSIA) 503
NITROGEN PURGE PRESSURE (PSIG) 100
SPECTROMETER SLIT WIDTH (MM) 0.058
WAVELENGTH (MICRONS)
WAVELENGTH (MICRONS)
RELATIVE INTENSITY

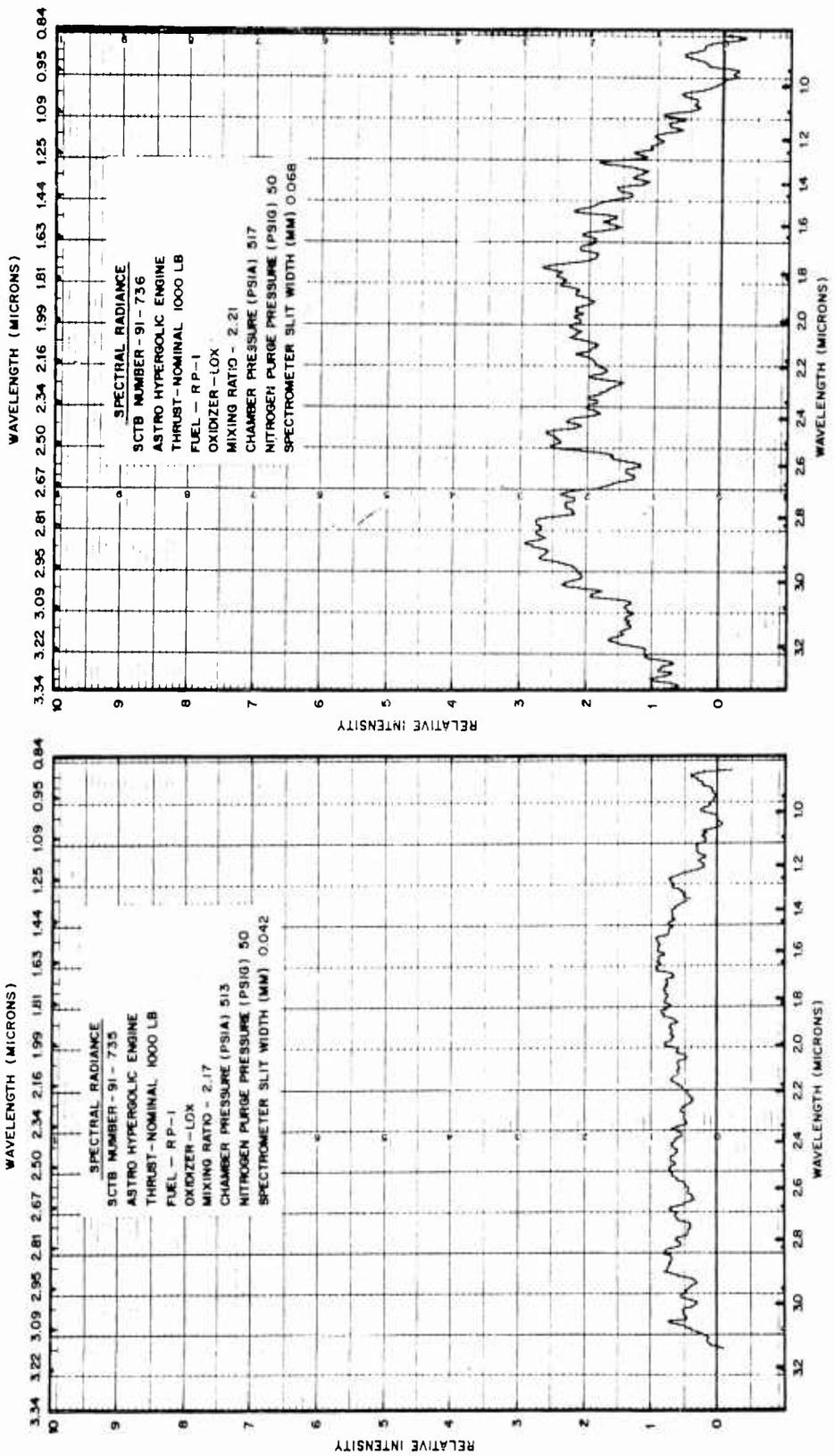
WAVELENGTH (MICRONS)
3.34 3.22 3.09 2.95 2.81 2.67 2.50 2.34 2.16 1.99 1.81 1.63 1.44 1.25 1.09 0.95 0.84
SPECTRAL RADIANCE
SCTB NUMBER - 91 - 735
ASTRO HYPERGOLIC ENGINE
THRUST - NOMINAL 1000 LB
FUEL - RP-1
OXIDIZER - LOX
MIXING RATIO - 2.17
CHAMBER PRESSURE (PSIA) 513
NITROGEN PURGE PRESSURE (PSIG) 50
SPECTROMETER SLIT WIDTH (MM) 0.042
RELATIVE INTENSITY
WAVELENGTH (MICRONS)
SPECTRAL RADIANCE
SCTB NUMBER - 91 - 736
ASTRO HYPERGOLIC ENGINE
THRUST - NOMINAL 1000 LB
FUEL - RP-1
OXIDIZER - LOX
MIXING RATIO - 2.21
CHAMBER PRESSURE (PSIA) 517
NITROGEN PURGE PRESSURE (PSIG) 50
SPECTROMETER SLIT WIDTH (MM) 0.068
RELATIVE INTENSITY
WAVELENGTH (MICRONS)

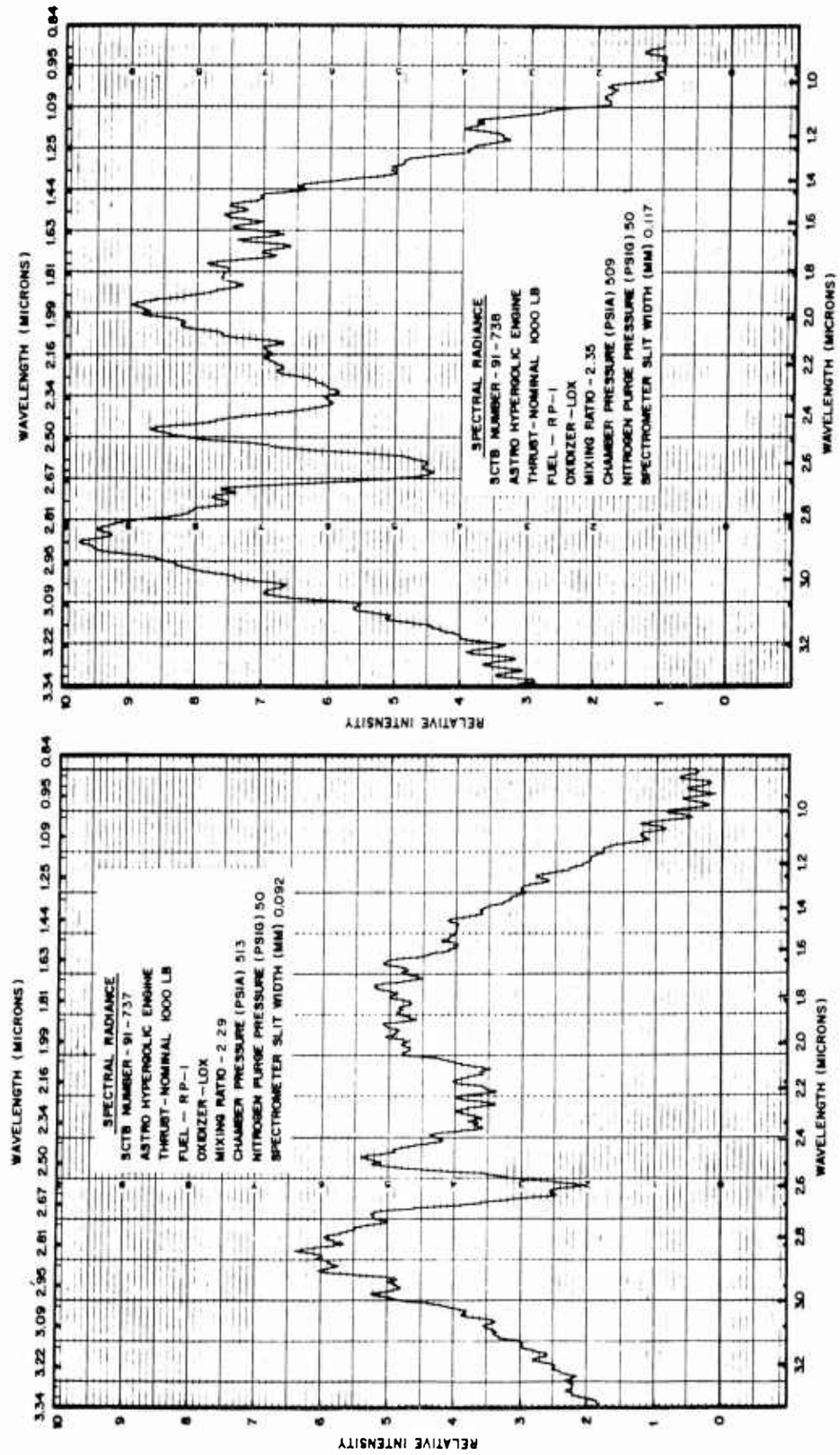
SPECTRAL RADIANCE
SCTB NUMBER - 91-738
ASTRO HYPERBOLIC ENGINE
THRUST - NOMINAL 1000 LB
FUEL - RP-1
OXIDIZER - LOX
MIXING RATIO - 2.35
CHAMBER PRESSURE (PSIA) 509
NITROGEN PURGE PRESSURE (PSIG) 50
SPECTROMETER SLIT WIDTH (MM) 0.117
WAVELENGTH (MICRONS)
RELATIVE INTENSITY
SPECTRAL RADIANCE
SCTB NUMBER - 91-737
ASTRO HYPERBOLIC ENGINE
THRUST - NOMINAL 1000 LB
FUEL - RP-1
OXIDIZER - LOX
MIXING RATIO - 2.29
CHAMBER PRESSURE (PSIA) 513
NITROGEN PURGE PRESSURE (PSIG) 50
SPECTROMETER SLIT WIDTH (MM) 0.092
WAVELENGTH (MICRONS)
RELATIVE INTENSITY

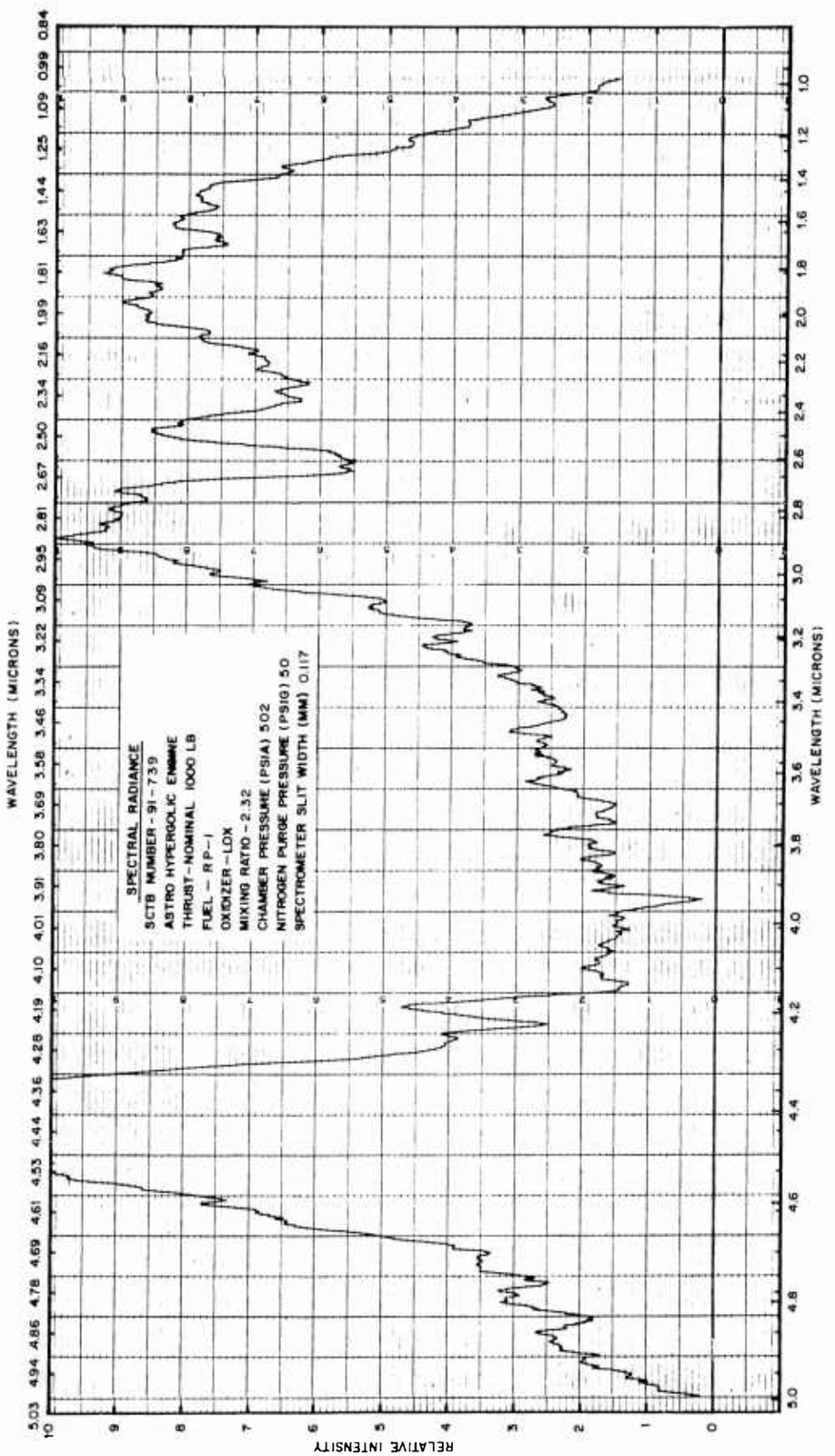
SPECTRAL RADIANCE
SCTB NUMBER - 91-739
ASTRO HYPERGOLIC ENGINE
THRUST - NOMINAL 1000 LB
FUEL - RP-1
OXIDIZER - LOX
MIXING RATIO - 2.32
CHAMBER PRESSURE (PSIA) 502
NITROGEN PURGE PRESSURE (PSIG) 50
SPECTROMETER SLIT WIDTH (MM) 0.117
WAVELENGTH (MICRONS)
WAVELENGTH (MICRONS)
RELATIVE INTENSITY

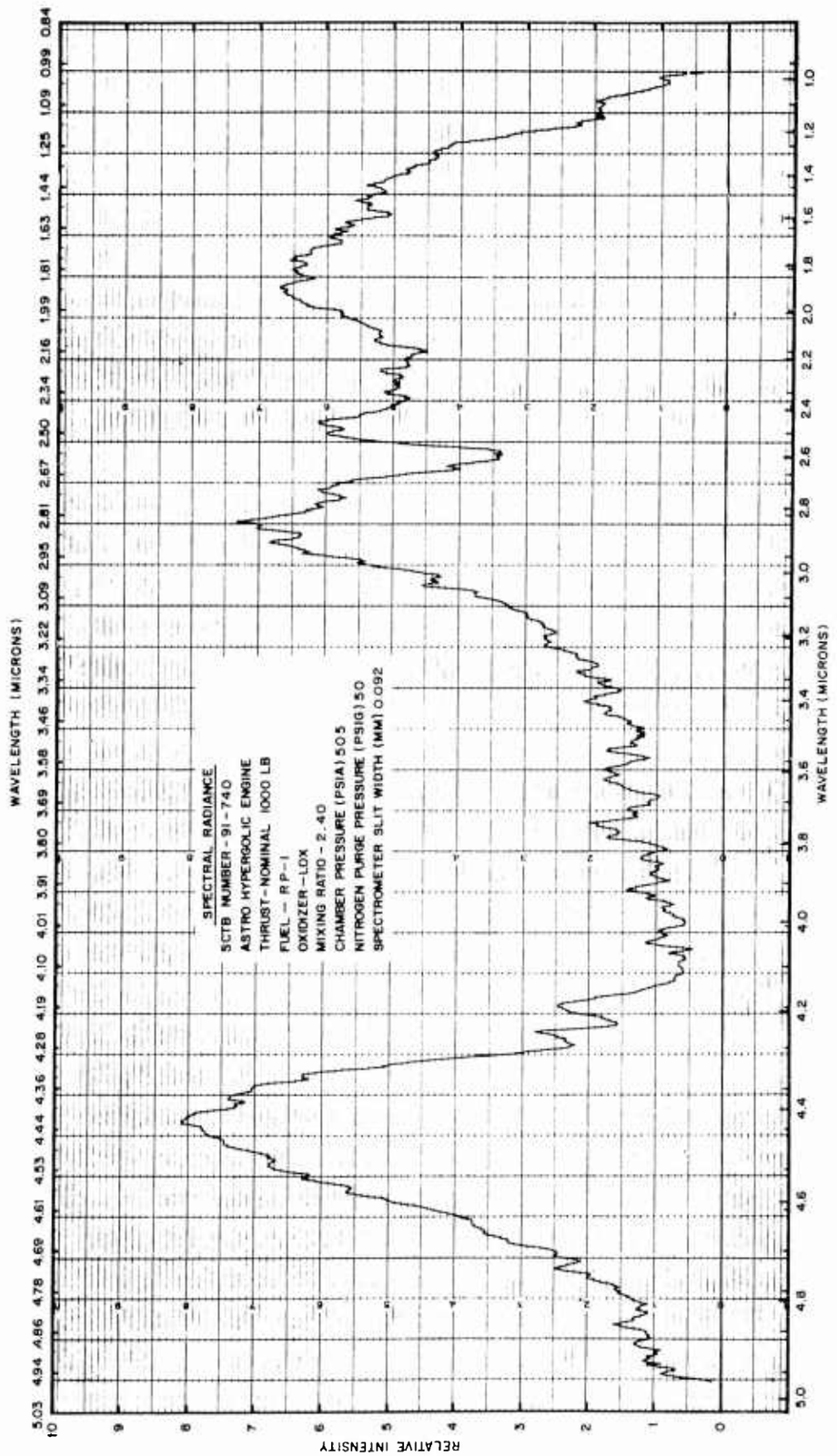
SPECTRAL RADIANCE
SCTB NUMBER - 91-740
ASTRO HYPERGOLIC ENGINE
THRUST - NOMINAL 1000 LB
FUEL — RP-1
OXIDIZER - LOX
MIXING RATIO - 2.40
CHAMBER PRESSURE (PSIA) 505
NITROGEN PURGE PRESSURE (PSIG) 50
SPECTROMETER SLIT WIDTH (MM) 0.092
WAVELENGTH (MICRONS)
RELATIVE INTENSITY

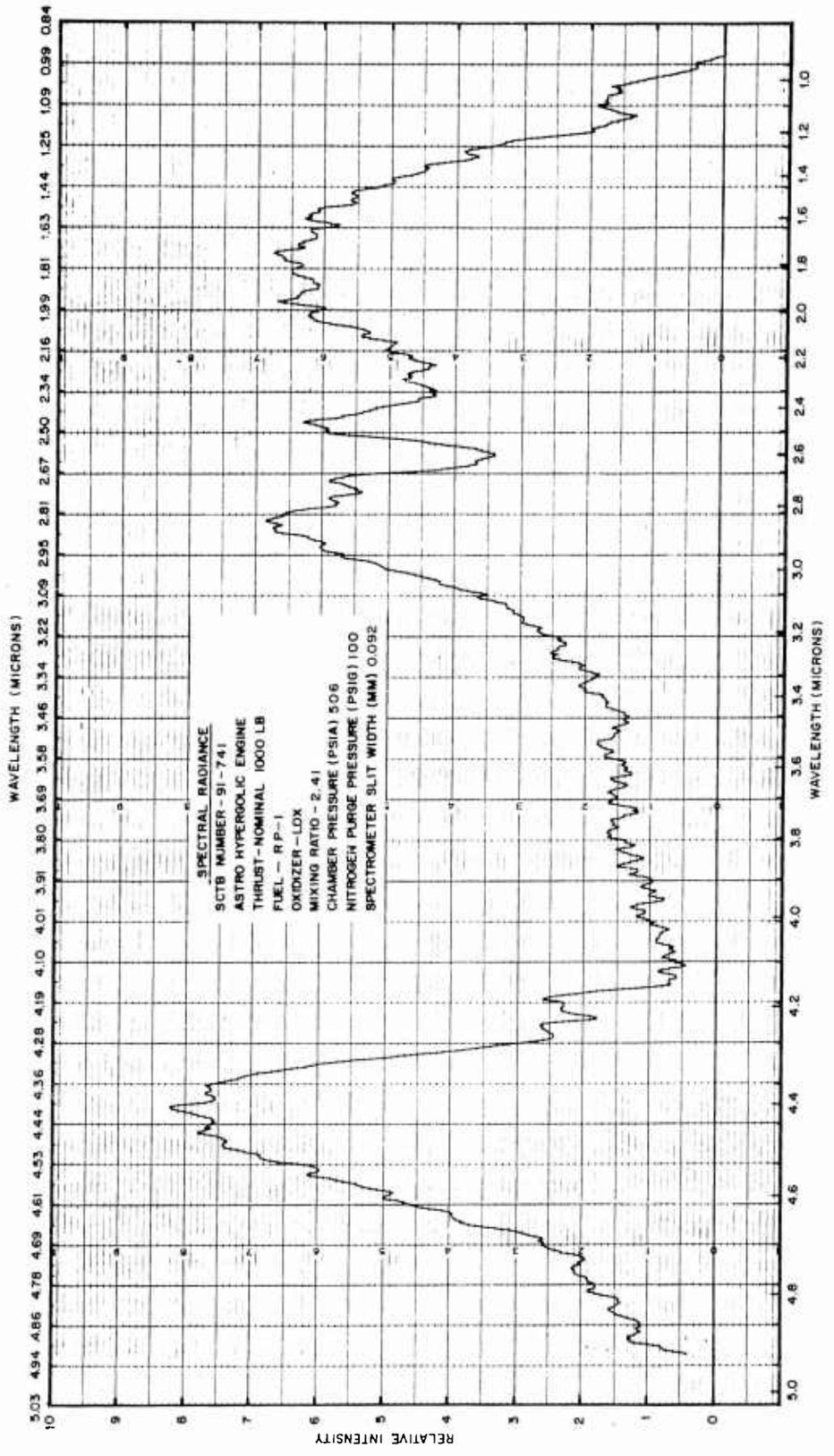
SPECTRAL RADIANCE
SCTB NUMBER - 91-741
ASTRO HYPERBOLIC ENGINE
THRUST - NOMINAL 1000 LB
FUEL - RP-1
OXIDIZER - LOX
MIXING RATIO - 2.41
CHAMBER PRESSURE (PSIA) 506
NITROGEN PURGE PRESSURE (PSIG) 100
SPECTROMETER SLIT WIDTH (MM) 0.092
WAVELENGTH (MICRONS)
RELATIVE INTENSITY
WAVELENGTH (MICRONS)

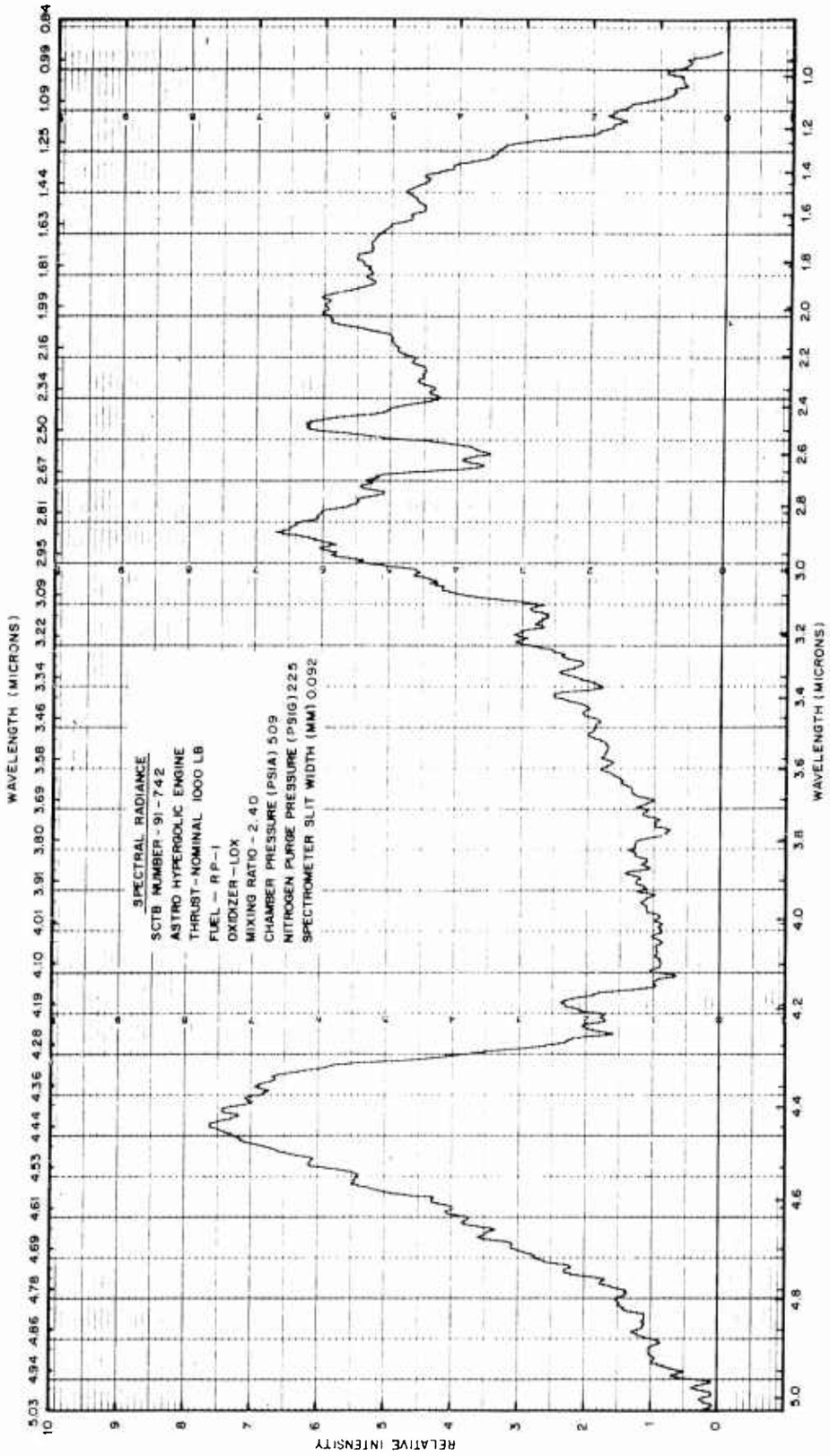
SPECTRAL RADIANCE
SCTB NUMBER - 91-742
ASTRO HYPERGOLIC ENGINE
THRUST-NOMINAL 1000 LB
FUEL — RP-1
OXIDIZER — LOX
MIXING RATIO - 2.40
CHAMBER PRESSURE (PSIA) 509
NITROGEN PURGE PRESSURE (PSIG) 225
SPECTROMETER SLIT WIDTH (MM) 0.092
WAVELENGTH (MICRONS)
RELATIVE INTENSITY

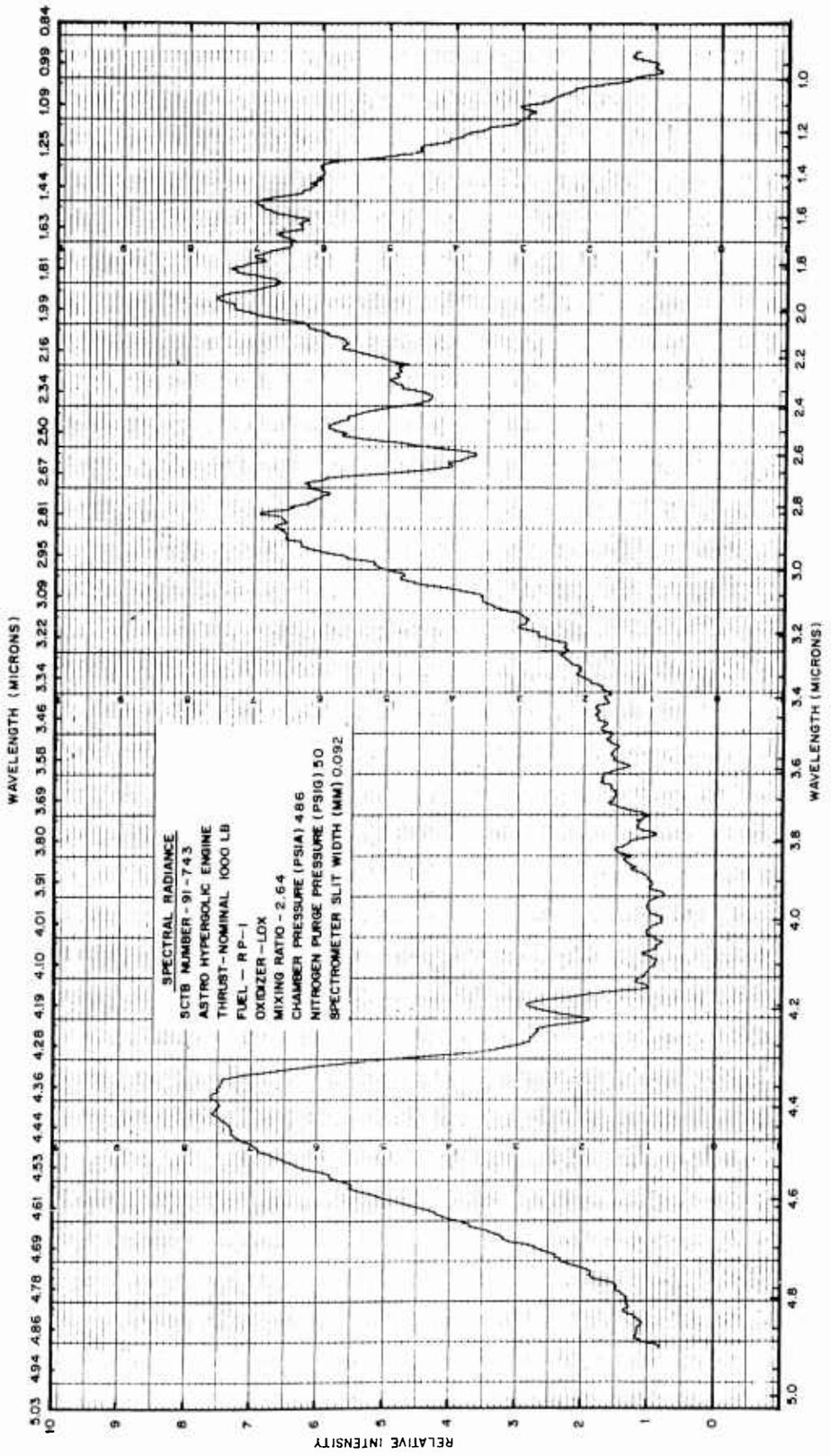
SPECTRAL RADIANCE
SCTB NUMBER - 91-743
ASTRO HYPERGOLIC ENGINE
THRUST-NOMINAL 1000 LB
FUEL — RP-1
OXIDIZER — LOX
MIXING RATIO - 2.64
CHAMBER PRESSURE (PSIA) 486
NITROGEN PURGE PRESSURE (PSIG) 50
SPECTROMETER SLIT WIDTH (MM) 0.092
WAVELENGTH (MICRONS)
RELATIVE INTENSITY

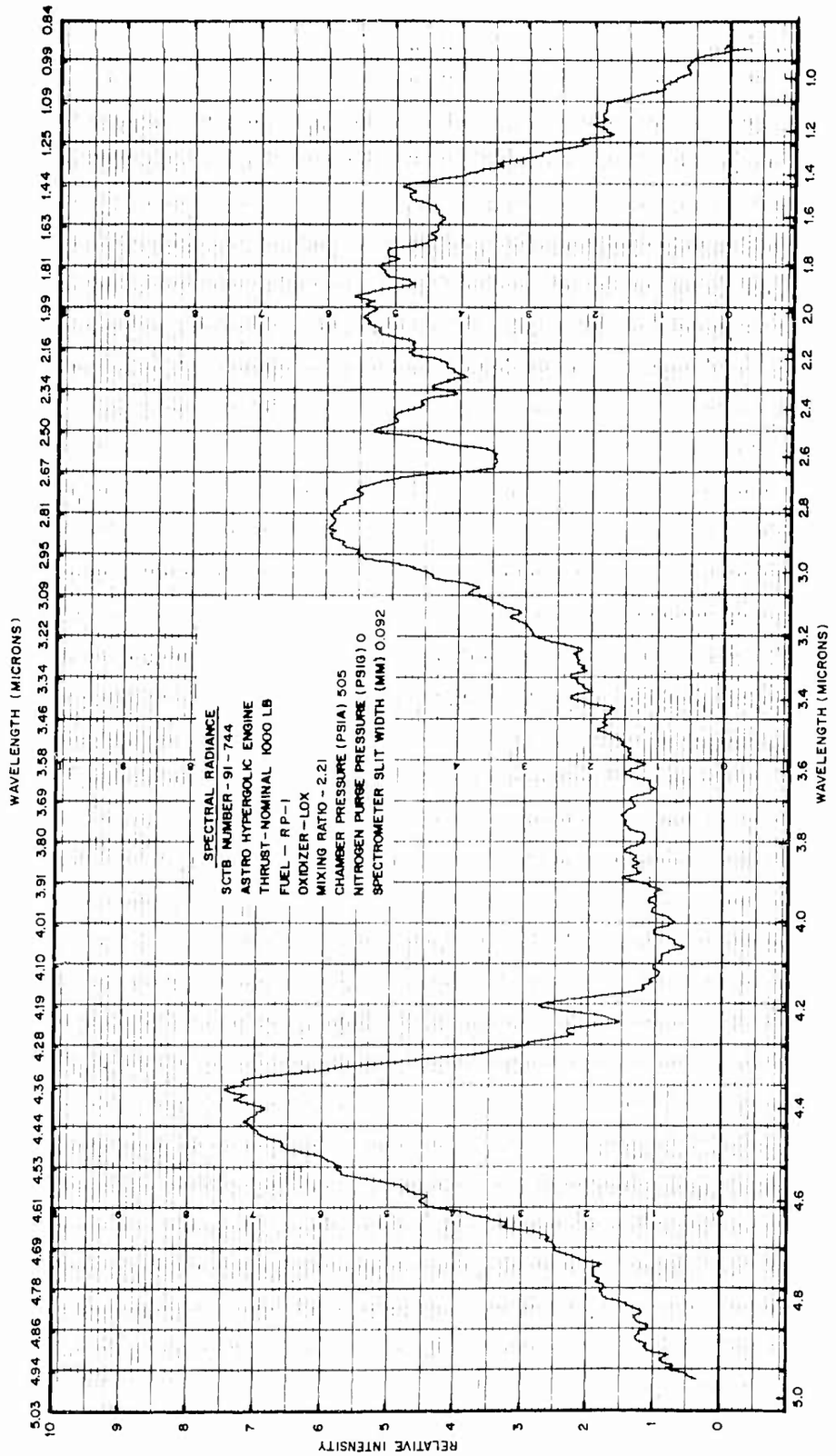
SPECTRAL RADIANCE
SCTB NUMBER - 91 - 744
ASTRO HYPERGOLIC ENGINE
THRUST - NOMINAL 1000 LB
FUEL - RP-1
OXIDIZER - LOX
MIXING RATIO - 2.21
CHAMBER PRESSURE (PSIA) 505
NITROGEN PURGE PRESSURE (PSIG) 0
SPECTROMETER SLIT WIDTH (MM) 0.092
WAVELENGTH (MICRONS)
RELATIVE INTENSITY
WAVELENGTH (MICRONS)

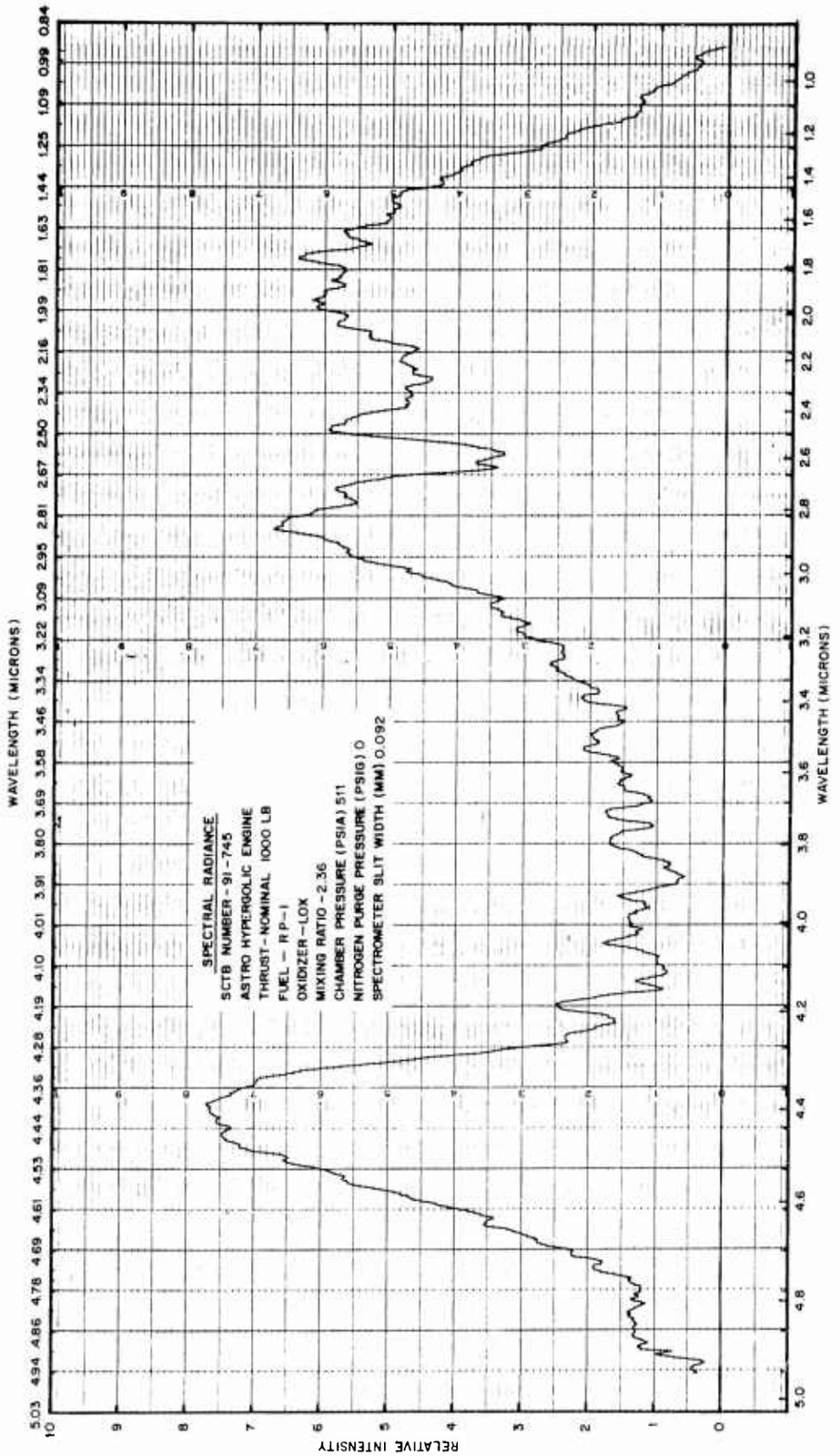
SPECTRAL RADIANCE
SCTB NUMBER - 91-745
ASTRO HYPERGOLIC ENGINE
THRUST - NOMINAL 1000 LB
FUEL - RP-1
OXIDIZER - LOX
MIXING RATIO - 2.36
CHAMBER PRESSURE (PSIA) 511
NITROGEN PURGE PRESSURE (PSIG) 0
SPECTROMETER SLIT WIDTH (MM) 0.092
WAVELENGTH (MICRONS)
RELATIVE INTENSITY
WAVELENGTH (MICRONS)

Appendix C

CALIBRATION OF THE MICHELSON (BLOCK I-4T) INTERFEROMETER SPECTROMETER

The theoretical approach to the vital problem of calibration is presented herein by Richard G. Clow, Org. 52-40, LMSC Research Laboratories at Palo Alto. This mathematical discussion is an integral and necessary contribution to the report as a whole and should be of considerable assistance to infrared scientists in their evaluation of the subject spectrometer for spectral analysis of radiating sources.

C.1 INTRODUCTION

An attempt is made in the following sections to complete the theory governing calibration of the Michelson interferometer spectrometer, particularly as it applies to one typical instrument, the Block I-4T. The excellent study of methods of radiometric calibration recently presented by Fred E. Nicodemus and George J. Zissis (Ref. 1) is a necessary reference in this work. Although the basic radiometer is covered very thoroughly in that report, the material on spectral-radiometers is sketchy in its application to Michelson interferometer spectrometers in general.

The Michelson interferometer spectrometer is different from all the other types of spectrometers considered by Nicodemus and Zissis (Ref. 1) in that the radiation from different wavelengths is not dispersed in space. The operation of the interferometer spectrometer is based on the fact that light of different wavelengths is modulated at different frequencies by the motion of one of the mirrors. It may be said to disperse in frequency rather than to disperse in space. Three important consequences of this difference are discussed here:

(1) The instrument more closely resembles a basic chopping radiometer than a space dispersing spectral radiometer. In fact, if a wave analyzer is tied directly to the output of the detector the instrument behaves almost exactly like a chopping radiometer with a narrow band optical filter (Fig. C-1). The center frequency of the filter is determined by the frequency of the wave analyzer, and the width of the filter is determined by the bandwidth of the wave analyzer (assuming that this bandwidth is larger than that corresponding to the spectral resolution of the instrument). The only difference is that

(a) INTERFEROMETER SPECTROMETER (WITHOUT RECORDING OF INTERFEROGRAM)

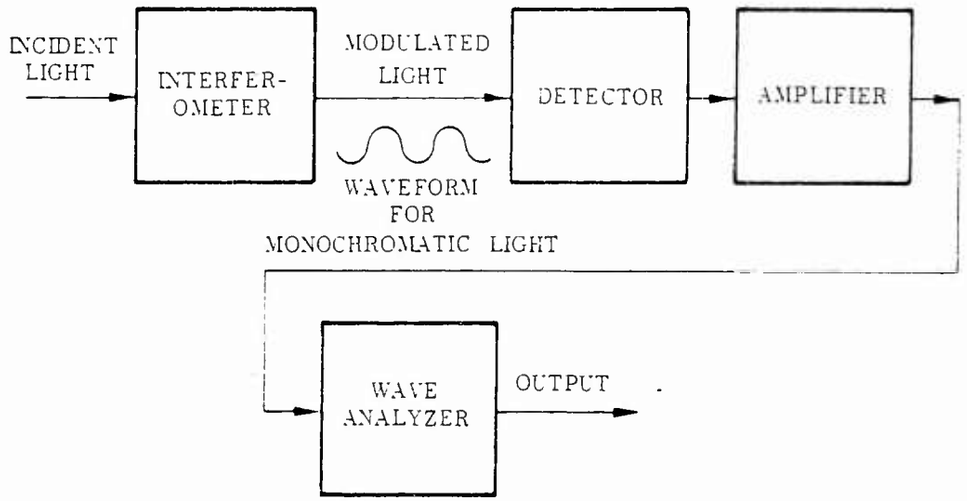

(b) CHOPPER RADIOMETER

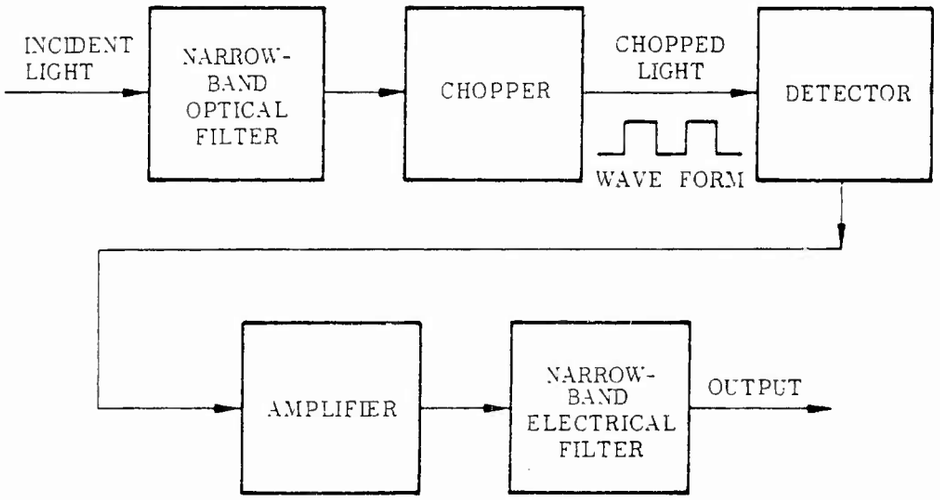

Fig. C-1 Comparison of Functional Operation of Interferometer Spectrometer With Copper Radiometer

the chopping action is obtained by interference rather than by interposition of an opaque chopper blade. The chopping action is strictly sinusoidal compared to the "square wave" chopping of the usual chopper wheel. These facts become immediately evident when the mode of action of the interferometer, as described herein, (e.g., in the I-4T manual) is considered.

Consequently, the calibration procedure for the interferometer spectrometer certainly should be reconsidered. That will be done at least partially in this report. Provided an absolute calibration can be achieved as well on a Block as on any other radiometer, there appears to be no need to run a relative spectral calibration on the Block, followed by an absolute calibration on some other radiometer. Furthermore, as pointed out by Nicodemus and Zissis (Ref. 1, p. 49) there is some risk of error in this dual type of calibration.

(2) All of the light entering the interferometer spectrometer falls on the detector at the same time (except for normal losses and the 0.5 modulation factor that occur in any chopping radiometer). This means that there is a much higher chance for saturation of the detector than there is in a space dispersing spectrometer. Following the basic principle (Ref. 1) that all conditions should be reproduced as exactly as possible, we see that calibration with a monochromatic beam of light is not acceptable. It would be possible that with monochromatic light (as from a monochrometer) no saturation would be observed, but when a total spectrum is used (as in a blackbody) the amount of light from all other wavelengths combined could induce saturation even though no more light was present at any particular wavelength. For this reason, calibration should be effected with a source whose spectral distribution, both in intensity, and (roughly) in distribution, is close to that expected if the detector sensitivity varies sharply with wavelength.

(3) Nonlinearity in the detector can completely invalidate the entire output. This is so because the method of Fourier analysis depends upon the linearity of the conversion from optical intensity to electrical voltage. If this conversion is linear, a given frequency of intensity variation in the input will produce only

that same frequency in the output. However, if nonlinearities occur, other frequencies will appear in the output, usually multiples or submultiples of the signal frequency. Since frequency corresponds to optical wavelength, a nonlinear detector will give not only erroneous intensity indications; it also will give rise to false lines and a general distortion of the spectrum as well. Thus, the warning of Nicodemus and Zissis (Ref. 1, p. 34) that nonlinearity means trouble is well justified in this case. The conclusion is reached that in an interferometer spectrometer, nonlinearity must be absolutely avoided. Avoidance implies that thermal-type detectors such as bolometers and thermistors are preferred to photoconductive detectors. Their use is usually adequate because they collect radiation constantly rather than during only a part of the scan cycle as is the case with ordinary spectral radiometers. When extreme sensitivity is needed, and therefore photoconductive cells must be used, extreme precautions should be taken to avoid nonlinearities. It is necessary to be very sure that the detector is in the same degree of saturation in the calibration as in actual use. This means that the light level on the detector must not vary. Then small variations from this level will linearly change detector output, but the responsivity depends upon the general light level.

C.2 REFERENCE SOURCE

It is necessary in the case of a chopping radiometer to ask what radiation is falling on the detector when the chopper blade is in the optical path (Ref. 1, p. 7). Considerations taken into account in the introduction, pose this analogous question concerning the interferometer: What radiation is falling on the detector when light from the source cannot pass to the detector because of interference?

Before answering the above question, we need to consider the basic operating principles of the instrument. Complete information is given by J. Connes (Ref. 2) and by Block Associates, Inc. (Ref. 3). A brief description will be given here.

Reference to Fig.C-2 shows that light from the source falls on the partially reflecting surface, M; part is reflected to M_2 and thus passes to the detector; and part is transmitted to M_1, where reflection returns the ray to M. Here the ray divides again, part being returned to the source, and part being reflected to the detector.

When the distances MM_1 and MM_2 are equal, light from the source reflected from M_1 reinforces light reflected from M_2. As the distance MM_1 increases, the two rays passing to the detector will alternately reinforce and cancel each other. The intensity transmitted to the detector for a monchromatic source will be

$$I = I_o (1 + \sin 4\pi \nu x)$$

where

I_o is proportional to the initial intensity

ν is the wave number of the incident light

x is the displacement of M_1 from the zero position

If the mirror excursion takes place uniformly over a distance B/2 in time T, the distance x at time t will be $x_t = Bt/2T$, and the transmitted intensity will be

$$I = I_o \left[1 + \sin 2\pi \left(\frac{\nu B}{T}\right) t\right]$$

In other words, the intensity from a monochromatic source of wave number ν will be modulated at a frequency

$$f_\nu = \frac{\nu B}{T}$$

A statement in Ref. 3 indicates that the light is returned to the source when it is not passing the detector. This is plausible since, according to geometrical optics, the ray shown in Fig. C.2 can terminate only in either the detector or the source.

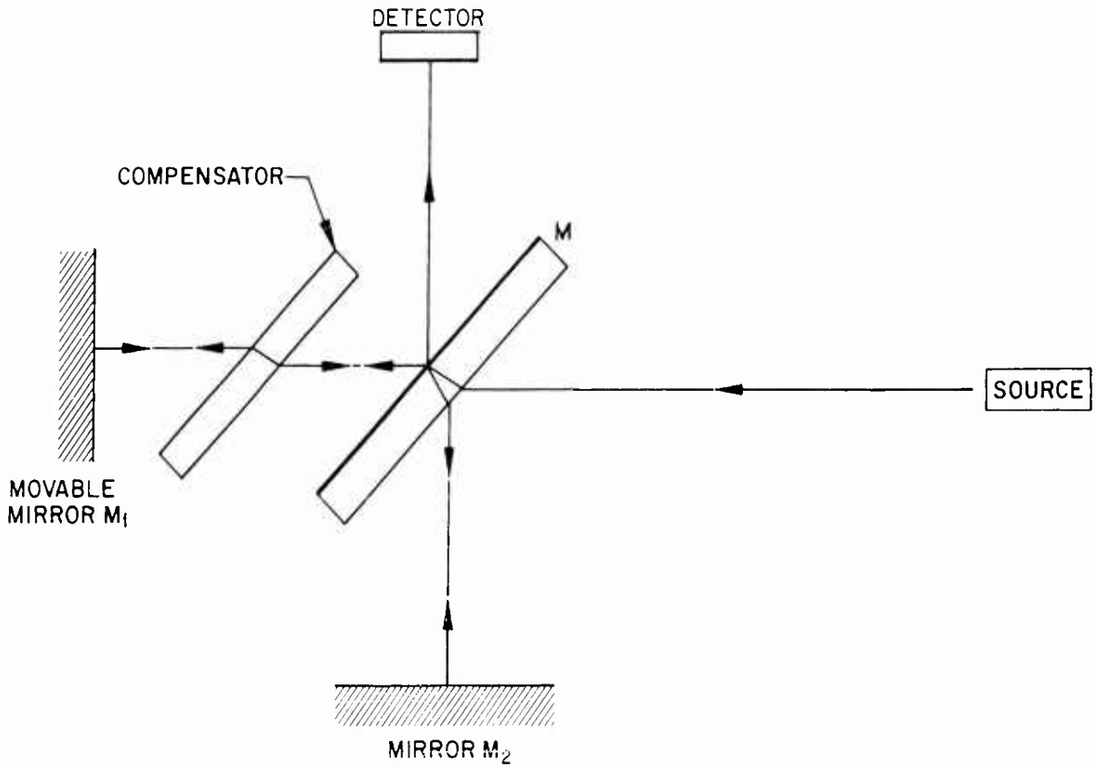

Fig. C-2 Typical Path of Radiation Originating in Detector When Mirror Displacement Produces Destructive Interference in Light From Source

However, light originating in the detector traverses a reverse path. Considerations of the interchangeability of the source and detector in a linear medium indicate that the detector looks at itself when it is not looking at the source. As x is increased, this intensity is modulated also, but 180 deg out of phase with radiation coming from the source; hence it subtracts from the source. It must be concluded that, at least in part, the interferometer responds to differences between source and detector spectral radiance. This consideration will be an important one in making long wavelength measurements, since it means that the detector acts essentially as a reference source.

Actually, the semireflecting surface M will be a very thin metalic coating on a glass surface. Reflection from metalic surfaces do not follow the same laws as reflection from dielectrics. The situation is very complex, as is indicated Born and Wolf (Ref. 4. Ch. XIII). The quantity which must be determined is the difference in the phase shift at M on internal and external reflection (Ref. 4, p. 300) (Ref. 2, p. 231). Further study of this question is needed. Moreover, the contributions of self-radiation from other parts of the instrument to the modulated radiation falling on the detector needs to be considered.

C.3 WAVEFORM VARIATION

That the waveform of the chopped radiation is not the same for every source is pointed out by Nicodemus and Zissis (Ref. 1, p. 40). An analogous effect is observed in interferometer spectrometers. This variation appears as a change in the frequency and phase of the modulated wave.

In the I-4T, the frequency at which a small monochromatic source is modulated depends upon its location in the field of view. When the source is at an angle γ from the center of the field, a mirror displacement x produces a retardation (Fig. C-3).

$$2r = 2x \sec \gamma$$

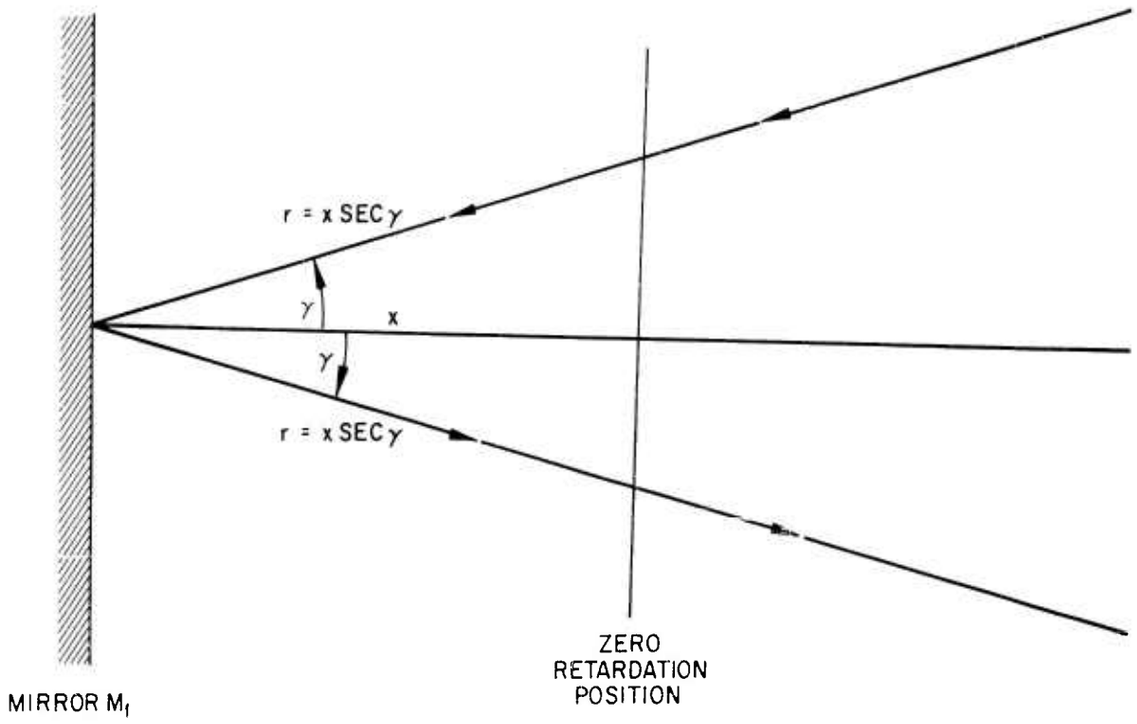

Fig. C-3 Variation of Retardation for an Oblique Ray

The radiation of wave number ν coming from this direction and modulated at a frequency

$$f'_\nu = 2\nu r = 2\nu x_t \sec\gamma = \frac{\nu B}{T} \sec\gamma$$

This differs from the frequency that would occur when the source is at the center of the field by an amount

$$\Delta f_\nu = f' - f = f_\nu (\sec\gamma - 1) \simeq f_\nu \frac{\gamma^2}{2}$$

since the series expansion for sec γ is sec $\gamma = 1 + \gamma^2/2 + \ldots$

Then, since

$$\nu = f \frac{T}{\nu B}$$

a monochromatic source will appear to change its color by

$$\Delta\nu = \Delta \frac{f_\nu T}{B} \simeq f_\nu \frac{\gamma^2}{2} \frac{T}{B} = \nu \frac{\gamma^2}{2} \text{ cm}^{-1}$$

as compared with its appearance at the center of the field of view.

Consider also the phase of sinusoidally modulated output resulting from a monochromatic point source. As the source changes its location in the field of view, the angle at which the ray is reflected from the semimetalic mirror is changed. For metallic surfaces, the difference for internal and external reflection (hereafter called the phase shift difference) generally may be expected to change with angle of reflection (Ref. 4, p. 612).

To summarize, both phase and frequency of the modulated waveform for a monochromatic point source may be expected to change with location of the point in the field of view.

In the interferometer spectrometer the "modulated" waveform (in the sense of Ref. 1) also changes with the wavenumber of the incident light. The variation in frequency has already been mentioned. This variation forms the basis of the operation of the instrument. The variation in phase of the modulated waveform is equally important, but, unfortunately, not so well understood. If the phase shift difference (referred to above) at M is zero, the modulated waveform will be a cosine wave. If the phase-shift difference is not exactly zero, a maximum intensity will not occur at $x = 0$. Suppose the phase-shift difference is θ radians. Then a displacement of

$$x_o = 2\left(\frac{\theta\lambda}{2\pi}\right) = \frac{\theta\lambda}{\pi}$$

is necessary to compensate for the phase shift to restore maximum intensity. The modulated intensity will then have phase of θ radians (i.e., will not be a cosine wave). As indicated in Ref. 4, Ch. XIII, such a variation of phase-shift difference with wavelength may be generally expected for metallic surfaces.

It may happen that the phase-shift difference is exactly zero for all wavelengths. In that case, all wavelengths will give a bright fringe at $x = 0$. If a fairly broad spectrum is being viewed, then $x = 0$ will be the only position for which all wavelengths will give a bright fringe, and a bright central fringe will result. This is the case assumed in the elementary theory. But if the phase-shift difference is not zero (say it is about π), each wavelength will produce a bright fringe at a displacement $x = \lambda$. If the spectrum is not too broad (i.e., all the visible) the maxima will coincide approximately at $x = \lambda$. A bright fringe will still be produced, but not at $x = 0$. Thus, the position of the bright fringe in white light cannot be taken as an absolute indication of the zero displacement position. Clearly some caution is necessary in applying the elementary theory.

It is well known that any shift Δx in the origin produces a shift in the phase of a sinusoidal waveform sine (ωx) proportional to ω. Thus, any error in the location of the zero displacement position will introduce a change in phase that is a function of frequency.

It may seem that consideration of phase of the modulated waveform is unimportant since the wave analyzer responds to the amplitude of the wave only. However, the signal voltage, $V(t)$, actually delivered at the output of the detector depends very much on the variation of the phase with frequency. To make this idea precise, consider that portion of $V(t)$ occurring in the interval $-T/2 < t < T/2$.

Let $S_V(f)$ be the spectrum of this portion of $V(t)$:

$$S_V(f) = \int_{-\frac{T}{2}}^{\frac{T}{2}} dt\ V(t)\ \exp(-i\,2\pi f t)$$

According to the sampling theorem (Ref. 5, p. 210)

$$S_V(f) = \sum_{m=-\infty}^{+\infty} S_V\left(\frac{m}{T}\right) \frac{\sin[\pi(fT - m)]}{\pi(fT - m)}$$

where $S_V(m/T)$ is the same function of m/T that $S_V(f)$ is of f; i.e.,

$$S_V\left(\frac{m}{T}\right) = \int_{-\frac{T}{2}}^{\frac{T}{2}} dt\ V(t)\ \exp\left(-i\,\frac{2\pi m t}{T}\right)$$

Let $s_V(f)$ be the spectrum of $V(t)$; then

$$V(t) = \int_{-\infty}^{\infty} df\, s_V(f)\, \exp(i2\pi ft)$$

Then

$$S_V\left(\frac{m}{T}\right) = \int_{-\frac{T}{2}}^{\frac{T}{2}} dt\, \exp\left(-i\,\frac{2\pi mt}{T}\right) \int_{-\infty}^{\infty} df\, s_V(f)\, \exp(i2\pi ft)$$

$$= \int_{-\infty}^{\infty} df\, s_V(f) \int_{-\frac{T}{2}}^{\frac{T}{2}} dt\, \exp\left[i2\pi t\left(f - \frac{m}{T}\right)\right]$$

Carrying out the integration over t, this becomes

$$S_V\left(\frac{m}{T}\right) = T \int_{-\infty}^{\infty} df\, s_V(f)\, \frac{\sin[\pi(fT - m)]}{\pi(fT - m)}$$

This means that all the information in the segment of $V(t)$ of length T is contained in the coefficients $S_V(m/T)$ which are weighted averages of the true spectrum $s_V(f)$. The weighting function in the integral is significantly different from zero only in a band of width $1/T$ around the frequency f.

At first, no difficulty seems apparent, but remember that $s_V(f)$ refers to the true complex-valued spectrum of $V(t)$; i.e., we are required to average its real and imaginary parts seperately. Now, if the phase of $s_V(f)$ varies rapidly with frequency f, the real and imaginary parts will each go through many cycles of positive and negative values in the interval $1/T$. For example, if $V(t) = \delta(t - T)$,

where the interval inspected ranges only over $-T/2$ to $T/2$, all spectral components (white light) will be present. Yet, because their phase varies rapidly with f, due to the displacement of the delta function from the origin, the averages over intervals $1/T$ will be zero. This means $S_V(m/T)$ will be zero. But this should hardly be surprising since $V(t) = 0$ identically in the interval referred to by $S_V(m/T)$.

One of the most immediate practical consequences of the above theory is that the position of zero retardation should be located within the observation interval and preferably centrally located. Another consequence refers to the existence of a situation in which concern for the variation of the phase-shift difference with frequency is not necessary: the case in which only a narrow band of frequencies is being used. This fact was exploited by Michelson in his work on the fine structure of spectral lines using this type of instrument. The practical implications for calibration of the I-4T will be discussed in Section. To summarize: The variation of Phase-shift difference with wavelength and position is certainly of importance in interferometer spectrometers.

C.4 THEORY OF RESPONSE

In this section, a brief sketch of a radiometric theory of interferometer spectrometers will be given. This theory is intended to complement that presented by Ref. 1, and should be easy reading for those thoroughly familiar with the reference report. It is assumed that all sources involved are self-luminous so that the response is to the intensity rather than to the amplitude of the electromagnetic radiation.

- Let x,y be coordinates in the source plane.
- Let λ be the optical wavelength.
- Let $N_\lambda(x,y,\lambda)$ be the source spectral radiance in watts/cm^2-ster-μ (actually this is the difference between source spectral radiance and instrument self-radiance).
- Let λ_o be the optical wavelength to which the spectrometer is adjusted.
- Let $p = k\lambda_o$ be the parameter in the output which indicates λ_o (e.g., inches of displacement along a recorder graph, dial setting on a wave analyzer, etc.). The units of k (the scale factor) are chosen appropriately.

- Let $V(k\lambda_o)$ be spectrometer output in units when setting is at $p = k\lambda_o$. (Basically this is the output of a Fourier cos analyzer, but may be indicated by inches of displacement across recorder paper at position p along paper, meter reading of wave analyzer when dial is set at p, etc.)
- Let $R_{SN}(x,y,k\lambda_o,\lambda)$ be system spectral radiance responsibity (should really be R_{N_λ}) defined to make the following equation hold:

$$V(k\lambda_o) = \int_x \int_y \int_\lambda R_{SN}(x,y,k\lambda_o,\lambda)\, N_\lambda(x,y,\lambda)\, dx\, dy\, d\lambda \qquad (1)$$

where the integration is over all relevant values of x, y and λ.

The assumption that R_{SN} can be defined to make an equation like this hold is equivalent to an assumption of linearity in radiance. In writing this equation it is assumed that all other parameters not mentioned above are held fixed. Some of these fixed parameters are

- All knob settings on
  - (a) Radiometer, specifically retardation and scan time
  - (b) Wave Analyzer (except frequency)
  - (c) Recorder
  - (d) All other instruments
- Tape parameters, including tape speed
- Distance to source and atmospheric conditions between source and radiometer
- Radiometer aperture
- Radiometer orientation relative to source plane

It will be apparent that the above list of fixed parameters is a specific expression of the philosophy of Nicodemus and Zissis (Ref. 1) in that all possible conditions should be the same in use and in calibration. One may think that the requirement for a fixed

distance to the source is going too far, and that perhaps an angular calibration should be made which would be applicable (through a simple mathematical adjustment) at various distances. Unfortunately, when source distance is changed, atmosphere also is changed; and this change in transmission is so complex as to almost defy analysis. Although performing this adjustment is possible, it is certainly not in the spirit of a laboratory "calibration." If at all possible, then, source distance should be fixed; and if this is not possible, it should be recognized that the adjustment is a major scientific problem and not a "calibration."

Only the spectral radiance responsivity is considered in this section since it is most closely associated with the actual physical characteristics of the source. The irradiance responsivity and power responsivity can be derived from it when source and instrument characteristics are taken into account.

Equation (1) corresponds to a combination of Eq. (10) or Eqs. (36) and (27) of Ref. 1. The combined treatment is better because it allows for the possibility of treating the case in which spectral responsivity varies with position. It also shows more clearly the relationship between them. In addition, Eq. (1) has the direct physical interpretation of a sum of the contributions from each element of source area and optical wavelength. However, the instrument imposes a weighting factor [determined by $R_{SN}(x, y, p, \lambda)$] on the contribution from each element, according to the adjustment of p. Since R_{SN} is an instrumental characteristic, the output V measures a weighted average of $N\lambda(x, y, \lambda)$ and not a power. The output may be considered as a measure of a power only when referred to an instrument with the same system spectral radiance responsivity, R_{SN}. The corresponding consideration for the basic radiometer is made quite clear by Ref. 1 (p. 14), but the exposition for the spectral radiometer is not as complete.

The linearity of the instrument, expressed by Eq. (1), is an assumption that must be verified before Eq. (1) can be used. The question will be discussed further in the next section.

C.5 CALIBRATION THEORY (LINEAR CASE)

If Eq. (1) holds, and $R_{SN}(x, y, k\lambda_o, \lambda)$ is known as a function of all its variables, the problem of the spectrometer use is that of determining $N(x, y, \lambda)$ from a set of values of $V(k\lambda_o)$. (It is permissible to shift the source in the source plane to do this.) However, in the beginning, $R_{SN}(x, y, k\lambda_o, \lambda)$ is not known. The calibration problem consists of the determination of $R_{SN}(x, y, k\lambda_o, \lambda)$ from values of $V(\lambda_o)$ obtained from sources with known spectral radiance distributions, $N_\lambda(x, y, \lambda)$. This is equivalent to inverting the integral operator on $R_{SN}(x, y, k\lambda_o, \lambda)$ defined by $N(x, y, \lambda)$.

The quantity $p = k\lambda_o$ occurs in $R_{SN}(x, y, p, \lambda)$ as a parameter. For a fixed p the instrument behaves like a radiometer with a narrow band filter, as shown in Fig. C-1. The problem of determining the dependence of $R_{SN}(x, y, p, \lambda)$ on λ, when p is fixed, is referred to (Ref. 1) as the problem of determining the spectral responsivity. The problem of determining the dependence of $R_{SN}(x, y, p, \lambda)$ on x and y when p is fixed; is referred to (in Ref. 1) as the problem of determining the spatial responsivity. If the spectral responsivity turns out to be independent of x and y, in the sense that $R_{SN}(x, y, p, \lambda)$ plotted as a function of λ has the same shape for different values of x and y, then it is possible to consider the spectral and spatial responsivity separately, as is done in Ref. 1. This will not necessarily be the case.

In fact, from consideration of the discussion given in Section above on wave shape, it is clear that the spectral responsivity does, in general, depend on position of the source in the field of view. Suppose the maximum retardation is very long, so that the spectral resolution as determined by it is much less than $\nu\ \lambda^2/2\ \text{cm}^{-1}$ where γ is the maximum obliquity angle. Then, if at the center of the field the peak of the spectral response curve is at $\lambda_o = 1/\nu_o$, the peak of the spectral response curve for a point at an angle $\gamma/2$ will occur at wavelength

$$\lambda = \frac{1}{\nu_o(1 + \gamma^2/\delta)}$$

It is evident that the spectral response has shifted its peak and therefore is not independent of position in the field of view.

Consider then the system spectral responsivity function $R_{SN}(x, y, k\lambda_o, \lambda)$. Denote

$$R'_N(k\lambda_o, \lambda) = \iint_{x,y=-\infty}^{+\infty} R_{SN}(x, y, k\lambda_o, \lambda)\, dx\, dy$$

and

$$R_N(\lambda_o) = \int_{\lambda} R'_N(k\lambda_o, \lambda)\, d\lambda$$

Then define

$$\tau(k\lambda_o, \lambda) = \frac{R'_N(k\lambda_o, \lambda)}{R_N(\lambda_o)}$$

so that

$$\int_x \tau(k\lambda_o, \lambda)\, d\lambda = 1$$

for all λ_o. Thus

$$R'_N(k\lambda_o, \lambda) = \tau(k\lambda_o, \lambda)\, R_N(\lambda_o)$$

The function $R_N(\lambda_o)$ is called the spectral radiance responsivity. For the I-4T it includes the effect of the detector frequency response function as well as other material effects.

In a spectrometer $\tau(k\lambda_0, \lambda)$ must be nearly zero unless λ is close to λ_0. This is what we mean be a spectrometer. The "half-width" of τ may be defined as that interval of λ for which τ is greater than one half its maximum value. The "half width" is essentially what we mean by the spectral resolution of the instrument. The function τ defined here has the same general significance as the τ function of Nicodemus and Zissis (Ref. 1) except that the normalization procedure is not necessarily the same. It often happens that τ depends only on $\lambda - \lambda_0$ and not on λ and λ_0 separately. This means that the spectral resolution is the same for all settings of the instrument, but we need not require that condition for adequate radiometric calibration.

In all cases considered here it will be assumed that the phase-shift difference is identically zero for all angles and wavelengths. In this case, the position of zero retardation corresponds to a bright central fringe for white light, and this fringe can be used to locate the zero position. The amount of light in the input at wave number ν is given by the inverse cosine transform at frequency $\nu B/T$ of the detector output (interferogram). However, since only a finite length of data is available, we can obtain only averages of the inverse cosine transform as described in the preceding section. Since phase shift is essentially constant with frequency, the power delivered to the wave analyzer is in proportion to the magnitude of the cosine transform, provided the zero retardation is centrally located in the observation interval. If the zero position is located at the edge of the interval, the phase of the output frequency will shift by π radians in a frequency range $1/T$. Since this corresponds to the zero of the weighting function that gives the weighted average, an output indication can still be obtained, but the signal-to-noise has been reduced and the resolution affected as explained in Ref. 2.

C.5.1 Special Case I – Spectral and Spatial Responsivity Are Independent

This case occurs in the I-4T when the resolving power is limited by the retardation, i.e, $R = \nu B/k$ where k is of the order of unity. In this case, the change in

frequency in an oblique ray of maximum angle γ is small enough that it cannot be detected. For wave number ν, there are νB waves in the retardation interval B. For in the oblique ray at angle γ there are νB sec γ waves, or $\sim \nu B\gamma^2/2$ more. If $\nu B\gamma^2/2 < 1/2$, i.e., $B < 1/\nu\gamma^2$ then the change in frequency cannot be determined easily. The spectral responsivity is then (approximately) the same at all points in the field of view. Further, for a nearly monochromatic source of wave number ν, the interferogram is a cosine function of time with frequency $f_\nu = \nu B/T$. Then, if the wave analyzer is set at bandwidth $1/T$, the integration time is just T seconds. The output at the end of the scan is a measure of the Fourier cosine transform since all the waves of frequency f_ν are of the same phase. A wider bandwidth will cause a loss of spectral resolution as well as a decrease in signal-to-noise ratio for narrow spectral lines. A narrower bandwidth will cause a sawtooth appearance in the spectrum due to the fact that the integration time of the analyzer now includes several scans. Those frequencies which are in phase on successive scans will add and give a peak in the spectral graph; those which are out-of-phase will subtract and give a trough in the spectral graph. The peaks are separated by a frequency interval $f_2 - f_1$ corresponding to the presence of just one more wave in the scan interval: $f_2/T - f_1/T = 1$, i.e., $\Delta f = 1/T$. The peaks give a true measure of the output. Since the resolution cannot be better than $1/T$ cycles per second, there is nothing lost by reading only the peaks. These results accord with the recommendations given in section IV of the I-4T manual, but the reasons are not explained there. Of course, if the playback speed up ratio, P, is greater than unity, the required wave analyzer band-width is P/T, and usually P is adjusted to make this quantity equal to the fixed wave-analyzer bandwidth. This discussion indicates that the wave-analyzer output can be made to correspond to $V(k\lambda_o)$, so that Eq. (1) can be used.

For every particular point (x, y), the function $R_{SN}(x, y, p, \lambda)$ defines a function of (p, λ) [by considering (x, y) fixed]. This curve is called the spectral-response curve at (x, y). In the case being considered, this function has the same shape for every value of (x, y). That is what is meant by a spectral responsivity that is independent of position in the field of view. This means that $R_{SN}(x, y, p, \lambda)$ can be

expressed as a product of a function of (x, y) and another function of (p, λ), say as

$$R_{SN}(x, y, p, \lambda) = h(x, y)\, g(p, \lambda)$$

The values of $h(x, y)$ determine the relative heights of the spectral response curve (described above) that is associated with (x, y). It is always possible to have $h(x, y)$ normalized so that $\iint h(x, y)\, dx\, dy = 1$.

If $h(x, y)$ did not satisfy the latter requirement, but

$$\int_{-\infty}^{+\infty}\int h(x, y)\, dx\, dy = h_o$$

then it would be possible to normalize $h(x, y)$ by defining

$$h'(x, y) = \frac{h(x, y)}{h_o}$$

$$g'(p, \lambda) = h_o\, g(p, \lambda)$$

so that the requirement would be satisfied.

The above operation can be described as separating the variables. The function $h(x, y)$ is usually zero outside of some very small area. That area in which $h(x, y)$ is not zero is called the field of view.

Now, it is seen that

$$\int_{x, y=-\infty}^{+\infty}\int h(x, y)\, g(p, \lambda)\, dx\, dy = g(p, \lambda)$$

But since the integrand is equal to $R_{SN}(x, y, p, \lambda)$, and since we have already set its integral over all x, y equal to $R'_N(p, \lambda)$, it is clear that

$$g(p, \lambda) = R'_N(p, \lambda) = \tau(k\lambda_o, \lambda)\, R_N(\lambda_o)$$

Summarizing:

$$R_N(x, y, k\lambda_o, \lambda) = h(x, y)\, \tau(k\lambda_o, \lambda)\, R_N(\lambda_o)$$

where

$$\iint_{-\infty}^{+\infty} h(x, y)\, dx\, dy = 1$$

$$\int_{-\infty}^{+\infty} \tau(k\lambda_o, \lambda)\, d\lambda = 1$$

All variables have now been separated and the way is paved for a separate consideration of spectral and spatial responsivity. The function $h(x, y)$ can be determined by mapping the field of view with a small source, as described by Nicodemus and Zissis (Ref. 1). The source need not be of any particular spectral distribution. The response to a source so small that $h(x, y)$ is nearly constant for values of x, y for which the radiance is nonzero is given by

$$V_{x_o, y_o}(k\lambda_o) = \iint_{x, y = -\infty}^{+\infty} \int_{\lambda} h(x, y)\, \tau(k\lambda_o, \lambda)\, R_N(\lambda_o)\, N_\lambda(x_o, y_o, \lambda)\, dx\, dy\, dx$$

$$= h(x_o, y_o)\, R_N(\lambda_o) \left[\int_{\lambda} \tau(k\lambda_o, \lambda)\, N_\lambda(x_o, y_o, \lambda)\, d\lambda \right] \Delta S \qquad (2)$$

where ΔS is the area of the source and x_o, y_o is a point in the source (usually its center). As the source is moved from point to point all factors are constant except

$h(x_o, y_o)$. Hence, $h(x_o, y_o) = K\left[V_{x_o, y_o}(k\lambda_o) - V_o(k\lambda_o)\right]$ where $V_o(k\lambda_o)$ is the system response with the source removed. The constant K can then be chosen easily to give the correct normalization as described above.

When $N_\lambda(x_o, y_o, \lambda)$ has a known dependence on λ, it is possible to use Eq. (2) to determine $R_N(\lambda_o)$. This is particularly simple when N_λ varies so slowly with λ that it may be considered constant for values of λ for which $\tau(k\lambda_o, \lambda)$ is nonzero. Then

$$\int_\lambda \tau(k\lambda_o, \lambda)\, N_\lambda(x_o, y_o, \lambda)\, d\lambda = N_\lambda(x_o, y_o, \lambda_o)$$

and Eq. (2) yields

$$R_N(\lambda_o) = \frac{V_{x_o, y_o}(k\lambda_o)}{h(x_o, y_o)\, N_\lambda(x_o, y_o, \lambda_o)\, \Delta S} \tag{2a}$$

This completes the calibration in this case since $\tau(k\lambda_o, \lambda)$ is usually calculated from instrument characteristics as in Nicodemus and Zissis.

The linearity of the system should be checked in two different ways. First, by using sources of increasing temperature; and next, by using sources of greater area. The latter requirement can be met by using two or more small sources located in different parts of the field of view. A simple linearity check procedure is to recalibrate the instrument under the various situations and then to verify that the same calibration functions are obtained in each case.

C.5.2 Special Case II – Uniform Spectral Radiance

The case of intertwined spectral and spatial responsivity is much more complicated than that previously discussed. However, if attention is restricted to cases in which $N_\lambda(s, y, \lambda)$ is independent of x, y throughout the field of view, a simple result can

be obtained. Uniform spectral radiance can often be obtained either by using a small field of view, or by using an extended source in which the spectral radiance is carefully controlled to be uniform.

In this case, the interferogram for a uniform monochromatic source of wave number ν will have a complicated shape, not necessarily a sinusoidal function. For a retardation interval B, long enough to prevent treatment by the simple methods of Case I, the spectrum of the interferogram will be distributed over a band of frequencies near $f_\nu = \nu B/T$ of width approximately $\nu B/T\ \gamma^2/2$ where γ is the maximum obliquity angle. Thus the resolution will be no better than $\nu\,(\gamma^2/2)\ \text{cm}^{-1}$. A source of nearby wave number ν_1 will have a similar, possibly overlapping spectrum. But in this case, the overlapping components at a given frequency ν will have the same phase; hence they will add to a sum proportional to the intensities of the two sources multiplied by the appropriate weighting factors.

Now suppose the interferogram was fed into a wave analyzer with bandwidth $\nu B/T\ \gamma^2/2$ cycles/sec, which corresponds to a resolution of $\nu(\gamma^2/2)\ \text{cm}^{-1}$. Since there are within this band two or more frequencies that can be distinguished in time interval T, there will be beats in the output. The power delivered (at any one time) will not vary linearly with changes in the intensity of any particular frequency components. The intensities of spectral lines will not be properly recorded. However, if all components are increased approximately proportionally, as when $N_\lambda\,(x, y, \lambda)$ is a blackbody spectral radiance, the total output will increase linearly with input. Beats will occur in the output of the narrow band filter, but if the total power delivered in time T is measured, an indication of a weighted average of the squares of the intensities in the various sub-bands will be obtained. The analysis could be carried out on this basis, but this is not the case referred to by Eq. (1) or by Ref. 1, either.

If the recorder speed P is adjusted so that the wave analyzer bandwidth is P/T regardless of the maximum obliquity angle, no beats will occur. The result will be a weighted average of the intensities as required by Eq. (1), provided the readings

are made at the end of the scan time, or at the peaks of the "saw-teeth" in the spectrum. Further, if this method is used, the signal-to-noise ratio for narrow spectral lines will be improved and all the information in the interferogram will be preserved. However, it must be remembered that the spectral resolution is determined by the obliquity angle and not by the retardation (which would give an apparently better result). The resulting spectrum can be smoothed, if desired, to remove any spurious structure finer than this resolution.

The most important result of the above discussion is the conclusion that the wave analyzer output can be made to measure a weighted average of $N_\lambda(x, y, z)$ so that

$$V(k\lambda_o) = \iint_{xy=-\infty}^{+\infty} \int_\lambda R_{SN}(x, y, k\lambda_o, \lambda)\, N_\lambda(x_o, y_o, \lambda)\, dx\, dy\, d\lambda$$

$$= \int_\lambda \left[\iint_{x,\, y=-\infty}^{+\infty} R_{SN}(x, y, k\lambda_o, \lambda)\, dx\, dy \right] N_\lambda(x_o, y_o, \lambda)\, d\lambda$$

$$= \int_\lambda R'_N(k\lambda_o, \lambda)\, N_\lambda(x_o, y_o, \lambda)\, d\lambda$$

$$= R_N(\lambda_o) \int_\lambda (k\lambda_o, \lambda)\, N_\lambda(x_o, y_o, \lambda)\, d\lambda \qquad (3)$$

where x_o, y_o is a point in the field of view and the integral over λ is over all contributing wavelengths.

In cases $N_\lambda(x_o, y_o, \lambda)$ varies slowly with λ (as for a blackbody), then

$$V(k\lambda_o) = R_N(\lambda_o)\, N_\lambda(x_o, y_o, \lambda) \qquad (3a)$$

This corresponds to Eq. (39) of Nicodemus and Zissis (Ref. 1), but here the reference to the τ function can be omitted because of the method of normalization. The inclusion

of the factor $\Delta\lambda_S$ in the referred to Eq. (39) is somewhat misleading. It suggests that the output is a spectral radiance integrated over wavelength, and therefore should be expected to have the dimensions of radiance (watts/cm^2-ster). The notation used in this part of Vol. 1 correctly indicates that the integration variable is dimensionless; hence, the system output is a measure of a spectral radiance (dimensions watts/cm^2-ster$-\mu$). The interpretation of the integral is that the output measures a weighted average of the spectral radiance with weights given by the smoothing function $\tau(k\lambda_o, \lambda)$ as explained in greater generality in section .

If $N_\lambda(x, y, \lambda)$ varies substantially throughout the field of view, much more complicated mathematical techniques are needed to get back to the radiance from $V(\lambda_o)$. So far as $h(x, y)$ is concerned, the practical solution to this difficulty is to make the field of view small enough to insure the constancy of $N_\lambda(x, y, \lambda)$ throughout that area. This can usually be checked visually.

The situation with regard to variations of $N_\lambda(x, y, \lambda)$ with λ are, however, completely different. The presence of spectral lines creates a structure much finer than the spectral resolution of the I-4T or the eye. The instrument output must be thought of as a smoothed spectrum made with the function $\tau(k\lambda_o, \lambda)$ as the smoothing function. Since the data are to be interpreted in this way, it is desirable to give the function $\tau(k\lambda_o, \lambda)$ of the instrument with the data obtained from it. This can usually be most easily done by giving $\tau(k\lambda_o, \lambda)$ as a family of curves in the $\tau, \lambda - \lambda_o$ plane with λ_o as a parameter. If the spectral response of the instrument is constant, there will be only one curve. With the aid of the $\tau(k\lambda_o, \lambda)$ curves, the user of the data may, if he wishes, attempt to reconstruct the fine structure of the spectral variations of $N_\lambda(x, y, \lambda)$.

For the case mentioned above, the problem of radiometric calibration has been resolved to the determination of the function $R_N(\lambda_o)$. To find this, it is merely necessary to use a source of known spectral radiance, such as a blackbody source, which fills the field of view of the instrument. Then

$$R_N(\lambda_o) = \frac{V(\lambda_o)}{N_B(x_o, y_o, \lambda_o)}$$

where $V(\lambda_o)$ is the observed output and N_B is the blackbody spectral radiance.

As before, a convenient check for linearity is to calibrate the instrument at different intensity levels and verify that the same function $R_N(\lambda_o)$ is obtained in each case.

C.6 TOPICS NOT COVERED

No consideration has been given in this report to the effects of errors in the alignment of the interferometer. The action of the instrument has been treated as if it were functioning perfectly. It is possible that the effects of these errors may be taken up in the calibration, but a more detailed analysis is needed to investigate this.

An entire set of topics not covered are associated with the notion of advanced data processing of the interferogram. This processing would probably be done by digitilizing the output of the detector and processing the resulting output on a digital computer. In this way it may be possible to increase the spectral resolution to disclose very narrow lines, or to improve spatial resolution to disclose source structure smaller than the field of view, thus aiding in background suppression. Further, the problem of intermixed spatial and spectral responsivity could be attacked in this way.

This could be done by using the fact that the phase-shift difference for a monochromatic point source is a constant of the instrument. Hence, the phase of the pure sinusoidal component contributed by this source is known for any assumed zero position (not necessarily the actual zero retardation position). The output can be processed linearly to give the component, which could be taken as the fundamental output rather than the total power delivered from all points.

More general methods of data processing could increase signal-to-noise ratio. For example, if the phase-shift difference is identically zero, and a record is obtained with the zero retardation position at one edge, the symmetry of the interferogram about the zero position could be used to effectively double the recorded data, thus increasing signal-to-noise ratio and/or resolution, as described in Ref. 2. When optimum methods of data processing have been clarified, it is possible that improved methods of gathering data may be indicated.

Before advanced data processing or consideration of alignment errors can be undertaken, a more exact and complete theory of interferometer operation is needed. Reference 2 presents a good starting point for this theory. The development of an improved theory is the first step toward any advanced work.

C.7 REFERENCES

1. Fred E. Nicodemus and George J. Zissis, Report of BAMIRAC Methods of Radiametric Calibration, Univ. of Mich. Institute of Science and Technology, Report No. 4613-20-R, October 1962 (ASTIA No. AD-289,375) Contract SD-91
2. J. Connes, "Recherches sur la Spectroscope por Transformation de Fourier," Rev. Optic 40
3. Block Associates, Inc., Cambridge, Mass., I-4 Interferometer Spectrometer, (Instruction Manual)
4. M. Born and E. Wolf, Principles of Optics, Pergamon, 1959
5. David Middleton, Introduction to Statistical Communication Theory, McGraw Hill, New York, 1960